学位論文

Evolution of shell microstructure in Protobranchia (Mollusca: Bivalvia)

（原鰓類（軟体動物：二枚貝綱）における貝殻微細構造の進化）

平成 26 年 12 月博士（理学）申請

東京大学大学院理学系研究科

地球惑星科学専攻

佐藤　圭

Abstract

Molluscan shells are composed of structural units of calcium carbonate called shell microstructure. Variation in molluscan shell microstructure is more noticeable relative to other animal phyla and subphyla. Generally shell microstructure is similar among phylogenetically close taxa. Shell microstructural variation also reflects differences in mechanical properties such as shell strength. Hence, shell microstructural architecture has significance in studies on adaptive radiation and macro-/microscopic morphological evolution. This study focusses on protobranchs to clarify evolution of shell microstructures through the origin and diversification of the basal groups of bivalves. Various shell microstructures were examined through scanning electron microscopy and characterized by crystallographic textures. Furthermore, they were evaluated phylogenetically through molecular phylogenetic analysis using DNA sequences.

An ML-based phylogenetic analysis was performed based on nine molecular loci (16S rRNA, 18S rRNA, 28S rRNA, cytochrome c oxidase subunit 1 [COI], histone H3, ATP synthase β, elongation factor-1α, myosin heavy chain type II and RNA polymerase II) in 107 protobranch species in total. The resulting ML tree supported the monophyly of four superfamilies of Protobranchia with a major change in the position of the family Sareptidae. Sareptidae has been considered as the Nuculoidea but was paraphyletic to the Nuculanoidea in the resulting ML tree. In addition, multiple polyphyletic conditions were revealed among genera and families validated in previous classifications.

Shell microstructures of 38 protobranch species were newly described using scanning electron microscopy. The topology of the obtained phylogenetic tree and shell microstructural composition are consistent at the superfamily level in protobranchs. The microstructural design is similar among Nuculidae in having outer prismatic and middle/inner nacreous structures in common. Outer prismatic structures of protobranchs were divided into five subtypes. In Solemyoidea, four groups were recognized in accordance with the genus-level phylogeny. On the other hand, fine prismatic, homogeneous and fine complex crossed lamellar structures are shared in Nuculoidea. Sareptids were previously classified in Nuculidae but here were transferred to Nuculanoidea based on the molecular phylogenetic tree. In agreement with the molecular phylogeny, similar shell microstructures are shared by sareptids and other nuculanoideans.

The crystallographic textures of shell microstructures in protobranch bivalves were analyzed for 14 specimens of 13 species. Six groups of crystallographic patterns were recognized among 12 microstructures in 13 species. By comparing the crystallographic textures within each type of shell microstructure, several cases of convergence were found among closely related taxa, for instance, the inner layer of solemyids and the outer layer of nuculids. These examples may imply that morphologically similar microstructures have different phylogenetic origins.

Shell microstructural grouping found in this study was consistent with the division of higher taxa suggested by molecular phylogenetic analysis. This indicates that shell microstructure of protobranchs reflect their phylogenetic origin. In addition, the descriptions of shell microstructures in previous studies suggest that all ancestral protobranchs had a nacreous structure, although the nacreous structure is never found in

the Recent Solemyoidea and Nuculanoidea, suggesting that the shell microstructure of protobranchs evolved from a nacreous to non-nacreous structure, in general. These changes seem to have occurred during the Silurian to Carboniferous in “Malletidae-like” Nuculanoidea and Nuculoidea, and in the Cenozoic in Nuculanoidea. The homogeneous structure, which is dominant in non-nacreous species is advantageous to the energy cost of shell formation. In the latter event, the distribution of Nuculanoidea shifted to high-latitude and deep-water regions and increased their diversity, probably related to the appearance and divergence of infaunal heterodont bivalves, which occupy a similar habitat. A possible driving force for the shell microstructural evolution is insoluble in the former event. However, species appeared after those event is superior in having low-cost shell microstructure.

Table of contents

Chapter 1 Introduction

1-1. Shell microstructure of molluscs

Molluscan shells are composed of structural units of calcium carbonate called shell microstructures; these microstructures are categorized by their crystal form and orientation. Shell microstructure has long been studied in paleontology, because they can be preserved in fossil specimens and therefore are considered to provide a clue for the evolution and phylogeny of the past life. Details of various microstructures have been described in several monographs (e.g. Bøggild, 1930; Taylor et al., 1969; Carter, 1990a). According to the definition in Carter (1990a), 40 types of mineralized microstructures are recognized in molluscan shells and periostraca (Table 1.1) in terms of variety in their mineralogies. This variety is more noticeable relative to other animal phyla and/or subphyla. Many researchers believe that the variety have phylogenetic significance. Similarities of shell microstructures in phylogenetically close taxa of molluscs have been reported in many papers (Veneridae: Uozumi & Suzuki, 1981; Shimamoto, 1986; Littorinidae: Taylor & Reid, 1990; Cardiidae: Schneider & Carter, 2001; Patellogastropoda: Fuchigami & Sasaki, 2005). Therefore, the investigation of shell microstructures can provide clues for systematic and phylogenetic relationship of molluscs, including fossil taxa.

Compared to authigenic calcium carbonate, mechanical properties of each shell microstructures are variable (e.g. Currey, 1976; Frýda et al., 2013). This variation is probably reflect the degree of resistance to predatory attack, for example. West & Cohen (1996) argued that the number of crossed lamellar layers in snails increased with

Table 1.1. Taxonomic distribution of skeletal microstructure and mineralogy (modified the table from Carter, 1990b). Abbreviations: ara., aragonite; cal., calcite; pho., phosphate.

	Shell microstructure	Mollusca			Corals			Brachiopoda		Bryozoa		Annelida			Arthropoda	Echinodermata	Vertebrata	
	Mineralogy	ara.	cal.	pho.	ara.	cal.	pho.	cal.	pho.	ara.	cal.	ara.	cal.	pho.	cal.	cal.	ara.	pho.
Prismatic structures	Regular simple prismatic	O	O					O		O								
	asymmetric prismatic	O				O												
	Radially elongate simple prismatic	O																
	Lathic simple prismatic		O															
	Irregular simple prismatic	O	O		O	O		O		O	O		O		O	O		
	Blocky prismatic	O			O					O								
	Pavement prismatic		O															
	Rod-type fibrous prismatic	O	O		O													O
	Lath-type fibrous prismatic	O	O					O			O							
	Anvil-type fibrous prismatic		O					O			O							
	Simple lamellar fibrous prismatic	O													O			
	Irregular fibrous prismatic	O	O		O	O		O		O	O		O		O			O
	Denticular composite prismatic	O			O	O				O	O							O
	Non-denticular composite prismatic	O			O?					O?	O?							O?
	Compound composite prismatic	O																
	Crossed composite prismatic	O									O							
	Regular spherulitic prismatic	O								O?								
	Irregular spherulitic prismatic	O	O		O	O		O		O	O				O			
	Planar sperulitic prismatic		O		O	O				O	O							
	Spherulitic	O			O	O			O	O	O				O		O	O
Laminaar structures	Sheet nacreous	O																
	Row stack nacreous	O																
	Columnar nacreous	O																
	Semi-nacreous	O	O					O		O?	O							
	Orthogonal plywood																	O
	Twisted plywood	?	?												?			O
	Lamello-fibrillar	O	O												O			O
	Plywood with transverse fibers	O																O
	Crossed bladed		O					O			O							
	Regularly foliated		O					O			O							
	Semi-foliated		O			O		O			O							
	Matted	O							O			O						O
	Homogeneous	O	O		O	O	O	O	O	O	O	O	O		O	O	O	O
Crossed structures	Crossed acicular	O																
	Intersected crossed platy	O																
	Dissected crossed prismatic	O																
	Oriented crossed lamellar	O	O															O
	Non-oriented crossed lamellar	O									O							
	Prismatic enamel structures																	O
	Decussated enamel structures																	O
	Fine complex crossed lamellar	O			O				O			O			O			O
	Irregular complex crossed lamellar	O	O		O	O			O	O	O	O			O	O		
	Cone complex crossed lamellar	O	O															
	Helical	O																
	Isolated spicules or spikes	O		O		O		O						O		O		O
	3-D sterom + trabecular structures															O		O
	Decapod horizontal laminate														O			
	Total	**40**			**15**			**16**		**19**		**7**			**10**	**5**	**17**	

increasing of predation intensity. This layer has plywood-like arrangement of aragonite needles, and play an important role in the strengthening of shells (Currey, 1999). The relationship between molluscan ‘macroscopic’ morphology and their life habitat has long been studied (e.g. Stanley, 1970). Shell microstructural variation also seems to have significance in adaptive radiation and macroscopic morphological evolution. Microscopic as well as macroscopic shell morphology is expected to reveal molluscan evolutionary history in fossil records.

1-2. Protobranch bivalves

1-2-1. Subclass Protobranchia

To characterize the phylogenetic significance and evolutionary history of the molluscan shell microstructure, it is desirable to focus on basal taxa of a particular molluscan class. The shell microstructure of bivalves has been previously comparatively well studied (Carter, 1990). Therefore, for this study, Protobranchia which is considered as the primitive taxon of bivalves, was used for analyses (e.g. Zardus, 2002).

Protobranchs are considered as possibly the oldest clade of the Bivalvia (e.g. Allen, 1983). The first occurrence of protobranchs dates back at least to early Ordovician (Cox et al., 1969) and they have not changed their morphology drastically over time (Morris & Fortey, 1976). Recent protobranchs encompass about 700 species (Huber, 2010). Protobranchia have four superfamilies according to the current classification: Nuculanoidea (Order Nuculoida), Solemyoidea, Manzanelloidea (Order Solemyoida), and Nuculanoidea (Order Nuculanoida) (Bouchet et al., 2010. See table 1.2). Protobranchs are united by the following characteristics: gill structure, hinge

Table 1.2. Systematics of Protobranchia based on Bouchet et al. (2011). Original description was noted. A dagger (†) before the name indicates the species is a fossil.

Subclass	Order	Superfamily	Family	Genus	Type species
Protobranchia	**Nuculoida**	**Nucloidea**	**Nuculidae**	***Acila***	***Acila divaricata***
Pelseneer, 1889	Dall, 1889	Gray, 1824	Gray, 1824	Adams & Adams, 1858	(Hinds, 1843)
				Austronucula	***Austronucula schencki***
				Powell, 1939	Powell, 1939
				Brevinucula	***Brevinucula verrillii***
				Thiele, 1934	Dall, 1886
				Condylonucula	***Condylonucula cynthiae***
				Moore, 1977	Moore, 1977
				Ennucula	***Ennucula obliqua***
				Iredale, 1931	(Lamarck, 1819)
				Linucula	***†Linucula ruatakiensis***
				Marwick, 1931	(Marwick, 1926)
				Neonucula	***Neonucula pratasensis***
				Lan & Lee, 2001	(Lan & Lee, 2001)
				Nucula	***Nucula nucleus***
				Lamarck, 1799	(Linnaeus, 1758)
				Pronucula	***Pronucula decorosa***
				Hedley, 1902	Hedley, 1902
				Rumptunucula	***Rumptunucula vincentiana***
				Bergmans, 1978	(Cotton & Godfrey, 1938)
				Sinonucula	***Sinonucula cyrenoides***
				Xu, 1985	(Kuroda, 1929)
				Varinucula	***Varinucula gallinacea***
				Maxwell, 1988	(Finlay, 1930)
			Sareptidae	***Pristigloma***	***Pristigloma nitens***
			Stoliczka, 1870	Dall, 1900	(Jeffreys, 1876)
				Sarepta	***Sarepta speciosa***
				Adams, 1860	Adams, 1860
				Setigloma	***Setigloma japonica***
				Schileyko, 1983	(Smith, 1885)
	Solemyoida	**Manzanelloidea**	**Manzanellidae**	***Huxleyia***	***Huxleyia sulcata***
	Dall, 1889	Chronic, 1952	Chronic, 1952	Adams, 1860	Adams, 1860
				Nucinella	***Nucinella ovalis***
				Wood, 1851	(Wood, 1840)
		Solemyoidea	**Solemyidae**	***Acharax***	***Acharax johnsoni***
		Gray, 1840	Gray, 1840	Dall, 1908	Dall, 1891
				Solemya	***Solemya togata***
				Lamarck, 1818	(Poli, 1795)
	Nuculanida	**Nuculanoidea**	**Nuculanidae**	**Ledella**	**Ledella bushae**
	Carter ete al., 2000	Adams & Adams, 1858 (1854)	Adams & Adams, 1858 (1846)	Verrill & Bush, 1987	Warén, 1978
				Ledellina	***Ledella olivacea***
				Filatova & Schileyko, 1984	Filatova & Schileyko, 1984
				Parayoldiella	***Parayoldiella ultraabyssalis***
				Filatova, 1971	(Filatova, 1971)
				Adrana	***Adrana electa***
				Adams & Adams, 1858	(Adams, 1856)
				Jupiteria	***Jupiteria concava***
				Bellardi, 1875	(Bronn, 1831)
				Lamellileda	***Lamellileda typica***
				Cotton, 1930	Cotton, 1930
				Nuculana	***Nuculana pernula***
				Link, 1807	(Müller, 1779)
				Politoleda	***Politoleda polita***
				Hertlein & Strong, 1940	(Sowerby, 1833)
				Poroleda	***Poroleda lanceolata***
				Hutton, 1893	(Hatton, 1885)
				Propeleda	***Propeleda ensicula***
				Iredale, 1924	(Angas, 1877)
				Saccella	***Saccella commutata***
				Woodring, 1925	(Philippi, 1844)
				Teretileda	***Teretileda oculata***
				Iredale, 1929	Iredale, 1929

Table 1.2. Continued.

Subclass	Order	Superfamily	Family	Genus	Type species
Protobranchia	**Nuculanida**	**Nuculanoidea**	***Bathyspinulidae***	***Bathyspinula***	***Bathyspinula calcarella***
Pelseneer, 1889	Carter ete al., 2000	Adams & Adams, 1858 (1854)	Coan & Valentich-Scott, 1997	Allen & Sanders, 1982	(Dall, 1908)
				Tindariopsis	***Tindariopsis agathida***
				Verrill & Bush, 1897	(Dall, 1890)
			Malletiidae	***Carinineilo***	***Carinineilo carinifera***
			Adams & Adams, 1858 (1846)	Kuroda & Habe, 1971	(Habe, 1951)
				Clencharia	***Clencharia abyssorum***
				Clarke, 1961	(Verril & Bush, 1898)
				Katadesmia	***Katadesmia vincula***
				Dall, 1908	(Dall, 1908)
				Malletia	***Malletia chilensis***
				Desmoulins, 1832	Desmoulins, 1832
				Neilo	***Neilo cumingii***
				Adams, 1854	Adams, 1854
				Protonucula	***Protonucula verconis***
				Cotton, 1930	Cotton, 1930
				Pseudoglomus	***Pseudoglomus pompholyx***
				Dall, 1898	(Dall, 1889)
				Taiwannuculana	***Taiwannuculana exotica***
				Okutani & Lan, 1999	(Okutani & Lan, 1999)
			Neilonellidae	***Neilonella***	***Neilonella corpulenta***
			Schileyko, 1989	Dall, 1881	(Dall, 1881)
			Phaseolidae	***Lametila***	***Lametilla abyssorum***
			Scarlato & Starobogatov, 1971	Allen & sanders, 1973	Allen & sanders, 1973
				Prelametila	***Prelametilla clarkei***
				Allen & Sanders, 1973	Allen & Sanders, 1973
			Siliculidae	***Silicula***	***Silicula fragilis***
			Allen & Sanders, 1973	Jeffreys, 1879	Jeffreys, 1879
			Tindariidae	***Tindaria***	***Tindaria arata***
			Verrill & Bush, 1897	Bellardi, 1875	Bellardi, 1875
			Yoldiidae	***Adranella***	***Adranella casta***
			Dall, 1908	Verrill & Bush, 1898	(Verril & Bush, 1898)
				Megayoldia	***Megayoldia thraciaeformis***
				Verrill & Bush, 1897	(Storer, 1838)
				Microgloma	***Microgloma yongei***
				Sanders & Allen, 1973	Sanders & Allen, 1973
				Orthoyoldia	***Orthoyoldia scapania***
				Verrill & Bush, 1897	(Dall, 1890)
				Portlandia	***Portlandia arctica***
				Mörch, 1857	(Gray, 1824)
				Scissileda	***Scissileda parceplicata***
				Kiburn, 1994	(Barnard, 1964)
				Yoldia	***Yoldia hyperborea***
				Mörch, 1842	Torrell, 1859
				Yoldiella	***Yoldiella lucida***
				Verrill & Bush, 1897	(Lovén, 1846)

conformation, shell microstructure, larval development, foot morphology, respiratory pigments, trophic mode, and digestion (Zardus, 2002). Nuculoidea and Nuculanoidea share taxodont teeth but generally differ in the following aspects of shell morphology (Coan et al., 2000): short posterior end in Nuculanoidea and usually elongate posterior end in Nuculanoidea. Pallial sinuses indicating the existence of siphons are absent in

Nuculoidea and present in several families in Nuculanoidea. Manzanelloidea and Solemyoidea are characterized by unique feeding habitat and chemosynthetic system (e.g. Stewart & Cavanaugh, 2006; Oliver & Taylor, 2012) but differ in the presence or absence of hinge teeth. Manzanelloidea have few vertical teeth, but Solemyoidea is edentate.

Each superfamily of Protobranchia is diagnosed by morphological characteristics. However, these characteristics are not always obvious, because their shell morphology is generally simple. The current classification of protobranchs is summarized below.

1-2-2. Higher classification of protobranchs

Allen (1985) described the shell morphology of protobranchs as "never extravagant". Indeed the taxonomy of protobranchs has long been problematic.

The current classification of bivalves above a family level was summarized in two recent papers, Bouchet et al. (2010) and Carter et al. (2011). Multiple sources of phylogenetic inference, including molecular, soft anatomical, shell morphological, shell microstructural, bio- and paleobiogeographic characteristics, were integrated into the classification in these papers. According to the scheme in Carter et al. (2011), protobranchs are relegated to a subclass rank, and the Subclass Protobranchia consist of two superorders, Nuculiformii and Nuculaniformii. The Superorder Nuculiformii is classified into two orders, Nuculida and Solemyida, while extinct order Afghanodesmatida and extant order Nuculanida are united as the superorder Nuculaniformii. Bouchet et al. (2010) divided protobranchs into three orders: Nuculida,

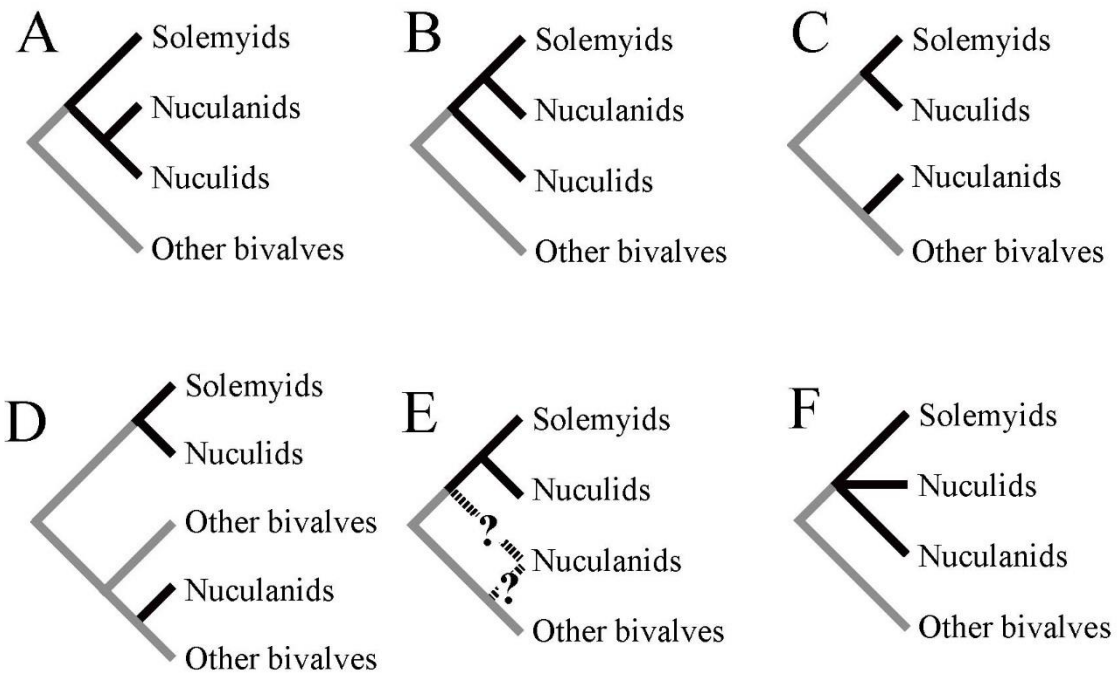

Figure 1.1. Phylogenetic hypothesis of protobranchs bivalves and other bivalve taxa. **A.** Cryptodonta and Paleotaxodonta hypothesis. Genetic relationship supported by Purchon (1987) based on morphological data, parsimony analyses of morphological data of Salvini-Plawen & Steiner (1996), evolutionary tree in Cope (1997),(Carter et al. 2011) Smith et al. (2011) based on phylogenomic analysis (transcriptome date containing up to 216402 sites and 1185 gene regions) and Sharma et al. (2012) based on four molecular markers (Myosin heavy chain, ATP synthase subunit B, Elongation factor-1α and RNA polymerase II). **B.** The proposed evolutional elationship of Morton (1996). Waller (1990, 1998) based on non-numerical cladistics analyses of morphology. **C.** Opponobranchia formed paraphyletic group of bivalves by Giribet &Wheeler (2002) analysis based on three molecular markers (18S rRNA, 28S rRNA and COI) and morphology. **D.** Giribet & Distel (2003) proposed monophyly of opponobranchia whereas nuculanides are the sister group of heterodont biralves by the parsimony analysis of molecular data (18S rRNA, 28S rRNA, COI and histone H3). Three studies situated nuculanids as a sister group of pteriomorph bivalves (Plazzi & Passamonti (2010) based on Bayesian analysis of four molecular markers (12 rRNA, 16S rRNA, COI and CytB), Wilson et al. (2010) based on Bayesian analysis of five molecular markers (16S rRNA, 18S rRNA, 28S rRNA, COI and histone H3) and Plazzi et al. (2011) based on Bayesian analysis of four molecular markers (12 rRNA, 16S rRNA, COI and CytB)). **E.** Opponobranchia hypothesis suggested by Giribet (2008). Giribet (2008) didn't resolved the monophyly of protobranchs but Carter et al. (2011)suggested it. **F.** Synoptic classification of Bouchet et al. (2010).

Solemyida and Nuculanoida. Although these two studies used the same phylogenetic information, these two schemes of classification are quite different. However, they both recognize three major taxa in protobranchs: that is, Nuculids, Solemyids and Nuculanids. These taxa have long been united as protobranchs (e.g. Cox et al., 1969), although there are various hypotheses on phylogenetic relationships among these three groups (Figure 1.1. Purchon, 1987; Waller, 1990; Waller, 1998; Morton, 1996; Salvini-Plawen &Steiner, 1996; Cope, 1997; Giribet & Wheeler., 2002; Giribet & Distel, 2003; Giribet, 2008; Bouchet et al., 2010; Plazzi & Passamonti, 2010; Wilson et al., 2010; Carter et al., 2011; Plazzi et al., 2011; Smith et al., 2011; Sharma et al., 2012; Sharma et al., 2013; Bieler et al., 2014). The principal hypotheses of protobranch phylogeny supported by morphological characteristics are summarized as follows. **1)** Cryptodonta (mostly equivalent to Lipodonta proposed by Cope (1996): Solemyids + Paleotaxodonta (Nuculids + Nuculanids; Newell, 1965). **2)** Opponobranchia: (Solemyids + Nuculids) + Nuculanids. The former is based on hinge tooth morphology used in the traditional taxonomy of protobranchs, and the criterion for the latter is the arrangement of gill filaments. Solemyids and Nuculids have the opposite arrangement of gill filaments along the gill axis (Waller, 1998), which was shown to result in a unique pattern of ciliary mechanism described by Atkins (1937); Giribet (2008) named this clade (Solemyids + Nuculids) Opponobrancia. Morphological data have supported cryptodont and paleotaxodont concepts in many cases (Figure 1.1A: Purchon, 1987; Salvini-Plawen & Steiner, 1996; Cope, 1997). On the other hand, early studies using molecular data suggested non-monophyly of protobranchia (Figure 1.1C: Giribet & Wheeler, 2002; Figure 1.1D: Giribet & Distel, 2003; Plazzi & Passamonti, 2010; Wilson et al., 2010; Plazzi et al., 2011). Recent molecular studies using multiple genes (Smith et al., 2011;

Sharma et al., 2012; Sharma et al., 2013) support the monophyly of protobranchs and the division into Criptodonta and Paleotaxodonta (Figure 1.1A). This classification seems to be feasible in spite of several different hypotheses by recent studies. Carter et al. (2011) suggested the monophyly of Protobranchs and Opponobranchia. Bieler et al. (2014) reconstructed the phylogenetic relationships of Bivalvia with nine genes (18S rRNA, 28S rRNA, 16S rRNA, histone H3, COI, and four nuclear protein-encoding genes, Myosin heavy chain, ATP synthase subunit B, Elongation factor-1α, and RNA polymerase II provided by Sharma et al., 2012) and 13 morphological data. Several phylogenetic trees with different topology were obtained in Bieler et al. (2014), but all of them support the monophyly of protobranchs.

Below the order rank, classification of protobranchs is more problematic. Table 1.2 shows the current classification of protobranchs following Bouchet et al. (2010), Huber (2010), Coan & Valentich-Scott (2012) and the World Register of Marine Species (WoRMS, http://www.marinespecies.org/index.php). These above-mentioned papers have a consensus on the monophyly of protobranchs; however, classification among Protobranchia remains controversial. Indeed the classification by Carter et al. (2011) is entirely different from that of Bouchet et al. (2010). For instance, the classification among nuculanids differs widely. Superfamily and order-level classification is also mentioned below.

One of the most doubtful grouping occurs in the family Sareptidae. This family contains the genera *Sarepta*, *Setigloma* and *Pristigloma* and belongs to the order Nuculoida according to the classification in the above-mentioned papers, but Carter et al. (2011) separately classifies *Sarepta* and *Setigloma* into the family Sareptidae (Nuculanida) and *Pristigloma* into the family Pristiglomidae (Nuculida). In the original

descriptions, the genera *Pristigloma* and *Sarepta* were placed in Nuculanidae in the superfamily Nuculanoidea (nuculanids) (*Pristigloma* by Dall, 1900; *Sarepta* by Adams, 1860). Sanders & Allen (1973) classified the genus *Pristigloma*, together with the new genus *Microgloma*, in the superfamily Nuculoidea (nuculids). They considered these genera as Nuculoidea because of the characteristics such as: an anterior rather than posterior inhalant current; lack of mantle fusion; siphons absent; palp large, broad, deep and almost square rather than elongate. However, Ockelmann & Warén (1998) classified *Microgloma* in the family Yoldiidae because of the difference in the hinge ontogeny compared to other nuculids. *Microgloma* have a long slender ligament similar to Nuculanids. In particular, *Yoldiella* resembles *Microgloma* in the shell morphology in young specimens and the sculpture of the prodissoconch. This placement has been accepted in the recent classification, but remains controversial (Huber, 2010). Characteristics such as reproduction mode, monoecious and brooding are unique to *Yoldiella* and doubtfully to *Microgloma*. Ockelmann & Warén (1998) also mentioned the similarity between *Setigloma* and *Sarepta* in contrast to Schileyko (1983) who considered *Setigloma* and *Pristigloma* as related. Thus, the family Sareptidae has been used for three genera, *Sarepta*, *Setigloma* and *Pristigloma*. Moreover, Coan et al. (2000) assigned *Pseudoglomus*, which was originally classified in the Nuculanidae, to the 'Pristiglomidae'. This classification is currently rejected based on Ockelmann & Warén (1998), because *Pseudoglomus* does not have a resilifer and *Pseudoglomus* is now considered to belong to the family Malletiidae. However this grouping is still questionable, because *Pseudoglomus fragilis* has a resilifer, and the anatomy of *Pseudoglomus* is unknown (Huber, 2010). These complicated situations in the classification of Sareptidae bring to light the problems involved in the protobranchs classification: the classification of

protobranchs even above a superfamily rank can possibly be modified further. It is not always true that all species belonging to the same groups definitely have similar characteristics. For example, the recent molecular phylogenetic analysis by Sharma et al. (2013) indicates the movement of Sareptidae from the superfamily Nuculoidea to Nuculanoidea. However, there still remains the possibility that some sareptids are close to Nuculoidea and not to Nuculanoidea.

The second example is the family Manzanellidae. Cox et al. (1969) allocated them to the subclass Pteriomorphia and not to Protobranchia, based only on the shell characteristics. In contrast, Allen & Sanders (1969) referred to their similarities to solemyids in anatomical features, including gill morphology, pedal morphology and the presence of small palps. This interpretation has widely been accepted (e.g. Pojeta, 1988; Bieler & Mikkelsen, 2006) and also corroborated recently (Oliver & Taylor, 2012). Molecular phylogenetic analysis focusing on protobranchs using five genes (Sharma et al. 2013) showed non-monophyly of the superfamily Solemyoidea, but did not emphasize the resulting topology, because the likelihood-based tests of topology did not deny the monophyly of Solemyoidea. Bieler et al. (2014) showed the monophyly of the order Solemyoida by molecular analysis, using nine genes, and again the bootstrap support value is not significant. In the case of Manzenellids the conflict exists between the interpretations of shell morphology and anatomical characteristics. As described before, the anatomy of this superfamily indicates its closeness to solemyids, though the shell morphology of Manzanellids is nuculoidean-like in shape (Cox et al., 1969).

1-3. Objectives of this study

The purpose of this study is to understand the shell microstructural evolution of protobranchs and reveal the relationship between shell microstructural evolution and adaptive radiation of protobranchs.

Protobranchs are suitable materials to understand the overall evolutional history of the shell microstructure of bivalves, Protobranchs are considered as the primitive taxa of bivalves, and it is desirable to focus on basal taxa to characterize the shell microstructure. On the other hand, classification of protobranchs is somewhat problematic as mentioned above. Thus, to review the classification of protobranchs is also the purpose of this study. Therefore I focused on Recent protobranchs by extracting the data for shell microstructure and molecular phylogeny from the same specimens. For the shell microstructure description, I performed observations with SEM and analyzed crystallographic textures of shell microstructures to characterize the microstructural morphology in detail.

Chapter 2

A molecular phylogenetic analysis of protobranch bivalves

2-1. Introduction

As mentioned in Chapter 1, the classification of protobranchs needs considerable revision, in part due to their ecology. Protobranchs are primarily associated with the deep sea (Allen, 1978) and generally utilize an infaunal habitat (Stanley, 1970). These specialized habitats make the taxon sampling difficult, hindering the collection of live materials to describe soft-part characteristics and perform molecular analyses. The simplicity of shell form in protobranchs can cause an underestimation of their anatomical and phylogenetic complexity. For instance, the inner and outer gill lamellae arrange in an opposed format in the Nuculidae and Solemyoida, but the gill lamellae of Nuculanoidea show an alternate arrangement (Ridewood, 1903; Yonge, 1939; Allen & Sanders, 1969; Sanders& Allen, 1973; Allen & Hannah, 1986). The Solemyoida possesses chemoautotrophic bacteria within their gills (Fisher, 1990; Distel, 1998; Fujiwara, 2003; Stewart & Cavanaugh, 2006; Oliver & Taylor, 2012), while other protobranchs are generally deposit feeders (Zardus 2002). Recent molecular studies indicate significant genetic divergence within putative morphological species. Neulinger et al. (2006) found two distinct genetic variations among *Acharax* cf. *johnsoni* whose classification was supported by experts on bivalve taxonomy from multiple localities. Genetic variations of protobranchs that occur along a depth gradient in the same locality

have been well studied using gene markers (Chase et al., 1998; Etter et al., 1999, 2005; Glazier & Etter, 2014). Glazier & Etter (2014) indicated that *Neilonella salicensis* in the western North Atlantic has a sharp genetic break between the populations that reside above 2800 m and below 3200 m. Etter et al. (2005) found remarkable diversity in each of four protobranch species (*Nucula similis*, *Nucula atacellana*, *Clencharia abyssorum* and *Ledella ultima*) and Zardus et al. (2006) showed that genetic divergence among populations in *Nucula atacellana* is much greater at different depths within the same basin (the North American, West European and Argentine basins) than at similar depths and thousands of kilometres apart. These studies suggest that protobranch bivalves include many cryptic species. Besides, molecular phylogenetic analysis of protobranch bivalves by Sharma et al. (2013) showed considerable non-monophyletic relationships within and among genera. These previous studies strongly suggest that species distinction in protobranch bivalves based on shell morphology alone causes an underestimation of true species diversity.

To reveal the protobranch phylogenetic relationship and evolutional history, molecular phylogenetic analysis was performed in protobranch bivalves from Japanese water. Data on shell microstructure, crystallographic characteristics, and DNA sequences were obtained from each specimen to enhance the reliability of taxonomic identification.

2-2. Materials and methods

2-2-1. Materials

All specimens in this study were collected from Japanese waters. In addition, various specimens were provided by other researchers. The following three specimens were obtained from the subtidal zone obtained by Dr. Seike while scuba diving. *Acila insignis* and *Yoldia notabilis* were from Otsuchi Bay, Iwate Prefecture and two *Solemya pusilla* specimens were from Kurihama Bay, Kanagawa prefecture. They were collected alive at ca. 5 to 15.2 m depth and preserved in 99% ethanol. Another *Solemya pusilla* specimen was collected alive off Johgashima Island at 135–150 m depth by dredging. The soft part of this specimen was not preserved. Specimens of five species, *Acharax johnsoni*, *A. japonica*, *Solemya tagiri*, *S. flava* and tindarids were obtained from the collections of the Japan Agency for Marine-Earth Science and Technology (JAMSTEC. *Acharax johnsoni* specimens were collected as dead shells at two different sites. One was collected at Hiroo Canyon, where Fujikura et al. (2008) reported chemosynthetic communities, at 1246 m depth during dive #351 of the remotely operated vehicle (ROV) Hyper-Dolphin (42°10.7′N, 144°10.5′E). The other was collected from a methane seep site at Sagami Bay (Okutani & Egawa, 1985; Fujikura *et al*., 2008) at 1174 m depth off Hatsushima Island (35°00.0′N, 139°13.5′E) during dive #917 of the submersible Shinkai 6500. Both specimens were dead shells. *Solemya tagiri* specimens were collected alive from a methane seep site (Hashimoto *et al*., 1993; Yamanaka *et al*., 1999) in Kagoshima Bay, south Japan at 104 m depth by the ROV Dolphin-3K (31°39.565′N, 130°48.199′E). These were fixed by 10% formalin and later preserved in 99% ethanol. For this reason, DNA analysis was less than successful in this species. *Solemya flava* specimens were obtained from a hydrothermal vent site in Iheya Ridge, situated in the mid-Okinawa Trough, south Japan (Ohta & Kim, 2001) during dive #1246 of the Hyper-Dolphin. These specimens were preserved during the cruise at -30 °C in light-shielded conditions and fixed in 99%

ethanol in the laboratory. This species was described as a new species by Sato et al. (2013b). A tindarid? specimen was collected alive from a hydrothermal vent site in Izena Hole, which is also situated in the mid-Okinawa trough, south Japan (Fujikura et al., 2008), and preserved in 99% ethanol. *Solemya pervernicosa* specimens were collected alive from a cold-water methane seep site in the Sea of Japan off Joetsu at depths of around 1000 m (Matsumoto *et al*., 2005). Both specimens of *S. pervernicosa* were preserved at -30 °C. *Yoldia seminude* specimens were from 94–95 m depth off the Nemuro peninsula, north Japan. *Bathyspinula oceanica* and *Setigloma japonica* specimens were obtained from the hadal zone (5179–5223 m depth) off Kamchatka during the research cruise KH14-2 of Hakuho-maru, the research vessel of JAMSTEC. These specimens were stored in 99% ethanol after being boiled alive at 80–99 °C within 1 min in order to deactivate DNase (Ueshima, 2002).

Other specimens were collected during the author's field work. *Acharax japonica* specimens were collected alive from sinks (1.1 m × 4.2 m × 0.5 m high) at the Shimoda Marine Research Center, University of Tsukuba (34°40′N, 138°56′E), by using a stainless steel sieve with 1 mm mesh. This site is an unusual habitat for this species (Yamanaka *et al*., 2008). The following six species were collected from an area off Misaki, Kanagawa prefecture at 95.0 to 345 m depth by dredging performed by the Rinkai-maru which is a survey ship at the Misaki Marine Biological Station, University of Tokyo: *Acila minutoides, Sarepta speciosa*, *Huxleyia sulcata*, *Nuculana yokoyamai*, *Nuculana gordonis* and *Megayoldia lischkei* specimens were collected alive and Ennucula sp. 2 were collected as dead shells. The former specimens were stored in 99% ethanol after being boiled alive in at 80–99 °C within 1 min. The following seven species, *Acila mirabilis, Ennucula nipponica*, *Nucula tokyoensis*, *Nuculana tanseimaruae*, *Malletia*

Table 2.1. The list of specimen used in this study. Analyses for which each specimen used is also indicated.

Classification	Species	Latitude	Longitude	Depth (m)	Locality/ Voucher	Date	Condition	DNA	SEM	XRD
Superfamily Nuculoidea										
Nuculidae	*Acila mirabiris*	33° 34.6' N	135° 00.0' E	556.53	Off-Wakayama/ KT11-14	2011/6/5	with soft part	○	○	
	Acila minutoides	-	-	-	Off Misaki	2011/7/25	with soft part	○	○	
	Acila insignis	39° 20.28' N	141° 54.56' E	15.2	Otsuchi Bay	2010/9/7	with soft part	○	○	○
	Brevinucula sp.	28° 32.27' N - 28° 34.15' N	127° 02.28' E - 127° 02.53' E	606-610	Off Amami-Ohshima/ C365	2012/11/16	with soft part	○	○	
	Ennucula nipponica	33° 34.6' N	135° 00.0' E	556.53	Off-Wakayama/ KT11-14	2011/6/5	with soft part	○	○	
	Ennucula nipponica	28° 33.89' N - 28° 32.96' N	127° 02.62' E - 127° 02.20' E	610-611	Off Amami-Ohshima/ C365	2012/11/16	with soft part			○
	Ennucula siberutensis	32° 22.15' N - 32° 23.35' N	129° 02.41' E - 129° 03.05' E	304-310	Kasayama Bank/ C365	2012/11/19	with soft part	○	○	
	Ennucula tenuis	32° 09.07' N - 32° 09.02' N	128° 59.03' E - 129° 00.45' E	508-514	Okikasayama Bank/ C365	2012/11/19	with soft part	○		
	Ennucula tenuis	28° 32.27' N - 28° 34.15' N	127° 02.28' E - 127° 02.53' E	606-610	Off Amami-Ohshima/ C365	2012/11/16	with soft part	○	○	
	Ennucula sp.1	28° 33.89' N - 28° 32.96' N	127° 02.62' E - 127° 02.20' E	610-611	Off Amami-Ohshima/ C365	2012/11/16	with soft part	○	○	
	Ennucula sp.2	-	-	-	Off Misaki	2011/10/27	Dead shell		○	
	Nucula tokyoensis	33° 31.8' N	134° 59.3' E	998.92	Off-Wakayama/ KT11-14	2011/6/5	with soft part		○	
	Nucula tokyoensis	33° 31.8' N	134° 59.3' E	998.92	Off-Wakayama/ KT11-14	2011/6/5	with soft part			○
	Nucula tokyoensis	32° 22.15' N - 32° 23.35' N	129° 02.41' E - 129° 03.05' E	304-310	Okikasayama Bank/ C365	2012/11/19	with soft part	○	○	
	Nucula toressi	32° 09.07' N - 32° 09.02' N	128° 59.03' E - 129° 00.45' E	508-514	Okikasayama Bank/ C365	2012/11/19	with soft part	○	○	
Sareptidae	*Sarepta speciosa*	35° 07.90' N - 35° 08.09' N	139° 34.11' E - 139° 33.86' E	95.0-96.2	Off Misaki	2012/4/25	with soft part	○	○	
	Sarepta speciosa	35° 07.82' N - 35° 07.64' N	139° 34.34' E - 139° 34.22' E	96-98.7	Off Misaki	2013/2/14	with soft part	○		
	Setigloma japonica	47° 00.22' N - 47° 00.91' N	160° 02.62' E - 160° 01.29' E	5179-5223	Off Kamchatka/ KH-14-2	2014/5/27	with soft part	○		
Superfamily Manzanelloide										
Manzanellidae	*Huxleyia sulcata*	35° 07.19' N - 35° 06.86' N	139° 34.10' E - 139° 33.75' E	210-345	Off Misaki	2012/3/14	with soft part	○	○	
	Huxleyia sulcata	35° 07.19' N - 35° 06.86' N	139° 34.10' E - 139° 33.75' E	210-345	Off Misaki	2012/3/14	Dead shell			○
Superfamily Solemyoidae										
Solemyidae	*Acharax japonica*	34° 40.04' N	138° 56.08' E	0.5 (Depth of sink)	Shimoda Marine Resarch Center	2009/8/6	with soft part	○		
	Acharax japonica	34° 40.04' N	138° 56.08' E	0.5 (Depth of sink)	Shimoda Marine Resarch Center	2009/8/6	with soft part	○		
	Acharax japonica	34° 40.04' N	138° 56.08' E	0.5 (Depth of sink)	Shimoda Marine Resarch Center	2009/8/6	with soft part			○
	Acharax japonica	34° 40.04' N	138° 56.08' E	0.5 (Depth of sink)	Shimoda Marine Resarch Center	2009/8/6	Dead shell		○	
	Acharax johnsoni	35° 00.072' N	138° 13.470' E	1166	Off Hatsushima	2011/6/25	with soft part	○	○	
	Acharax johnsoni	42° 10.70' N	144° 10.50' E	1246	Hiroo Canyon	2004/10/5	Dead shell		○	
	Acharax johnsoni	35° 00.00' N	139° 13.50' E	1174	Off Hatsushima	2005/12/11	Dead shell		○	
	Acharax johnsoni	28° 33.89' N - 28° 32.96' N	127° 02.62' E - 127° 02.20' E	610-611	Off Amami-Ohshima/ C365	2012/11/16	Dead shell			○
	Solemya perernicosa	-	-	ca. 1000	Joetsu Knoll	-	with soft part	○		
	Solemya tagiri	31° 39.57' N	130° 48.20' E	104	Kagoshima Bay	-	with soft part			
	Solemya flava	27° 32.99' N	126° 58.23' E	1402	Iheya Ridgle/ HPD #1246	2011/2/9	with soft part	○	○	
	Solemya flava	27° 32.99' N	126° 58.23' E	1402	Iheya Ridgle/ HPD #1246	2011/2/9	with soft part	○	○	
	Solemya pusilla	ca. 35° 13.50' N	ca. 139° 42.9' E	ca. 5	Kurihama	2011/6/1	Dead shell	○		
	Solemya pusilla	ca. 35° 13'30" N	ca. 139° 42.9' E	ca. 5	Kurihama	2011/6/1	with soft part	○		
	Solemya pusilla	ca. 35° 13'30" N	ca. 139° 42.9' E	ca. 5	Kurihama	2011/6/1	with soft part			○
	Solemya pusilla	-	-	135-150	Off Johgashima Island	-	Dead shell		○	
Superfamily Nuculanoidae										
Nuculanidae	*Nuculana soyoae*	35° 07.21' N	139° 33.93' E	250	Off Misaki	2011/10/24	with soft part	○	○	
	Nuculana tanseimaruae	33° 34.6' N	135° 00.0' E	556.53	Off-Wakayama/ KT11-14	2011/6/5	with soft part	○		
	Nuculana tanseimaruae	33° 34.6' N	135° 00.0' E	556.53	Off-Wakayama/ KT11-14	2011/6/5	with soft part			○
	Nuculana tanseimaruae	32° 09.07' N - 32° 09.02' N	128° 59.03' E - 129° 00.45' E	508-514	Okikasayama Bank/ C365	2012/11/19	with soft part	○		
	Nuculana tanseimaruae	32° 09.07' N - 32° 09.02' N	128° 59.03' E - 129° 00.45' E	508-514	Okikasayama Bank/ C365	2012/11/19	with soft part			○
	Nuculana leonina	32° 22.15' N - 32° 23.35' N	129° 02.42' E - 129° 03.05' E	304-310	Kasayama Bank/ C365	2012/11/19	with soft part	○	○	
	Nuculana yokoyamai	35° 07.73' N - 35° 07.68' N	139° 34.13' E - 139° 33.83' E	-	Off Misaki	2012/3/14	with soft part	○	○	
	Nuculana gordonis	-	-	-	Off Misaki	2011/7/25	with soft part	○	○	
	Nuculana gordonis	35° 10.31' N - 35° 10.24' N	139° 34.81' E - 139° 34.74' E	85.5-87.7	Off Misaki	2011/10/27	Dead shell			○

Table 2.1. Continued.

Classification	Species	Latitude	Longitude	Depth (m)	Locality/ Voucher	Date	Condition	DNA	SEM	XRD
Bathyspinulidae	*Bathyspinula oceanica*	47˚00.22' N - 47˚00.91' N	160˚02.62' E - 160˚01.29' E	5179-5223	Off Kamchatka/ KH-14-2		with soft part	○	○	
Malletiidae	*Malletia takaii*	33˚31.8' N	134˚59.3' E	998.92	Off-Wakayama/ KT11-14	2011/6/5	Dead shell		○	
	Malletia takaii	38˚29.83' N - 38˚29.77' N	143˚06.98' E - 143˚04.66' E	2307	Off Onagawa/ KT14-5	2014/4/26	with soft part			○
	Malletia humilior	28˚33.89' N - 28˚32.96' N	127˚02.62' E - 127˚02.20' E	610-611	Off Amami-Ohshima/ C365	2012/11/16	with soft part	○	○	
Neilonellidae	*Neilonella soyoae*	33˚34.6' N	135˚00.0' E	556.53	Off-Wakayama/ KT11-14	2011/6/5	with soft part	○	○	
	Neilonella dubia	33˚34.6' N	135˚00.0' E	556.53	Off-Wakayama/ KT11-14	2011/6/5	with soft part	○	○	
	Neilonella dubia	32˚09.07' N - 32˚09.02' N	128˚59.03' E - 129˚00.45' E	508-514	Okikasayama Bank/ C365	2012/11/19	with soft part	○		
	Neilonella dubia	28˚32.27' N - 28˚34.15' N	127˚02.28' E - 127˚02.53' E	606-610	Off Amami-Ohshima/ C365	2012/11/16	with soft part	○	○	
	Neilonella dubia	28˚32.94' N - 28˚33.78' N	127˚02.41' E - 127˚02.78' E	647-637	Off Amami-Ohshima/ C365	2012/11/16	with soft part	○		
	Neilonella kirai	32˚16.98' N - 32˚17.23' N	129˚02.99' E - 129˚04.67' E	384-378	West Sanpo Sone/ C365	2012/11/19	with soft part	○	○	
Tindariidae	*Tindaria soyoae*	28˚32.27' N - 28˚34.15' N	127˚02.28' E - 127˚02.53' E	606-610	Off Amami-Ohshima/ C365	2012/11/16	with soft part	○	○	
	Tindaria soyoae	28˚32.27' N - 28˚34.15' N	127˚02.28' E - 127˚02.53' E	606-610	Off Amami-Ohshima/ C365	2012/11/16	with soft part			○
	Tindaria?	27˚14.815' N	127˚04.089' E	1617	NT11-20/ HPD #1329	2011/10/5	with soft part	○		
Yoldiidae	*Megayoldia lischkei*	35˚07.73' N - 35˚07.68' N	139˚34.13' E - 139˚33.83' E	-	Off Misaki	2012/3/14	with soft part	○	○	
	Megayoldia japonica	32˚16.98' N - 32˚17.23' N	129˚02.99' E - 129˚04.67' E	384-378	West Sanpo Sone/ C365	2012/11/19	with soft part	○	○	
	Yoldia johanni	43˚06.68' N - 43˚06.61' N	145˚45.67' E - 145˚45.40' E	94-95	Off Nemuro peninsula	2011/4/26	with soft part	○	○	
	Yoldia johanni	43˚06.68' N - 43˚06.61' N	145˚45.67' E - 145˚45.40' E	94-95	Off Nemuro peninsula	2011/4/26	with soft part			○
	Yoldia notabilis	39˚20.22' N	141˚54.21' E	10	Otsuchi Bay	2010/9/7	with soft part	○	○	
	Yoldia notabilis	39˚20.22' N	141˚54.21' E	10	Otsuchi Bay	2010/9/7	with soft part			○

takaii, *Neilonella soyoae* and *Neilonella dubia*, were collected by beam trawling from several points off Wakayama, mid Japan during a deep-sea survey by the KT11-14 cruise by Tanseimaru, JAMSTEC's research vessel. Except *Malletia takaii*, all these specimens were collected alive and stored in 99% ethanol after being boiled alive at 80–99 °C within a minute. During the 365 cruise of Nagasaki-maru, Nagasaki University's fisheries training boat, *Brevinucula* sp., *Ennucula teramachii*, *Ennucula tenuis*, *Ennucula* sp1., *Nucula toressi*, *Nuculana tanseimaruae*, *Nuculana sagamiensis*, *Malletia humilior*, *Neilonella dubia*, *Tindaria soyoae* and *Megayoldia japonica* were collected from several points, including a hydrothermal vent site (Hashimoto et al., 1995) called "Off Amami-Ohshima" in the East China sea by beam trawling. All specimens and their usages were listed in Table 2.1.

Comprehensive sequence data of protobranchs were previously reported by Sharma et al. (2013). They decoded the sequences of 74 protobranch species from five molecular loci (16S rRNA, 18S rRNA, 28S rRNA, cytochrome c oxidase subunit 1 [COI] and histone H3). In this study, we obtained an additional 33 species from 9 family groups of protobranchs for molecular analysis (Table 2.2). These sequenced specimens consisted of 5 species in Solemyidae, 1 in Manzanelloidae, 16 in Nuculanoidea and 11 in Nuculoidea. Among the sequences we obtained, the *Acila mirabilis* sequence already exists in GenBank. However this data is also novel because all sequenced specimens were obtained from different localities. Monophyly of protobranchs has already been demonstrated in previous studies with large-scale phylogenomic approaches (Smith et al., 2011; Sharma et al., 2012; Bieler et al., 2014). Sharma et al. (2012) suggested that the four nuclear protein-encoding genes (ATP synthase β, elongation factor-1α, myosin heavy chain type II and RNA polymerase II) employed the robust assessment of phylogenetic relationship of various depths. Thus, four nuclear protein-encoding genes were added to the above-mentioned five genes, following the method used of Sharma et al. (2012) and Bieler et al. (2014). The data collected in previous studies (e.g., Giribet & Wheeler, 2002; Taylor et al., 2008; Giribet et al., 2006) were additionally accessed from GenBank.

Specimens of the same species and locality were used in this study for shell microstructural observation, crystallographic texture analysis and molecular analysis. The voucher materials were preserved for further taxonomic studies.

In order to confirm the monophyly of protobranchs, ten bivalves covering the whole taxon (Pteriomorphia, Paleoheterodonta, Archiheterodonta, Anomalodesmata and Inaequidonta) and three gastropod sequences from GenBank including nine genes (16S rRNA, 18S rRNA, 28S rRNA, cytochrome c oxidase subunit 1 [COI], histone H3, ATP

synthase β, elongation factor-1α, myosin heavy chain type II and RNA polymerase II) were used. A full list of specimens included in this study is shown in Tables 2.2 and 2.3.

Table 2.2. List of species, genes and their accession numbers used in molecular phylogenetic analyses. Newly acquired data were highlighted in gray with the length of the decoded sequences. The classification of superfamily was based on Bouchet et al (2010).

Classification	Species	18S rRNA	28S rRNA	16S rRNA	histone H3	COI
Superfamily Nuculoidea						
Nuculidae	*Nucula tokyoensis*	1366	1089	485	249	613
	Nucula torresi	1040	1281	481	359	609
	Nucula sulcata	DQ279937	KC984827	-	-	KF369159
	Nucula sulcata	KC984713	KC984816	KC984679	KC984776	KF369158
	Nucula sulcata	KC984725	KC984815	-	KC984777	KC984746
	Nucula sulcata	AF207642	DQ279960	DQ280029	DQ280001	DQ280017
	Nucula sulcata	AF120525	AF120582	-	AY070147	-
	Nucula sulcata	-	AF207649	-	-	-
	Nucula nuculeus	EF105223	-	GQ166568	-	-
	Nucula nuculeus	EF105222	-	-	-	-
	Nucula nuculeus	EF105221	-	-	-	-
	Nucula nuculeus	EF105220	-	-	-	-
	Nucula nuculeus	EF105219	-	-	-	-
	Nucula nuculeus	EF105218	-	-	-	-
	Nucula nuculeus	EF105217	-	-	-	-
	Nucula nuculeus	EF105216	-	-	-	-
	Nucula atacellana	KC984723	KC984818	KC984676	-	KC984742
	Nucula atacellana	-	-	-	-	KF563182
	Nucula atacellana	-	-	-	-	KF563183
	Nucula profundorum	KC984720	KC984830	KC984677	-	KC984741
	Nucula proxima	AF120526	AF120583	AY377617	-	AF120641
	Nucula proxima	AF022477	-	-	-	-
	Nucula proxima	AF022476	-	-	-	-
	Nucula proxima	AH005593	-	-	-	-
	Nucula proxima	L78847	-	-	-	-
	Nucula atacellana	-	-	DQ269458	-	-
	Nucula atacellana	-	-	DQ269459	-	-
	Ennucla similis	-	-	AY762142	-	-
	Ennucla similis	-	-	AY762141	-	-
	Ennucula nipponica	1504	1400	504	320	631
	Ennnucula siberutensis	1298	1328	-	313	-
	Ennucula tenuis	1330	2127	459	350	-
	Ennucula tenuis	1209	1364	487	149	662
	Ennucula sp. 1	1237	1239	475	318	-
	Ennucula cumingii	KC984724	KC984813	KC984683	KC984752	KC984750
	Ennucula granulosa	KC984721	KC984817	KC984678	KC984774	KC984749
	Ennucula cardara	KC984716	KC984829	KC984681	KC984751	KC984748
	Ennucula tenuis	KC984684	KC984826	KC984682	KC984775	KC984747
	Ennucula tenuis	-	-	-	-	EF528308
	Ennucula decipiens	-	-	JF496759	-	-
	Brevinucula sp	1139	1470	305	243	-
	Brevinucula verrillii	KC984722	KC984814	KC984680	KC984782	-
	Acila minutoides	1500	1495	519	333	522
	Acila insignis	-	-	-	-	526
	Acila mirabilis	1402	1503	475	319	636
	Acila divaricata	-	-	-	-	KC120813
	Acila divaricata	-	-	-	-	KC120812
	Acila mirabilis	-	-	-	-	KC120808
	Acila mirabilis	-	-	-	-	KC120807
	Acila castrensis	KC429319	KC429408	KC429241	-	KC429087
	Acila castrensis	AF120527	AF120584	-	-	-

Table 2.2. Continued.

Classification	Species	18S rRNA	28S rRNA	16S rRNA	histone H3	COI
Sareptidae	*Sarepta speciosa*	1596	1509	492	237	491
	Sarepta speciosa	1616	1532	421	264	-
	Setigloma japonica	1605	1464	321	356	578
	Pristigloma nitens	KC984708	KC984833	KC984670	KC984786	-
	Pristigloma sp.	KC984709	KC984835	-	KC984791	-
	Pristigloma alba	KC984704	KC984834	-	KC984784	-
Superfamily Manzenelloidea						
Manzanellidae	*Nucinella* sp.	KC429324	KC429414	-	KC429158	KC429089
	Huxleyia sulcata	1499	1330		202	533
	Huxleyia munita	KC429323	KC429413	-	KC429157	-
	Huxleyia munita	-	KC429412	-	-	-
Superfamily Solemyoidea						
Solemyidae	*Solemya pervernicosa*	1599	1482	506	330	294
	Solemya pusilla	1160	1446	476	346	500
	Solemya pusilla	1408	1414	505	-	610
	Solemya flava	1439	1427	458	365	625
	Solemya flava	1422	1147	-	270	622
	Solemya velesiana	KC984717	KC984794	KC984674	KC984780	KC984744
	Solemya velesiana	AM293669	AM293668	-	-	-
	Solemya elarraichensis	KC984719	KC984795	KC984673	KC984779	KC984743
	Solemya sp.	FR715296	FR715297	-	-	FR715326
	Solemya velum	KC984718	KC984796	KC984675	KC984778	KC984745
	Solemya velum	AF120524	KC429415	JQ728447	AY070146	U56852
	Solemya velum	AF022474	AF120581	KC429243	KC429159	GQ280820
	Solemya velum	AH005592	AY145421	DQ280028	-	GQ280819
	Solemya velum	AF022475	-	-	-	GQ280818
	Solemya velum	-	-	-	-	GQ280817
	Solemya velum	-	-	-	-	GQ280816
	Solemya velum	-	-	-	-	JN165237
	Solemya togata	AJ389658	AJ307552	-	-	-
	Solemya reidi	AF117737	-	-	-	-
	Solemya sp.	AM293672	AM293673	-	-	-
	Solemya sp.	AM293666	AM293667	-	-	-
	Solemya sp.	HG942544	-	HG942545	-	HG942539
	Solemya sp.	-	FR715297	-	-	-
	Acharax japonica	1533	1482	465	314	-
	Acharax japonica	-	1162	496	276	-
	Acharax johnsoni	1605	1597	451	293	-
	Acharax gadirae	KC984715	KC984793	KC984672	-	-
	Acharax barstchii	KC984714	KC984828	KC984671	KC984781	-
	Acharax sp.	AJ563763	-	-	-	-
	Acharax sp.	AJ563762	-	-	-	-
	Acharax sp.	AJ563761	-	-	-	-
	Acharax sp.	AJ563760	-	-	-	-
	Acharax sp.	AJ563759	-	-	-	-
	Acharax sp.	AJ563758	-	-	-	-
	Acharax sp.	AJ563757	-	-	-	-
	Acharax sp.	AJ563756	-	-	-	-
	Acharax sp.	AJ563755	-	-	-	-
	Acharax sp.	AJ563754	-	-	-	-
	Acharax sp.	AJ563753	-	-	-	-
	Acharax sp.	AJ563752	-	-	-	-
	Acharax sp.	AJ563751	-	-	-	-
	Acharax sp.	-	HE863781	-	-	-
Superfamily Nuculanoidea						
Nuculanidae	*Ledella ultima*	KC984685	KC984820	KC984667	KC984769	KC984740
	Ledella ultima	-	-	AY762136	-	-
	Ledella ultima	-	-	AY762135	-	-

Table 2.2. Continued.

Classification	Species	18S rRNA	28S rRNA	16S rRNA	histone H3	COI
Superfamily Nuculanoidea						
Nuculanidae	*Ledella ultima*	KC984700	KC984839	-	KC984770	KC984739
	Ledella pustulosa	KC984710	KC984804	KC993873	KC984771	-
	Ledella ecaudata	KC984701	KC984843	KC984666	KC984792	-
	Ledella sp.	KC984711	KC984805	-	KC984772	KC984738
	Nuculana tanseimaruae	1587	1039	-	-	162
	Nuculana tanseimaruae	1140	1461	-	353	571
	Nuculana soyoae	392	503	-	360	301
	Nuculana acinacea	1180	1109	-	363	568
	Nuculana pernula	KC984693	KC984801	-	KC984766	KC984737
	Nuculana pernula	AY145385	AY145419	-	-	EF528302
	Nuculana pernula	AF207644	AF207651	-	KC984764	-
	Nuculana minuta	DQ279938	DQ279961	DQ280030	DQ280002	DQ280018
	Nuculana minuta	AF120529	AF120586	KC984664	KC984765	AF120643
	Nuculana commutata	-	-	-	-	GQ166587
	Nuculana conceptionis	KC984688	KC984800	-	KC984763	-
	Nuculana caloundra	-	-	KC984660	-	-
	Nuculana pella	AJ389665	AJ307553	-	-	-
	Nuculana pella	AY070111	AY070124	-	AY070148	-
	Nuculana caloundra	KC429321	KC429410	KC429242	KC429155	-
	Nuculana caloundra	AM293663	AM293664	-	-	-
	Nuculana gordonis	1450	455	483	337	517
	Propeleda longicaudata	KC984692	KC984802	KC984665	KC984785	KC984736
	Propeleda carpenteri	KC984687	KC984799	-	KC984761	KC984735
	Jupiteria sp.	-	KC984825	-	KC993885	-
	Jupiteria sp.	-	KC984821	-	KC993886	-
	Jupiteria sp.	-	KC984824	-	KC993884	-
	Jupiteria sematensis	-	AB103131	-	-	-
	Adrana scaphoidea	KC984691	KC984819	-	KC984753	-
Bathyspinulidae	*Bathyspinula oceanica*	1088	1472	-	293	304
	Bathyspinula hilleri	KC984712	KC984806	KC993874	KC984773	KC984733
	Bathyspinula filatovae	KC993876	KC984841	KC993871	KC993889	-
	Bathyspinula calcar	KC993875	-	KC993870	-	-
	Tindariopsis agathida	KC993877	-	KC993869	-	-
	Tindariopsis sulcata	KC993878	-	KC993868	-	-
Malletiidae	*Malletia humilior*	1229	1431	-	292	608
	Malletia johnsoni	KC993879	KC984837	KC993872	KC993888	-
	Malletia abyssorum	-	-	AY762143	-	-
	Malletia abyssorum	-	-	AY762144	-	-
	Katadesmia cuneata	KC984697	KC984809	KC984669	KC984759	-
	Katadesmia cuneata	KC984698	KC984810	-	KC984758	-
	Clencharia abyssorum	KC429320	KC429409	-	KC429154	-
Neilonellidae	*Neilonella whoii*	KC984695	KC984822	KC984659	KC984756	KC984732
	Neilonella salicensis	KC993881	KC984838	-	KC993887	-
	Neilonella subovata	AF207645	AF207652	-	-	AF207656
	Neilonella kirai	1200	1018	-	346	559
	Neilonella soyoae	-	1070	-	324	-
	Neilonella dubia	-	440	-	243	-
	Neilonella dubia	1069	1328	-	324	540
	Neilonella dubia	1018	477	-	348	514
	Neilonella dubia	643	1283	-	328	496
Phaseolidae	*Lametila abyssorum*	KC984705	KC984798	KC984661	KC984783	-
Siliculidae	*Silicula* sp.	KC984703	KC984840	-	KC984762	KC984734
	Silicula sp.	KC984694	KC984803	-	KC984760	-
	Silicula rouchi	KC984686	KC984836	KC984663	KC984767	-
Tindariidae	*Tindaria soyoae*	1399	1418	515	221	585
	Tindaria ?	1549	1376	-	-	-
	Tindaria kennerlyi	KC984702	KC984812	-	KC984755	KC984731
	Tindaria sp.	KC993882	KC984823	-	-	-

Table 2.2. Continued.

Classification	Species	18S rRNA	28S rRNA	16S rRNA	histone H3	COI
Yoldiidae	*Megayoldia lischkei*	1505	1506	468	272	-
	Nuculana yokoyamai	979	1399	-	232	-
	Yoldia limatula	KC429322	KC429411	-	KC429156	KC429088
	Yoldia limatula	AF120528	AF120585	-	AY070149	AF120643
	Yoldia limatula	-	JF509735	-	AY377768	-
	Yoldia limatula	-	AY145424	-	-	-
	Yoldia eightsi	KC984696	KC984808	-	KC984754	KC984730
	Yoldia scissurata	KC984706	KC984797	-	KC984790	KC984729
	Yoldia myalis	AF207643	AF207650	-	-	AF207655
	Yoldia notabilis	1332	1483	-	278	624
	Yoldia johanni	1550	1698	487	65	223
	Megayoldia sp.	KC984699	KC984811	-	KC984757	-
	Megayoldia japonica	1024	1291	403	364	348
	Yoldiella nana	AJ389659	-	-	-	HQ919200
	Yoldiella orcia	KC984690	KC984832	-	KC984789	KC984728
	Yoldiella inconspicua	KC984689	KC984807	KC984668	KC984788	KC984727
	Yoldiella americana	KC984707	KC984842	KC984662	KC984787	KC984726
	Yoldiella valettei	KC993880	KC984831	-	KC993883	-
OUTGROUPS: Autobranchia						
Prteriomorphia	*Glycymeris glycymeria*	KC429328	KC429421	KC429246	KC429163	KC429093
	Pteria hirundo	KC429332	KC429425	KC429250	KC429167	AF120647
Palaeoheterodonta	*Neotrigonia lamarckii*	KC429345	KC429443	KC429262	KC429182	KC429105
Archiheterodonta	*Encrassatella cumingii*	KC429350	KC429448	KC429267	KC429187	KC429110
Anomalodesmata	*Lyonsia floridana*	KC429353	KC429451	KC429268	KC429191	AF120654
	Cardiomya sp.	KC429362	KC429463/KC429464	KC429276	KC429198	KC429118
Inaequidonta	*Anodontia omissa*	KC429363	KC429465	KC429277	KC429199	KC429120
	Scissula similis	KC429394	KC429502	KC429304	KC429225	KC429142
	Teredo clappi	-	KC429518	KC429316	KC429238	-
	Solen vaginoides	KC429399	KC429507	KC429308	KC429230	-
OUTGROUPS: Class Gastropoda						
Haliotidae	*Haliotis tuberculata*	AF120511	AY145418	AY377622	AY377775	AY377729
Calyptraeidae	*Crepidula fornicata*	AY377660	AY145406	AY377625	AY377778	AY353154
Siphonariidae	*Siphonaria pectinata*	X91973	DQ256744	AY377627	AY377780	AF120638

2-2-2. Notes on sample identification

All scientific names of protobranch specimens used in this study follow the recent classification (e.g. Bouchet et al., 2010; Huber, 2010; Coan & Valentich-Scott, 2012 and World Register of Marine Species; http://www.marinespecies.org/index.php). Photos of specimen used in this study were shown in Figures 2.1-13. The specimens in

these figures were used in the molecular analysis and/or observations of shell microstructures in most cases. Diagnosis of species with doubtful identification is described below.

2-2-2-1. Identification of *Acila*

In the north-west Pacific Ocean, three species of *Acila* (s.s.) that have rostrate in the posteroventral margin unlike *Acila* (*Truncacila*) are recognized: *Acila divaricata*, *Acila mirabilis*, and *Acila vigilia*. *Acila vigilia* is distinguished from other *Acila s.s.* species in having a strong black periostracum in fresh specimens. However, *A. mirabilis* and *A. divaricata* are difficult to distinguish. *A. divaricata* was originally described by Hinds (1843). The holotype of this species was reported from the China Sea but not illustrated. However, a number of studies have suggested that *A. divaricata* is a juvenile of *A. mirabilis* and a senior synonym of *A. mirabilis* (e.g. Dall, 1898; Habe, 1958; Habe, 1977; Knudsen, 1967; Kuroda & Habe, 1981; Lutaenko & Noseworthy, 2012; Okutani, 2000; Schenck, 1934, 1935, 1936). On the other hand, several studies insist that these are two distinct species (e.g. Bernard et al., 1993; Hanley, 1860; Huber, 2010; Smith, 1892; Sowerby II, 1871; Xu, 1984, 1999; Xu & Zhang, 2008). Zhang et al. (2014) showed the distinctiveness of the two species through molecular identification using mitochondrial COI genes. The presence of a strong rostrate form corroborates the identification of the material as *A. mirabilis*.

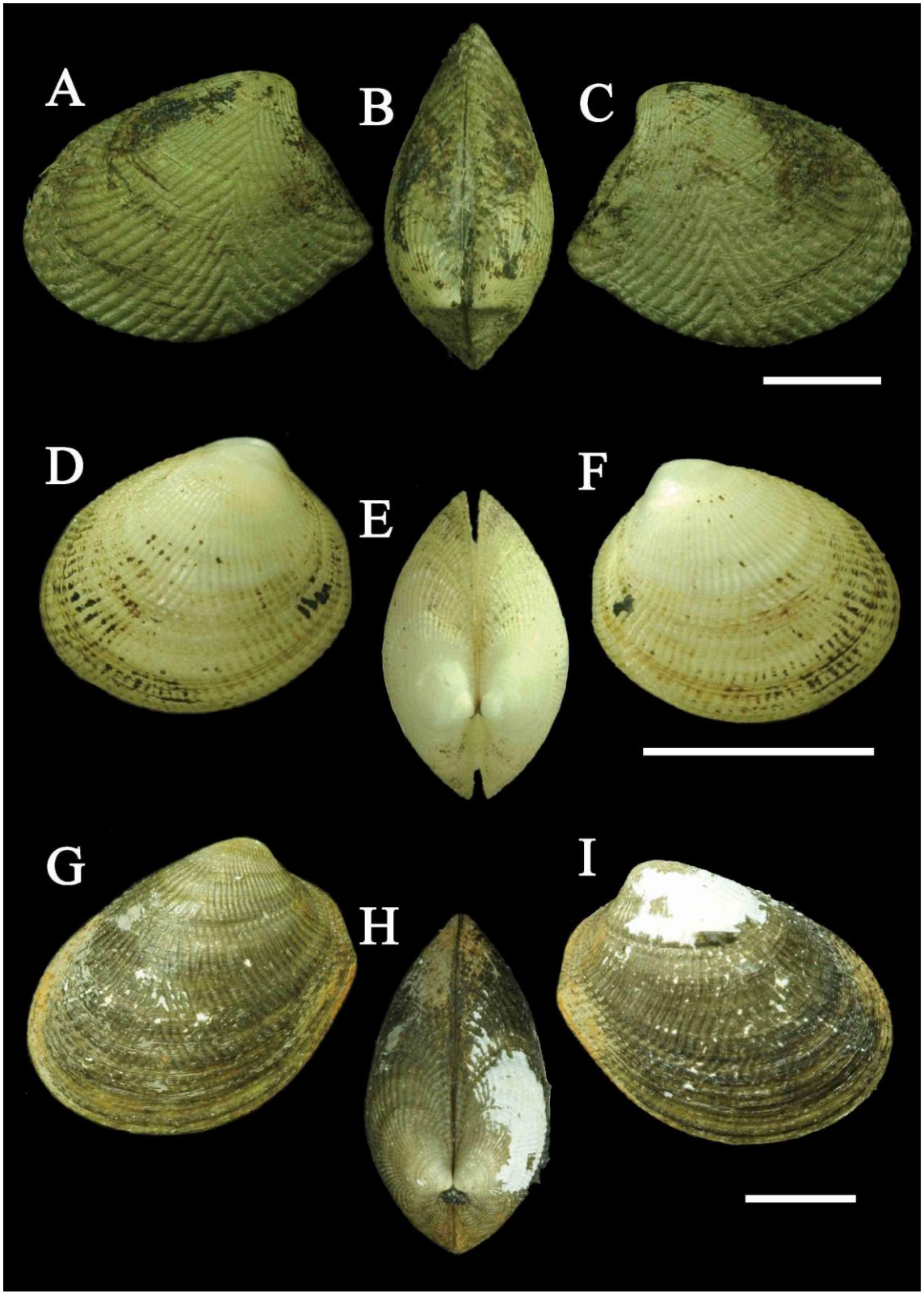

Figure 2.1. External shell morphology of genus *Acila* species (Family Nuculidae; Superfamily Nuculoidea). Scale bars = 5 mm. **A-C.** *Acila mirabilis*. A, left valve; B, dorsal. C, right valve. **D-F.** *Acila minutoides*. D, left valve; E, dorsal. F, right valve. **G-I.** *Acila insignis*. G, left valve; H, dorsal. I, right valve.

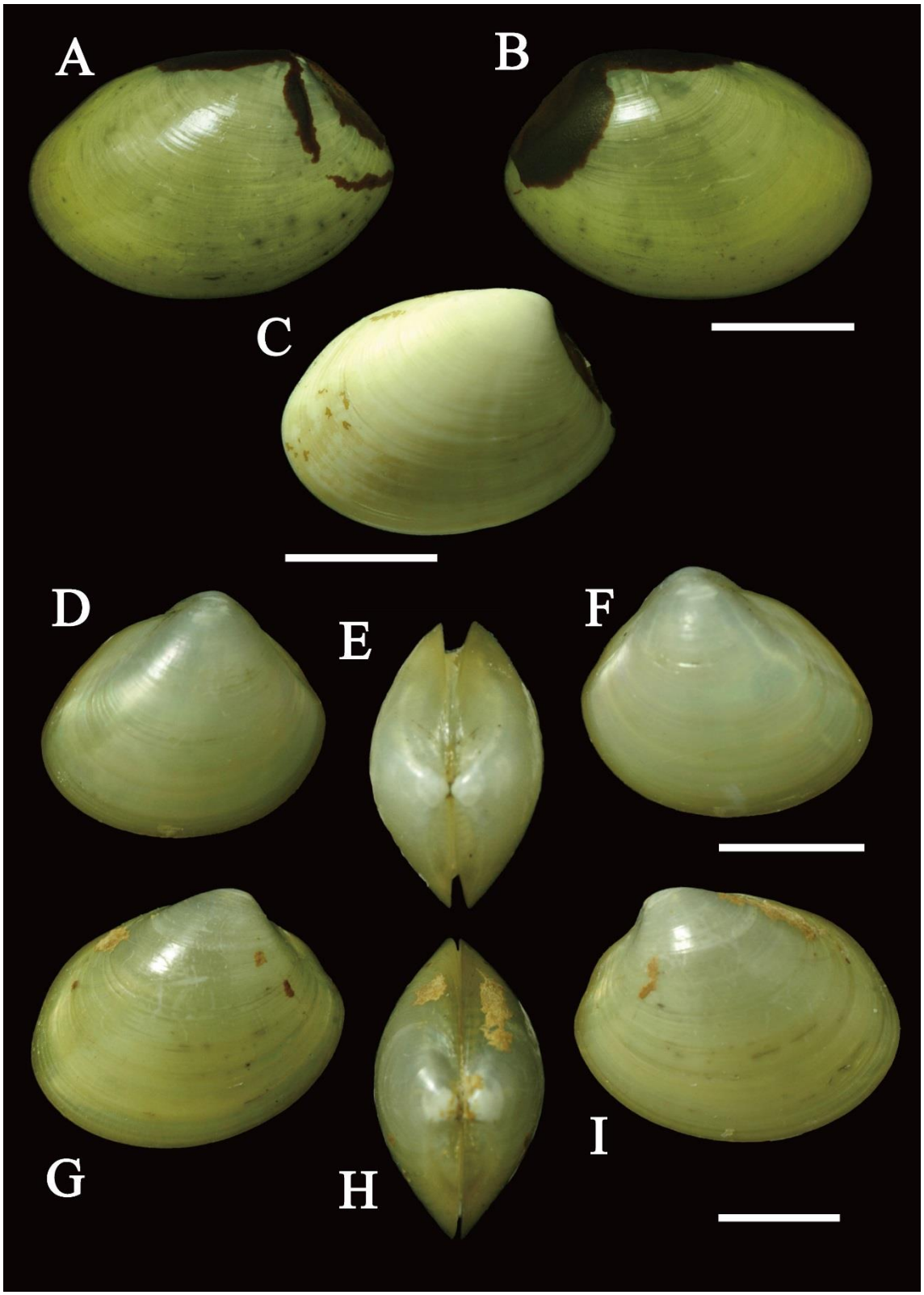

Figure 2.2. External shell morphology of genus *Ennucula* and *Brevinucula* species (Family Nuculidae; Superfamily Nuculoidea). Scale bars = 5 mm. **A, B.** *Ennucula nipponica*. A, left valve; B, right valve. **C.** left valve of *Ennucula sp.* 2. **D-F.** *Ennucula siberutensis*. A, left valve; B, dorsal; C, right valve. **G-I.** *Ennucula tenuis*. G, left valve; H, dorsal. I, right valve.

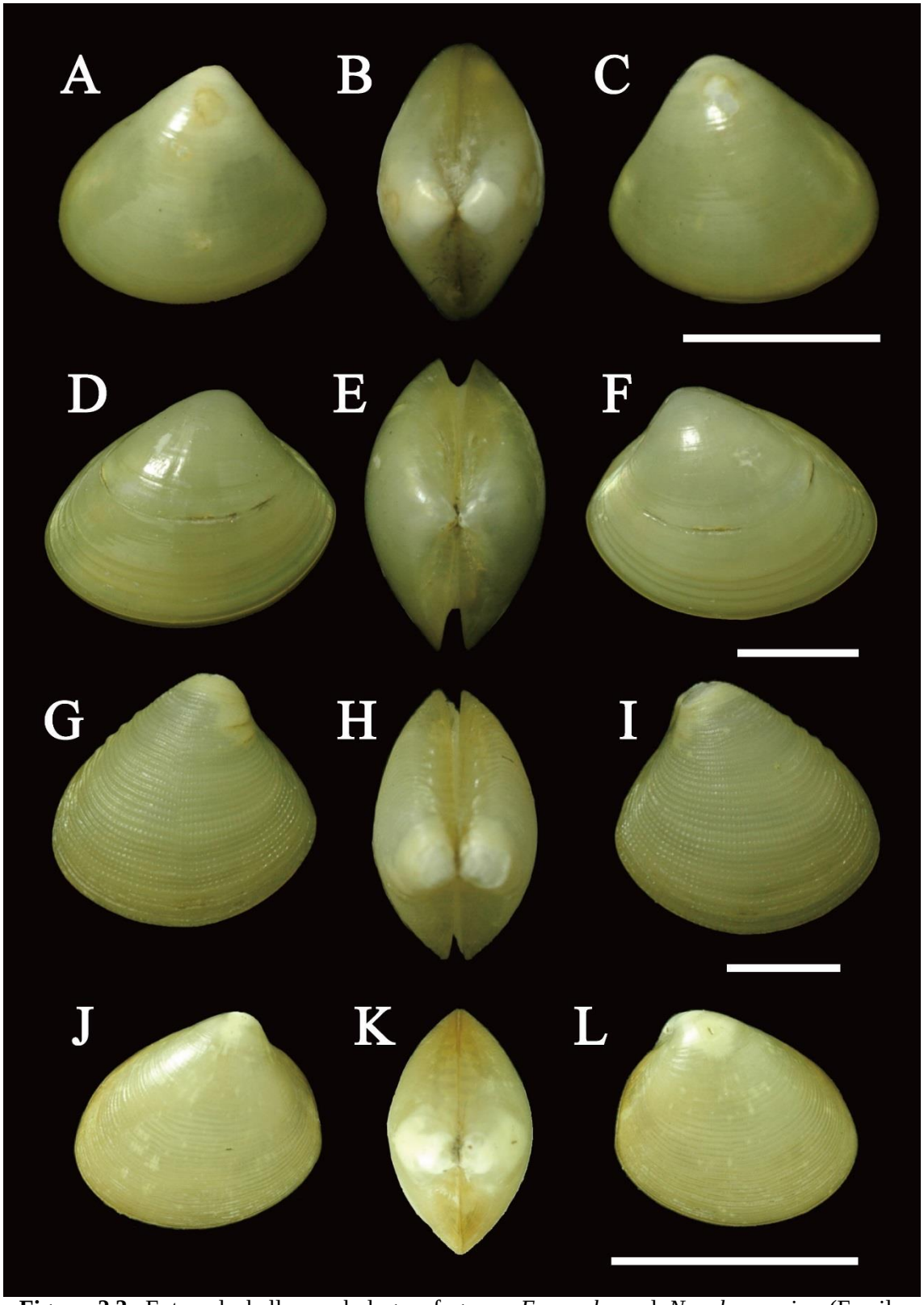

Figure 2.3. External shell morphology of genus *Ennucula* and *Nucula* species (Family Nuculidae; Superfamily Nuculoidea). Scale bars = 5 mm. **A-C.** *Brevinucula sp.*. D, left valve; E, dorsal. F, right valve. **D-F.** left valve of *Ennucula sp. 1*. D, left valve; E, dorsal; F, right valve. **G-I.** *Nucula torresi*. G, left valve; H, dorsal. I, right valve. **J-L.** *Nucula tokyoensis*. J, left valve; K, dorsal. L, right valve.

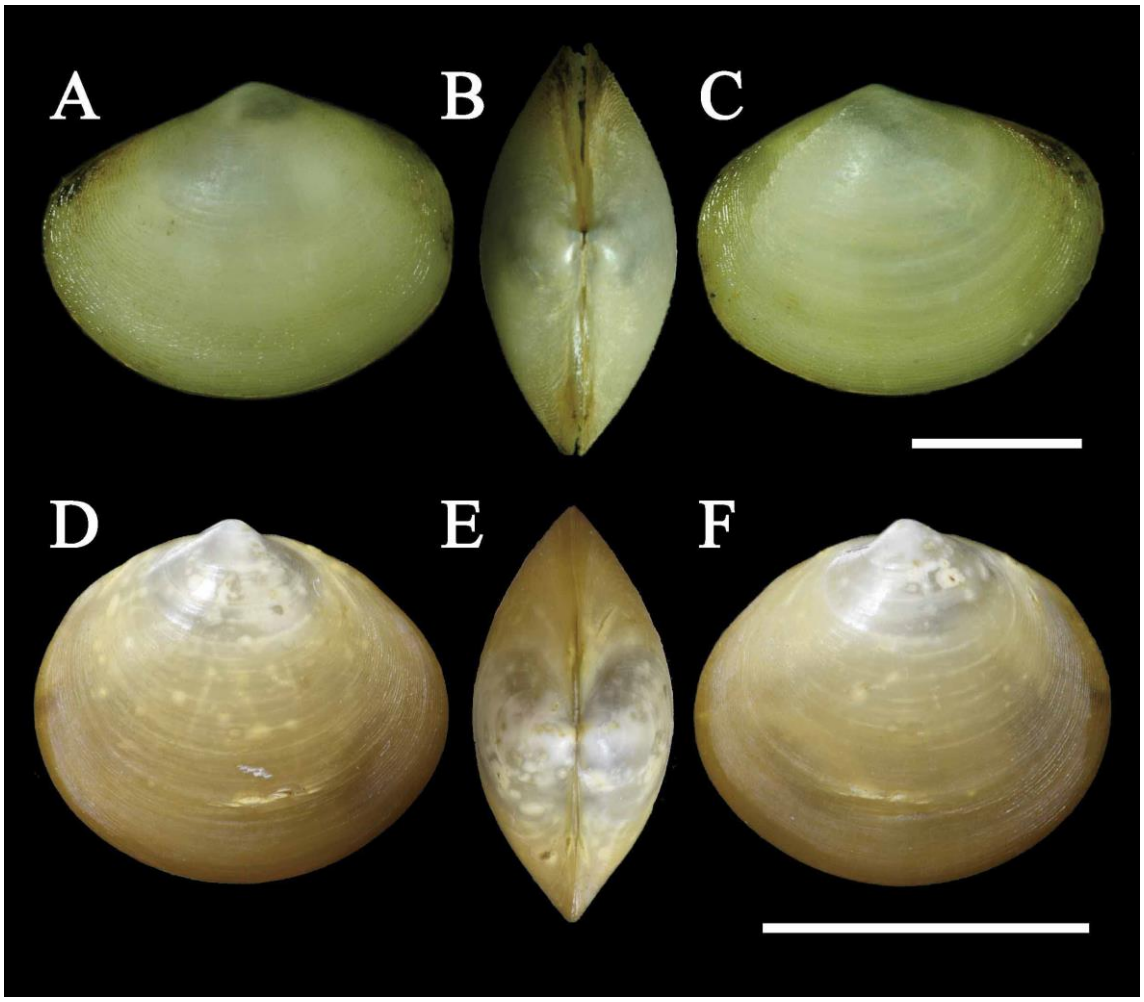

Figure 2.4. External shell morphology of family Sareptidae species (Superfamily Nuculoidea). Scale bars = 5 mm. **A-C.** *ASarepta speciosa*. A, left valve; B, dorsal. C, right valve. **D-F.** *Setigloma japonica*. D, left valve; E, dorsal. F, right valve.

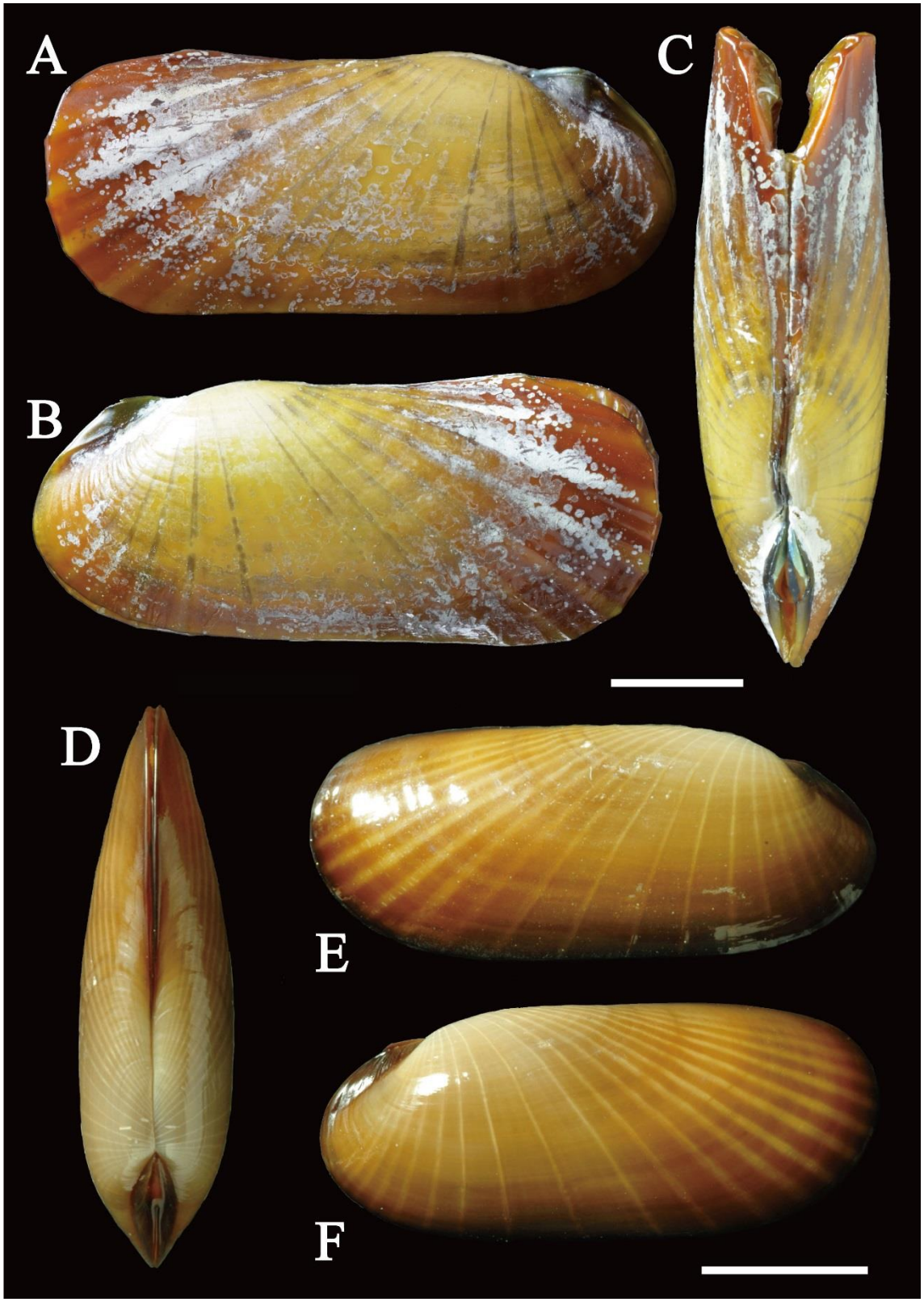

Figure 2.5. External shell morphology of genus *Acharax* species (Family Solemyidae; Superfamily Solemyoidea). Scale bar = 5 mm. **A-C.** *Acharax johnsoni*. A, left valve; B, dorsal; C, right valve. **D-F.** *Acharax japonica*. D, dorsal; E, left valve; F, right valve.

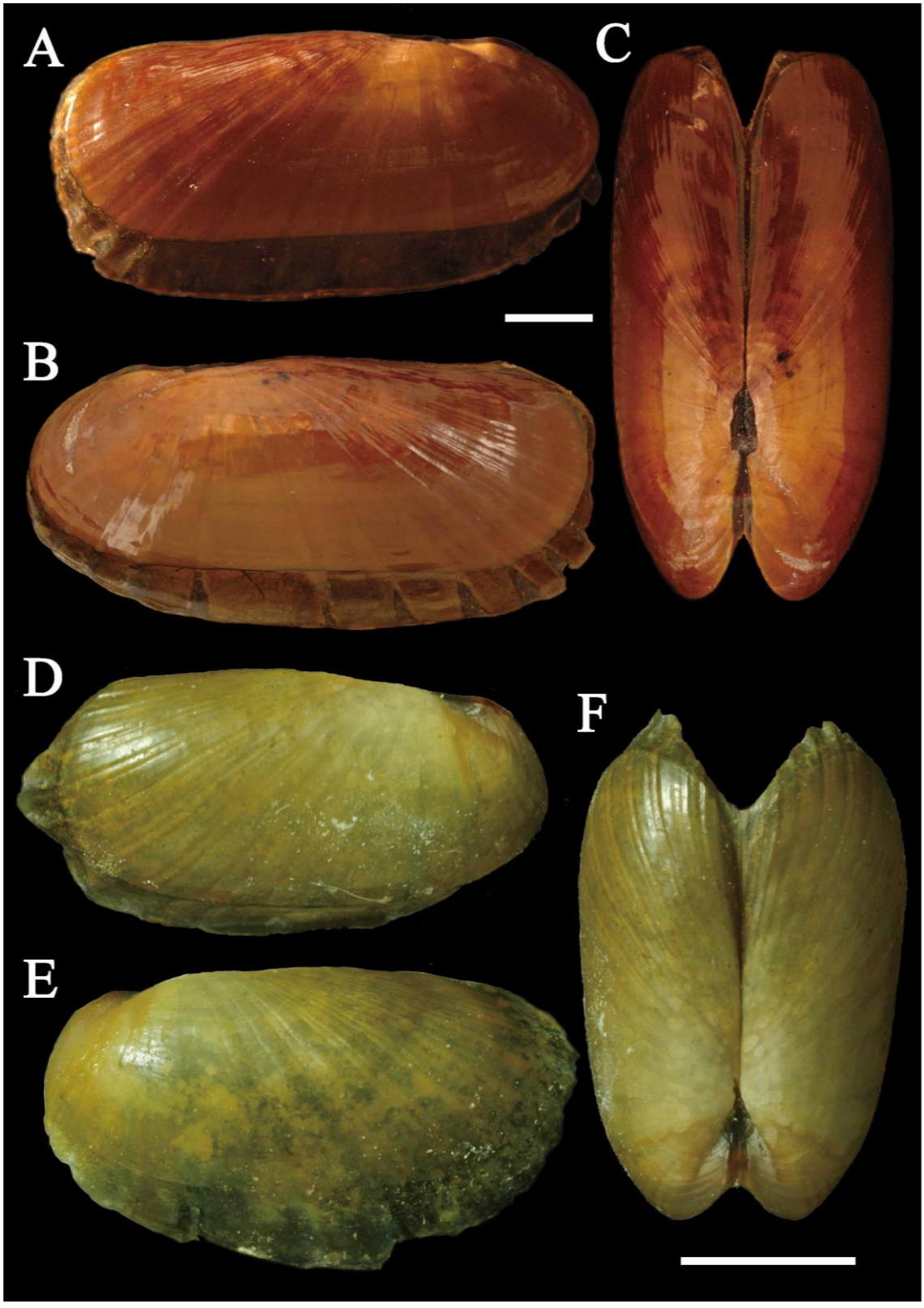

Figure 2.6. External shell morphology of genus *Solemya* species (Family Solemyidae; Superfamily Solemyoidea). Scale bar = 5 mm. **A-C.** *Solemya percernicosa*. A, left valve; B, right valve; C, dorsal. **D-F.** *Solemya flava*. D, left valve; E, right valve; F, dorsal.

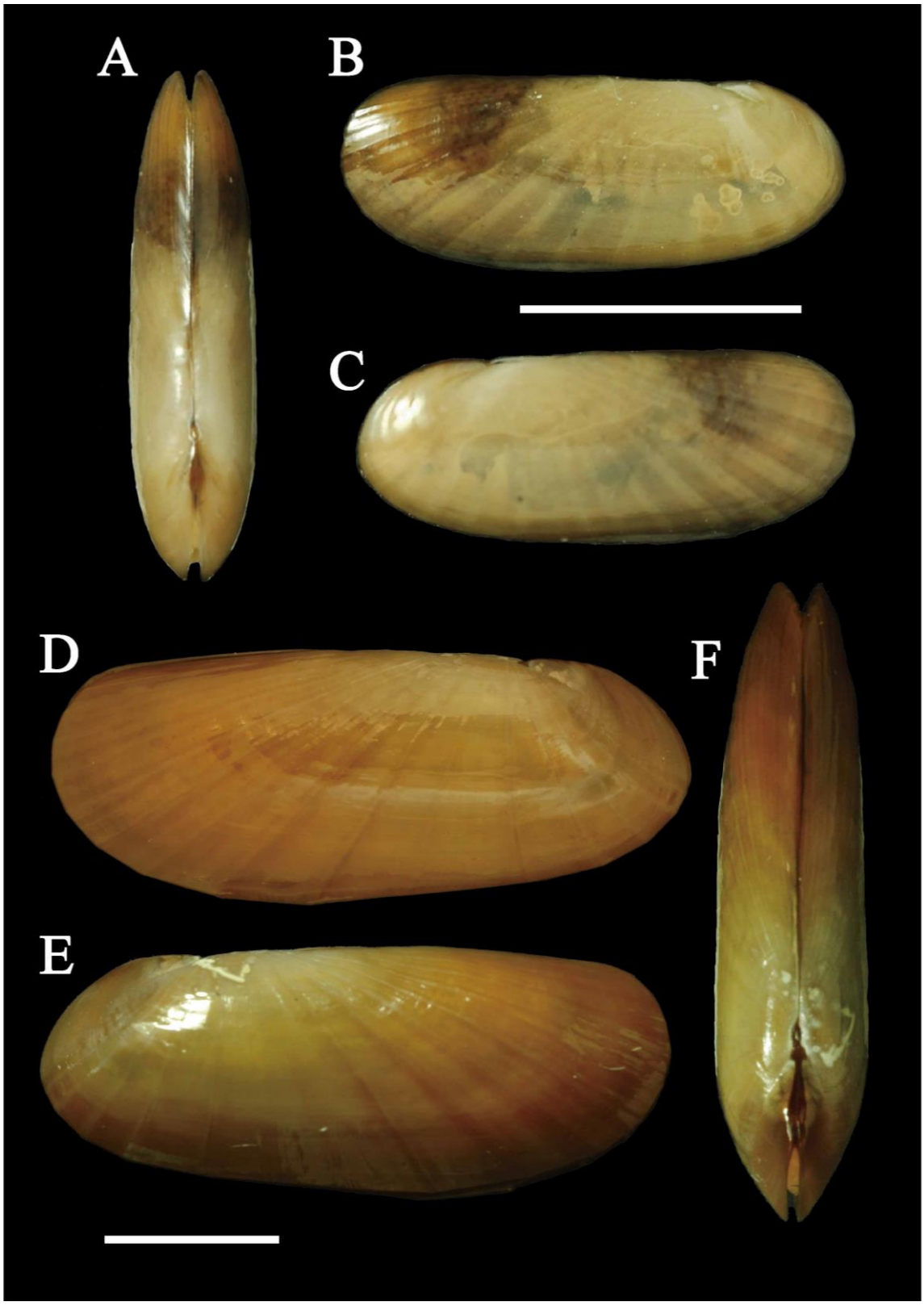

Figure 2.7. External shell morphology of genus *Solemya* species (Family Solemyidae; Superfamily Solemyoidea). Scale bar = 5 mm. **A-C.** *Solemya pusilla*. A, dorsal; B, left valve; C, right valve. **D-F.** *Solemya tagiri*. D, left valve; E, right valve; F, dorsal.

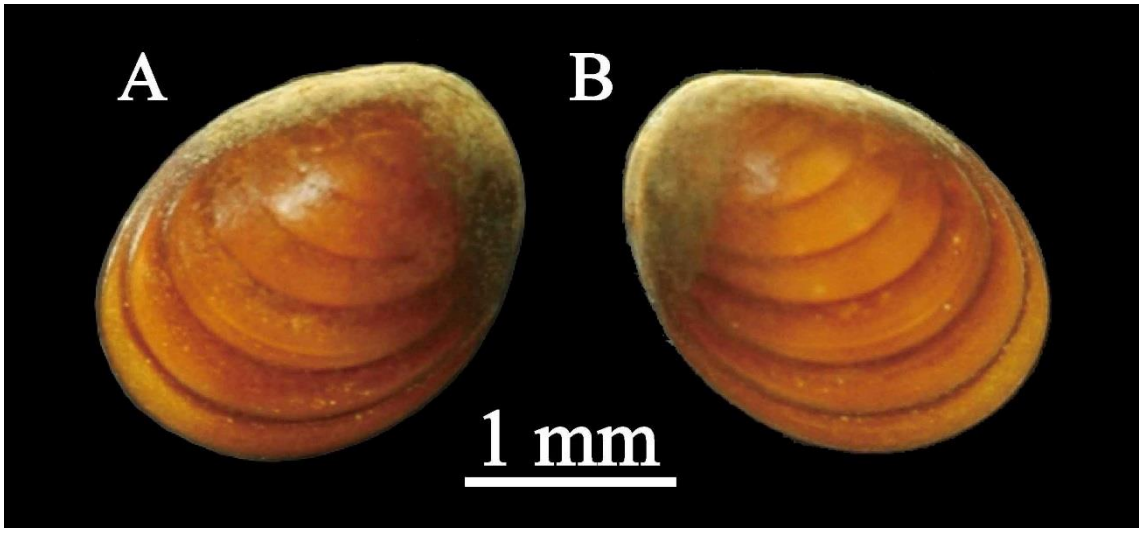

Figure 2.8. External shell morphology of family Manzanellidae species (Superfamily Solemyoidea). Scale bar = 1 mm. **A, B.** *Huxleyia sulcata*. A, left valve; B, right valve.

2-2-2-2. Identification of *Yoldia*

Okutani (2000) illustrated three *Yoldia* (*Cnesterium*) species, *Yoldia johanni*, *Yoldia seminuda* and *Yoldia notabili*s, among eight *Yoldia* species from Japanese waters. Among these species, the specimens (see Figure 2.13G-I) in this study appears to be *Yoldia johanni* Dall, 1925 by having oblique striae, slightly recurved posterior end and slightly pointed rostrum. *Yoldia notabilis* is characterized by a pointed rostrum. *Yoldia seminuda* differs from other species in the umbo position and shell outline. The umbo of *Y. johanni* is situated at a more posterior position (ca. posterior 2/3 of shell length) than that of *Y. seminude* (mid part of shell length). In addition, *Y. seminude* have a more elongate outline than *Y. johanni*. However, Coan et al. (2000) synonymized *Y. johanni* with *Y. seminude* Dall, 1871 and recent classification has followed them. I doubt this classification because the shell morphology of '*Yoldia johanni*' shown in several papers (Kira, 1954; Habe, 1977; Okutani, 2000) differs from that of *Y. seminude* (photographs

are showed in Coan et al., 2000; Huber, 2010) as described before. The distribution of the two species is also varies considerably. The type locality of *Y. johanni* is north Japan and that of *Y. seminuda* is the American coast (Dall, 1925). *Y. notabilis* was described using a fossil specimen from the upper Pleistocene of central Japan (Yokoyama, 1925). Illustrations of the original descriptions show resemblances between *Y. johanni* and *Y. notabilis* (Dall, 1925; Yokoyama, 1925). Although further inquiry is needed on the *Yoldia* species, this study follows the current interpretation by Okutani (2000).

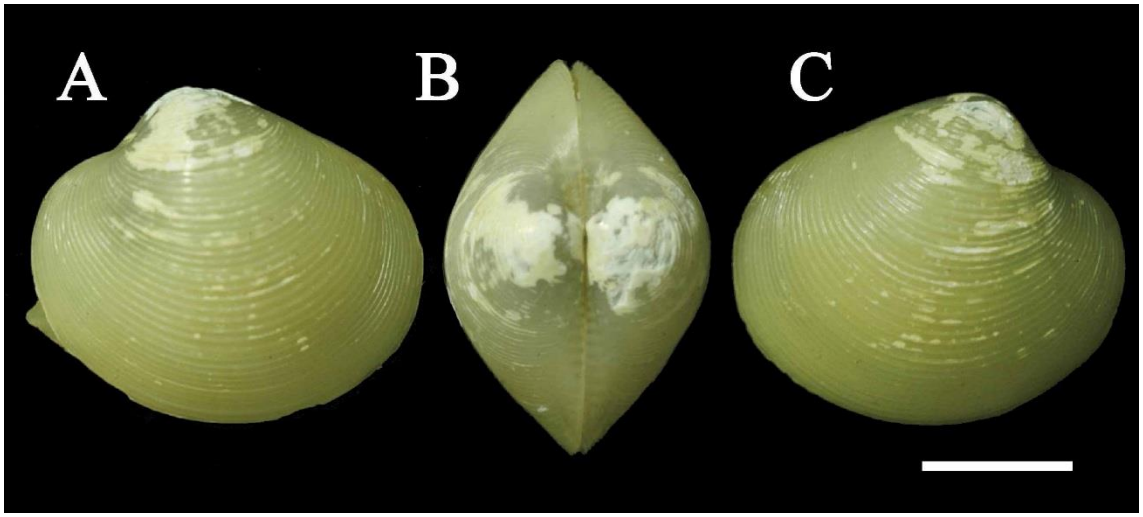

Figure 2.9. External shell morphology of family TIndariidae (Superfamily Nuculanoidea). Scale bar = 5 mm. **A-C.** *Tindaria soyoae*. A, left valve; B, dorsal; C, right valve.

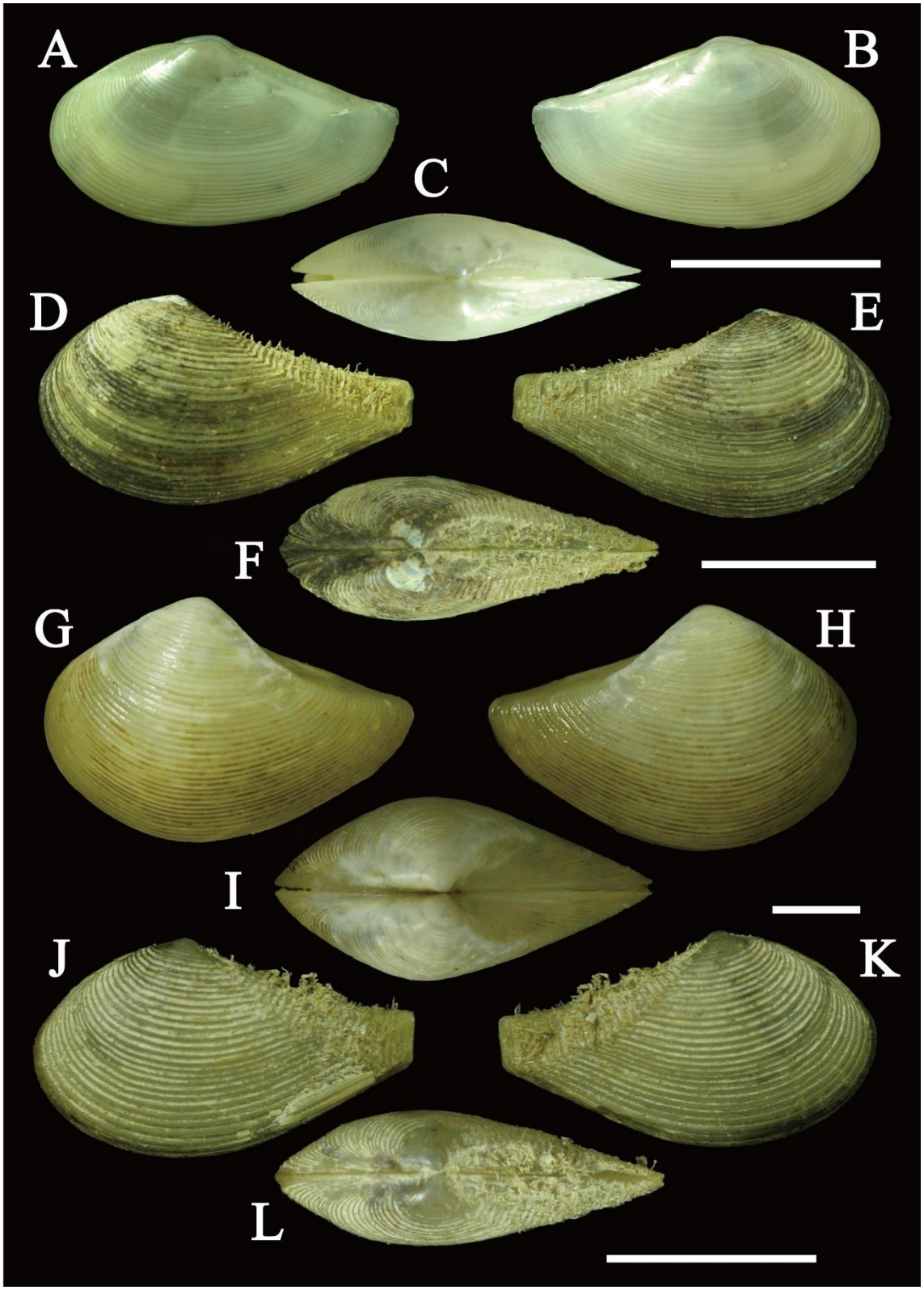

Figure 2.10. External shell morphology of family Nuculanidae species (Superfamily Nuculanoidea). Scale bars = 5 mm. **A-C.** *Nuculana gordonis*. A, left valve; B, right valve; C, dorsal. **D-F.** *Nuculana soyoae*. D, left valve; E, right valve; F, dorsal. **G-I.** *Neilonella kirai*. G, left valve; H, right valve; I, dorsal. **J-L.** *Nuculana yokoyamai.* J, left valve; K, right valve; L, dorsal.

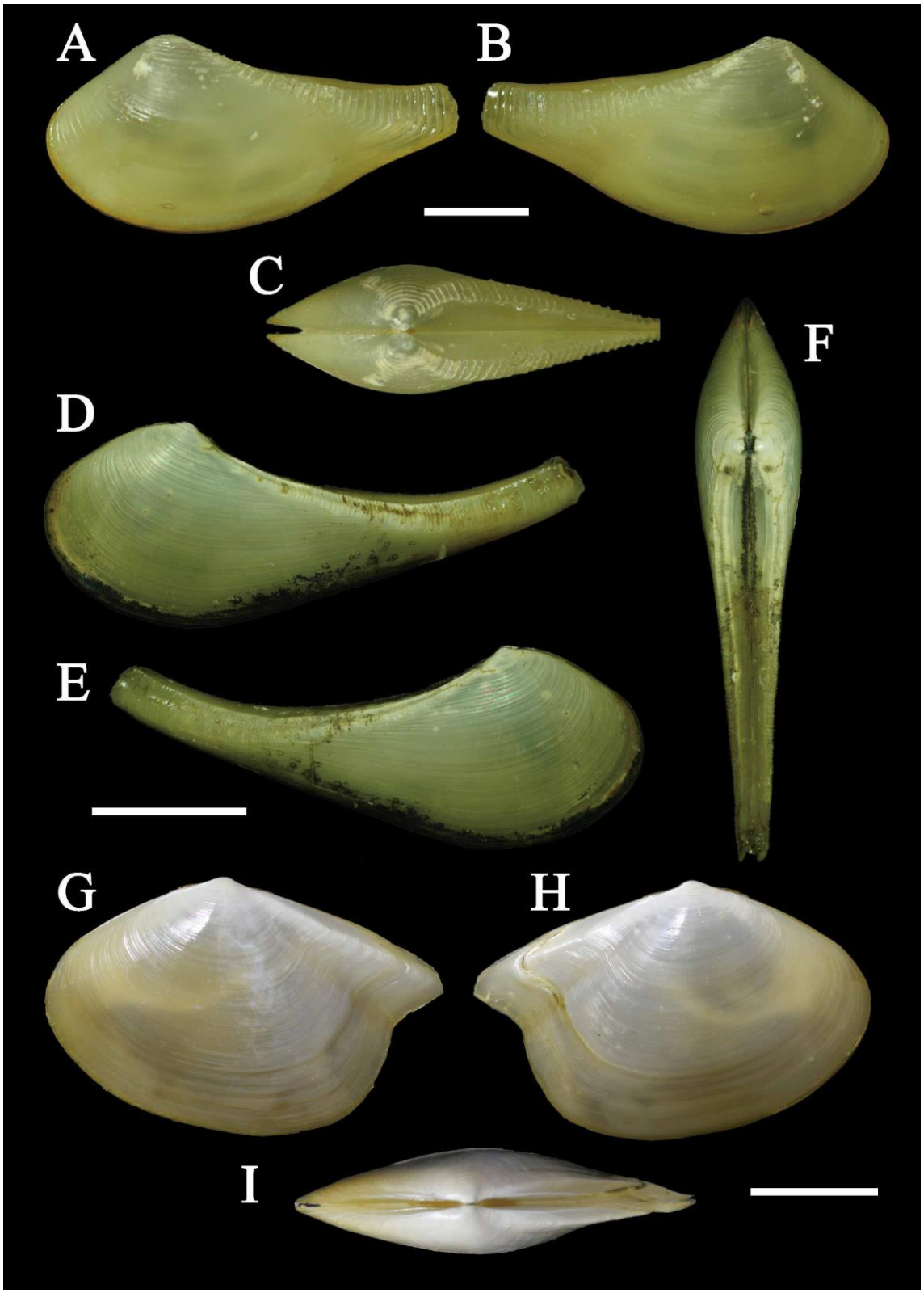

Figure 2.11. External shell morphology of family Nuculanidae and Bathyspinulidae species (Superfamily Nuculanoidea). Scale bar = 5 mm. **A-C.** *Nuculana leonina*. A, left valve; B, right valve; C, dorsal. **D-F.** *Nuculana tanseimaruae*. D, left valve; E, right valve; F, dorsal. **G-I.** *Bathyspinula carcarella*. G, left valve; H, right valve; I, dorsal.

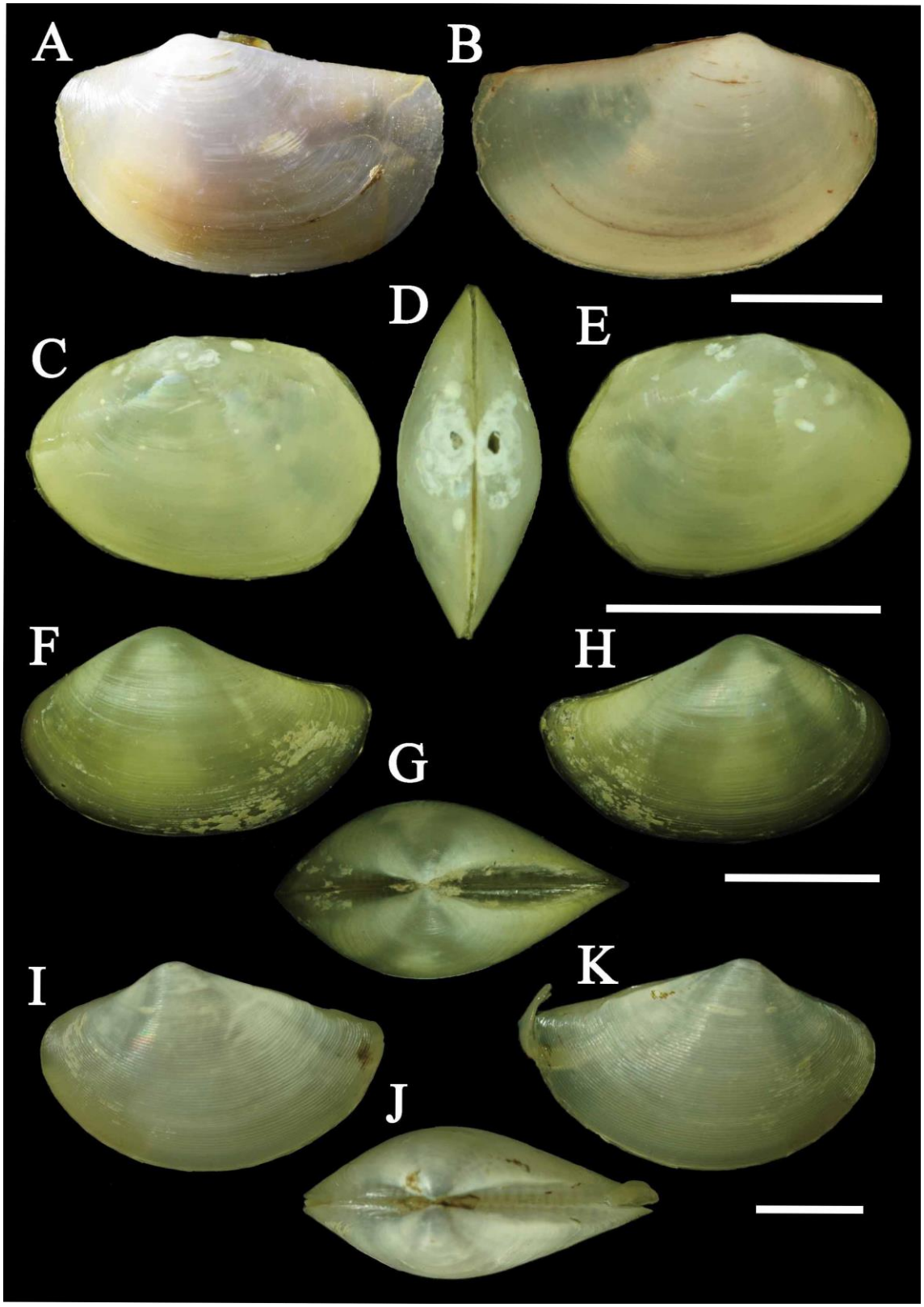

Figure 2.12. External shell morphology of family Malletiidae and Neilonellidae species (Superfamily Nuculanoindea). Scale bar = 5 mm. **A, B.** *Malletia humilior*. A, left valve; B, right valve. **C-E.** *Malletia takaii*. C, left valve; D, dorsal; E, right valve. **F-H.** *Neilonella soyoae*. F, left valve; G, dorsal; H, right valve. **I-K.** *Neilonella dubia*. I, left valve; J, dorsal; K, right valve.

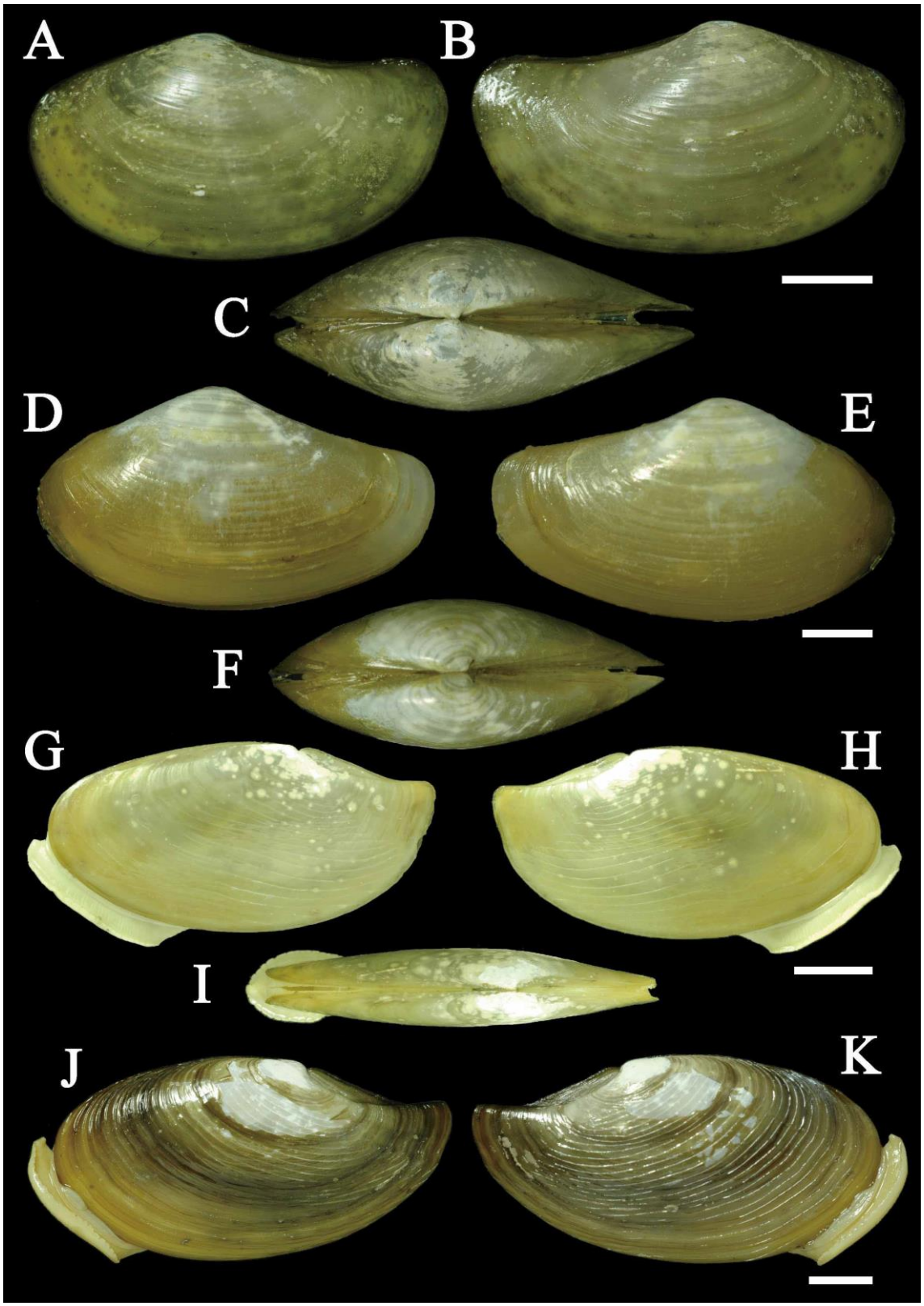

Figure 2.13. External shell morphology of family Yoldiidae species (Superfamily Nuculanoindea). Scale bar = 5 mm. **A-C.** *Megayoldia lischkei*. A, left valve; B, right valve; C, dorsal. **D-F.** *Megayoldia japonica*. D, left valve; E, right valve; F, dorsal. **G-I.** *Yoldia johanni*. G, left valve; H, right valve; I, dorsal. **J, K.** *Yoldia notabilis*. J, left valve; K, right valve.

2-2-3. DNA extraction, amplification and sequencing

DNA was extracted from the mantle or the whole animal using DNeasy Blood and Tissue Kit (Quiagen) and purified by GeneReleaser (Bioventures) following the manufacturer's protocols. Two mitochondrial genes (16S rRNA and cytochrome c oxidase subunit I: COI), two nuclear ribosomal genes (18S rRNA and 28S rRNA), and one nuclear protein-encoding gene (Histone H3) were amplified. The process cycled 30-35 times. The standard PCR profile for mitochondrial genes was as follows: for mitochondrial genes, 120 seconds at 94 °C for denaturation, 30 seconds at 50 °C for annealing, 60 seconds at 72 °C for elongation. Denaturing in the initial step was 150 min at 94 °C and elongation in the terminal steps was conducted for 180 seconds at 72 °C. The standard PCR condition for nuclear genes was the same as that for mitochondrial genes except for settings of annealing. For annealing nuclear genes, PCR was performed in the touch down manner (Don et al., 1991) with a starting annealing temperature of 70 °C. Each subsequent cycle had an annealing temperature 1 °C lower until 65 °C was reached, with the final 25-30 cycles annealing at these final temperatures. The primer sequences for each of the five genes are listed in Table 2.4 and the length of the PCR products are listed in Table 2.5.

After purification by ExoStar (Illustra), sequence reactions were performed using GenomeLab DTCS Quick Start Kit (Beckman Coulter) following the manufacturer's protocol. Suitable sequencing primers were designed and synthesized for sequence reaction (also see Table 2.4). Capillary electrophoresis was conducted with CEQ 2000 (Beckman Coulter).

Table 2.3. List of species and gene fragments of nuclear protein-encoding genes included in phylogenetic analyses.

Classification	Species	ATP synthase β	elongation factor-1α	myosin heavy chain type II	RNA polymerase II
Protobranchia					
Solemyidae	*Solemya velum*	-	JQ781158	JQ781084	JQ781112
Nuculanidae	*Nuculana caloundra*	-	JQ781176	-	JQ781109
Malletiidae	*Clencharia abyssorum*	-	JQ781184	-	JQ781120
Yoldiidae	*Yoldia limatula*	JQ781128	JQ781157	JQ781082	JQ781106
OUTGROUPS: Autobranchia					
Prteriomorphia	*Glycymeris glycymeria*	JQ781124	JQ781168	JQ781074	JX036496
	Pteria hirundo	JQ781123	JQ781164	JQ781077	JQ781105
Palaeoheterodonta	*Neotrigonia lamarckii*	JQ781127	JQ781177	JQ781086	JQ781098
Archiheterodonta	*Encrassatella cumingii*	JQ781143	JQ781167	-	JQ781104
Anomalodesmata	*Lyonsia floridana*	JQ781132	JQ781148	-	JQ781110
	Cardiomya sp.	JQ781129	JQ781149	-	JQ781113
Inaequidonta	*Anodontia omissa*	JQ781140	JQ781182	JQ781094	JQ781102
	Scissula similis	JQ781139	JQ781180	JQ781091	JQ781115
	Teredo clappi	JQ781138	JQ781186	JQ781089	JQ781100
	Solen vaginoides	JQ781141	JQ781185	JQ781093	JQ781101

2-2-4. Phylogenetic analyses

Maximum likelihood (ML) analyses were performed using the alignments of each marker and the concatenated dataset, which were edited by the following methods. Sequences of five genes were aligned individually using the online program MAFFT version 7 (Katoh & Standley 2013). Alignment strategy was set up as Q-INS-i for ribosomal genes (18S, 28S, and 16S) and G-INS-i for protein coding genes (H3 and COI) on MAFFT version 7. The nuclear gene data set (ATP synthase β, elongation factor-1α, myosin heavy chain type II and RNA polymerase II) was set up as Q-ins-i. Alignments were confirmed by eye and the absence of initiation and stop codons in the protein-coding gene sequences (H3 and COI) was checked by translating them into protein sequences using MEGA version 6 (Tamura et al., 2013). Each alignment was masked to remove alignment ambiguous sites using Gblocks version 0.91b (Castresana 2000) with parameters allowing for smaller final blocks, gap positions within the final blocks and less strict flanking positions. Mesquite version 2.75 (Maddison & Maddison,

2011) was used for data set concatenation.

ML analyses of each generated alignment were conducted using RAxML GUI version 1.3 (Silvestro and Michalak 2011). For the ML searches, concatenated sequences were partitioned for each gene. MEGA version 6 (Tamura et al. 2013) specified the GTR + Γ + I substitution model as the best nucleotide substitution model estimation method. Although not all of all nine genes prefer the GTR + Γ + I model by MEGA version 6 estimation, it was preferred by the majority. It is considered to be the most complicated substitution model. The bootstrap (bs) support values were estimated by 1000 iterations.

Table 2.4. Nucleotide sequences of primers.

Locus	primer	Sequence (5' - 3')	Direction	Sourse
18S rRNA	18Se	CTG GTT GAT CCT GCC AGT	Forward	Palumbi (1996)
	18S-A	GCA GCA GGC GCG CAA ATT AC	Forward	Designed form aligned protobranch sequences (this study)
	18S-B	GAA GGC AGC AGG CGC GCA	Forward	Designed form aligned protobranch sequences (this study)
	18S-C	GGT AAT TCC AGC TCC AAT AG	Forward	Designed form aligned protobranch sequences (this study)
	18S-D	AGC TCG TAG TTG GAT CTC G	Forward	Designed form aligned protobranch sequences (this study)
	18S-E	AGT TCT GAC CAT AAA CGA TGC	Forward	Designed form aligned protobranch sequences (this study)
	18S-F	CGG TGT TAG AGG TGA AAT TC	Forward	Designed form aligned protobranch sequences (this study)
	18S-G	AGG ATT GAC AGA TTG AGA GC	Forward	Designed form aligned protobranch sequences (this study)
	18S3	CGG TAG TAG CGA CGG GCG GTG TG	Reverse	Modified from 18d in Palumbi (1996)
28S RNA	LSU5	TAG GTC GAC CCG CTG AAY TTA AGC A	Forward	Littlewood et al. (2000)
	LSU900	CCG TCT TGA AAC ACG GAC CAA G	Forward	Olsen et al. (2003)
	LSU1600	AGC GCC ATC CAT TTT CAG G	Reverse	Williams et al. (2003)
	28S-A	AGA GAG AGT TCA AGA GTA CG	Forward	Designed form aligned protobranch sequences (this study)
	28S-B	AGC GAA TGA TTA GAG GCC TTG	Forward	Designed form aligned protobranch sequences (this study)
	28S-C	CAA GGC CTC TAA TCA TTC GCT	Reverse	Designed form aligned protobranch sequences (this study)
Histone H3	H3aF	ATG GCT CGT ACC AAG CAG ACG GC	Forward	Colgan et al. (1998)
	H3-A	CCG TCG TTA CCA GAA GAG CA	Forward	Designed form aligned protobranch sequences (this study)
	H3aR	ATA TCC TTR GGC ATR ATR GTG AC	Reverse	Colgan et al. (1998)
COI	LCO1490	GGT CAA CAA ATC ATA AAG ATA TTG G	Forward	Folmer et al. (1994)
	HCO2198	TAA ACT TCA GGG TGA CCA AAA AAT CA	Reverse	Folmer et al. (1994)
16S rRNA	16S-1	CGC CTG TTT ATC AAA AAC AT	Forward	Palumbi (1996)
	16S-4	CCG GTC TGA ACT CAG ATC ACG T	Reverse	Palumbi (1996)

Table 2.5. Data partition size and Modeltest recommendations for each molecular marker.

Partitions	Original length of alignment (bp)	Fraction retained by Gblocks (%)	Final length of alignment (bp)	Model selected (AIC)	Model selected (BIC)
16S rRNA	754	52	397	GTR+G+I	HKY+G
18S rRNA	2158	70	1531	GTR+G+I	K2+G+I
28S rRNA	3306	34	1152	GTR+G+I	T92+G
COI	742	83	620	GTR+G+I	GTR+G+I
H3	420	77	324	GTR+G+I	GTR+G
ATP synthase β	852	98	839	GTR+G+I	GTR+G+I
elongation factor-1α	933	96	905	GTR+G+I	K2+G+I
myosin heavy chain type II	645	94	610	TN93+G+I	K2+G
RNA polymerase II	351	99	347	GTR+G+I	K2+G+I

2-3. Results

2-3-1. Sequence data

A total of 6725 base pairs (bp) with 186 aligned sequences (including 43 new sequences) of nine genes were concatenated and used for ML analysis. The breakdown is as follow; 154 aligned sequences (including 39 new sequences) of 1531 bp in length (70% of the originally sequenced 2158 bp) for 18S rRNA genes, 135 aligned sequences (including 42 new sequences) of 1152 bp in length (34% of the originally sequenced 3306 bp) for 28S rRNA genes, and 115 aligned sequences (including 40 new sequences) of 324 bp in length (77% of the originally sequenced 420 bp) for histone H3 genes were used as the dataset of the nuclear genetic markers. For the mitochondrial markers, 86 aligned 16S rRNA sequences (including 26 new sequences) of 397 bp in length (52% of the originally sequenced 754 bp) and 88 aligned COI sequences (including 32 new sequences) of 620 bp in length (86% of the original sequenced 742 bp). Four nuclear genes from Sharma et al. (2012) were also concatenated; 11 aligned sequences of the ATP synthase β gene, 14 aligned sequences of the elongation factor-1α gene, 9 aligned sequences of the myosin heavy chain type II gene, and 11 aligned sequences of the RNA polymerase II gene. The original length of each sequence, rate of the fraction retained by GBlocks and final length of each alignment are listed (Table 2.4). Table 2.4 also lists the best substitution model of each gene under the Akaike's information criterion (AIC) and Schwartz's Bayesian information criterion (BIC).

The following sequence data were excluded because of their high evolutionary rates: three 18S rRNA sequences of *Nucula ploxima* from Campbell et al. (1998), the COI sequence of *Nuculana commutata* provided by Plazzi & Passamonth (2010), three

genes (18S rRNA, 16S rRNA, and COI) of *Solemya* sp. registered on GenBank by Vestheim & Kaartvedt (data unpublished), and two set of genome data of *Solemya togata* [18S rRNA data from Steiner & Hammer (2000) and 28S rRNA data from Hammer (2001)].

2-3-2. Maximum likelihood analyses

A phylogenetic tree based on ML analysis using the combined nine genes (16S + COI + 18S + 28S + H3 + ATP synthase β + elongation factor-1α + myosin heavy chain type II + RNA polymerase II) with 186-ingroup taxon was constructed (Figure 2.14). In addition, three phylogenetic trees based on ML analyses were reconstructed. An ML tree using two mitochondrial genes (16S +COI) and three nuclear genes (18S rRNA + 28S rRNA + histone H3) were provided (Figure 2.15), following the method of Sharma et al. (2013). Reconstructed phylogenetic trees of the ML analyses using both two mitochondrial genes (16S +COI) and seven nuclear genes (18S + 28S+ H3 + ATP synthase β + elongation factor-1α + myosin heavy chain type II + RNA polymerase II) were separately reconstructed (the mitchondrial tree is shown in Figure 2.16 and nuclear tree for Figure 2.17).

The monophyly of the subclass Protobranchia was supported in a nine-gene tree (16S rRNA + cytochrome c oxidase subunit I + 18S rRNA + 28S rRNA + histone H3 + ATP synthase β + elongation factor-1α + myosin heavy chain type II + RNA polymerase II; Figure 2.14) but with negligible support (bs = 42%). The monophyly of each protobranch superfamily (Nuculoidea, Nuculanoidea, Solemyoidea and Manzanelloidea) were strongly supported with significant ML bootstrap values (at least

97%) except for the family Sareptidae. Nuculoidea formed a paraphyletic group to other protobranchs (Solemyoidea, Manzanelloidea and Nuculanoidea), and those taxa formed a monophyletic group comprising Solemyoida (Solemyoidea and Manzanelloidea) and Nuculanoidea. These relationships have significant nodal support (bs = 51% for the clade Solemyoidea and Manzanelloidea, bs = 46% for Solemyoida and Nuculanoidea). In Nuculoidea, genera *Acila* and *Brevinucula* formed a monophyletic group (bs = 91% for *Acila*, bs = 95% for *Brevinucula*), while genera *Nucula* and *Ennucla* were polyphyletic due to a partial exclusion of taxa. Two genera of Solemyoidea, *Acharax* and *Solemya* formed a monophyly and were well separated from each other with strong support (bs = 100% for *Solemya* and bs = 94% for *Acharax*). Similarly, the monophyly of two genera of Manzanelloidea (*Nucinella* and *Huxleyia*) were well supported (bs = 100%), although sampling of this taxon was insufficient. The family Sareptidae, regarded as a taxon of Nuculoidea in the current systematics (e.g. Bouchet et al., 2010), was polyphyletic. In addition, it was paraphyletic to other Nuculanoidea. Groups of Nuculanoidea without Sareptidae formed considerable non-monophyletic relationships within and among genera. The support value of the Nuculanoidea was generally low.

The ML analysis using seven nuclear genes (18S rRNA + 28S rRNA + histone H3 + ATP synthase β + elongation factor-1α + myosin heavy chain type II + RNA polymerase II) yielded almost the same result as that of the nine-gene analysis. The monophyly of subclass Protobranchia was supported in an insignificant bootstrap value (44%), while the monophyly of four superfamilies was supported significantly (at least 85 % in bs value). The seven-gene ML tree differs from the nine-gene tree slightly in the species-level topology and substantially in the phylogenetic position of the families Sareptidae and Tindariidae. Three sareptids provided by this study (two *Sarepta*

speciosa and *Microgloma japonica* specimens) are paraphyletic to other Nuculanoidea in the seven-gene ML tree and the nine-gene ML tree. However, three taxa of Sareptidae from Sharma et al. (2013), *Pristigloma nitens*, *Pristigloma* sp., and *Pristigloma alba*, were situated in the 'ingroup of other Nuculanoidea' in the seven-gene ML tree, but they were also paraphyletic to other Nuculanoidea in the nine-gene ML tree. Similarly, two tindarids (*Tindaria soyoae* and *Tindaria* sp.) were paraphyletic to other Nuculanoidea in the seven-gene ML tree, while they were included in the other Nuculanoidea clade in the nine-gene ML tree. The ML tree using two mitochondrial genes did not support the monophyly of Protobranchia but supported five major clades; Nuculoidea (bs = 92%), Solemyoidea (bs = 85%), Nuculanoidea excluding Sareptidae (bs = 96%), and Sareptidae (bs = 100%).

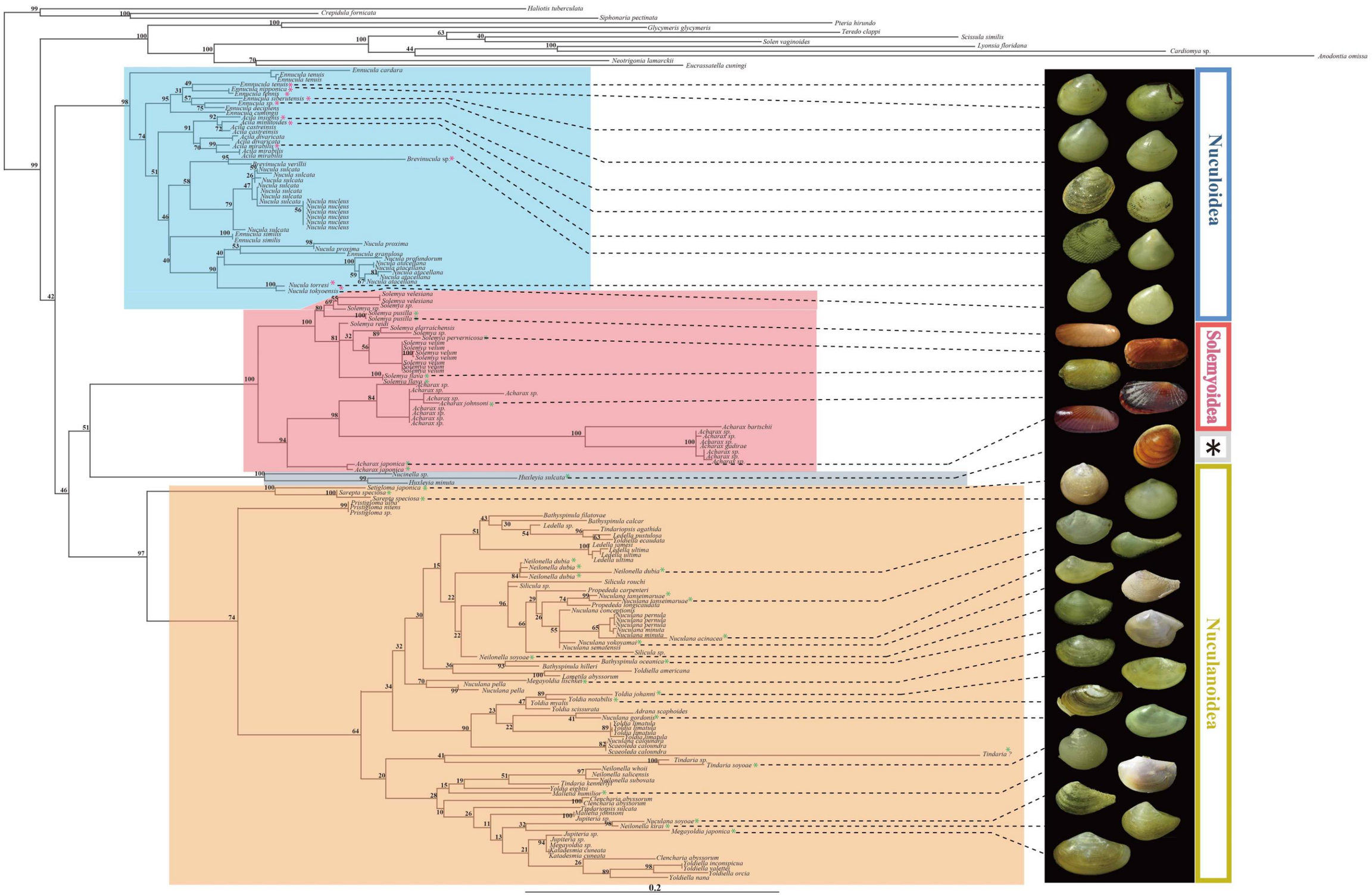

Figure 2.14. Phylogenetic relationships of Protobranchia based on the maximum likelihood analysis of nine genes. Numbers on nodes indicate bootstrap resampling frequencies. Major lineages were hilighted [blue: Nuculioidea (without Sareptidae), red: Solemyoidea, gray: Manzanelloidea, orange: Nuculanoidea (with Sareptidae)]. OTU names with asterisk mark is from this study. The photographs of the specimens for molecular analysis are exhibited in the right of this figure. Asterisk mark in the right bar indicates Manzanelloidea.

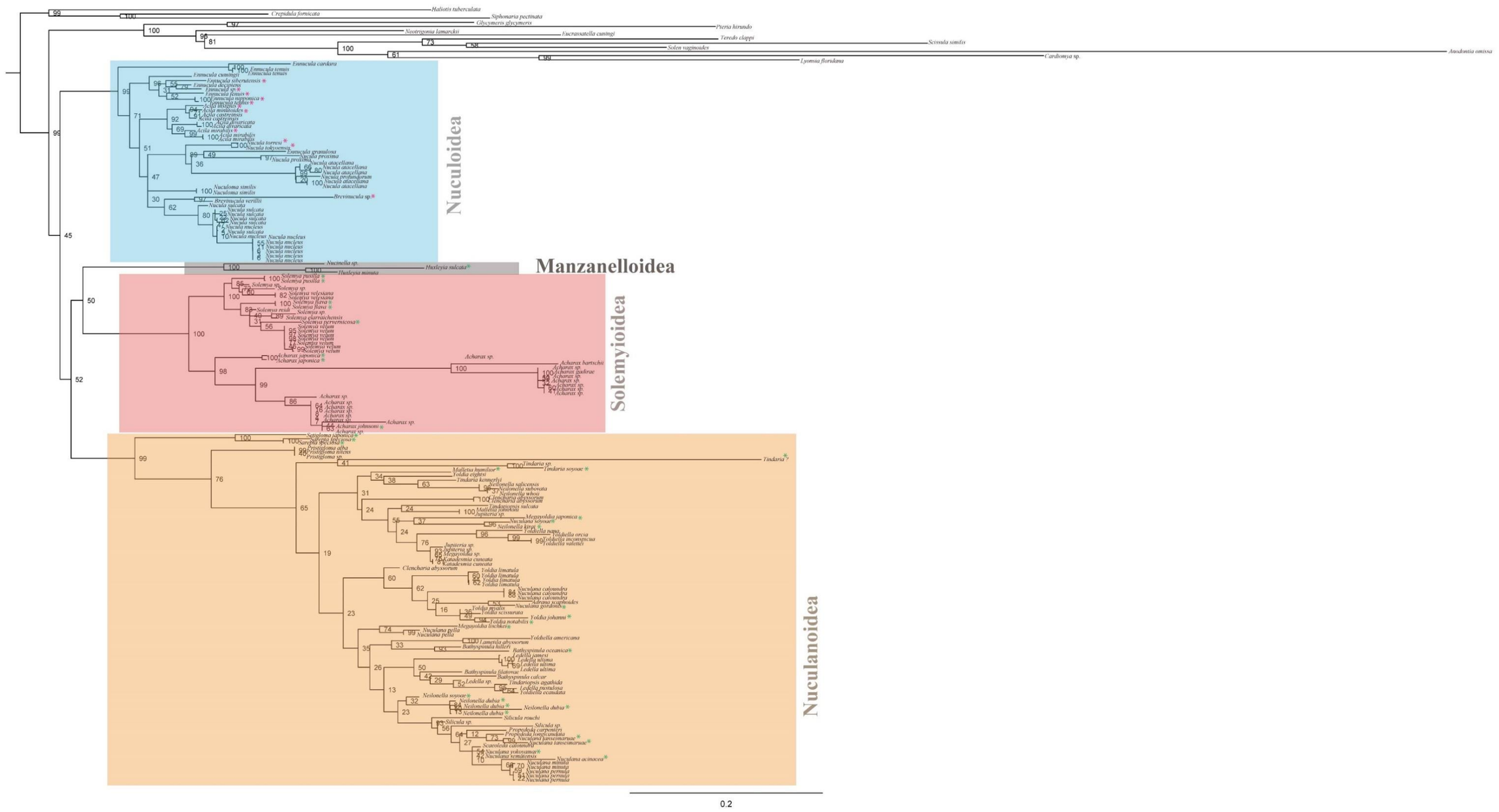

Figure 2.15. Phylogenetic relationships of Protobranchia based on the maximum likelihood analysis of five genes. Numbers on nodes indicate bootstrap resampling frequencies. Major lineages were hilighted [blue: Nuculioidea (without Sareptidae), red: Solemyoidea, gray: Manzanelloidea, orange: Nuculanoidea (with Sareptidae)]. OTU names with asterisk mark is from this study.

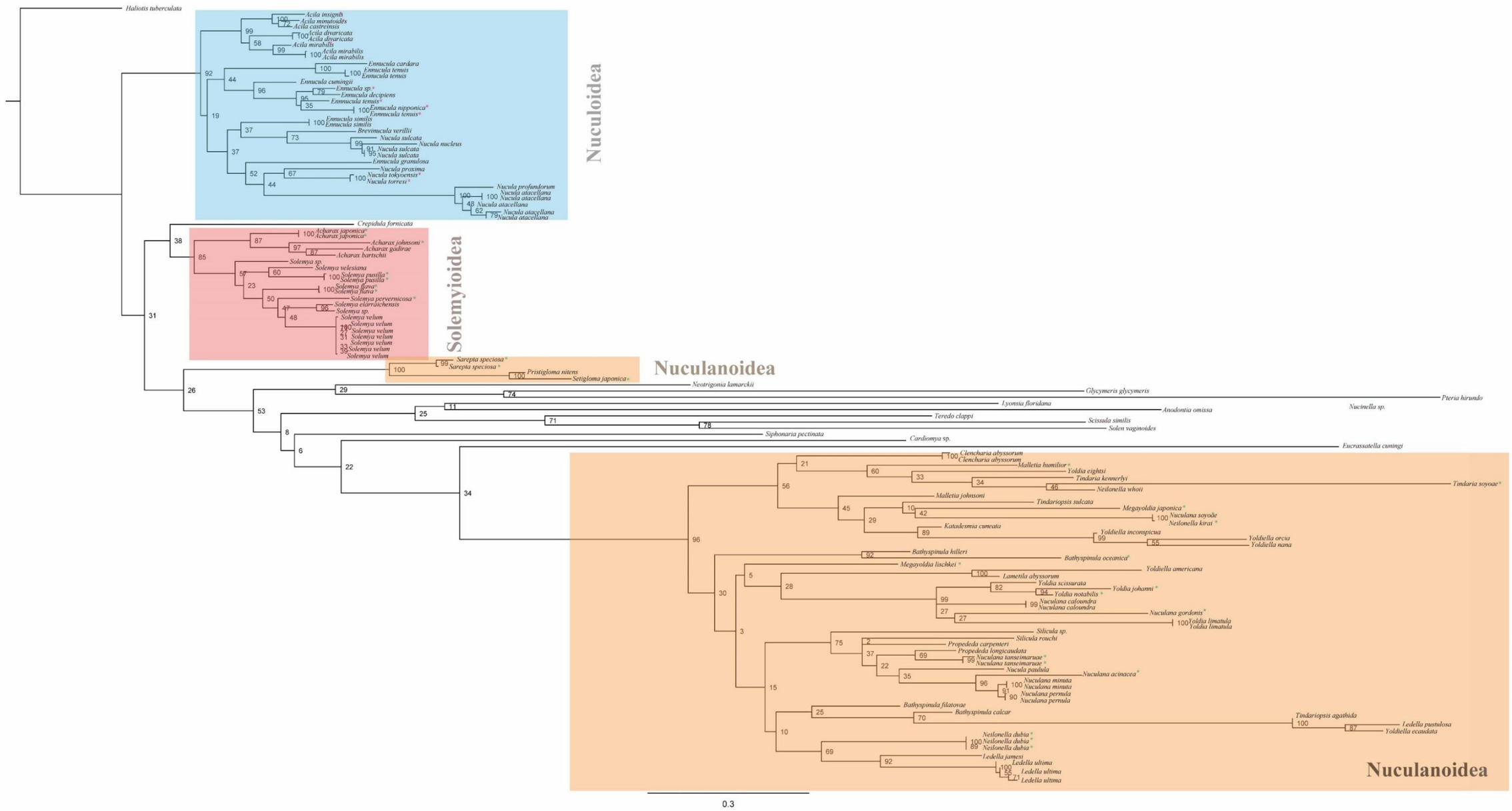

Figure 2.16. Phylogenetic relationships of Protobranchia based on the maximum likelihood analysis of two mitochondrial genes. Numbers on nodes indicate bootstrap resampling frequencies. Major lineages were hilighted [blue: Nuculioidea (without Sareptidae), red: Solemyoidea, gray: Manzanelloidea, orange: Nuculanoidea (with Sareptidae)]. OTU names with asterisk mark is from this study.

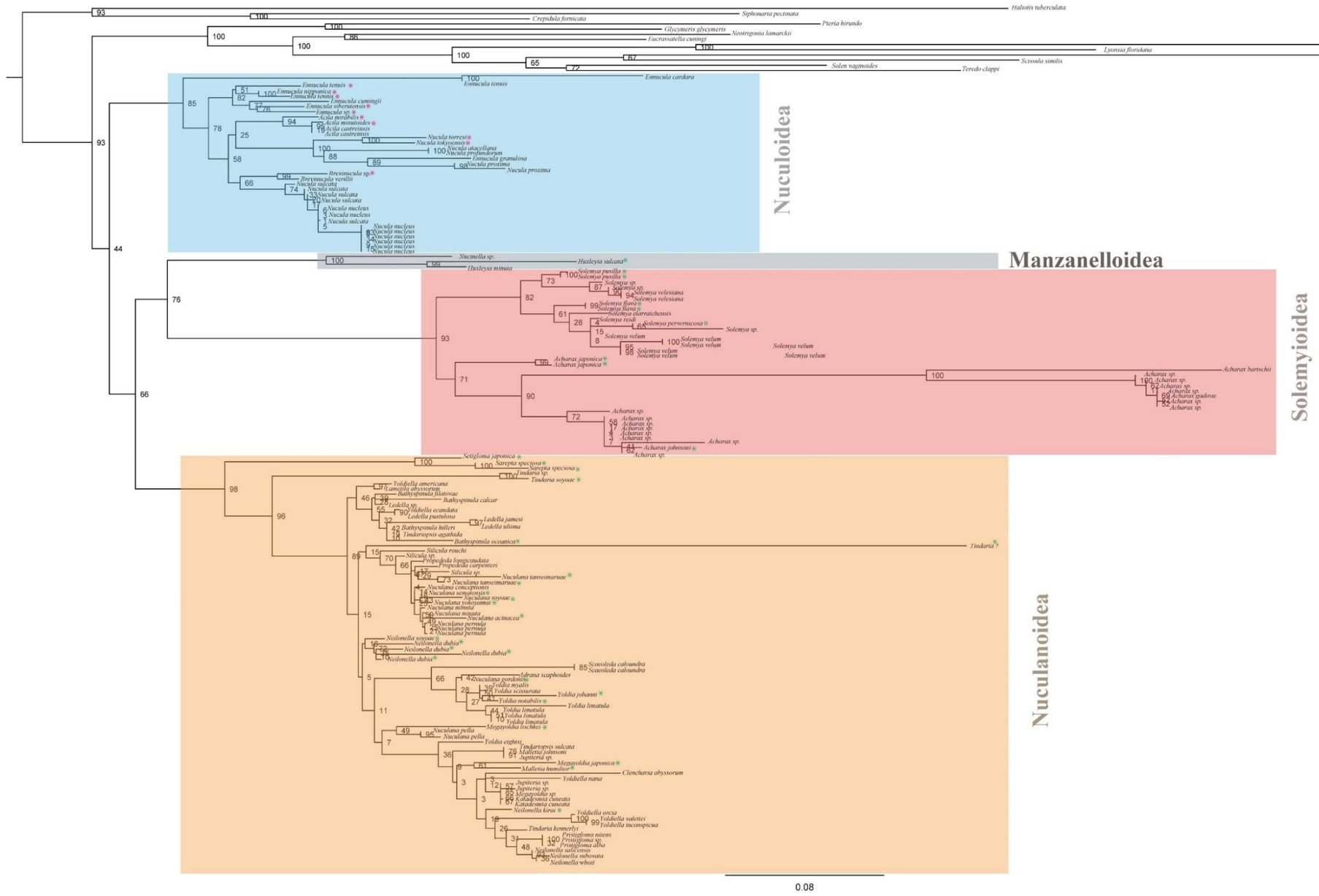

Figure 2.17. Phylogenetic relationships of Protobranchia based on the maximum likelihood analysis of seven nuclear genes. Numbers on nodes indicate bootstrap resampling frequencies. Major lineages were hilighted [blue: Nuculioidea (without Sareptidae), red: Solemyoidea, gray: Manzanelloidea, orange: Nuculanoidea (with Sareptidae)]. OTU names with asterisk mark is from this study.

2-4. Discussion

2-4-1. Higher-level relationship of Protobranchia

Protobranchs were traditionally proposed as a monophyletic group based on morphological characters (e.g. Cope, 1996; Morton, 1996), but this was not supported by molecular studies until recent years (e.g. Giribet & Distel, 2003; Wilson et al., 2010.). Recent phylogenomic study supported this hypothesis (Smith et al. 2011). Bieler et al. (2014) also exhibited the monophyly of protobranchs, both in their ML-based molecular phylogenetic tree using nine genes, and in Bayesian inference analysis using nine genes and morphological characters such as shell microstructure, larval characteristics, and muscle characteristics. Sharma et al. (2013) first implemented a comprehensive molecular phylogenetic analysis of protobranch bivalves, but they were not monophyletic (see supplementary figure 1 in Sharma et al., 2013). In this study, phylogenetic trees using five genes (Figure 2.15), seven genes (Figure 2.17) and nine genes (Figure 2.14) supported the monophyly of protobranch bivalves, although support values were low in all cases.

The major hypothesis of the superfamily-level relationship of protobranch bivalves is summarized as follows: 1) Cryptodonta (Solemyoidea)-Paleotaxodonta (Nuculoidea + Nuculanoidea) (Cope, 1996; Newell, 1965), and 2) Opponobranchia (Solemyids + Nuculoidea) and Nuculanoidea (Giribet, 2008). Nuculoidea and Nuculanoidea form mutual sister groups in Smith et al. (2011) and Sharma et al. (2013), and this result was consistent with the Cryptodonta-Paleotaxodonta hypothesis. On the other hand, the phylogenetic trees in Bieler et al. (2014) and in this study did not support either hypothesis, resulting in the sister groups of Solemyoidea, Manzanelloidea

and Nuculanoidea being reconstructed with anomalistic taxa as the family Sareptidae. This topology was unsupported in many previous studies but supported by Morton (1996) (see figure 1.1 in Chapter 1). Morton (1996) sited the Nuculoidea as a paraphyletic group of protobranchs based on feeding habit. Settled juveniles of *Nucula* use their foot to collect food prior to the development of their gills (Mortimer, 1962), and Morton deduced that ancestral bivalves had such a feeding habit. Though the result of recent phylogenomic study (Smith et al. 2011) does not agree with Morton's hypothesis, this deduction can be considered feasible, because phylogenomic analysis with insufficient taxon sampling inhibited the reconstruction of the true phylogenetic relationship. Smith et al. (2011) used only three species of protobranchs in their analysis. It is necessary to add further gene markers (particularly samples of Manzanelloidea) in order to reconstruct a robust phylogenetic tree. In terms of morphology, the earliest representation of protobranch bivalves was most likely in the form of nuculoid bivalves (e.g. Waller, 1998; Zardus, 2002). The provided topology in this study seems reasonable in this respect.

2-4-2. Superfamily Nuculoidea

According to the current classification, twelve genera are recognized in the family Nuculidae (Table 1.2). In this study, four genera, *Nucula*, *Ennucula*, *Brevinucula* and *Acila*, were used for phylogenetic analysis. *Acila* and *Brevinucula* formed a distinct monophyletic clade with strong support (bs = 91% for *Acila* and bs = 95% for *Brevinucula*), while *Nucula* and *Ennucula* formed polyphyletic groups.

The presence or absence of shell sculptures and crenulated inner ventral

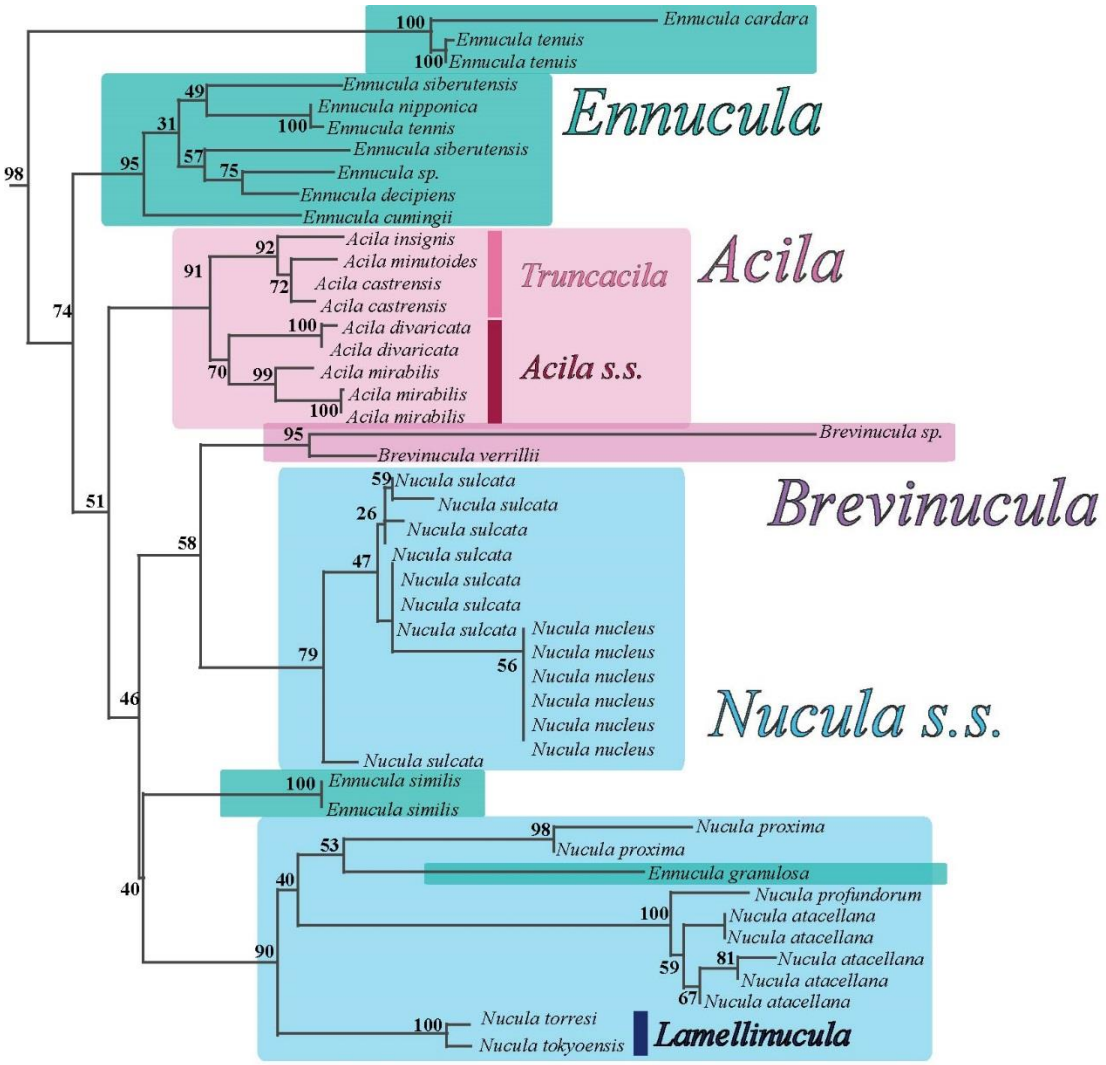

Figure 2.18. Part of ML based phylogenetic tree of nine genes (Figure 2.14) showing the Nuculiodea (without Sareptidae) topology. Numbers on nodes indicate bootstrap resampling frequencies. Each subgenera of Nuculanidea were hilighted.

margins are the basic diagnostic characteristics of Nuculoidea (e.g. Coan & Valentich-Scott, 2012). *Acila* can be easily distinguished from other nuculids by their divaricate riblets and crenulate inner margins. The genus *Acila* is further divided into two subgenera *Acila s.s.* and *Truncacila* based on the posteroventral morphology. *Acila s.s.* have a rostrate posterior end, and the posteroventral margins of *Truncacila* are rounded,

not rostrate. These two subgenera of *Acila* are well separated in the provided phylogenetic tree (bs = 91%). *Ennucula* is characterized by non-crenulated margins and a smooth shell surface, while *Nucula* has crenulated margins. The distinguishing characteristics of *Brevinucula* are the non-crenulate, smooth margins and the triangular shape. The topology of these three genera suggests that classification based on the existence of crenulate margins is questionable, as recognized by Gofas & Salas (1996), Kilburn (1999), and Sharma et al. (2013). *Lamellinucula*, a subgenus of *Nucula*, is different in having a strong commarginal sculpture. This subgenus formed a monophyly in the provided ML tree. However taxon sampling of *Lamellinucula* is not sufficient and there still remains the possibility that this subgenus is polyphyletic. The oldest fossil record among the all extant genera of Nuculoidea is the Cretaceous (*Nucula*, *Ennucula* and *Acila*) (Cox et al., 1969). Known extinct species of Nuculidae do not have crenulate margins in general. Ordovician-Devonian Nuculoidea species are the exception, and they have microscopically crenate margins (Cox et al., 1969). Crenate margins were never recognized in Praenuculidae, the extinct family of Nuculoidea. Thus, the lack of marginal crenulations seem to be a symplesiomorphy in Nuculoidea (Gofas & Salas, 1996). Coan et al. (2000) pointed out the possibility that the smooth margins in Nucuoidea can actually have microscopic crenulations.

Sareptidae, another family of Nuculoidea, was placed in the clade of Nuculanoidea by the ML analysis conducted by Sharma et al. (2013). They suggested the replacement of the family Sareptidae and, in addition, placed them as the superfamily Sareptoidea (order Nuculanida). For that reason, I discuss a systematic position of Sareptidae in the chapter ‘Superfamily Nuculanoidea’.

2-4-3. Superfamilies Solemyoidea and Manzanelloidea

The superfamily Solemyoidea consists of two genera, *Solemya* and *Acharax* which are distinguished by the position of a ligament (e.g. Cox, 1969; Pojeta, 1988). *Acharax* species have an external ligament while *Solemya* have an internal ligament. These two genera are clearly separated, forming distinct clades with strong support (bs = 100%) in the nine-gene ML tree provided by this study (Figure 4.6). The systematics of solemyids has long been controversial due to the simplicity of their external shell morphology and misunderstandings in the original descriptions. This dispute was resolved by Taylor et al. (2008) and widely accepted by other authors (Kamenev, 2009; Bailey, 2011; Oliver et al., 2011; Sato et al., 2013a). Taylor et al. (2008) redefined the five subgenera of *Solemya*; *Solemya s.s.*, *Petrasma*, *Solemyarina*, *Austrosolemya* and *Zesolemya* based on ligament characteristics and the poseterodorsal part of shell. In this study, the monophyly of *Solemyarina* was supported (bs = 80%) but not in *Solemya s.s.*. The subgenus *Petrasma* also showed a polyphyletic condition. According to the redefinition by Taylor et al. (2008), the difference between *Petrasma* and *Solemyarina* exists in the condition of the posterior adductor scar. *Petrasma* is diagnosed by the posterior adductor scar impressed into the shell surface with its anteroventral margin adjoined to the chondrophore. *Solemyarina* is characterized by an unimpressed posterior adductor scar that is not adjoining anteroventral margin of chondrophore. *Solemya s.s.* is distinguished from *Solemyarina* in the lack of an internal ligament expansion in front of the chondrophore. According to the topology in the provided nine-gene ML tree (Figure 4.6), the chondrophore seems to be an informative morphological character. Species of *Solemya* formed two distinct clades (bs = 100%) consisting of the *Solemyarina* + *Solemya*

s.s. (*Solemya pusilla*) clade and the *Petrasma* + *Solemya s.s.* (*Solemya flava*) clade. The species in the former clade have a weak, short chondrophore, and those in the latter develop the chondrophore, strong and wide in *Petrasma* and long in *Solemya flava* (see Taylor et al., 2008; Kamenev, 2009; Oliver et al., 2011; Sato et al., 2013b), while chondrophore morphology is unknown in *Solemya* sp. (data source in Rodrigues et al., 2011). Although *Solemya reidi* was synonymized with *Solemya pervernicosa* by Kamenev (2009), this study suggests that they are two distinct species.

Huber (2010) suggested *Pseudacharax* as a subgenus of *Acharax* based on shell morphology and habitat. *Pseudacharax* has an ovate shape and marginal fringes as in *Solemya*, but has an external ligament as in *Acharax*. The *Pseudacharax* species usually resides shallow intertidal or thalassic waters. The validity of *Pseudacharax* is supported by the topology of *Acharax japonica* in the ML analyses of this study with a strong support value (bs = 98%).

Although the support value was low (bs = 51%), Manzanelloidea formed a sister group to Solemyoidea with homologous anatomical characteristics, pointed out by Allen & Sanders (1969). Species of Solemyoidea generally lack an alimentary system (Kuznetsov & Schileyko, 1984; Reid, 1980; Kamenev, 2009) and commonly possess chemoautotrophic bacteria in their gills (Fisher, 1990; Distel, 1998; Fujiwara, 2003; Stewart & Cavanaugh, 2006). The Solemyid linage originated by the early Middle Ordovician (Whiterochkian) and its general morphology has been conservative since that time (Pojeta, 1988). Host and endosymbiont phylogenies are in agreement (Imhoff et al., 2003). These conditions suggest that the life habits of Solemyids are similar to those of living species. In fact, the Silurian solemyid *Janeia silurica* was associated with sediments interpreted as having reducing conditions, similar to habitats of recent

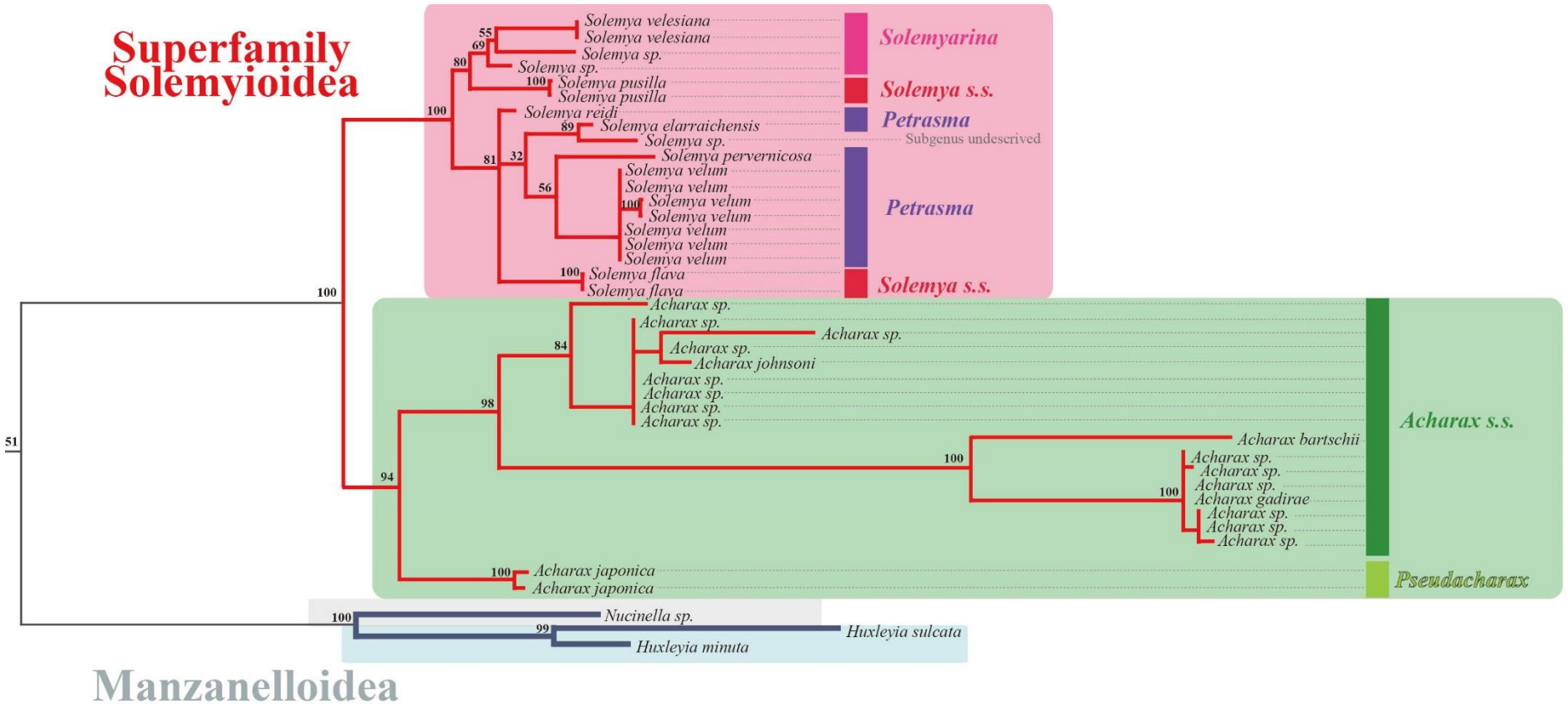

Figure 2.19. Part of ML based phylogenetic tree of nine genes (Figure 2.14) showing the Solemyoidea and Manzanelloidea topology. Numbers on nodes indicate bootstrap resampling frequencies. Each subgenera of Solemyoidea were noted.

species (Liljedahl, 1984, 1991) and to that of *Ilionia prisca*, an early lucinid, whose recent counterparts are known as chemosymbiotic bivalves (Taylor & Glover, 2010). The existence of possibly chemosynthetic rod-shaped bacteria was confirmed in species of Manzanelloidea, and an alimentary system suggests particulate feeding both in *Nucinella* and *Huxleyia* (Oliver & Taylor, 2012). These conditions support the acquisition of a chemosymbiotic life style before the differentiation between Solemyoidea and Manzanelloidea rather than parallel independent evolution in the two superfamilies. Manzanelloidea and Solemyoidea have been diverged at least since Permian (Pojeta, 1988; Cope, 2000). The Permian *Manzanella* is considered a possible ancestor of the Recent Manzanelloidea. Jurassic species of Manzanelloidea are associated with dysaerobic or organic rich sediments (e.g. Harries & Little, 1999; Wignall et al, 2005). Furthermore a large *Nucinella* species is associated with cold-seep deposits (Amano et al., 2007), suggesting that it employs chemosymbiosis. However, there is no evidence for the presence of symbionts in manzanelloidean species from the Paleozoic.

2-4-4. Family Sareptidae

Species of Sareptidae were paraphyletic to the Nuculanoidea in the nine-gene ML tree (Figure 2.20). The clade consisting of *Setigloma japonica* and the two specimens of *Sarepta speciosa*, were paraphyletic to the Nuculanoidea clade in all analyses, while the topology of the three *Pristigloma* species was unstable (see Figures 2.14-17). The *Pristigloma* clade is contained in Nuculanoidea and is sister to the clade of three *Neilonella* species in the ML tree using seven nuclear genes (Figure 2.17), but

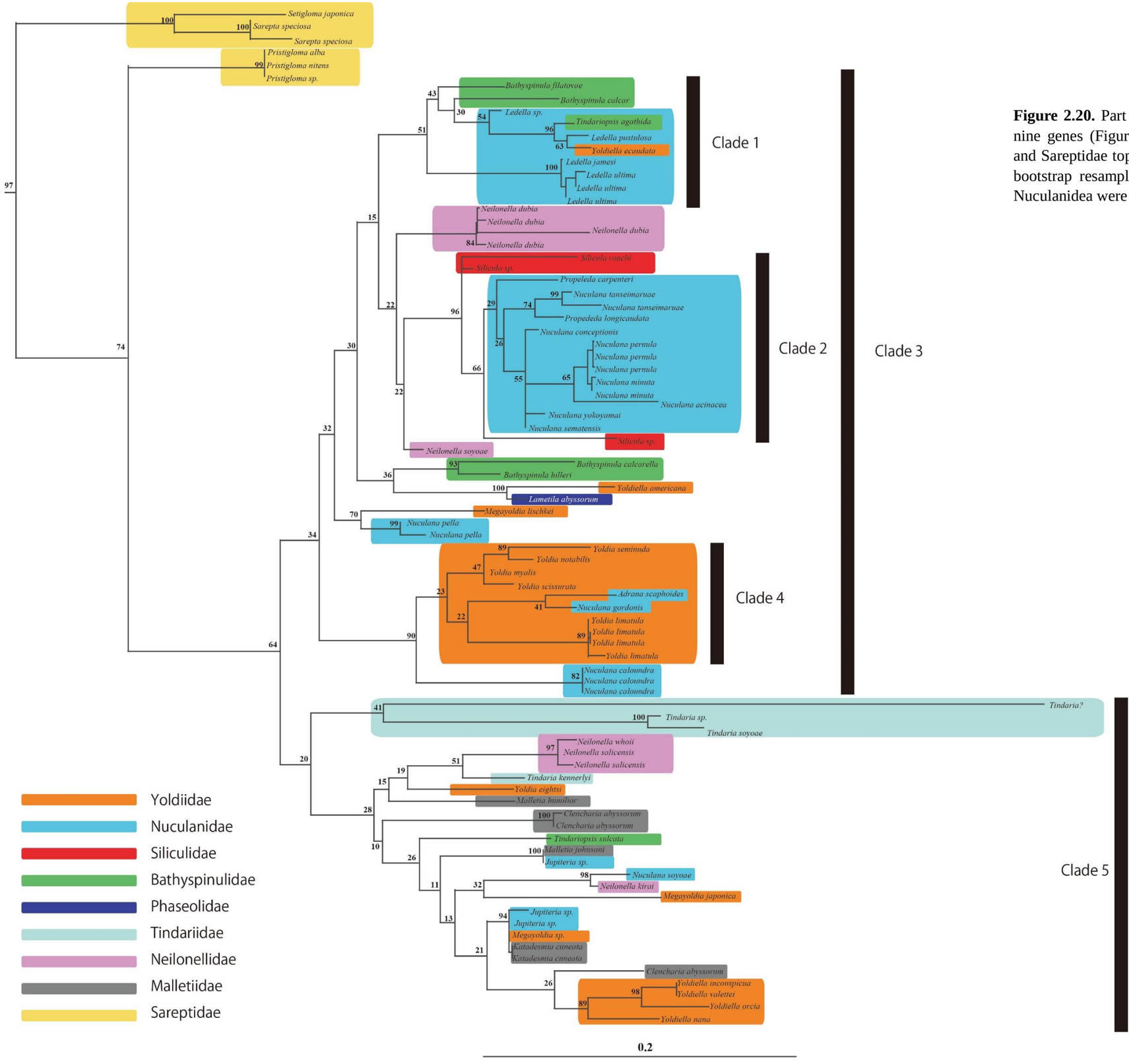

Figure 2.20. Part of ML based phylogenetic tree of nine genes (Figure 2.14) showing the Nucuanoidea and Sareptidae topology. Numbers on nodes indicate bootstrap resampling frequencies. Each families of Nuculanidea were hilighted.

not in the five- and nine-gene trees. This discrepancy may be due to the missing mitochondrial gene data in the *Pristigloma* species (Table 2.2), suggesting that it is necessary to add nuclear protein-encoding genes to the dataset used by Sharma et al. (2012). However, the topology of Sareptidae suggests inadequacy in the current classification scheme (e.g. Huber, 2010), and that the family is more closely allied to Nuculanoidea than to Nuculoidea in agreement with Sharma et al. (2013). Allen & Sanders (1973) recognized many shared characteristics between Pristiglomidae (*Pristigloma* and *Microgloma*) and Nuculidae (e.g., an anterior rather than a posterior inhalant current; lack of mantle fusion; mucus glands of the mantle located anteriorly, not posteriorly; siphons absent; palp large; and ligament internal). In contrast, Pristiglomidae and Nuculidae are distinguished by shell outline, ctenida size and filament number, ganglion morphology and hindgut morphology and position. The earliest representatives of protobranchs were most likely nuculoids (Waller, 1998) and Sareptidae was paraphyletic to Nuculanoidea in the nine-gene analysis of this study. Thus, the topology of Sareptidae in the provided molecular phylogenetic tree suggests that these shared characters may be symplesiomorphies of protobranchs. Sharma et al. (2013) estimated the divergence time of Sareptidae (*Pristigloma* in their analysis) from other Nuculanoidea based on their parsimonion tree, which has a similar topology to that of the ML tree in this study. According to them, divergence dated back to the Ordovicain and/or Early Silurian. This estimation seems to be plausible, however, fossil records do not agree with it, because there is no fossil record of Sareptidae for conformation (Cox, 1969). One hypothesis explaining this contradiction is the confusion of fossil Sareptidae and Nuculoidea, due to their similar shell morphology.

As mentioned in Chapter 1, the placement of the family Sareptidae has long

been confused until this study, and five genera possibly related to the family Sareptidae are controversial (see Table 2.6). Molecular data of three of the five 'sareptid-like' genera, *Pristigloma*, *Setigloma* and *Sarepta*, were used in this study. As stated above, *Sarepta* and *Setigloma* formed a monophyletic group but did not include *Pristigloma*. Ockelmann & Warén (1998) showed the similarity in hinge and ligament morphologies between *Sarepta speciosa* and *Setigloma japonica*. Schileyko (1983) assumed that *Setigloma* and *Pristigloma* were closely related to one another. The former study agreed with the provided topology, while the latter did not. Five genera of probable Sareptidae may be polyphyletic, and the identification of additional anatomical characteristics is required for better understanding.

Table 2.6. List of the papers refering to the classification of probable sareptids and their interpretations.

	Cox (1969)	Allen & Sanders (1973)	Schileyko (1983)	Allen & Hannah (1986)	Ockelmann & Warén (1998)	Coan (2000)	Huber (2010)
***Pristigloma* Dall (1990)**	Superfamily Nuculanoidea, Family Nuculanidae	Superfamily Nuculoidea, Family Pristiglomidae	Superfamily Nuculanoidea, Family Pristiglomidae	Superfamily Nuculoidea, Family Pristiglomidae	not mentioned, but refered to the description of Schileyko (1983)	Order Nuculoida, Superfamily Pristiglomoidea, Family Pristiglomidae	Order Nuculoida, Superfamily Sareptoidea, Family Sareptidae
***Setigloma* Shileyko (1983)**	-	not mentioned	Superfamily Nuculanoidea, Family Pristiglomidae	not mentioned	not mentioned, but refered to the description of Schileyko (1983)	Order Nuculoida, Superfamily Pristiglomoidea, Family Pristiglomidae	Order Nuculoida, Superfamily Sareptoidea, Family Sareptidae
***Sarepta* Adams (1860)**	Superfamily Nuculanoidea, Family Nuculanidae	not mentioned	not mentioned	Superfamily Nuculanoidea, Family Yoldiidae	not mentioned	not mentioned	Order Nuculoida, Superfamily Sareptoidea, Family Sareptidae
***Microgloma* Allen & Sanders (1973)**	-	Superfamily Nuculoidea, Family Pristiglomidae	not mentioned	Superfamily Nuculoidea, Family Pristiglomidae	Close to Superfamily Nuculanoidea, Family Yoldiidae?	not mentioned	Superfamily Nuculanoidea, Family Yoldiidae
***Pseudoglomus* Dall (1898)**	Superfamily Nuculanoidea, Family Malletiidae	not mentioned	not mentioned	Superfamily Nuculoidea, Family Pristiglomidae	Close to Superfamily Nuculanoidea, Family Malletidae, Neilonellidae and Tindaridae?	Order Nuculoida, Superfamily Pristiglomoidea, Family Pristiglomidae	Superfamily Nuculanoidea, Family Malletidae
Other description	-	Suggested family Pristiglomidae	-	-	Considered Pristiglomidae as junior synonym of Sareptidae Adams, 1860.	-	-

2-4-5. Superfamily Nuculanoidea

Sharma et al. (2013) performed ML and Bayesian phylogenetic analyses using 77 in-group datasets and recognized considerable inconsistencies in the phylogenetic

relationships within and among genera of Nuculanoidea. The additional taxon sampling and the extra four gene markers in this study could not recover this condition. All known eight families of Nuculanoidea (i.e., Nuculanidae, Bathyspinulidae, Maletiidae, Neilonellidae, Phaseolidae, Siliculidae Tindariidae and Yoldiidae) were analyzed, and none of them formed monophyletic groups. In general, support values of clades in Nuculanoidea are low in this study. Hence, provided topology indicates that a true genetic relationship is doubtful and that adding more gene markers is necessary for molecular phylogenetic analysis. However, some topology in the ML tree is consistent with the findings of previous studies on anatomical analysis (as discussed later).

Bathyspinulidae (*Bathyspinula* and *Tindariopsis*) and *Ledela* (Nuculanidae) formed a clade (clade 1 in Figure 2.20), while *Yoldiella ecaudata* (Yoldiidae) was contained in that clade. *Y. ecaudata* was originally described as *Ledella ecaudata* (Filatova & Schileyko, 1984), however Huber (2010) reclassified the species into the genus *Yoldiella*. My results suggest that the reclassification by Huber (2010) was invalid and, consequently, that the monophyly of the genus *Ledella* together with Bathyspinulidae was supported with relatively low reliability (bs = 51%). The same result was reported by Sharma et al. (2013), and the placement of *Bathyspinula* within *Ledella* was obtained by nuclear gene tree topologies (Boyle, 2011). Allen & Sanders (1982) reported that *Ledella* and *Bathyspinula* are closely related in having rostrate posterior margins and an internal, amphidetic ligament. By contrast, the paraphyletic condition in Bathyspinulidae was unexplainable (illustrated by clade 1 in Figure 2.20 and the clade consisting of *Bathyspinula calcarlella* and *Bathyspinula hilleri*).

Clade 2 (Figure 2.20) consists of two families; Nuculanidae (*Propeleda* and *Nuculana*) and Siliculidae. This is strongly supported by their monophyly (bs = 96%).

Allen & Sanders (1973) suggested that the anatomical characteristics, shell structure, hinge line, umbo size, and ligament indicate a close relationship between *Silicula* and *Propeleda*. The family Siliculidae differs from *Propeleda* in having unique elongated teeth. The family Phaseolidae is also characterized by elongated teeth as Siliculidae, although some species of Phaseolidae lack their teeth. While Siliculidae and Phaseolidae are considered related taxa (Allen & Sanders, 1973), elongated teeth seems to be a synapomorphy. Provided topology did not support validity of this characteristic as a tool to diagnose family. *Lametila abyssorum* in the family Phaseolidae seems to be related with *Yoldiella*, not with *Silicula*, because this species formed a distinct clade with *Yoldiella americana* (bs = 100%). Indeed, they resemble each other in their umbos with raised crest and an oblong, rounded outline, although their hinge teeth morphology is entirely different.

Our *Neilonella* specimens are paraphyletic to clade 2 (Figure 2.20), while *Neilonella* species from GenBank formed a distinct clade that was entirely detached from clade 2 (Figure 2.20). Species of *Neilonella* are clearly distinguished from other OTUs of clade 3 in not having a resilifer. I identified some species as *Neilonella* based on shell outline following Okutani (2000). However, I also recognized that some specimens of "*Neilonella"* having an internal ligament on a short gap in the dentition under the beaks. If so, reassessment of West Pacific *Neilonella* species may be required. *Neilonella* species from the East Pacific and the Atlantic were well analyzed anatomically by Allen & Sanders (1996).

The family Nuculanidae is not included in clade 2 and Yoldiidae is widely polyphyletic. These relationships were unexplainable, probably due to an insufficient data set. Several *Yoldia* species formed a clade (clade 4), but this clade included two

nuculanid species with a very low support value (bs = 23%).

Cox (1969) divided Nuculanoidea into two families, Malletiidae and Nuculaniidae based on the presence or absence of a resilifer. Malletiidae commonly lack a resilifer, which is present in Nuculaniidae. This classification is now rejected; however, the resilifer is one of the important characteristics in the systematics of Nuculanoidea. The geological range of fossil occurrence in Cox (1969) suggests that the absence of a resilifer is a probable symplesiomorphy of Nuculanoidea and other protobranchs. Clade 3 did not include taxa without a resilifer, if the above mentioned *Neilonella* hypothesis was correct. On the other hand, several taxa belonging to the families Neilonellidae, Tindariidae and Malletiidae, without resilifer are included in the clade 5.

Nuculanoidea evolved from the primitive state of inhalant flow to the advanced state of posterior inhalant flow (Allen, 1985) along with the development of an inhalant siphon and shell elongation. In this respect, *Tindaria* is considered a primitive nuculanoidean genus in possessing an oval shape and lacking siphons (Zardus, 2002). In this study, *Tindaria* species, excluding *Tindaria kennerlyi* were paraphyletic to other nuculanoideans in the five-gene ML and the seven-gene ML trees (without *Tindaria?* specimen) but included in Nuculanoidea in the nine-gene ML tree. *Tindaria kennerlyi* is a sister to three *Neilonella* species with a weak support value (bs = 51%). *Tindaria* species closely resemble *Neilonella* but differ in lacking siphons (Sanders & Allen, 1977). Thus, this topology suggests either polyphyly of *Tindaria* or misclassification of *Tindaria kennerlyi.*

In Nuculanoidea, anatomical and molecular phylogenetic analyses are necessary for future studies to avoid misclassification and probable false polyphyletic

condition. *Tindariopsis sulcata* was included in the ML tree of this study from Sharma et al. (2013). However, this species is supposed to be an extinct species (Griffin & Nielsen, 2008). Like this, molecular data from the GenBank may contain specimens with incorrect identifications.

2-5. Summary

The monophyly of the Protobranchia was supported by ML-based molecular analysis in this study, although the support value was not significant. Each of four superfamilies of protobranchs formed a distinct monophyletic clade with the exception of the family Sareptidae. The nine-gene ML tree in this study first demonstrated that species of Sareptidae was situated paraphyletic to the Nuculanoidea, while they have been classified into Nuculoidea. The family-level monophyly was not supported in the Nuculanoidea. Further molecular analysis and revision of classification are required in this taxon. On the other hand, genus/family-level monophyly was substantiated in Solemyoida and Nuculanoidea in general.

Chapter 3

Descriptions of shell microstructures

3-1. Introduction

To characterize the shell microstructure of protobranchs, SEM observations on shell microstructures were performed. This chapter contains descriptions of the shell microstructure of 38 modern protobranch species (see Table 2.1). The component of the shell layer and shell microstructures of each layer are described by taxa, and they are summarized in Table 3.3 and Table 5.1 (in Chapter 5) together with the descriptions of protobranch shell microstructures from previous studies for discussion of the shell microstructural evolution. Terminology for the shell microstructure is based on Carter & Clark (1985) and Carter (1990a) but some are newly classified into a new microstructure or sub-type of a known microstructure in case a definite difference is recognized.

3-2. Material and Methods

3-2-1. Material

To evaluate intra-and interspecific variations in shell microstructures and their crystallographic texture and genetic relationships, a total of 38 species were used in this study. This taxon sampling covers 10 of 12 known families and 16 of 54 genera of living protobranchs. Several specimens identified as the same species were used in all

analysis in order to detect the existence of cryptic species and intraspecific variations in shell microstructural and crystallographic texture. All specimens and their habitat, along with their applications are listed in Table 2.1.

3-2-2. Observations of shell microstructures

Shell microstructures were observed with a scanning electron microscope (Keyence-VE8800, JEOL-5600lv, Hitachi-S2250N) and field-emission-type scanning electron microscope (Hitachi-S4500) on fractured and polished planes in radial, transverse, and horizontal sections. Polished planes were filled with polyester resin (Polyester Solidifier; Nichika Corp.) or epoxy resin (S-31, Devcon Corp.) prior to cutting. The polished planes or fragments were treated by one of the following methods: (1) etching with 0.2% HCl for 1–30 minutes, (2) removal of organic materials with sodium hypochlorite for 10–120 minutes, (3) etching with 0.2% HCl for 1–5 minutes after immersion in sodium hypochlorite for 30 minutes, or (4) non-chemical treatment. After cleaning with an ultrasonic cleaner, the planes were coated with platinum or osmium.

In this study, we followed the terminologies of Carter & Clark (1985) and Carter (1990a) for the shell microstructure descriptions. Terms for the first-, second-, and third-order structures are used to describe the microstructural organizations at different scales. The first order indicates the primary microstructural element of a shell layer.

3-3. Abbreviations

CA, crossed acicular structure; cCCL, cone complex crossed lamellar structure; CN, columnar nacreous structure; CP, composite prismatic structure; dCL, diffuse crossed lamellar structure; DCP, denticular composite prismatic structure; FA, foliated aragonite structure; FC, flattened crystallites; fCCL, fine complex crossed lamellar structure; fCL, fine crossed lamellae; fLi, finely laminated structure; FP, fibrous prismatic structure; Fic, finely crystalline; Hom, homogeneous structure; iCCL, irregular complex crossed lamellar structure; ICN, irregularly columnar nacreous structure; ISP, irregular simple prismatic structure; IFP, irregular fibrous prismatic structure; ISPP, irregular spherulitic prismatic structure; Lam, laminar structure; Le, lamellar structure; Li, laminated structure; N, nacreous structure; nd, not described; P, prismatic structure; Por, porcelaneous; RESP, radially elongate prismatic structure; SN, sheet nacreous structure; SP, simple prismatic structure; Sph, spherulitic structure.

3-4. Results

Superfamily Nuculoidea

Family Nuculidae

Acila mirabilis (Adams & Reeve, 1850)

Figures 3.1-4

Shell layers.—The outer, middle, myostracum and inner layers are present (Figure 3.1). The outer layer is composed of a composite prismatic structure. The middle and inner layers are nacreous structures, but their neighboring tablets pile up

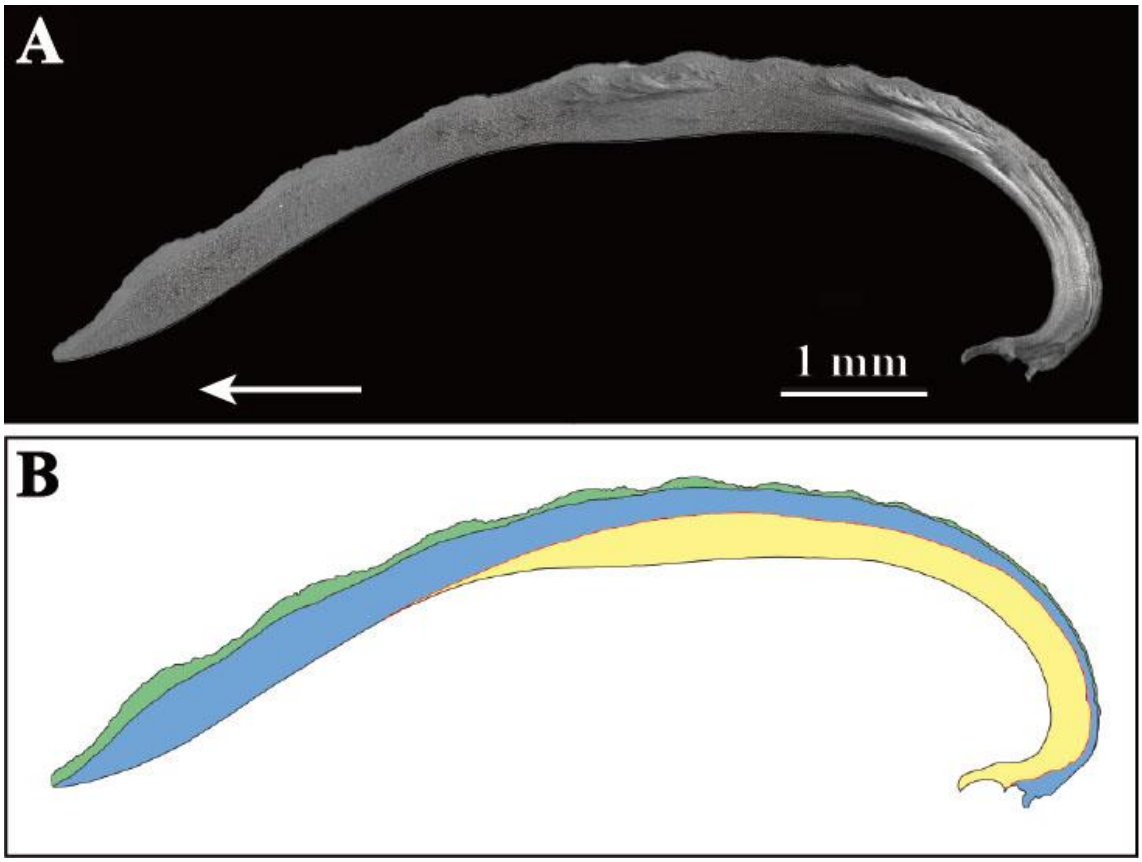

Figure 3.1. A, radial section of observed *Acila mirabilis*. White arrow indicates the growth direction. **B,** pattern diagram of A showing the distribution of shell layers. Outer layer, green; middle layer, blue; myostracum, red; inner layer, yellow.

differently. Vertically stacking nacre tablets dominate in the middle layer as a columnar nacreous structure and tablets show a brick-like appearance in all vertical sections as a sheet nacreous structure. Both middle and inner layers are divided by the myostracum composed of an irregular simple prismatic to homogeneous structure. The outer and middle layer thickens ventrally. The inner layer lies dorsal to the pallial line and also thickens dorsally, whereas the thickest part is distributed in the middle part of a radial section. The myostracum thickens ventrally with growth. However, it becomes thinner

subsequently and nearly disappears in the ventral part. The shell is up to approximately 550 μm thick in the observed specimen. The middle part of shell is the thickest.

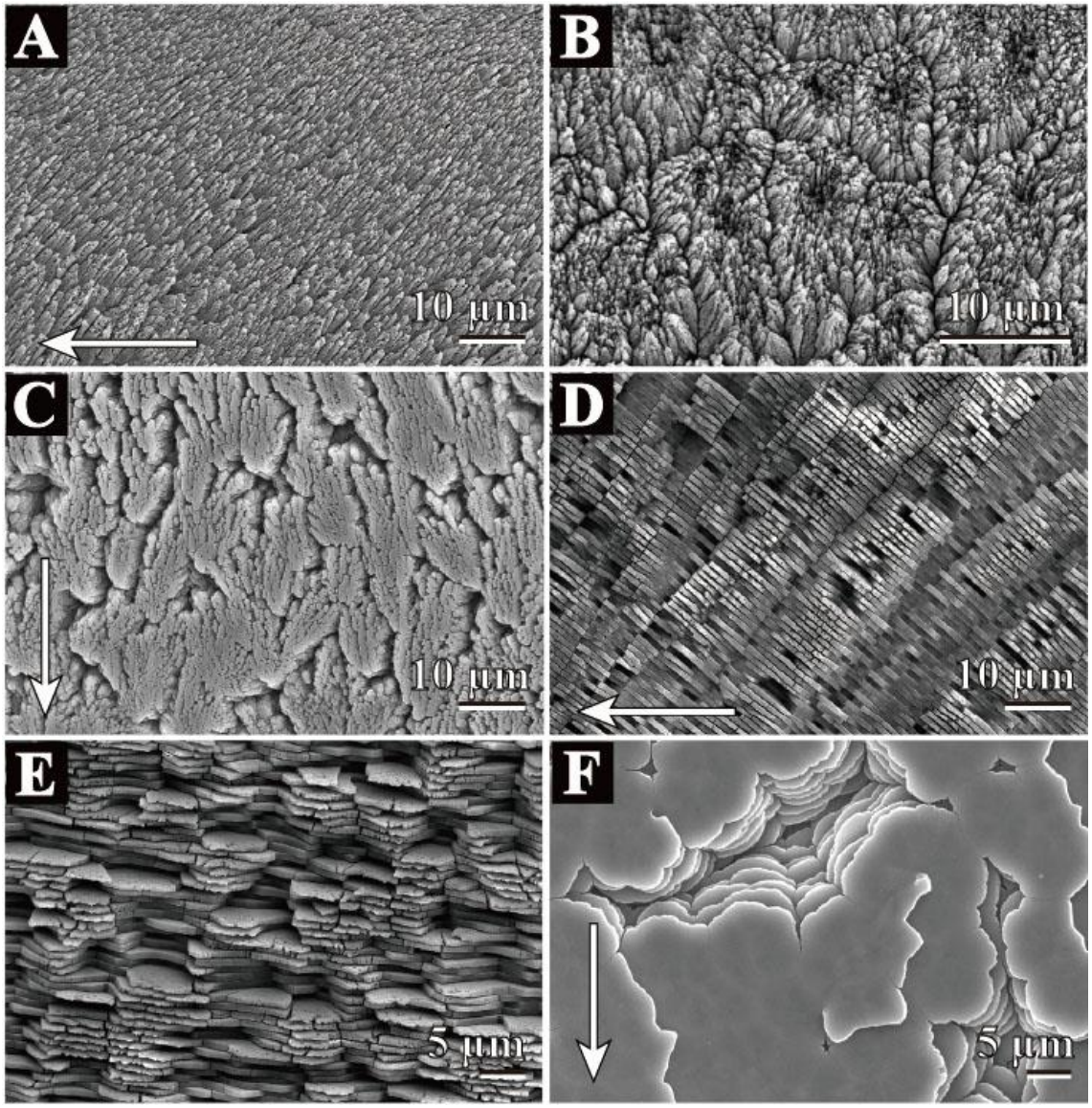

Figure 3.2. Scanning electron micrographs of *Acila mirabilis* microstructure. White arrow indicate growth direction. **A.** radial section of composite prismatic structure type-A of the outer layer. **B,** transverse section of composite prismatic structure type-A of the outer layer. **C,** inner surface of composite prismatic structure type-A of the outer layer. **D,** radial section of columnar nacreous structure of the middle layer. **E,** transverse section of columnar nacreous structure of the middle layer. F, inner surface of columnar nacreous structure of the middle layer. A, B, D, E, middle part of shell; C, F, ventral part of shell. A-F, Shell lengh = 11 mm.

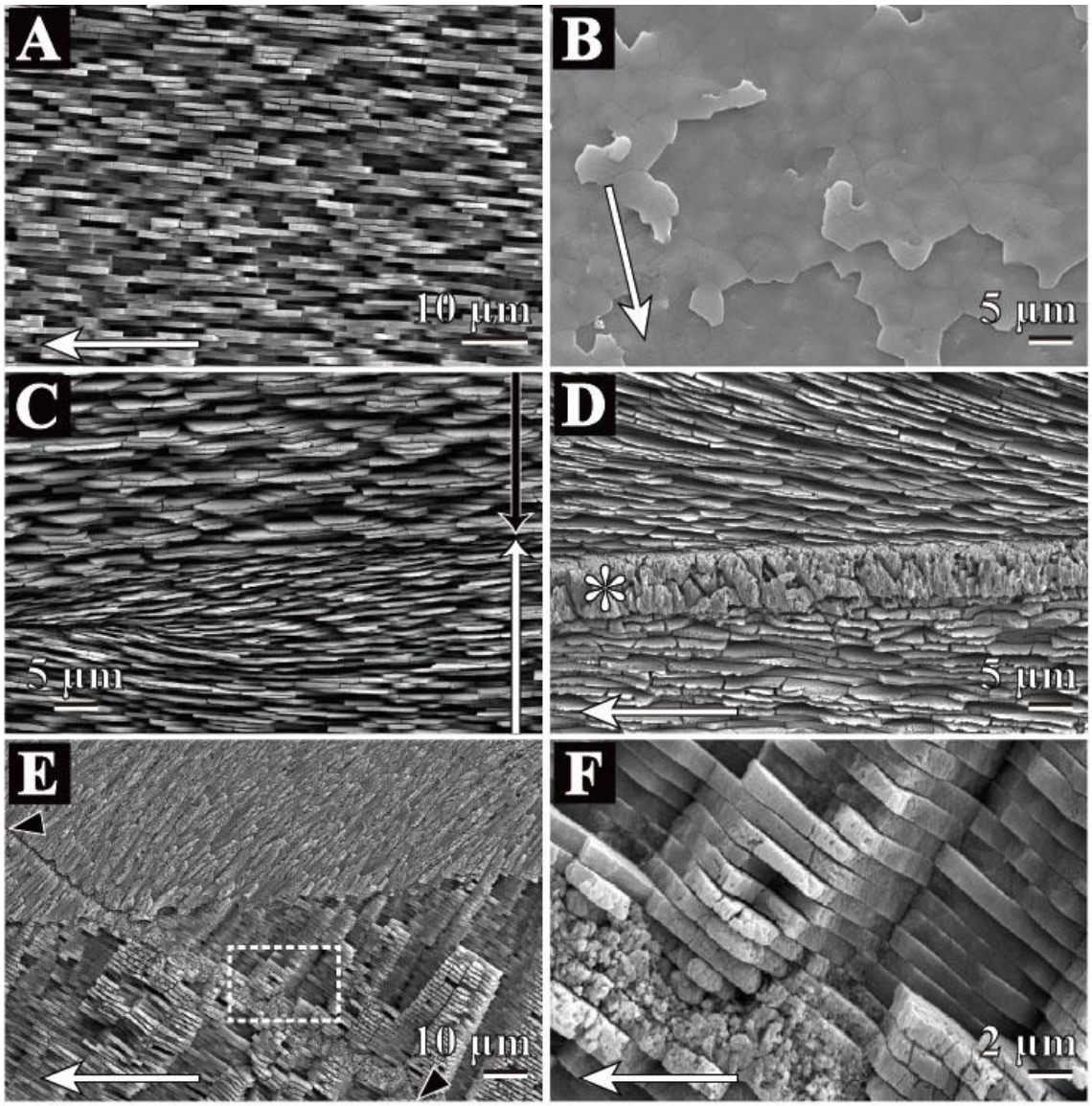

Figure 3.3. Scanning electron micrographs of *Acila mirabilis* microstructure. Holizontal white arrow indicate growth direction. **A.** radial section of sheet nacreous structure of the inner layer. **B,** inner surface of sheet nacreous of the inner layer. **C,** transverse section of nacreous structure of the middle and inner layers at ventral part of shell. Black arrow indicates the middle layer and white arrow exhibits the inner layer. **D,** radial section of nacreous structure of the middle and inner layers at dorsal part of shell. Asterisk mark indicates myostracum layer. **E,** radial section of the outer and middle layers. Black arrowhead indicates the growth line. **F,** closer view of broken-lined square in E. Homogeneous structure was recognized at the growth line. A, E, F, middle part of shell; B, C, ventral part of shell. D, dorsal part of shell. A-F, Shell lengh = 11 mm.

Outer layer.—Composite prismatic structure type-A (Figures 3.2A-C, 3.3E, 3.4D; for type of prismatic structures, see Table 3.1). The outer layer is consists of acicular crystals; it is approximately 3 μm in diameter and 30 μm long (Figures 3.2A, 3.3E). These crystals slant at angles of approximately 10–80° against the growth direction in a radial section and compose the first-order prisms weakly radiating toward the depositional surface (Figures 3.2B, C). The average width of the first-order prisms is approximately 10 μm.

Table 2.1. The characterization of the types of prismatic structure in nuculids.

Prism type	First order	Second order	Species
CP type-A	First order prisms consisting of acicular prisms that weakely radiate to depositional surface or align in parallel.	Long (high lengh/ width ratio) acicular crystals	*A. insignis, A. minutoides, A. mirabilis, E* sp.2
CP type-B	First order prisms consisting of acicular prisms that radiate to depositional surface or aline in parallel.	Short (low lengh/ width ratio) acicular crystals	*E. tenuis, E. nipponica,*
DCP	Consisted of second-order prisms spreading like a fan ventrally and the boundary between inner most part of the outr layer is recognized as dentateline.	Long (high lengh/ width ratio) acicular crystals	*N. torresi, N. tokyoensis*
IFP type-A	Consisted of two sublayers.	The outer sublayer is consisted of thin acicular crystals deeply slanting against the growth direction and the inner sublayer is composed of thick acicular crystals shortly slanting.	*B.* sp.
IFP type-B	Acicular crystals slant at deep angle against the growth direction at outer part and bend to the growth direction.	L shaped acicular crystals.	*E. siberutensis, E.* sp.1

Middle layer.—Columnar nacreous structure (Figure 3.2D-F). Nearly polygonal tablets stack vertically on the exterior side, but gradually shift to an irregularly stacked sheet nacre toward the shell interior. At the innermost part of the middle layer, they pile up like a brick wall and are hardly distinguishable from the inner layer, which consists of a sheet nacreous structure (Figures 3.2C, D). Nacre columns stack on a tilt parallel to the long axes of acicular crystals of the outer layer at the

outermost part of the middle layer and nearly vertically at the innermost part. While each tablet connects to the next tablet in a narrow sense (Figure 3.2F), the width of each assumed tablets is around 6 μm. Thickness of the tablets is approximately 1 μm at the outer part of the middle layer; it reduced inward, reaching 0.3 μm. Nacre tablets grow spirally unlike the columnar nacreous structure in gastropods and cephalopods (Bandel, 1990a, b) (Figure 3.2F). Homogeneous structure is recognized at growth lines (Figure 3.3F).

Myostracum.—Irregular simple prismatic structure and homogeneous structure (Figures 3.3C, D, 3.4C, D). At the most thickened part, irregularly shaped acicular crystals, which are around 5 μm long in the long axes, compose the myostracum (Figure 3.3D). At the thinned part, irregularly shaped blocky crystals, which are sort of false nacre tablets, compose the myostracum. Only nano-scaled granular crystals are distributed between nacre tablets where the myostracum is thinner (Figures 3.3C, 3.4B-E). Nacre tablets in the middle layer and granular crystals are distributed at the pallial line and adductor muscle scars in the observed specimen (Figure 3.4).

Inner layer.—Sheet nacreous structure (Figures 3.3A-D, 3.4B, C). Nacre tablets are approximately 0.7 μm thick and brick-like. Although the boundary of adjacent tablets is indistinct and fused with each other (Figure 3.3B), their width is around 4–10 μm. Nacre tablets in the inner layer show a spiral growth pattern as in the middle layer (Figure 3.3B).

Figure 3.4 (next page)**.** Scanning electron micrographs of *Acila mirabilis* microstructure. **A.** inner surface of *Acila mirabilis*. **B,** closer view of broken-lined square in A. Black arrow indicates the inner layer and white arrow exhibits the pallial line, where nacre tablets and granular crystals distribute. **C,** closer view of broken-lined square in B. **D,** closer view of broken-lined square in A. white arrow indicates the pallial line and gray arrow indicates the middle layer. Question mark implies indistinct boundary of them. **E,** closer view of broken-lined square in A, exhibiting nacre tablets and granular crystals of pallial line. A-E, Shell lengh = 11 mm.

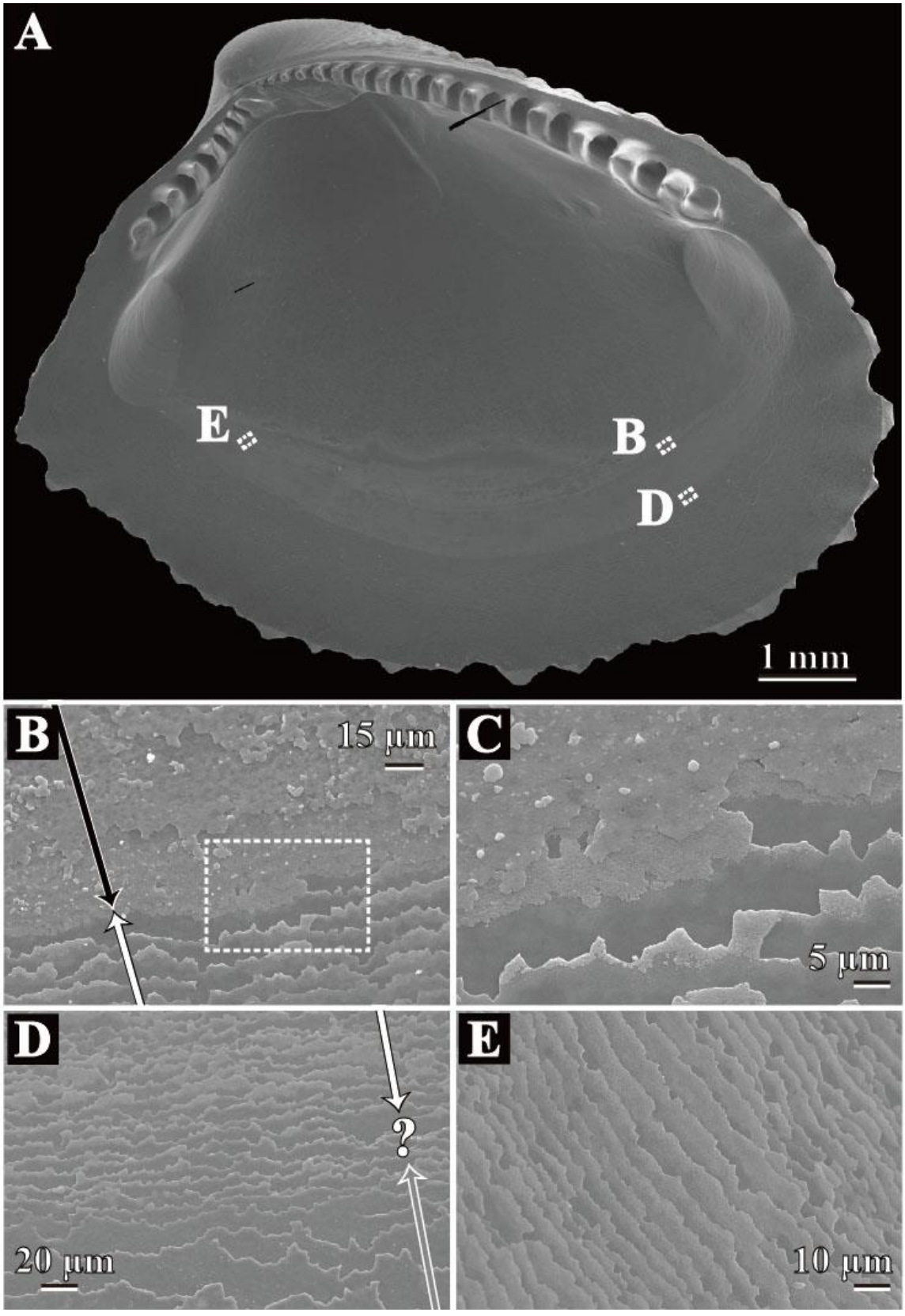
A
E
B
D
1 mm
B
15 µm
C
5 µm
D
?
20 µm
E
10 µm

Acila minutoides Kuroda & Habe in Habe, 1958

Figures 3.5, 6

Shell layers.—Outer, middle, myostracum and inner layers are present (Figure 3.5). The outer layer is composed of fibrous prismatic or rarely composite prismatic structure type-A. The middle layer is a columnar nacreous to sheet nacreous structure. The myostracum is composed of irregularly shaped blocky crystals at the dorsal part, but is indistinct at the ventral part. The inner layer is a sheet nacreous structure. The outer and middle layers thicken ventrally, and the inner layer generally thickens dorsally. The boundary between the middle and inner layers is indistinct at the ventral and dorsal parts due to thinning of the myostracum. The shell thickens at the ventral part and is up to approximately 270 μm thick in the observed specimen.

Outer layer.—Composite prismatic structure type-A and fibrous prismatic structure (Figure 3.5B–E). The outer layer consists of acicular crystals up to approximately 2.5 μm in diameter and approaches approximately 22 μm long in the long axis (Figure 3.5D, E). These crystals slant at an angle of approximately 40° to 90° against the growth direction in the radial section. Acicular crystals align parallel to nearby crystals and do not form the first-order prisms at the thickened part (fibrous prismatic; 3.5D, E), and compose the first-order prisms weakly at the thin part (composite prismatic, 3.5B), weakly radiating toward the depositional surface.

Middle layer.—Columnar nacreous structure (Figures 3.5B–C, 3.6A–B). Nacreous tablets weakly stack vertically at the exterior side (columnar nacreous) and are brick-like (sheet nacreous) due to inwards weakening vertical stacking. Nacre tablets are around 1.5 μm thick at the exterior side (Figure 3.6A, B) and become thinner inwards

(around 0.8 μm; Figure 3.6E, F). Although the boundary of adjacent tablets is indistinct due to fusion, the width of individual tablets is around 3–10 μm.

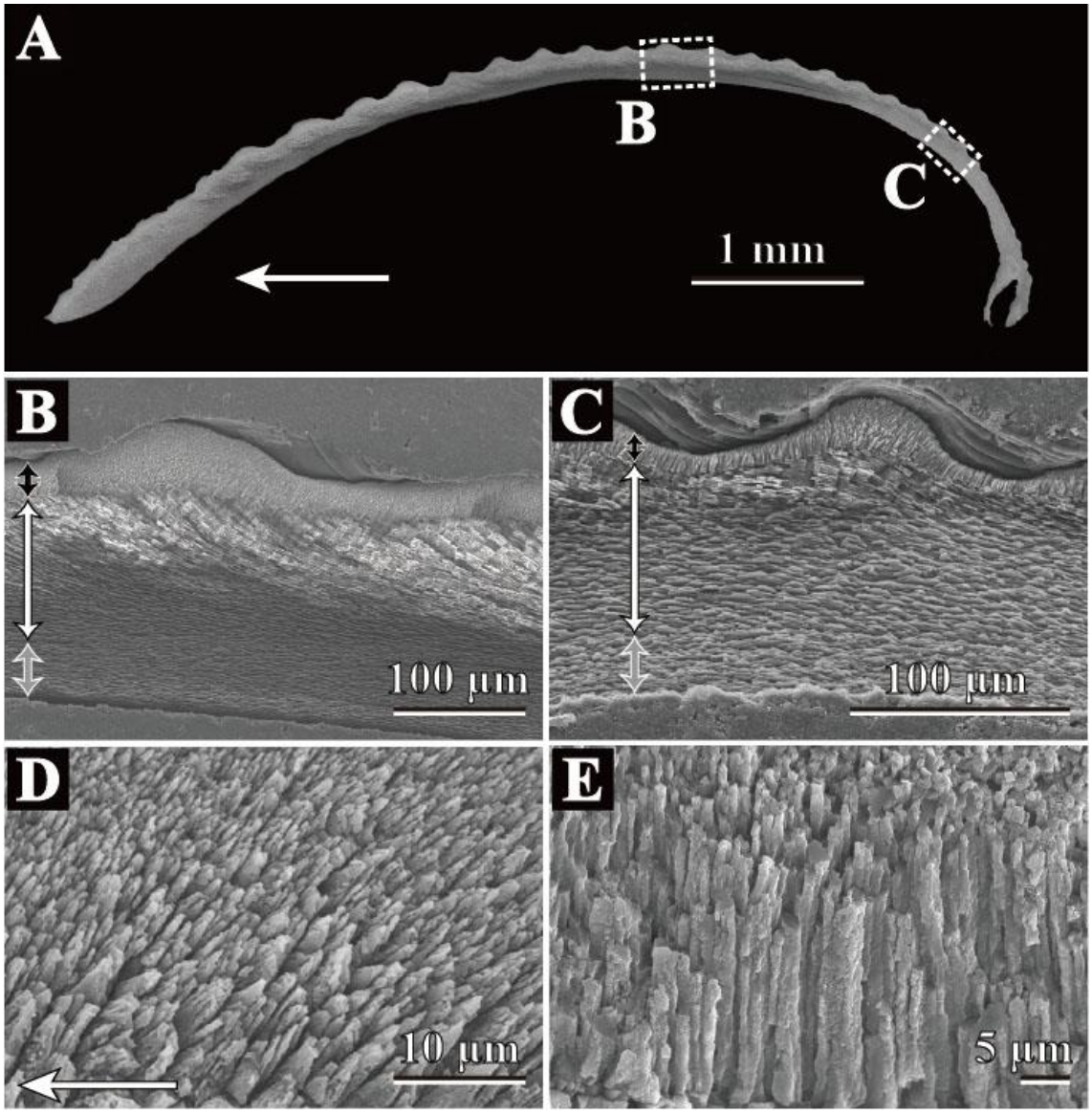

Figure 3.5. Scanning electron micrographs of *Acila minutoides* microstructure. White arrow indicate growth direction. **A.** radial section of observed *Acila minutoides*. **B,** closer view of broken-lined square in A showing middle part of the shell section. Black arrow, the outer layer; white arrow, the middle layer; gray arrow, inner layer. **C,** closer view of broken-lined square in A showing dorsal part of the shell section. Black arrow, the outer layer; white arrow, the middle layer; gray arrow, inner layer. **D,** radial section of composite prismatic structure type-A of the outer layer. **E,** transverse section of fibrous prismatic structure of the outer layer. D, E, middle part of shell. A-E, Shell lengh = 7 mm.

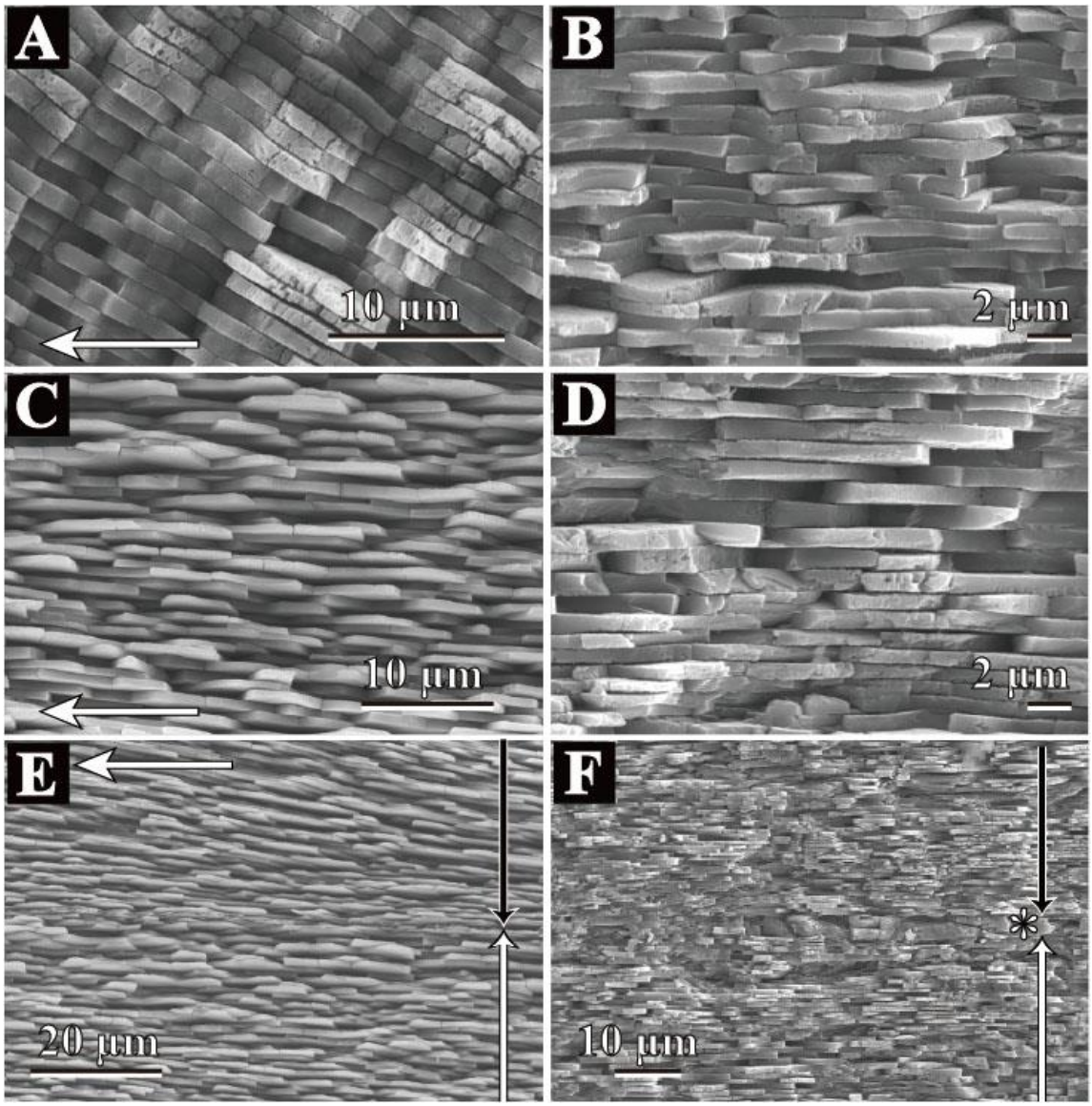

Figure 3.6. Scanning electron micrographs of *Acila minutoides* microstructure. Horizontal white arrow indicate growth direction. **A.** radial section of columnar nacreous structure of the middle layer. **B,** transverse section of nacreous structure of the middle layer. **C,** radial section of sheet nacreous structure of the inner layer. **D,** transverse section of sheet nacreous structure of the inner layer. **E,** radial section of nacreous structure of the middle and inner layers at ventral part of shell. Myostracum layer is indistinct. Vertical black arrow indicates the middle layer and white arrow indicates the inner layer. **F,** transverse section of nacreous structure of the middle and inner layers at dorsal part of shell. Myostracum layer is consist of irregular blocky crystals. Vertical black arrow indicates the middle layer. Asterisk mark shows the myostracum layer and white arrow is the inner layer. A-F, middle part of shell. A-F, Shell lengh = 7 mm.

Myostracum.—This layer consists of irregular blocky crystals or granular crystals (Figure 3.6E, F) which are mostly very thin (less than 1 μm) and filled with granular crystals (Figure 3.6E). The most thickened part exhibits irregular blocky crystals (up to 4 μm thick) (Figure 3.6F).

Inner layer.—Sheet nacreous (Figure 3.6C-F). Irregular polygonal tablets are approximately 0.6 μm thick and brick-like (Figure 3.6C, D). The boundary of adjacent tablets is indistinct and fused with each other. The width of each tablet is around 2–7 μm.

Acila insignis (Gould, 1861)

Figures 3.7, 8

Shell layers.—Outer, middle, myostracum and inner layers are present (Figure 3.7). The outer layer is composed of composite prismatic structure type-A. A columnar nacreous structure is dominant in the middle layer, and the inner layer is of a sheet nacreous structure. Both middle and inner layers are divided by the myostracum that is composed of a homogeneous structure. The outer and middle layers thicken ventrally. The inner layer lies dorsal to the pallial line and thickens dorsally, but the thickest part is distributed in the middle of the radial section. The shell is thickened ventrally and is up to approximately 920 μm thick in the observed specimen.

Outer layer.—Composite prismatic structure type-A (Figure 3.7D, E). The outer layer consist of acicular crystals up to approximately 1 μm in diameter. These crystals slant at an angle of approximately 10–70° against the growth direction in a radial section and compose the first-order prisms weakly radiating toward the

depositional surface.

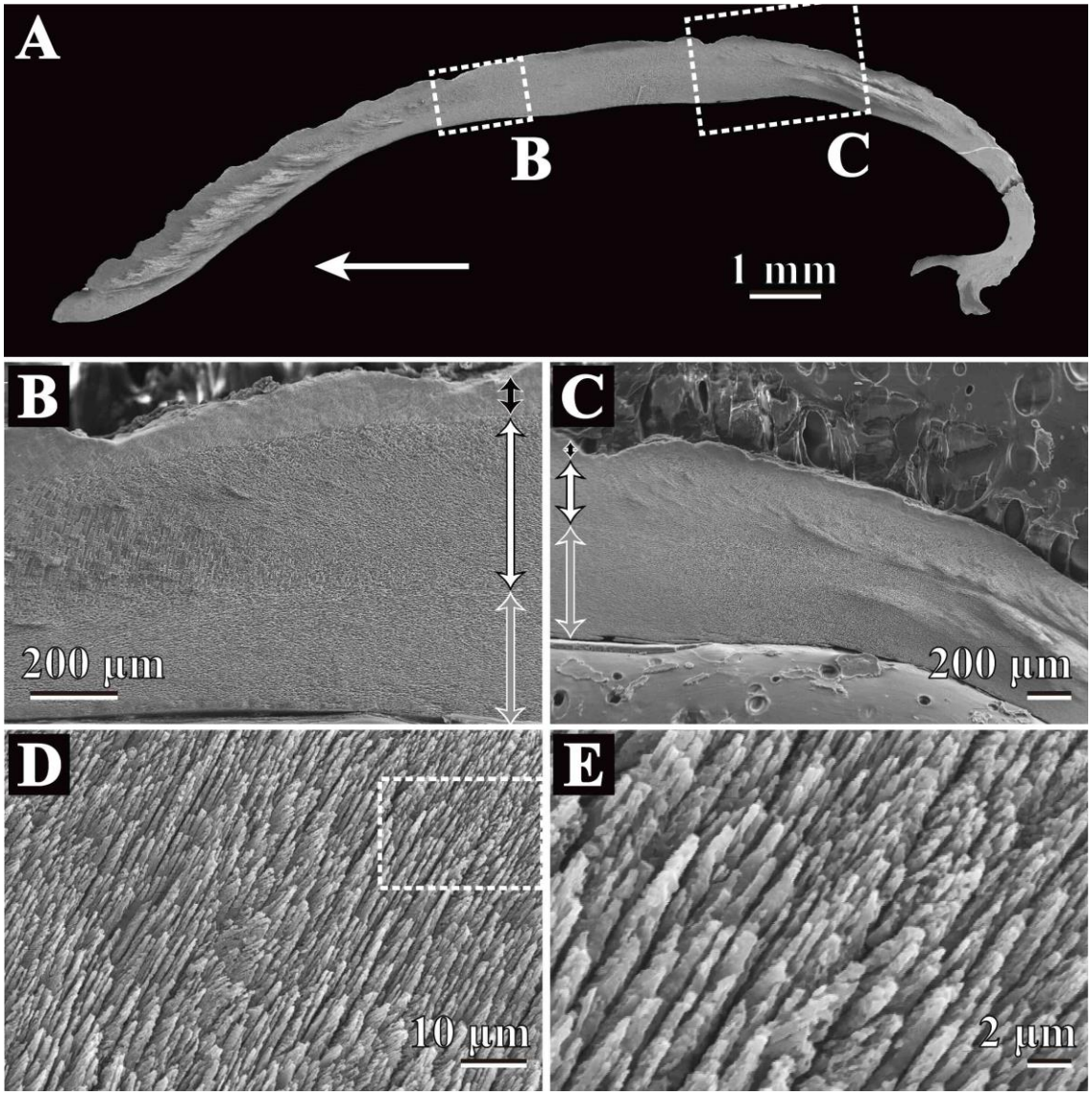

Figure 3.7. Scanning electron micrographs of *Acila insigniss* microstructure. Horizontal white arrow indicate growth direction. **A.** radial section of observed *Acila insignis*. **B,** closer view of broken-lined square in A showing middle part of the shell section. Black arrow, the outer layer; white arrow, the middle layer; gray arrow, inner layer. **C,** closer view of broken-lined square in A showing dorsal part of the shell section. Black arrow, the outer layer; white arrow, the middle layer; gray arrow, inner layer. **D,** radial section of composite prismatic structure type-A of the outer layer. **E,** closer view of broken-lined square in D. D, E, middle part of shell. A-E, Shell lengh = 15 mm.

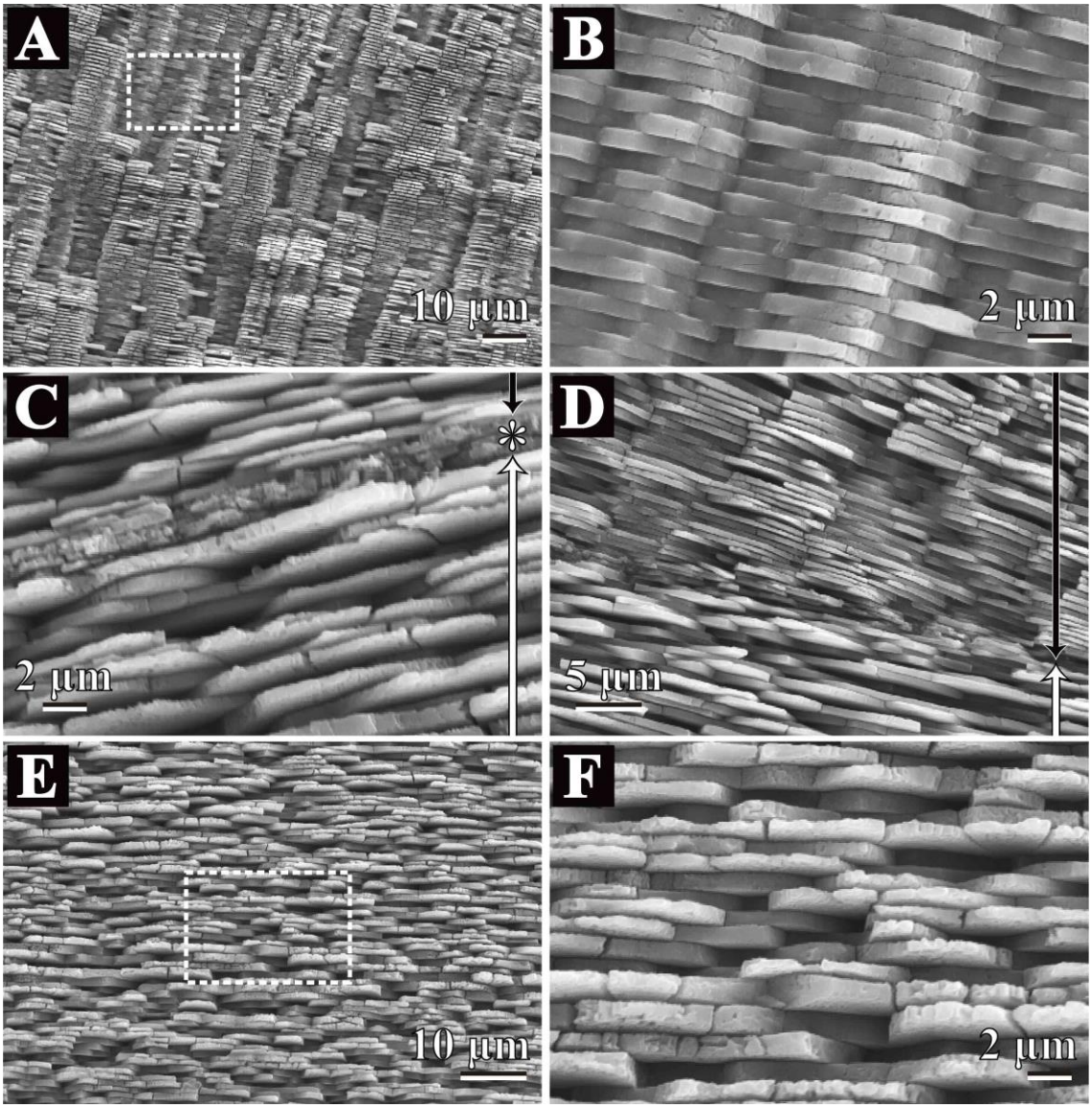

Figure 3.8. Scanning electron micrographs of *Acila insigniss* microstructure. Growth direction is left in all images. **A.** radial section of the columnar nacreous structure of the middle layer. **B,** closer view of broken-lined square in A, showing the columnar nacreous structure of the middle layer. **C,** nacreous structure of the middle and inner layers at middle part of shell. Myostracum layer is consist of homogeneous structure. Vertical black arrow indicates the middle layer. Asterisk mark shows the myostracum layer and white arrow is the inner layer. **D,** radial section of nacreous structure of the middle and inner layers at dorsal part of shell. Myostracum layer is indistinct. Vertical black arrow indicates the middle layer and white arrow indicates the inner layer. **E,** radial section of the sheet nacreous structure of the inner layer. **F,** closer view of broken-lined square in E. A-C, E, F, middle part of shell. D, dorsal part of shell. A-F, Shell lengh = 15 mm.

Middle layer.—Columnar nacreous structure (Figure 3.8A-D). Nearly polygonal tablets stack vertically in the exterior side (Figures 3.8A, B), but gradually shift to irregularly stacked sheet nacre towards the shell interior (Figures 3.8C, D). Nacre columns stack on a tilt at the outermost part of the middle layer and nearly vertically at its innermost part. Each tablet connects to the adjacent tablets mutually, and the width of each assumed each tablets is approximately 4–7 μm. The thickness of each tablet is approximately 1 μm.

Myostracum.— Homogeneous structure. Thickness of this layer reaches approximately 1.5 μm.

Inner layer.—Sheet nacreous (Figures 3.8C-F). Nacre tablets that are approximately 0.5–1.5 μm thick and brick-like. Although the boundary of adjacent tablets is indistinct due to fusion, their width is around 3–8 μm.

***Brevinucula* sp.**

Figure 3.9

Shell layers.—Outer, middle, myostracum and inner layers are present (Figure 3.9A). The outer layer has two sublayers. Both sublayers are of fibrous prismatic structure but their angle to the shell surface and width are different. The boundary between the innermost part of the outer layer and outermost part of the middle layer is smooth. Both the middle and inner layers are sheet nacreous structures, and they are divided by the myostracum composed of irregular blocky crystals or irregular simple prismatic structures. The outer and middle layers thicken ventrally, whereas the myostracum and inner layer thicken dorsally. This species has a relatively thick

(approximately 330 μm) shell for their small shell length.

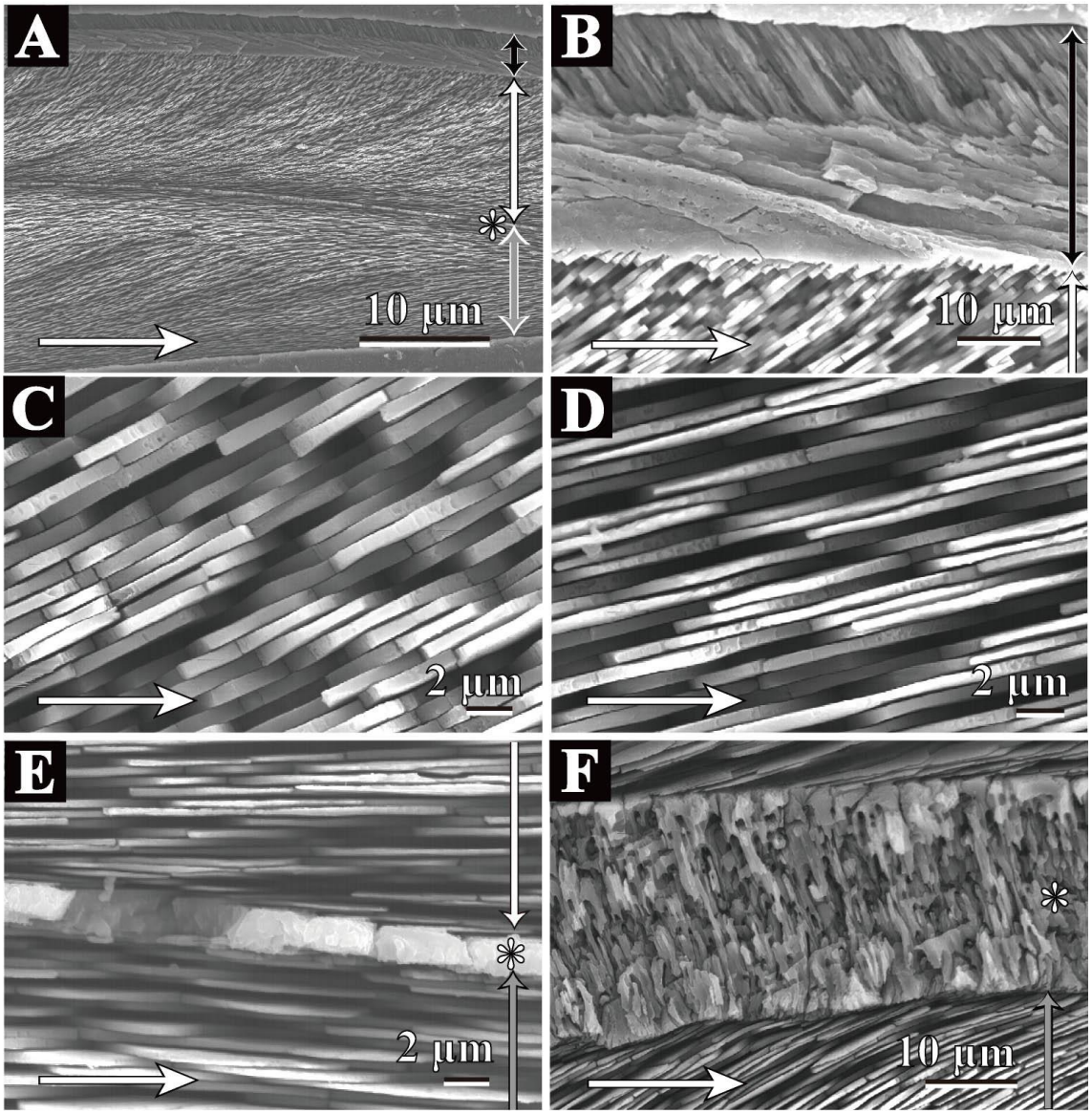

Figure 3.9. Scanning electron micrographs of *Brevinucula sp.* microstructure. Horizontal white arrow indicate growth direction. **A.** radial section of observed *Brevinucula sp.* **B,** radial section of irregular fibrous prismatic structure type-A (Black arrow). and middle sheet nacreous layer (White arrow). **C,** radial section of sheet nacreous structure of the middle layer. **D,** radial section of sheet nacreous structure of the inner layer. **E,** radial section of nacreous structure of the middle and inner layers at ventral part of shell. Asterisk mark indicates myostracum layer. Vertical white arrow indicates the middle layer and gray arrow indicates the inner layer. Asterisk mark shows the myostracum layer **F,** radial section of myostracum at dorsal part of shell. Asterisk mark indicates myostracum and vertical gray arrow indicates the middle layer.. A-E, middle part of shell. F, dorsal part of shell. A-F, Shell lengh = 7 mm.

Outer layer.—Irregular fibrous prismatic structure consisting of two sublayers (IFP type-A; figure 3.9B). Acicular crystals in the outer sublayer slant at a steep angle of approximately 60° against the growth direction in the radial section but 15° in the inner sublayer. The width of the crystals is approximately 0.8–1.5 μm in the outer sublayer and 2.5–40 μm in the inner sublayer.

Middle layer.—Sheet nacreous structure (Figure 3.9C, E and F). Nacre tablets are brick-like and stack parallel to the long axes of the acicular crystals of the inner sublayer of the outer layer and nearly vertically at its innermost part. The thickness of the nacre tablets is around 0.8 μm at the outer part, but thin inwards, reaching 0.2 μm.

Myostracum.— Irregular blocky crystals to irregular simple prismatic structures (Figure 3.9E, F). Irregularly shaped acicular crystals that are approximately 0.6–5 μm in width and up to approximately 20 μm long in the long axes. At the thinned part, irregularly shaped blocky crystals that are up to approximately 12μm in width form the myostracum. This layer never becomes indistinct ventrally.

Inner layer.— Sheet nacreous (Figure 3.9D-F). Nacre tablets are approximately 0.5 μm thick and their width is around 3.5–18 μm, piling-up like a brick wall. The nacre tablets in the inner layer are generally wider than those in the middle layer.

Ennucula nipponica (Smith, 1885)

Figures 3.10, 11

Shell layers.—Outer, middle, myostracum, and inner layers are present (Figure 3.10A). The outer layer is composed of composite prismatic structures (type-B). The middle and inner layers are similarly nacreous, but morphology and positional

relationship of their tablets are different. Vertically stacked nacre tablets are dominant in the middle layer (columnar nacreous structure), and tablets are brick-like in all vertical sections (sheet nacreous structure) in the inner layer. The boundary between the innermost part of the outer layer and the outermost part of the middle layer is smooth. Both the middle and inner layers are divided by the myostracum that is composed of irregular simple prismatic to irregular blocky crystals. The outer and middle layers thicken ventrally. The myostracum and inner layer generally thicken dorsally, whereas the thickest part is distributed in the middle part of a radial section. The shell is up to approximately 290 μm thick in the observed specimen.

Outer layer.—Composite prismatic structure type-B (Figure 3.10A-C). The outer layer consists of acicular crystals (Figure 3.10B, C). These crystals slant at angles of approximately 20–50° against the growth direction in the radial section and compose the first-order prisms weakly radiating toward the depositional surface (Figures 3.10C).

Middle layer.—Columnar nacreous structure (Figure 3.10D-F). Nacre tablets are around 0.7 μm thick at the outer part and have acute polygonal shapes (Figure 3.10F). Tablets stack vertically in the exterior side, while vertical stacking weakens inwards. At the innermost part of the middle layer, the thickness of the tablets reduces (up to 0.3 μm) and they become brick-like as in the inner layer that consists of sheet nacreous structures (Figures 3.11C, D). Nacre columns stack on a tilt and are nearly vertical at the innermost part. While each tablet connects to the adjacent tablets in a narrow sense (Figure 3.10F), the width of each assumed independent tablets is around 7μm. Thickness of the tablets is approximately 1 μm at the outer part of the middle layer and becomes thinner inwards, reaching 0.3 μm. Nacre tablets are stepped as sheet nacreous structures (Figure 3.10F).

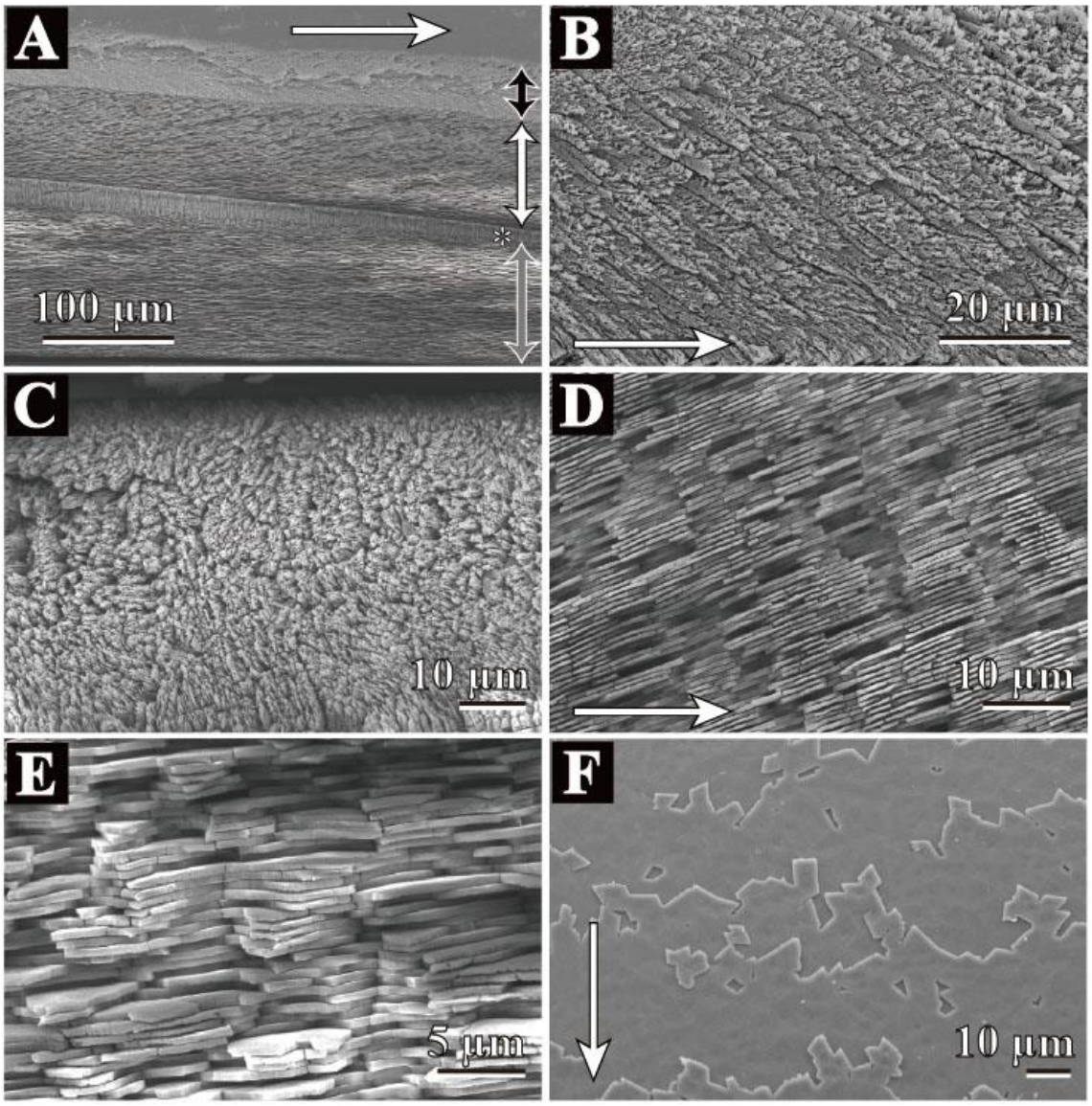

Figure 3.10. Scanning electron micrographs of *Ennucula nipponica* microstructure. Horizontal white arrow indicate growth direction. **A.** radial section which comprised of the outer, middle, myostracum and inner layers. Black double-headed arrow, the outer layer; white double-headed arrow, the middle layer; asterisk mark, myostracum; gray double-headed arrow, inner layer. **B,** radial section of composite prismatic structure type-B of the oueter layer. **C,** transverse section of composite prismatic structure type-B of the oueter layer. **D,** radial section of columnar nacreous structure of the middle layer. **E,** transverse section of columnar nacreous structure of the middle layer. **F,** inner surface of columnar nacreous of the middle layer. A, dorsal part of shell. B-E, middle part of shell. F, ventral part of shell. A-F, Shell lengh = 69 mm.

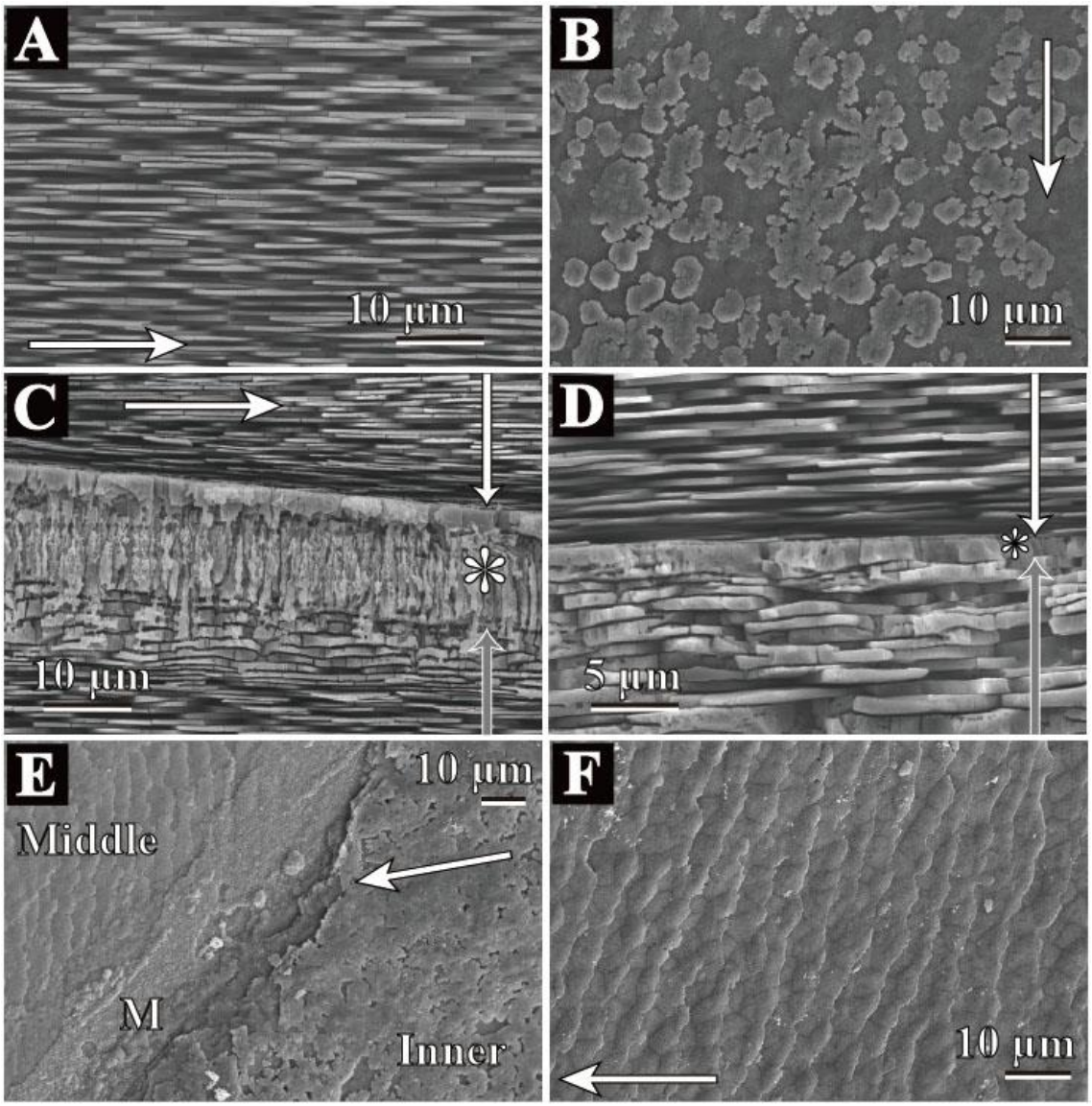

Figure 3.11. Scanning electron micrographs of *Ennucula nipponica* microstructure. White arrow indicate growth direction. **A** radial section of sheet nacreous structure of the inner layer. **B,** inner surface of sheet nacreous of the inner layer. **C,** radial section at dorsal part which comprised of the middle, myostracum and inner layers. Vertical white arrow, the middle layer; asterisk mark, myostracum; gray arrow, inner layer. **D,** radial section at middle part which comprised of the middle, myostracum and inner layers. Vertical white arrow, the middle layer; asterisk mark, myostracum; gray arrow, inner layer. **E,** inner surface around the posterior adductor muscle scar of left valve. Middle layer and myostracum layers distribute at the posterior adductor muscle scar. M, myostracum. **F,** closer view of the middle layer in E. A, B, D, middle part of shell. C, dorsal part of shell. E, F, ventral part of shell, around posterior adductor muscle scar. A-F, Shell lengh = 69 mm.

Myostracum.—Irregular simple prismatic structure with irregular blocky crystals (Figures 3.10A, 3.11C-E). The myostracum thickens dorsally and their thickness occupies the middle third of the total shell thickness. At the thickened part, the myostracum is composed of (1) the outer sublayer with irregular blocky crystals and irregular simple prismatic structure and (2) the inner sublayer with irregular acicular crystals around 0.8 μm in the short axes (Figure 3.11C). At the thinned part, the layer is formed of irregular blocky crystals (Figure 3.11D). The myostracum definitely separates the middle and inner nacreous layers but their formation is not derived from the attached muscles. The middle layer is distributed at the adductor muscle scars, not the myostracum (Figure 3.11E).

Inner layer.—Sheet nacreous (Figures 3.10A, 3.11A-F). Nacre tablets are approximately 0.7 μm and brick-like (Figure 3.11A). The nacre tablets in the inner layer grow as rounded tablets, while those in the middle layer show acute polygonal shapes (Figure 3.11B). Independent nacre tablets are around 4–14 μm in width and fused with adjacent tablets (Figure 3.11B, E).

Ennucula siberutensis (Thiele & Jaeckel, 1931)

Figure 3.12

Shell layers.—Outer, middle, myostracum, and inner layers are present (Figure 3.12). The outer layer is composed of bended fibrous prismatic structure (IFP type-B). The boundary between the innermost part of the outer layer and the outermost part of the middle layer is smooth. The middle and inner layers are sheet nacreous structures. The boundary between the two layers is indistinct due to an obscure myostracum. The

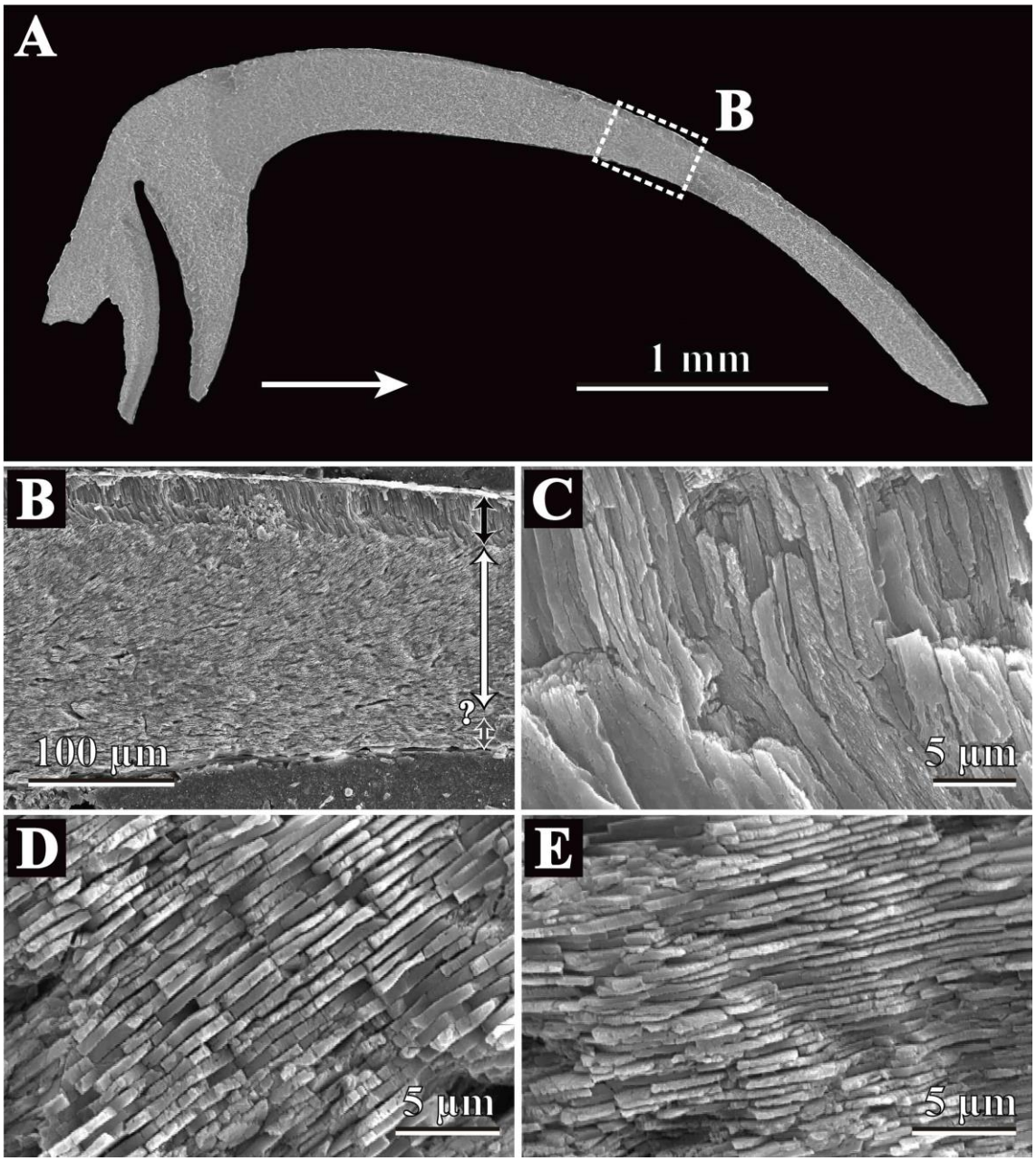

Figure 3.12. Scanning electron micrographs of *Ennucula siberutensis* microstructure. Horizontal white arrow indicate growth direction. Growth direction is right side in B-E. **A.** radial section of observed *Ennucula siberutensis*. **B,** closer view of broken-lined square in A showing middle part of the shell section. Black arrow, the outer layer; white arrow, the middle layer; gray arrow, inner layer. **C,** radial section of irregular simple prismatic structure type-B of the outer layer. **D,** radial section of sheet nacreous structure of the middle layer. **E,** radial section of sheet nacreous structure of the inner layer. B- E, middle part of shell. A-E, Shell lengh = 7 mm.

outer and middle layers thicken ventrally and the inner layer thickens dorsally. The shell is thickened in the ventral part and is approximately 360 μm thick in the observed specimen.

Outer layer.— Irregular fibrous prismatic structure type-B (Figures 3.12B, C). The outer layer consists of acicular crystals whose width is relatively thick for fibrous prismatic structures (up to 4 μm), and the long axes curve in an obtuse L-shape in a radial section. Bended acicular prisms deeply slant at angles of approximately 80° against the growth direction in a radial section but at shallow angles of around 45° in the curved inwards portion.

Middle layer.—Sheet nacreous structure (Figure 3.12D). Nacre tablets are approximately 0.6 μm thick brick-like and stack parallel to the long axes of acicular crystals of the inner sublayer of the outer layer and are nearly vertical at the innermost part.

Myostracum.— This layer is obscure.

Inner layer.— Sheet nacreous (Figure 3.12E). Brick-like nacre tablets are approximately 0.4 μm thick and their width is variable, up to 6 μm.

Ennucula tenuis (Montagu, 1808)

Figures 3.13, 14

Shell layers.—Outer, middle, myostracum and inner layers are present (Figure 3.13). The outer layer is composed of composite prismatic structures (type-B). The middle and inner layers are nacreous structures, but morphology and positional relationship of their tablets are different. Vertically stacking nacre tablets are dominant

in the middle layer as columnar nacreous structures and brick-like in all the vertical sections as sheet nacreous structures. The boundary between the innermost part of the outer layer and the outermost part of the middle layer is smooth. Both the middle and inner layers are divided by the myostracum that is composed of irregular simple prismatic structures. The outer and middle layers thicken ventrally. The myostracum and inner layer generally thicken dorsally, whereas the thickest part is distributed in the middle part of a radial section. The shell is up to approximately 240 μm thick in the observed specimen.

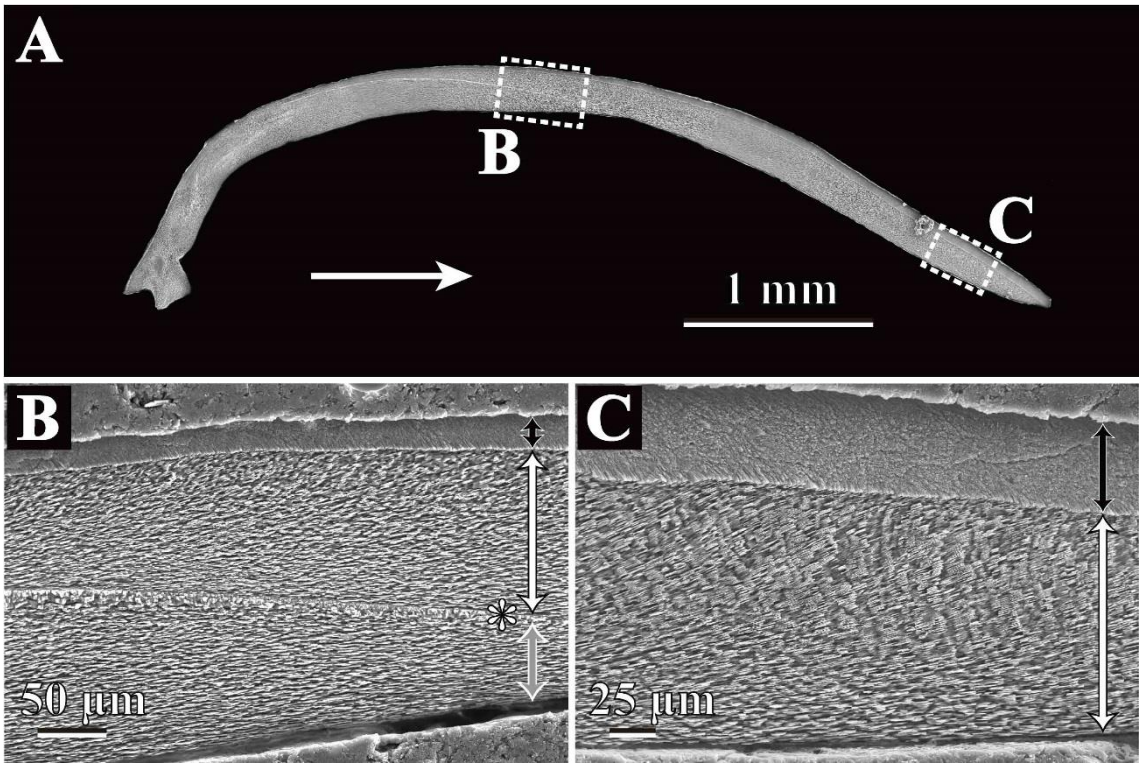

Figure 3.13. Scanning electron micrographs of *Ennucula tenuis* microstructure. Horizontal white arrow indicate growth direction. **A.** radial section of observed *Ennucula tenuis*. **B,** closer view of broken-lined square in A showing middle part of the shell section. Black arrow, the outer layer; white arrow, the middle layer; asterisk mark, myostracum; gray arrow, inner layer. **C,** closer view of broken-lined square in A showing ventral part of the shell section. Black arrow, the outer layer; white arrow, the middle layer. A-C, Shell lengh = 13 mm.

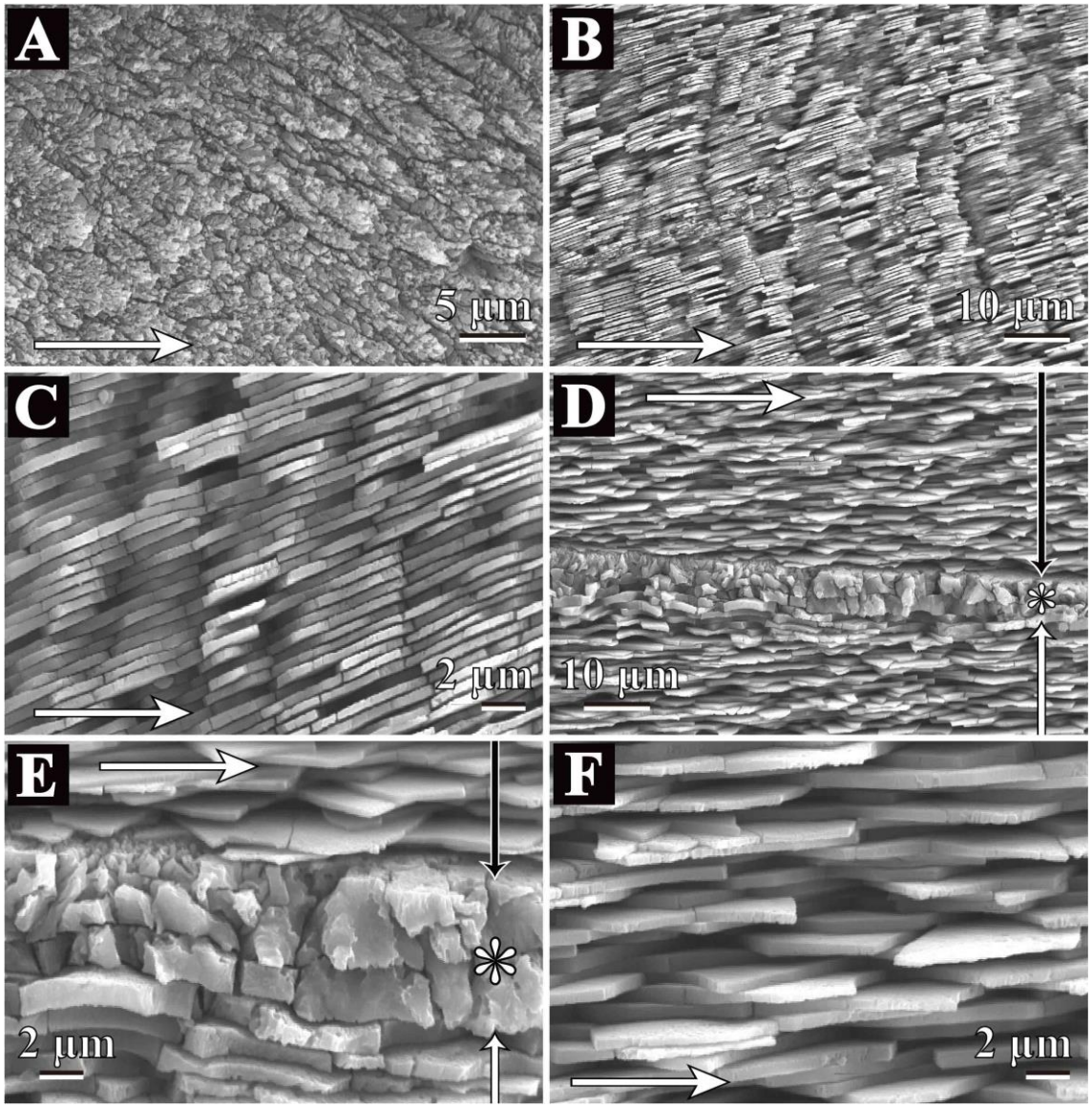

Figure 3.14. Scanning electron micrographs of *Ennucula tenuis* microstructure. Horizontal white arrow indicate growth direction.. **A,** radial section of composite prismatic structure type-B of the oueter layer. **B,** radial section of columnar nacreous structure of the middle layer. **C,** closer view of columnar nacreous structure of the middle layer. **D,** radial section at middle part which comprised of the middle, myostracum and inner layers. Vertical black arrow, the middle layer; asterisk mark, myostracum; white arrow, inner layer. **E,** closer view of E. Vertical black arrow, the middle layer; asterisk mark, myostracum; white arrow, inner layer. **F,** radial section of sheet nacreous structure of the inner layer. A-C, ventral part of shell. E-F, middle part of shell. A-F, Shell lengh = 13 mm.

Outer layer.—Composite prismatic structure type-B (Figures 3.13B, C, 3.14A). The outer layer consists of acicular crystals. These crystals slant at angles of around 60° against the growth direction in the radial section and compose the first-order prisms weakly radiating toward the depositional surface.

Middle layer.—Columnar nacreous to sheet nacreous structure (Figures 3.14B-E). Nacre tablets are around 0.7 μm thick and stack vertically in the exterior side (Figure 3.14B), but gradually shift to irregularly stacked sheet nacre toward the shell interior (Figure 3.14D). At the innermost part of the middle layer, the thickness of the tablets reduces (up to 0.4 μm) and they become brick-like as in the inner layer, which consists of sheet nacreous structures. While each tablet connects to the adjacent tablet in a narrow sense, the width of each assumed independent tablets is around 3–8 μm.

Myostracum.—Irregular simple prismatic structure (Figures 3.14D, E). This structure consists of acicular and irregular shaped crystals.

Inner layer.—Sheet nacreous (Figures 3.14D-F). Nacre tablets are approximately 0.6 μm thick and brick-like. Independent nacre tablets are around 3–12 μm in width and fused with adjacent tablets.

***Ennucula* sp. 1**

Figure 3.15

Shell layers.—Outer, middle, myostracum, and inner layers are present. The outer layer is composed of bended fibrous prismatic structures (IFP type-B). The boundary between the innermost part of the outer layer and the outermost part of the middle layer is smooth. The middle and inner layers are nacreous structures, but the

morphology and positional relationship of their tablets are different. Vertically stacking nacre tablets are dominant in the middle layer (columnar nacreous structure) and tablets are like brick walls in all vertical sections (sheet nacreous structure) in the inner layer. The boundary between the innermost part of the outer layer and the outermost part of the middle layer is smooth, probably due to their smooth shell surface. The myostracum, which consist of homogeneous structures, is thin but separates the two layers (the middle and inner layer). The outer and middle layer thickens ventrally and the inner layer thickens dorsally. The shell is up to approximately 280 μm thick in the observed specimen.

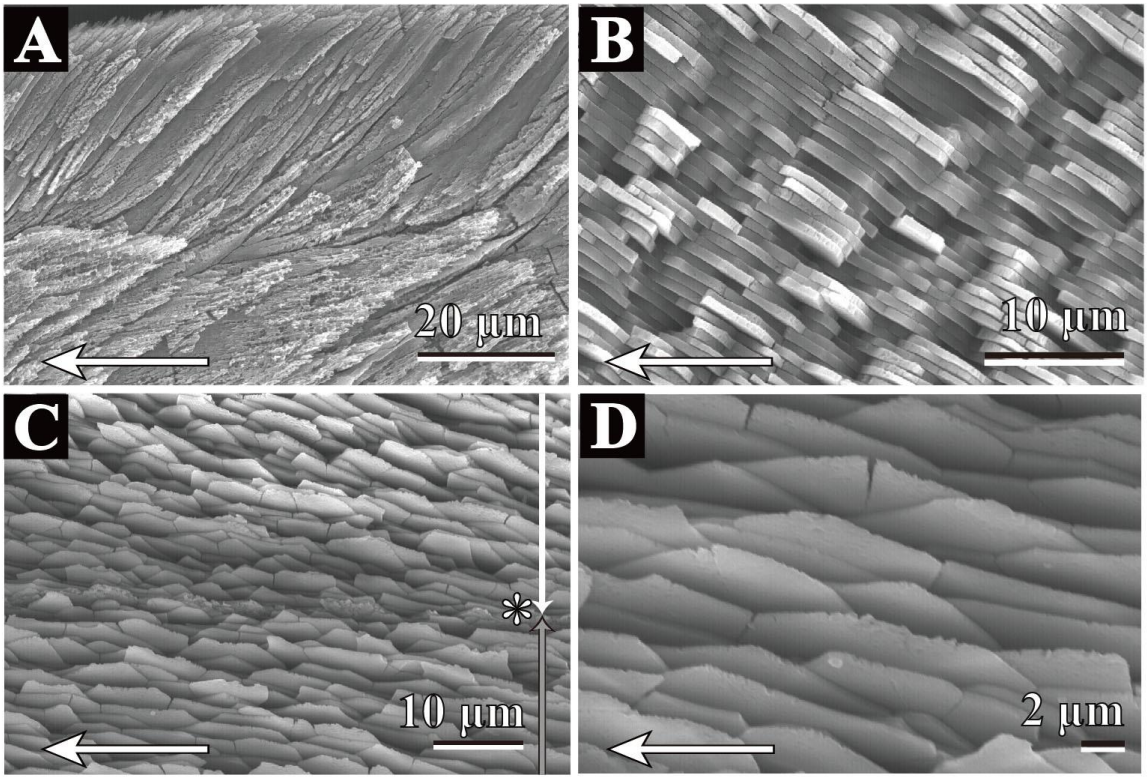

Figure 3.15. Scanning electron micrographs of *Ennucula* sp. 1 microstructure. Horizontal white arrow indicate growth direction. **A.** radial section of irregular fibrous prismatic structure type-B of the outer layer. **B,** radial section of sheet nacreous structure of the middle layer. **C,** radial section of nacreous structure of the middle and inner layers. Myostracum is obscure. Vertical white arrow indicates the middle layer and gray arrow indicates the inner layer. **D,** radial section of sheet nacreous structure of the inner layer. A-D, middle part of shell. A-D, Shell lengh = 12 mm.

Outer layer.—Irregular fibrous prismatic structure type-B (Figure 3.15A). The outer layer consists of acicular crystals whose width is relatively thick for fibrous prismatic (up to 10 μm) and the long axes curves, showing an obtuse L-shape in a radial section. Bended acicular prisms slant at an angle of approximately 70° against the growth direction in a radial section but at shallow angles of around 20° after being curved inwards.

Middle layer.—Columnar to sheet nacreous structure (Figures 3.15B, C). Tablets weakly stack vertically in the exterior side, while vertical stacking weakens inwards. Nacre tablets are around 0.7 μm thick, 1.7–9 μm in width and become thinner inwards (up to 0.4 μm). Tablets stack on a tilt parallel to the long axes of acicular crystals of the outer layer at the outermost part of the middle layer and nearly vertically at the innermost part of it.

Myostracum.— Homogeneous structure (Figure 3.15C). The mystracum layer is very thin (less than 0.4 μm) and consist of granular crystals that are around 0.7 μm in diameter.

Inner layer.— Sheet nacreous (Figures 3.15C, D). Nacre tablets which pile up like a brick wall are approximately 0.2 μm thick and their width is variable (up to 12 μm).

***Ennucula* sp. 2**

Figure 3.16

Shell layers.—Outer, middle, myostracum, and inner layers are present (Figures 3.16A-D). The outer layer is composed of composite or fibrous prismatic

structures (CP type-A). The middle and inner layer are nacreous structures, but their tablets pile up differently from each other. Vertical stacking nacre tablets are dominant in the middle layer (columnar nacreous structure) and tablets are brick wall-like in all vertical sections (sheet nacreous structure) in the inner layer. The boundary between the two layers is indistinct due to an obscure myostracum. The outer and middle layer thickens ventrally. The inner layer lies dorsal to the pallial line and generally thickens dorsally whereas its thickest part is distributed in the middle part of a radial section. The shell is up to approximately 360 μm thick in the observed specimen.

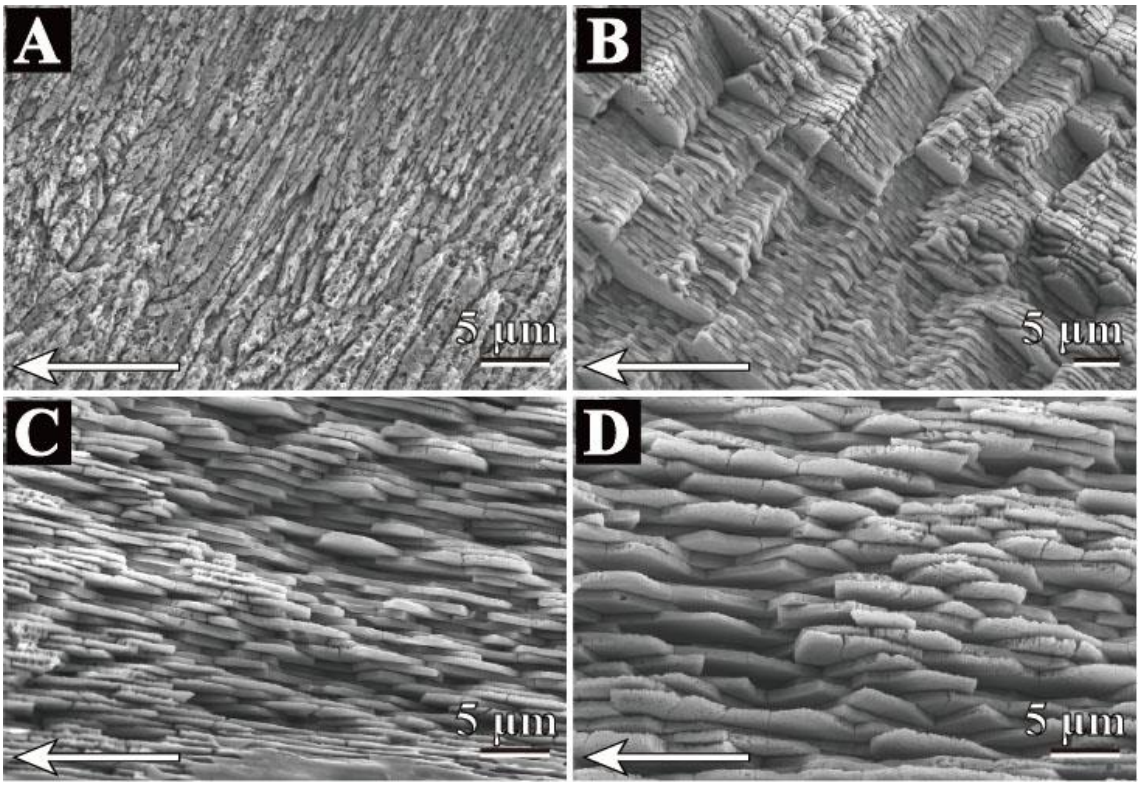

Figure 3.16. Scanning electron micrographs of *Ennucula* sp.2 microstructure. White arrow indicate growth direction. **A** radial section of fibrous prismatic structure type-A of the outer layer. **B,** radial section of columnar nacreous structure of outer part in the middle layer. **C,** radial section of sheet nacreous structure of inner part in the middle layer. **D,** radial section of sheet nacreous structure of the inner layer. A, B, D, middle part of shell. A-C, ventral part of shell. D, dorsal part of shell. A-D, Shell lengh = 11 mm.

Outer layer.—Composite prismatic structure type-A (Figure 3.16A). Acicular crystals are arranged parallel to one another tilting at an angle of around 55° against the growth direction in a radial section. These crystals thicken inwards by approximately 0.4 to 2 μm.

Middle layer.—Columnar nacreous structure to sheet nacreous (Figures 3.16B, C). Nearly polygonal tablets stack vertically in the exterior side (Figure 3.16B), while vertical stacking weakens inwards (Figure 3.16C). At the innermost part of the middle layer, they pile up like a brick wall, similar to the sheet nacreous structure in the inner layer (Figure 3.16C). Nacre columns stack on a tilt parallel to the long axes of the acicular crystals of the outer layer at the outermost part of the middle layer and nearly vertically at its innermost part. The width of the independent tablets is around 7–13 μm at the outer part. The thickness of the tablets is approximately 1 μm at the outer part of the middle layer, thinning inwards and reaching 0.5 μm.

Myostracum.—The myostracum of this species is obscure and is probably a homogeneous structure.

Inner layer.—Sheet nacreous (Figures 3.16D). Nacre tablets that are approximately 0.6 μm thick pile up like brick wall. Their width is around 3–10 μm.

Nucula tokyoensis **Yokoyama, 1920**

Figure 3.17

Shell layers.—Outer, middle, myostracum and inner layers are present (Figure 3.17). The outer layer is composed of a denticular composite prismatic structure. The middle and inner layers are sheet nacreous structures, and the myostracum is an

irregular prismatic structure. The outer and middle layers thicken ventrally and the myostracum and inner layer thicken dorsally. The shell is up to approximately 235 μm thick in the observed specimen.

Outer layer.—Denticular composite prismatic structure (Figures 3.17). Acicular crystals spread like a fan ventrally (Figure 3.17C) because these crystals are oriented perpendicular to the deposit surface (see correspondence between growth lines and the orientation of acicular crystals in Figure 3.17A). In a transverse section, the boundary between the innermost part of the outer layer and the outermost part of the middle layer is recognized as a dentate line due to a crenulate internal ventral margin. The width of crystals is around 3μm.

Middle layer.—Sheet nacreous structure (Figures 3.17D, E). Nearly polygonal tablets that are approximately 0.7-μm thick pile up like a brick wall (Figure 3.17D). Nacre columns stack on a tilt parallel to the long axes of the acicular crystals of the outer layer at the outermost part of the middle layer and nearly vertically at its innermost. The boundary of adjacent tablets is indistinct but their width is around 4–14 μm.

Myostracum.—Irregular simple prismatic structure (Figure 3.17E). Irregular shaped acicular crystals compose this layer. The myostracum layer thickens dorsally.

Inner layer.—Sheet nacreous (Figures 3.17E, F). Nacre tablets are approximately 0.7 μm thick and pile up like bricks almost parallel to the inner shell surface. Although the boundary of adjacent tablets is indistinct, their width is variable (around 4-20 μm).

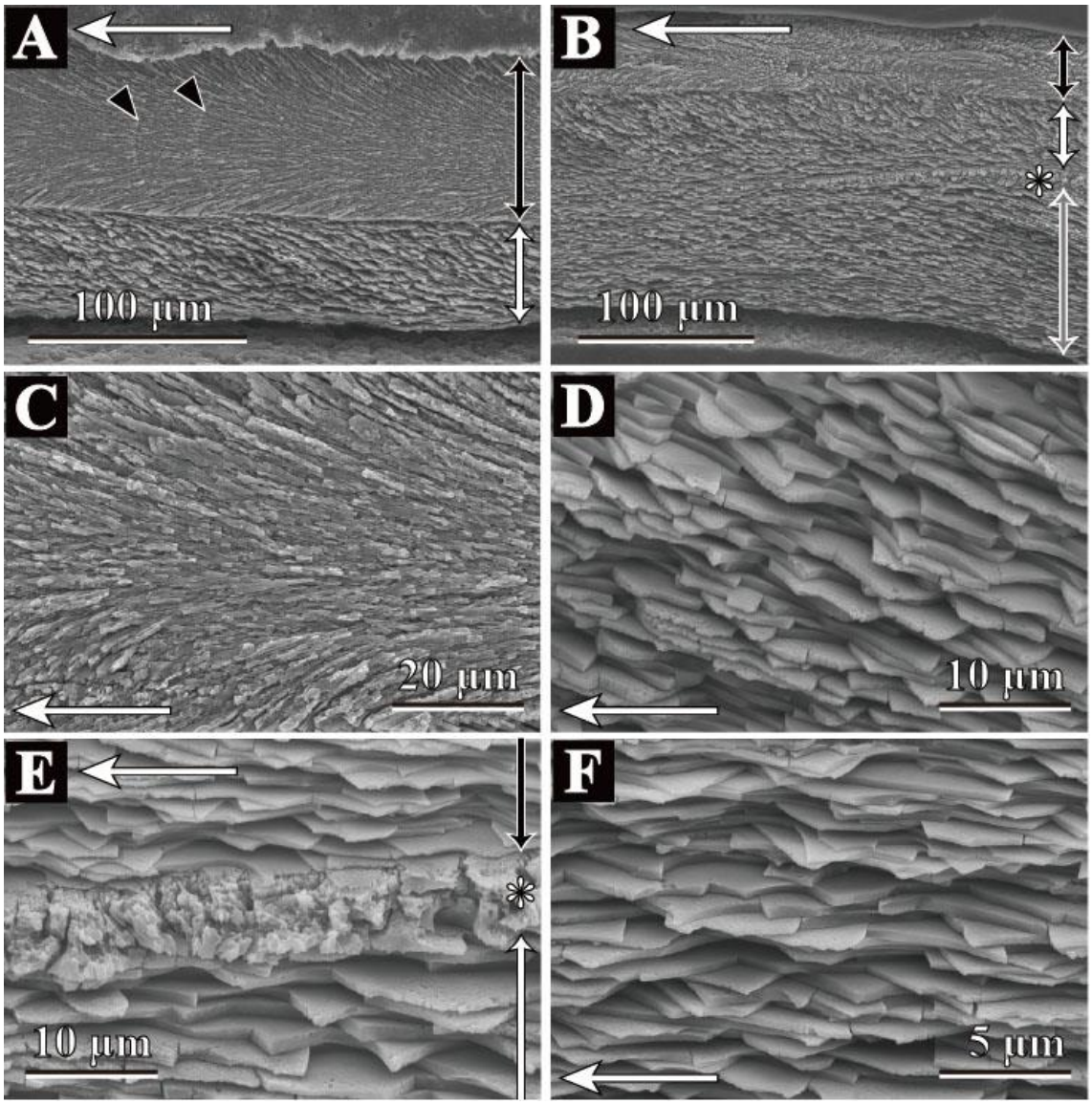

Figure 3.17. Scanning electron micrographs of *Nucula tokyoensis* microstructure. White arrow indicate growth direction. **A,** radial section at ventral part of shell which comprised of the outer and middle layers. Black double-headed arrow, the outer layer; white double-headed arrow, the middle layer. Black arrow-head indicates growth lines. **B,** radial section at dorsal part of shell which comprised of the outer, middle, myostracum and inner layers. Black double-headed arrow, the outer layer; white double-headed arrow, the middle layer; asterisk mark, myostracum; gray double-headed arrow, inner layer. **C,** radial section of denticular composite prismatic structure of the outer layer. **D,** radial section of sheet nacreous structure of the middle layer. **E,** radial section which comprised of the middle, myostracum and inner layers. Vertical black arrow, the middle layer; asterisk mark, myostracum; white arrow, inner layer. **F,** radial section of sheet nacreous structure of the inner layer. A, C, D, ventral part pf shell. B, E, F, dorsal part of shell. A-F, Shell lengh = 5 mm.

Nucula torresi Smith, 1885

Figure 3.18

Shell layers.—Outer, middle, myostracum, and inner layers are present. The outer layer is composed of denticular composite prismatic structures. The middle and inner layers are weakly organized columnar nacreous structures and sheet nacreous structures, respectively. The myostracum is obscure or consists of irregular blocky crystals. The outer and middle layers thicken ventrally and the myostracum and inner layer thicken dorsally. The shell thickness is up to approximately 480 μm thick in the observed specimen.

Outer layer.—Denticular composite prismatic structure (Figures 3.18A-C). Acicular crystals spread ventrally like a fan perpendicularly to the deposit surface. The width of the crystals is around 1 μm.

Middle layer.—Sheet nacreous structure; barely columnar nacreous structure (Figure 3.18D, E). Sheet nacreous structure is dominant in this layer, and tablets are slightly vertically stacked. Nearly polygonal tablets are around 0.6 μm thick at the outer part and thinner inwards (around 2 μm). Nacre columns stack on a tilt parallel to the long axes of the acicular crystals of the outer layer at the outermost part of the middle layer and nearly vertically at the innermost part. The boundary of adjacent tablets is indistinct but their width is around 2.5–5 μm at the outer part and 3–18 μm at the inner part.

Myostracum.—Irregular blocky crystals (Figure 3.18E). At the ventral side of the shell where this layer is mostly thickened, irregularly shaped blocky crystals, like a sort of false nacre tablets, compose the myostracum and become obscure ventrally.

Inner layer.—Sheet nacreous (Figure 3.18E, F). Nacre tablets are approximately 0.2–0.4 μm thick, and almost parallel to the inner shell surface. Their width is variable (around 4-10 μm).

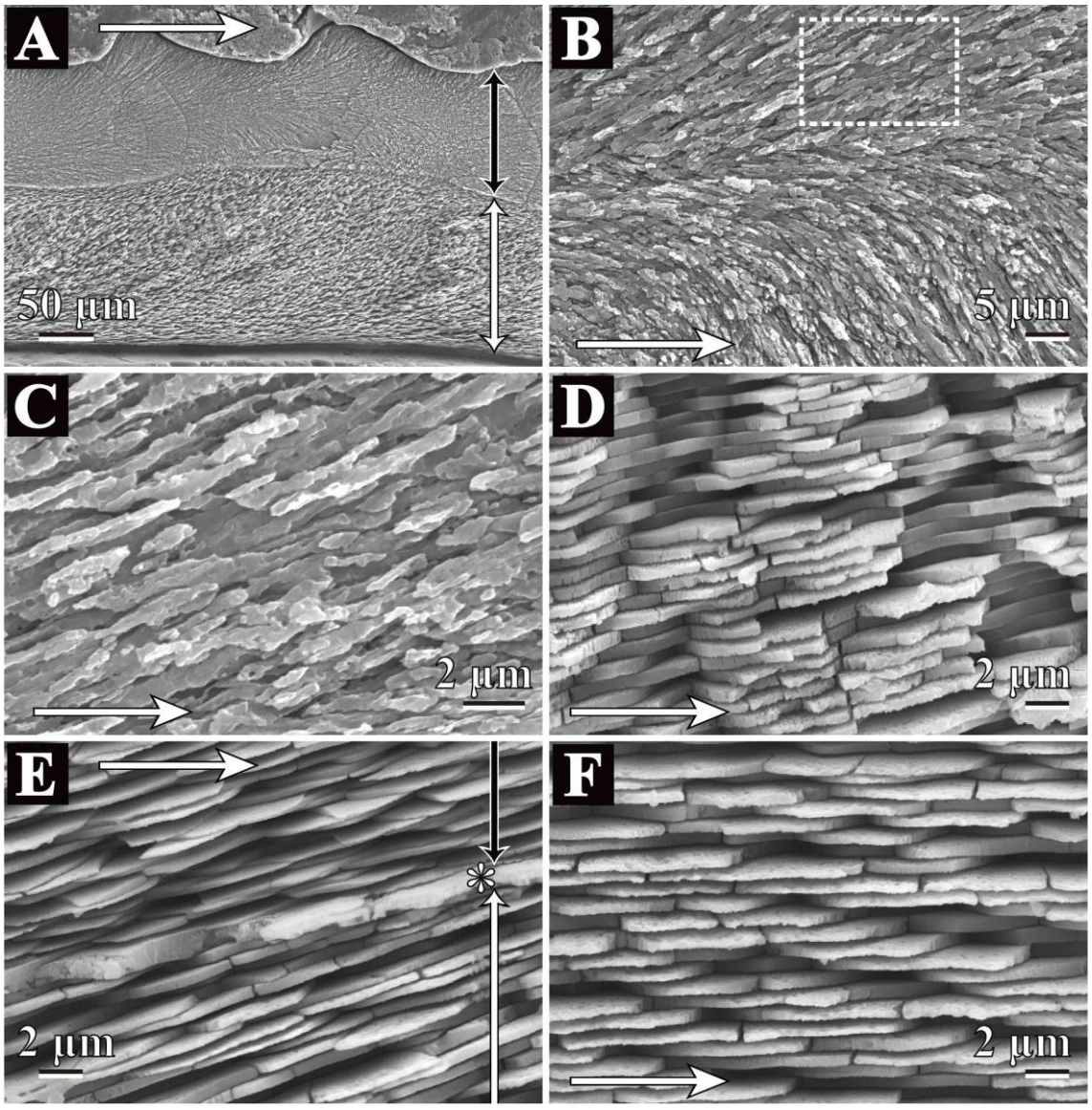

Figure 3.18. Scanning electron micrographs of *Nucula torresi* microstructure. White arrow indicate growth direction. **A,** radial section at ventral part of shell which comprised of the outer and middle layers. Black double-headed arrow, the outer layer; white double-headed arrow, the middle layer. **B,** radial section of denticular composite prismatic structure of the outer layer. **C,** closer view of broken-lined square in B. **D,** radial section of probable columnar nacreous structure of the middle layer. **E,** radial section which comprised of the middle, myostracum and inner layers. Vertical black arrow, the middle layer; asterisk mark, myostracum; white arrow, inner layer. **F,** radial section of sheet nacreous structure of the inner layer. A, D, ventral part pf shell. B, C, F, middle part of shell. E, dorsal part of shell. A-F, Shell lengh = 12 mm.

Family Sareptidae

Sarepta speciosa Adams, 1860

Figures 3.19, 20

Shell layers.—Outer, myostracum, and inner layers are present. The outer and inner layers are both homogeneous structures. A fine composite crossed lamellar structure is barely recognized at the ventral part in the outer layer. The myostracum is of an irregular simple prismatic structure. The outer layer weakly thickens ventrally, and the shell thickens up to 213 μm. The inner layer shows poor growth. The inner layer is restricted to the dorsal part, and it is questionable whether the myostracum reaches the pallial line.

Outer layer.—Mostly homogeneous structure (Figures 3.19, 3.20A, B, D–F). A fine complex crossed lamellar structure is barely recognized (Figure 3.20C). Granular crystals composed of a homogeneous structure moderately diminish in diameter inwards. The average diameter of the granular crystals is around 1.2 μm at the outer part (Figure 3.20A) and 0.4 μm at the inner part (Figure 3.20B). A fine complex crossed lamellar structure is recognized at the middle part of the outer layer in the dorsal and ventral sides along the growth lines (Figure 3.20C). Acicular crystals composed of first-order lamellae of fine complex crossed lamellar structure are up to 6 μm long in the long axes and incline at around 15° to the deposit surface and growth line.

Myostracum.—Irregular simple prismatic structure (Figure 3.20E). Very thin (up to 0.8 μm) and generally obscure. Acicular crystals composing the myostracum are around 0.4 μm at the thickest part.

Inner layer.—Homogeneous structure (Figures 3.20E, F). Granular crystals of

homogeneous structure are far smaller than those in the middle layer (around 0.2 μm in diameter).

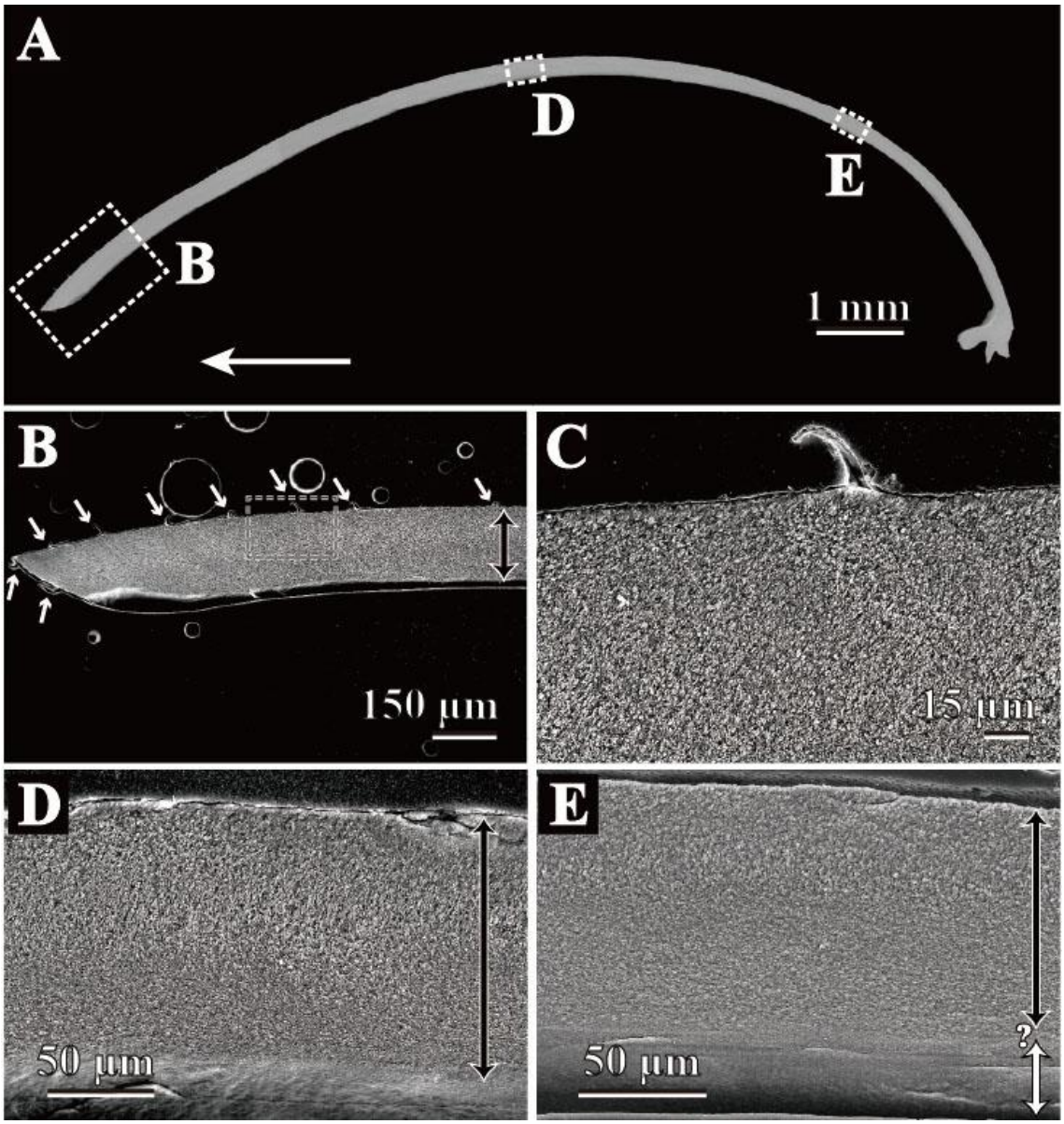

Figure 3.19. Scanning electron micrographs of *Sarepta speciosa* microstructure. White arrow indicate growth direction. **A** radial section of observed *Sarepta speciosa*. **B,** closer view of broken-lined square in A showing ventral part of the shell section. Black double-headed arrow, the outer layer; white arrow, radial rib of periostracum. **C,** closer view of broken-lined square in B. **D,** closer view of broken-lined square in A showing middle part of the shell section. Black double-headed arrow, the outer layer. **E,** closer view of broken-lined square in A showing dorsal part of the shell section. Black double-headed arrow, the outer layer; White double-headed arrow, the inner layer; Question mark implies obscure margin of two layers. A-F, Shell lengh = 13 mm.

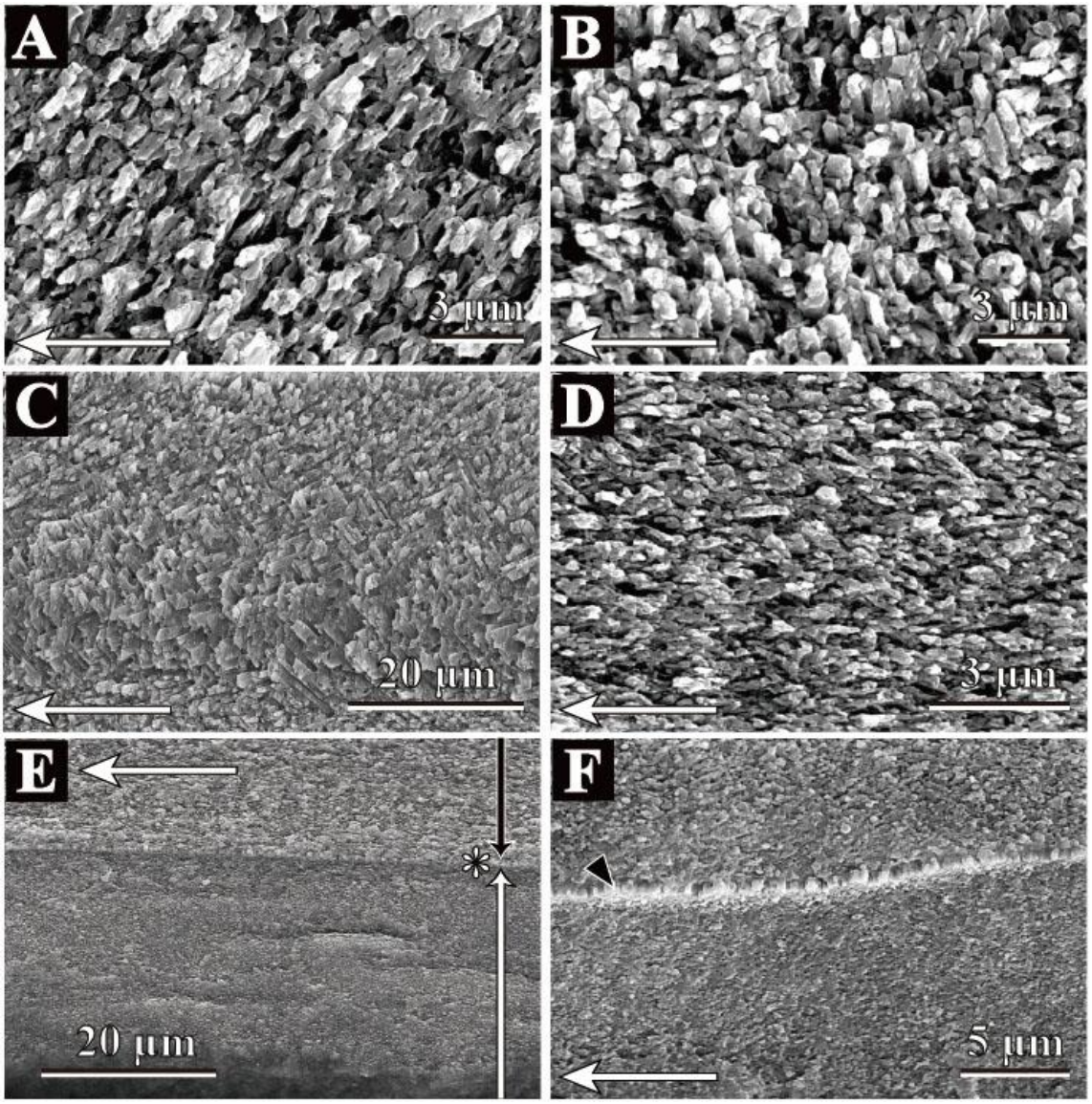

Figure 3.20. Scanning electron micrographs of *Sarepta speciosa* microstructure. White arrow indicate growth direction. **A** radial section of homogeneous structure of outer part of the outer layer. **B,** radial section of homogeneous structure of middle part of the outer layer. **C,** radial section of fine complex crossed lamellar structure of outer part at dorsal part of shell. **D,** radial section of homogeneous structure of inner part of the outer layer. **E,** radial section which comprised of the outer, myostracum and inner layers. Vertical black arrow, the outer layer; asterisk mark, myostracum; white arrow, inner layer. **F,** radial section of homogeneous structure of the inner layer. Black arrow-head indicates the growth line. A-D, middle part of shell. E, F, dorsal part of shell. Shell lengh = 13 mm.

Setigloma japonica (Smith, 1885)

Figure 3.21

Shell layers.—Outer, myostracum, and inner layers are present (Figure 3.21A). The outer and inner layers are both fine complex crossed lamellar structures. The myostracum is of an irregular simple prismatic structure. The outer and inner layers thicken ventrally, whereas the thickest part is in the middle of a radial section. The shell is up to approximately 120 μm thick in the observed specimen.

Outer layer.—Fine complex crossed lamellar structure (Figures 3.21A-E). Acicular crystals composing first-order lamellae of fine complex crossed lamellar structure are around 0.3 μm wide, up to 5 μm along the long axes, and inclined at around 15° to the deposit surface (i.e. growth line). Acicular crystals in the innermost part are larger than those in the outermost part. Irregular simple prismatic structure comprised of aligned acicular crystals is recognized at the growth lines (Figure 3.21D). Acicular crystals are 0.5 μm in width.

Myostracum.—Irregular simple prismatic structure (Figure 3.21E). The average width of these crystals is 0.5 μm

Inner layer.—Fine complex crossed lamellar structure (Figures 3.21E, F). Acicular crystals composing first-order lamellae are around 0.3 μm wide and up to 5 μm long in the long axes and inclined at around 15° to the deposit surface. Several growth lines are recognized in the irregular simple prismatic structure (Figure 3.21A).

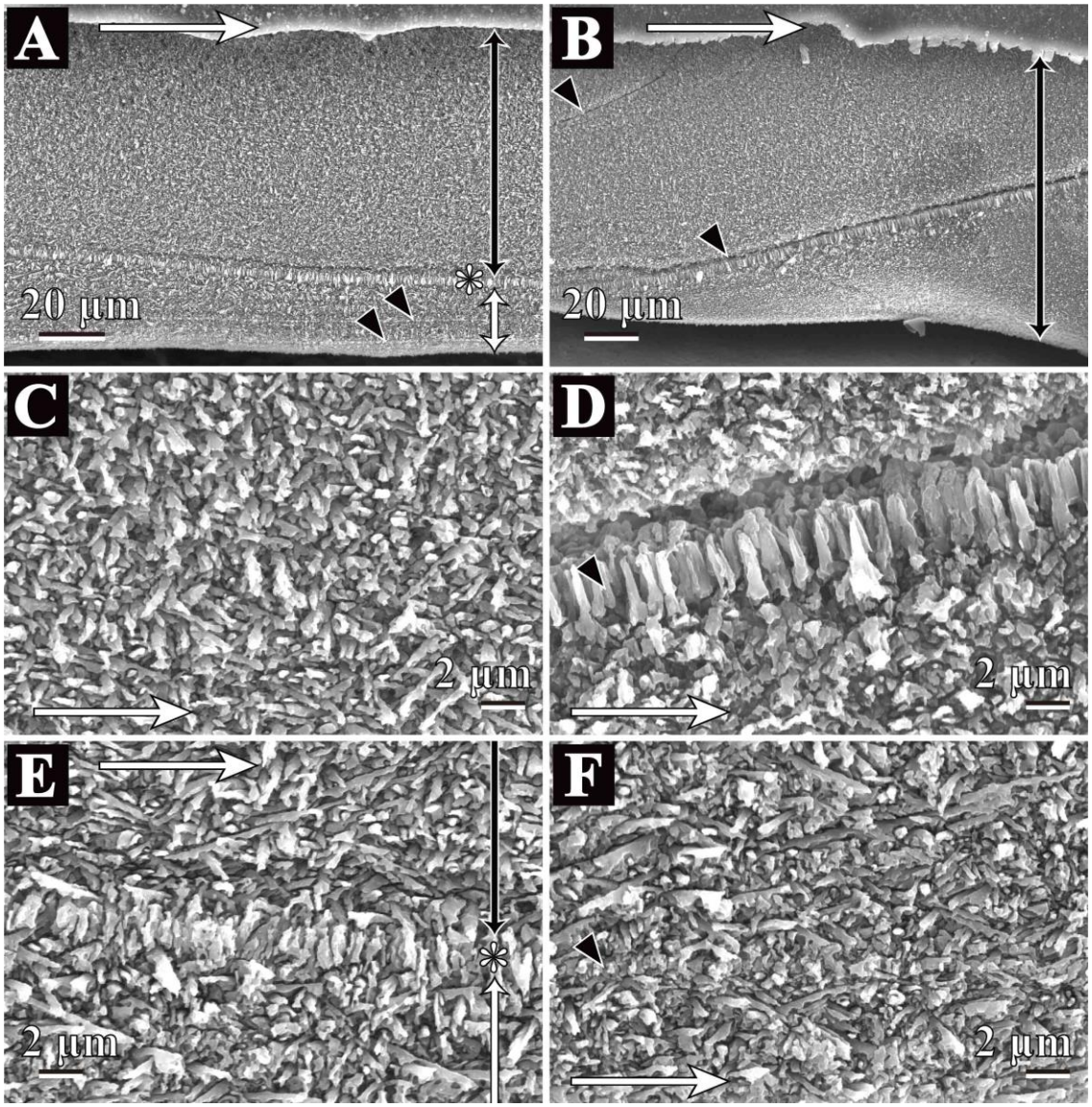

Figure 3.21. Scanning electron micrographs of *Setigloma japonica* microstructure. White arrow indicate growth direction. **A** radial section of middle part of the shell section. Black arrow, the outer layer; asterisk mark, myostracum; white arrow, the inner layer. Black arrow-head indicates growth lines. **B,** radial section of ventral part of the shell section. Black arrow, the outer layer. Black arrow-head indicates growth lines. **C,** radial section of fine complex crossed lamellar structure of the outer layer. **D,** radial section of fine complex crossed lamellar structure of the outer layer. Black arrow-head indicates growth lines. **E,** radial section which comprised of the outer, myostracum and inner layers. Vertical black arrow, the outer layer; asterisk mark, myostracum; white arrow, inner layer. **F,** radial section of fine complex crossed lamellar structure of the inner layer. A, C, E, F, middle part of shell. B, D, ventral part of shell. Shell lengh = 6 mm.

Superfamily Manzanelloidea

Family Manzanellidae

***Huxleyia sulcata* Adams, 1860**

Figure 3.22

Shell layers.—No layer construction is recognized due to the obscure or absent myostracum (Figure 3.22A). Thick periostracum with 10 μm average thickness covers the outer surface of the shell, periodically thickens inwards, and intrudes into the shell, where dark colored concentric ribs are recognized at the exterior shell surface. The shell thickens ventrally, reaching 142 μm.

Shell microstructures.—Mostly homogeneous structure and partly fine complex crossed lamellar structure (Figure 3.22B, D). The homogeneous structure is composed of granular crystals that are around 1 μm thick. Second-order crystals are less than 150 nm in diameter (Figure 3.22D). A fine complex crossed lamellar structure is distributed at the top one-third part of the shell. Acicular crystals in the fine complex crossed lamellar structure are 1 μm wide, up to 7 μm long in the long axes, and inclined at around 20° to the shell surface. At the inner part of the shell, several growth lines are distributed nearly parallel to the inner shell surface. Irregular simple prismatic structure composed of acicular crystals (up to 3 μm long, around 1 μm width) was observed at growth lines (Figure 3.22C, E). No growth lines are developed at the outer part of the shell, even where the periostracum thickens inwards, where growth breaks might have occurred.

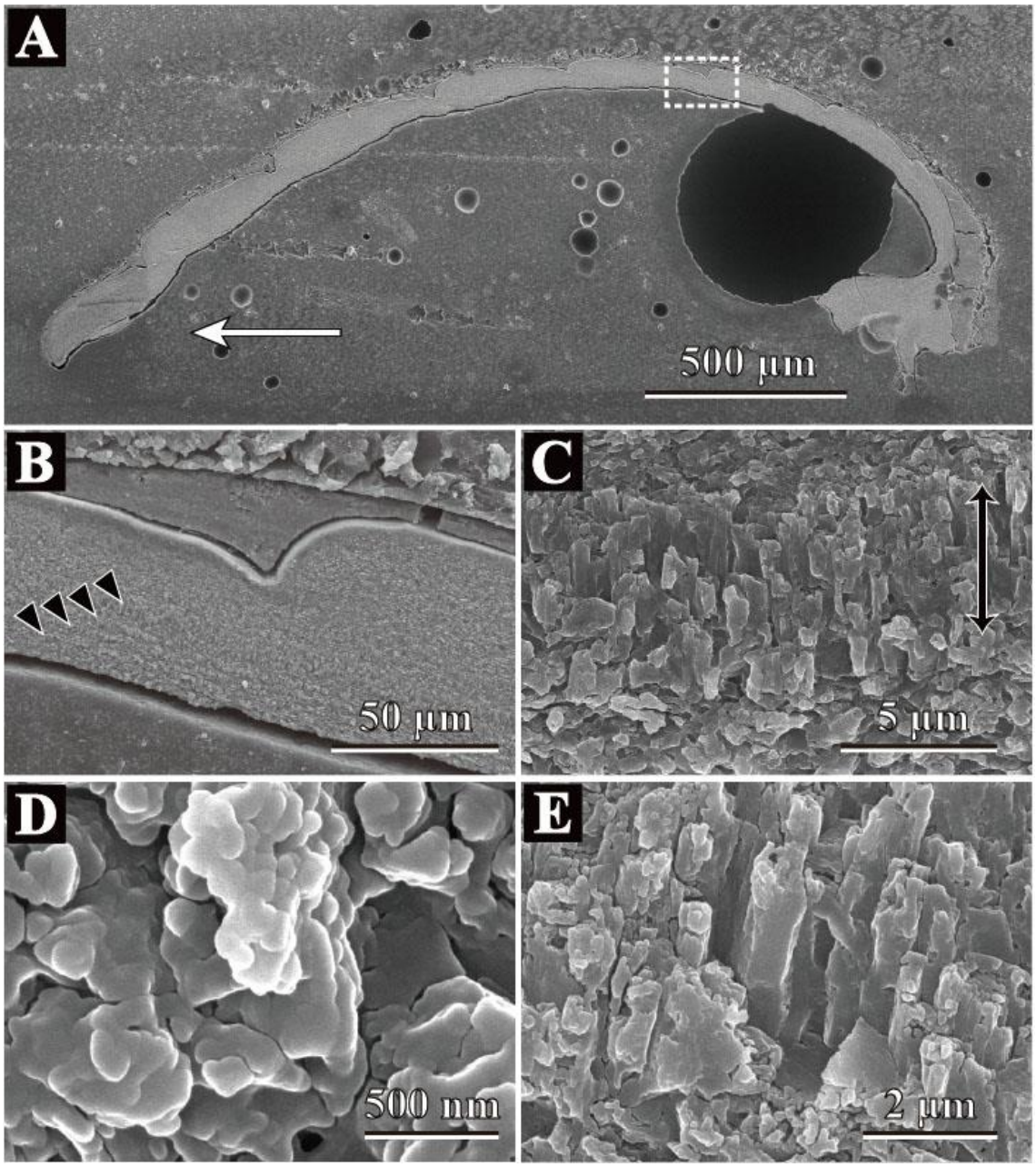

Figure 3.22. Scanning electron micrographs of *Huxleyia sulcata* microstructure. White arrow indicate growth direction. **A** radial section of observed *Huxleyia sulcata*. **B,** closer view of broken-lined square in A showing dorsal part of the shell section. Black arrow-head indicates growth lines. **C,** radial section of the outer layer which is comprised of homogeneous and irregular simple prismatic structures. Irregular simple prismatic structure (Black double-headed arrow) glow at growth line. **D,** radial section of homogeneous structure of the outer layer. **E,** more closed image of radial section of irregular simple prismatic structure of growth line of the outer layer. B-E, dorsal part of shell. . Shell lengh = 2 mm.

Superfamily Solemyoidea

Family Solemyidae

Solemya pervernicosa (Kuroda, 1948)

Figure 3.23

Shell layers.—Both outer and inner layers are present. The outer layer is composed of radially elongate simple prismatic structure (RESP; see Carter, 1990a; p. 610) (Figures 3.23A–D), and the inner layer is composed of irregular simple prismatic (ISP) structure (Figure 3.23E, F). The outer layer thickens ventrally, and the inner layer thickens dorsally. The inner layer is restricted to the area dorsal of the pallial line and adductor muscle scars. The boundary between the two layers is indistinct, and the myostracum is not observed. The periostracum is up to approximately 50 μm thick, and the shell is up to approximately 200 μm thick.

Outer layer.—RESP type A (for RESP types, see Table 3.2) (Figure 3.23A–D). The prisms are elongate in the radial direction (Figure 3.23A, C, and D), and their average width along the short axis is approximately 30 μm in a 31-mm-long specimen. Granular crystals, 0.5–1 μm in diameter that emerge in samples treated by chemical treatment method 3 (Figure 3.23B), are the second-order unit of the prisms. Neighboring crystals are frequently fused in a vertical direction toward the shell surface along interprismatic conchiolin sheets. In radial section, the fused granular crystals are visible as S-shaped structures (Figure 3.23A). A thin homogeneous layer (approximately 3 μm thick) is occasionally observed at the top of the outer layer (Figure 3.23B).

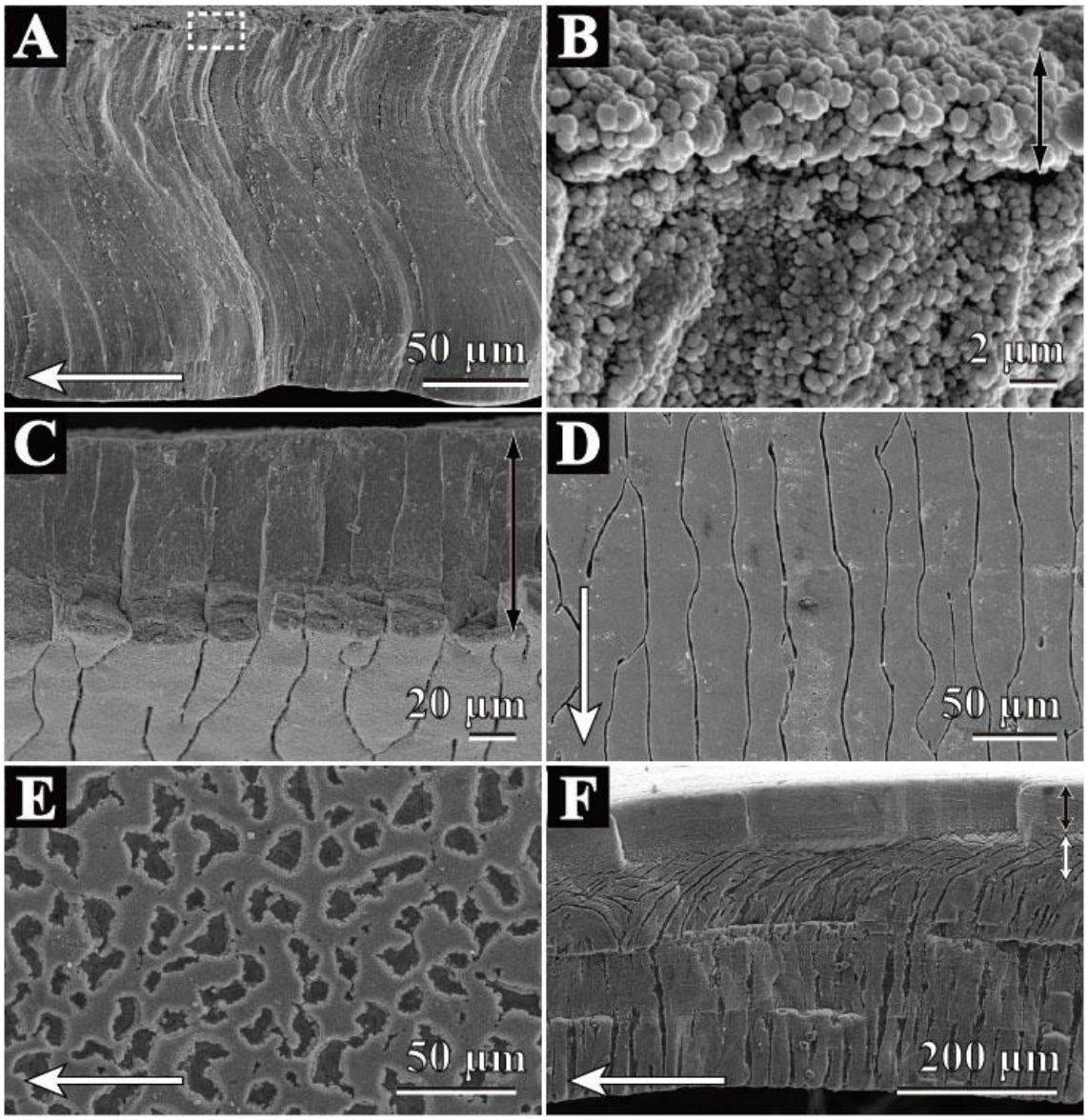

Figure 3.23. Scanning electron micrographs of *S.* (*P.*) *pervernicosa* shell microstructures, White arrows indicate growth direction. **A,** Radial section of radially elongate simple prismatic structure (RESP) of the outer layer; **B,** closer view of the broken-lined square in **A**. Granular crystals constituting RESP. A thin homogeneous layer is distributed above the outer layer as indicated by the black double-headed arrow. **C,** transverse section (black double-headed arrow) of the RESP of the outer layer. Inner shell surface is on the bottom side. **D,** inner surface of the RESP of the outer layer. Each prism is separated by conchiolin sheets and elongated in a radial direction. **E,** inner surface of irregular prismatic structure (ISP) of the inner layer. **F,** radial section of the RESP (black double-headed arrow) and ISP branching and bending in the outer part as indicated by the white double-headed arrow. (A), (B), anterior part of shell; (C), (D), anteroventral part; (E), (F), dorsal part. (A-F), RM30937. Shell length = 31 mm.

Inner layer.—ISP (Figure 3.23E, F). Interprismatic conchiolin sheets are observed as short discontinuous lines and dots on the inner shell surface (Figure 3.23E). In vertical section, the prisms, which are approximately 20 μm wide, become aggregated toward the shell surface (Figure 3.23F) because the irregular distribution of the conchiolin sheets allows the boundaries between prisms to fuse. The prisms branch and bend both ventrally and dorsally toward the outer shell layer. The complex of conchiolin sheets in the part of the inner layer next to the outer layer produces a blocky appearance in the sections.

Remarks: RESP is classified into three types (Types A, B, and C; Table 3.2).

Table 3.2. The characterization of the types of radially elongate simple prismatic structure (RESP) in solemyids.

RESP type	First order	Second order	Third order	Species
RESP type A	Elongated prisms.	S-shape structure	granular crystals	*S. pervernicosa* , *S. tagiri*
RESP type B	Elongated prisms in the radial direction perfectly.	three sublayers	-	*S. pusilla*
RESP type C	Elongated prisms that ramified into polygonal prisms.	granular crystals	-	*A. japonica*

Solemya tagiri Okutani, Hashimoto, and Miura, 2003

Figure 3.24

Shell layers.—Both outer and inner layers are present. The outer layer is composed of RESP type A (Figure 3.24A–D), and the inner layer is composed of ISP (Figures 3.24D, E). The outer layer thickens ventrally, and the inner layer thickens dorsally. The inner layer is restricted to the area dorsal of the pallial line and adductor

muscle scars. The boundary between the two layers is indistinct, and there is no myostracum. The periostracum is up to about 10 μm thick, and the shell is up to about 100 μm thick.

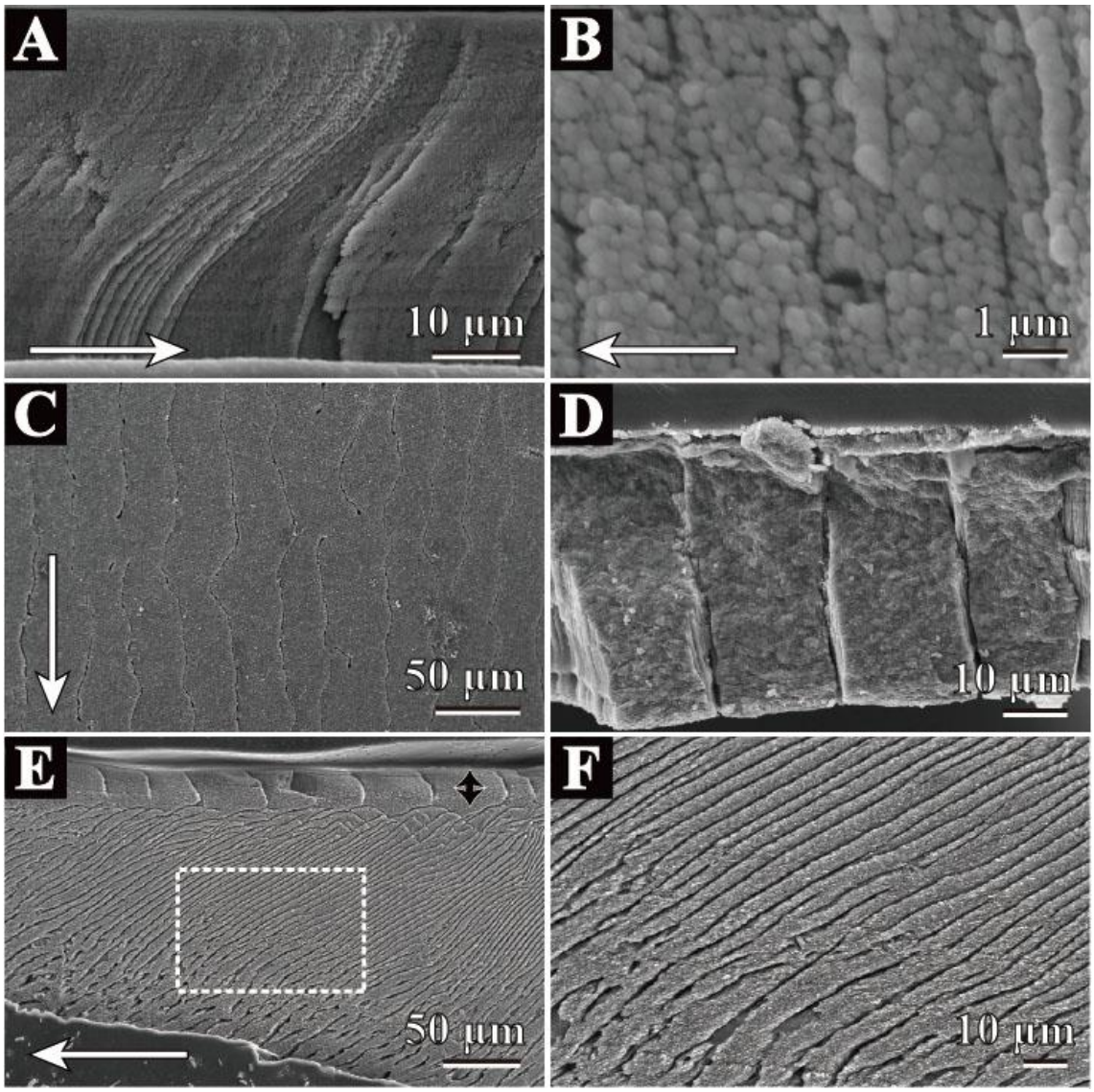

Figure 3.24. Scanning electron micrographs of *S.* (*S.*) *tagiri* shell microstructure. White arrows indicate growth direction. **A,** radial section of radially elongate simple prismatic structure (RESP) of the outer layer; **B,** closer view of the outer layer in a radial section; **C,** inner surface of the RESP of the outer layer. Each prism is partitioned by conchiolin sheets and elongated in a radial direction. **D,** transverse section of RESP of the outer layer. **E,** radial section of RESP (black double-headed arrow) and irregular prismatic structure (ISP). **F,** closer view of broken-lined square in (E). (A), middle part of shell; (B), (C), ventral part; (D), posteroventral part. (A), (E), (F), RM30936. (C), (D), RM30935. Shell length = 16.2 (RM30935) and 17 mm (RM30936).

Outer layer.—RESP type A (Figure 3.24A–D). The outer layer of this species resembles that of *S. pervernicosa*, but the orientation of the S-shaped structures is reversed (Figure 3.24A). The average width of the radially elongated prisms along their short axis is approximately 22 μm. The prisms are composed of granular crystals 0.5–1 μm in diameter (Figure 3.24B).

Inner layer.—ISP (Figure 3.24D, E). The inner layer of this species resembles that of *S. pervernicosa* but the conchiolin sheets do not exhibit ramification or fusing. Each prism is approximately 20 μm wide.

Solemya pusilla (Gould, 1861)

Figure 3.25

Shell layers.—This species has an outer and inner layer. The outer layer is composed of RESP type B (Figure 3.25A–E). The inner layer structure is homogeneous (Figure 3.25F). The outer layer increases in thickness ventrally, and the inner layer thickens dorsally. The inner layer is distributed only in the dorsal area. The boundary between the two layers is indistinct, and the myostracum was not observed. The periostracum and the shell are 7 μm and 75 μm thick, respectively.

Outer layer.—RESP type B (Figure 3.25A–E). The radially elongated prisms are aligned in parallel (Figure 3.25E) and obliquely to the radial ribs on the shell exterior. Their average width along the short axis is approximately 26 μm in an 8-mm-long specimen. The radially elongate prisms (Figure 3.25A) are composed of three sublayers characterized by crystals of different shapes and sizes. The outermost sublayer is composed of acicular crystals (3 μm long by 0.5 μm in diameter) aligned

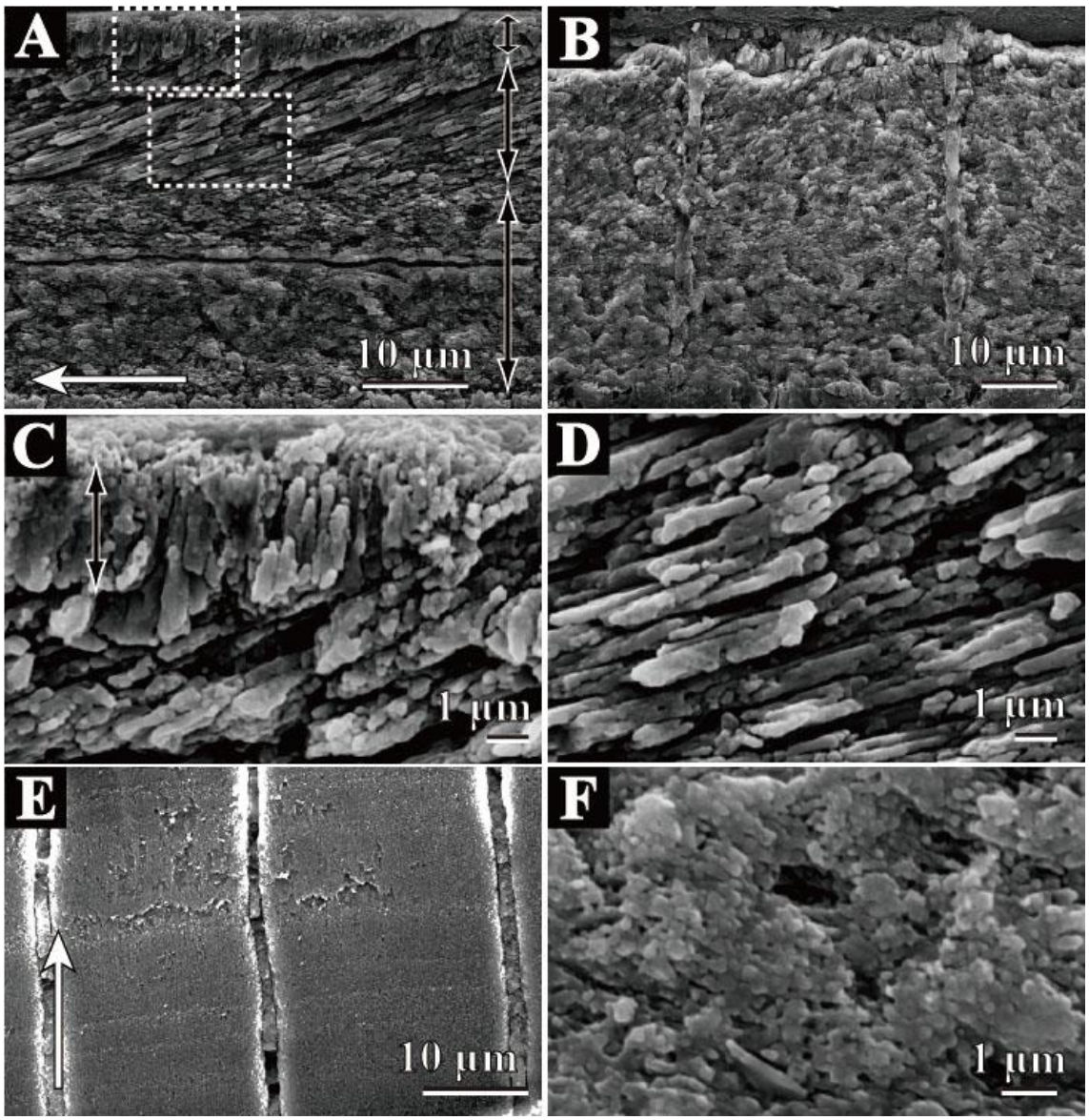

Figure 3.25. Scanning electron micrographs of *S. pusilla* microstructure. White arrows indicate growth direction. **A,** radial section of the outer and inner layers embedded in resin. The boundary between the two layers is indistinct. Upper and lower broken lined squares show (C) and (D), respectively. Black double-headed arrow indicates the three sublayers. The sample is partially delaminated. **B,** transverse section of RESP of the outer layer. The sample was embedded in resin. **C,** closer view of **A**, showing vertical acicular crystals in the outer sublayer of RESP and reclined acicular crystals in middle sublayer of RESP. **D,** closer view of (A), showing reclined acicular crystals in middle sublayer of RESP; **E,** Outer surface of RESP of the outer layer. The periostracum is removed. **F,** granular crystals of the inner layer in a radial section. (**A),** (C-F), ventral part of shell; (B). anterior part. (A-F), RM30939. Shell length = 6.1 mm.

perpendicular to the shell surface or of granular crystals (Figure 3.25C). The middle sublayer is composed of acicular crystals (up to 6 μm long and 0.5–1 μm in diameter) that slant downward at an angle of approximately 20° against the growth direction (Figure 3.25D). The innermost sublayer is composed of granular crystals that are 0.3–0.5 μm in diameter.

Inner layer.—Homogeneous structure (Figure 3.25F). Granular crystals are 0.5 μm in diameter and lack a clear first-order structural arrangement. Conchiolin sheets are absent in this layer, in contrast to the innermost sublayer of the outer layer.

Acharax japonica (Dunker, 1882)

Figures 3.26, 27

Shell layers.—This species has an outer and inner layer. The outer layer is composed of RESP type C structure (Figures 3.26A–F, 3.27A), and the inner layer is characterized by laminar, homogeneous, and irregular complex crossed lamellar structures (Figures 3.26A, C, 3.27B-D). The outer layer thickens ventrally, and the inner layer thickens dorsally. The inner layer is restricted to the area dorsal of the pallial line and adductor muscle scars. The boundary between the two layers is indistinct, and there is no myostracum. In a 16-mm-long specimen, the thicknesses of the periostracum and the shell are about 17 μm and 180 μm, respectively.

Outer layer.—RESP type C (Figures 3.26A–F, 3.27A). The radially elongated prisms (Figure 3.26D) branch toward the outer surface and bend dorsally (Figure 3.26A). In horizontal section, the branched outer part of the outer layer is similar in appearance to a polygonal prism (Figure 3.26E). The boundary between areas of

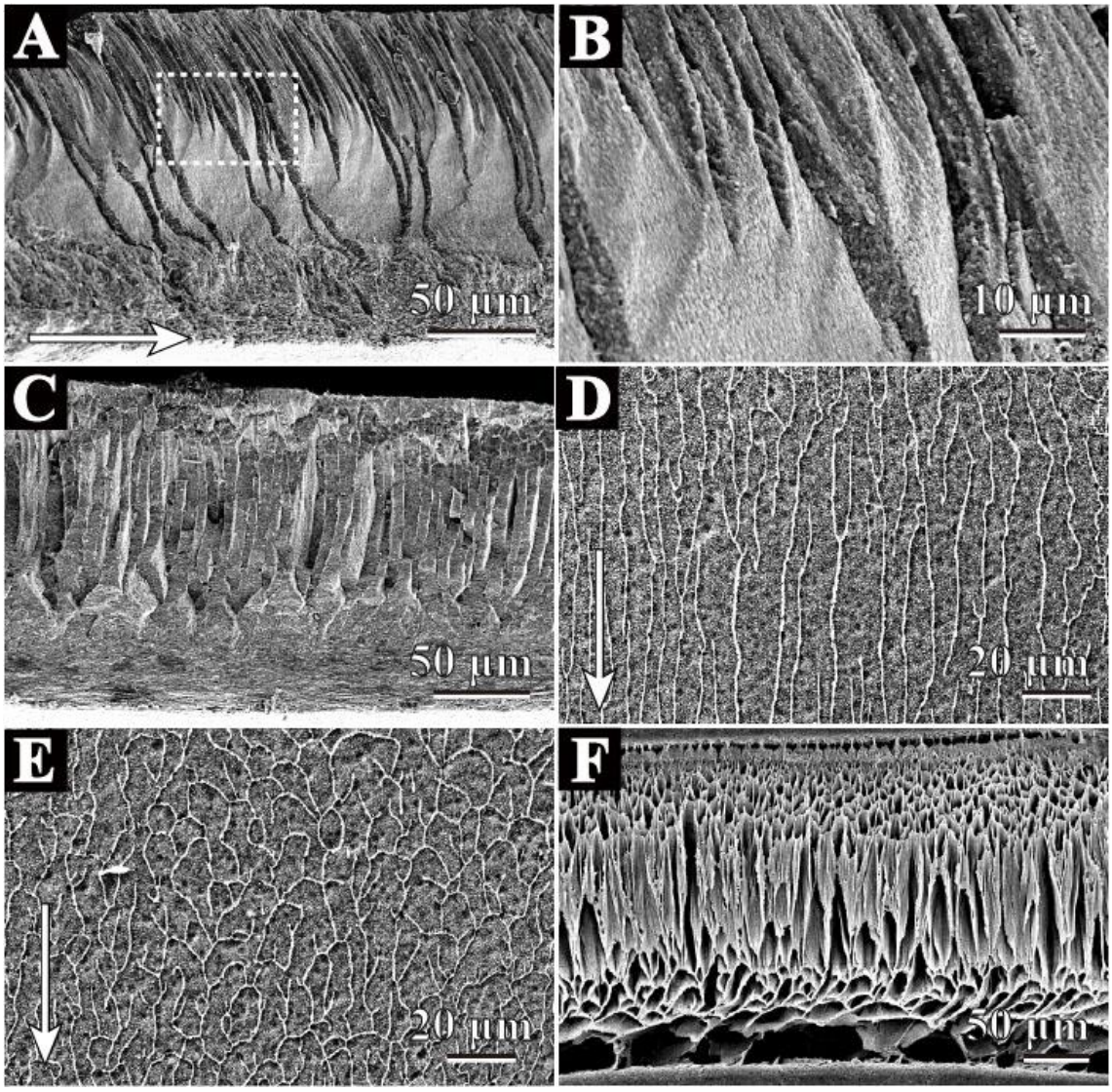

Figure 3.26. Scanning electron micrographs of *A. japonica*. White arrows indicate growth direction. **A,** radial section of radially elongate simple prismatic structure (RESP) of the outer layer with the laminar structure of the inner layer; **B,** closer view of the broken-lined square in (A). There is no clear boundary between the simple prisms (upper part) and elongated prisms (lower part); **C,** transverse section of RESP of the outer layer and the laminar structure of the inner layer. **D,** horizontal section of the lower part of the RESP. Each prism is elongated in the radial direction. **E,** horizontal section of the upper part of the RESP. **F,** decalcified transverse section of RESP embedded in resin (sample preparation part 1). RESP of this section is mostly composed of simple prisms. (A)-(C), anteroventral part of shell; (D), (E), dorsal part, (F), anterior part. (A)-(C), RM30919; (D), RM30921; (E), (F), RM30924. Shell length = 7.7-15.9 mm.

radially elongated and polygonal prisms is not clear (Figure 3.26B). The radially elongated prisms are distributed over the entire shell, whereas the polygonal prisms are dominantly in the anterior part (Figure 3.26F). The average width of both the radially elongated and the polygonal prisms is approximately 4 μm in a 15-mm-long shell. Both types of prisms are composed of granular crystals that are 0.3–0.5 μm in diameter. A thin layer of granular or acicular crystals is present at the top of the outer layer (Figure 3.27A).

Inner layer.—Laminar, homogeneous, and irregular complex crossed lamellar structures (Figures 3.26A, C, 3.27B–D). The microstructures of the inner layer vary among individual specimens in this species. In most specimens, the inner layer is characterized by laminar and homogeneous structures. Irregular complex crossed lamellar structures are rarely observed in the dorsal part of the inner layer (Figure 3.27D). The granular crystals composing the homogeneous structure are 0.5 μm in diameter and are without any clear first-order structural arrangement (Figure 3.27B). The laminar structure is composed of irregularly shaped lath crystals arranged in sheets parallel to the depositional surface. The long axes of the laths are oriented transversally (Figure 3.27C). The lath crystals occasionally are aggregated into irregularly shaped second- order units, producing an irregular complex crossed lamellar structure (Figure 3.27D).

Acharax johnsoni (Dall, 1891)

Figures 3.28-30

Shell layers.—This species has an outer and inner layer. The outer layer is composed of reticulate structure (Figure 3.28A–F), and the inner layer is composed of cone complex crossed lamellar structure (Figure 3.30A–F). The outer layer thickens ventrally, and the inner layer thickens dorsally. The inner layer is restricted to the area dorsal of the pallial line and adductor muscle scars. The boundary between the two layers is indistinct, and there is no myostracum. In a 62-mm-long specimen, the thickness of the periostracum is 20 μm, and that of the shell is 2 mm.

Outer layer.—Reticulate structure (Figures 3.28A–F, 3.29A–D). This structure consists of nested units: A units are blocky and B units are nonstructural and fill the spaces between the blocky A units (Figure 3.28A, C–E). Both types of units are variable in shape and are characterized by an irregular nested arrangement. The relative numbers of the two units change from the outer to the inner shell surfaces. B units up to 30 μm wide are dominant near the outer surface, but their width diminishes toward the inner shell surface (Figure 3.28A, B). The A units are rhomboidal and 10–20 μm wide in a 91- mm-long specimen in the inner part of the layer (lower side of Figure 3.28A); in the middle part they are trapezoidal, and in the outer part they are V-shaped or hexagonal. All of these A-unit shapes are similarly observed in both radial and transverse sections (Figure 3.28C, D). In a 91- mm-long specimen, the V-shaped units are up to 70 μm wide, and the hexagonal units are 10–20 μm wide. A network of conchiolin sheets separates the two types of units (Figures 3.28B, 3.29B–D). Both types of structural units are composed of granular crystals. Granular crystals composing A units are

approximately 0.4–0.5 μm in diameter, and those composing B units are approximately 0.3–0.4 μm in diameter (Figures 3.28F, 3.29A). The latter become fused in a direction vertical to the shell surface (Figures 3.28E, 3.29A).

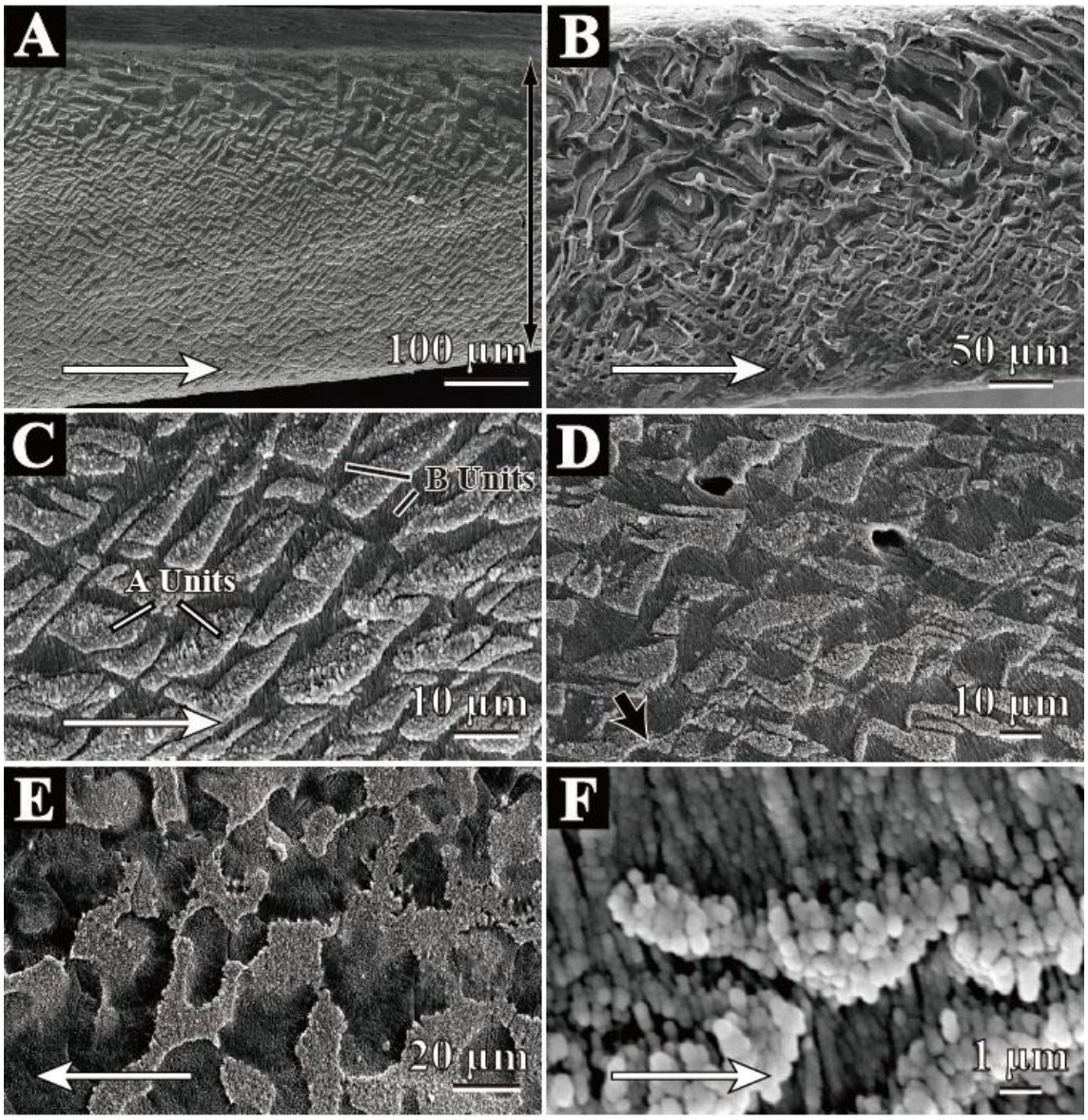

Figure 3.28. Scanning electron micrographs of the outer layer of *A. johnsoni*. White arrows indicate growth direction. **A,** radial section of reticulate structure (with black double-headed arrow) that is composed of blocky units (A units) and nonstructural units (B units); **B,** radial section of the reticulated structure. Conchiolin sheets rolled up in unit B. **C–E,** the reticulate structure sections at higher magnification. (C). radial section; (D). Transverse section. Black arrow indicates the direction of inner surface. (E). Outer surface. **F,** radial section of the reticulate structure at a higher magnification. (A), (F), anterior part of shell. (B), posteroventral part. (D). anterodorsal part. (E), ventral part. (A)-(D), (F), RM30912. (E), RM30913. Shell length = 62.9 (RM30913) and 91.7 mm (RM30912).

Inner layer.—Cone complex crossed lamellar structure (c-CCL) (Figures 3.30A–F). Elongated structural units are composed of stacked aggregated cones (Figure 3.30A, B) that interdigitate along their lateral boundaries. These structural units are up to 40 μm wide in a 91-mmlong specimen. The direction of stacking is normally perpendicular to the growing surface. The second-order lamellae are cone-like, and the apical angles of the cones range from 110° to 120°. The third-order lamellae are spicular or slightly platy (Figure 3.30C) and approximately 0.3 μm wide. Conchiolin sheets are distributed both obliquely (Figure 3.30D, E) and along growth lines (Figure 3.30D). Oblique conchiolin sheets have dip angles of about 20°–30° relative to the shell surface (Figure 3.30D, E). The sheets are irregularly distributed and transect the first order structural units.

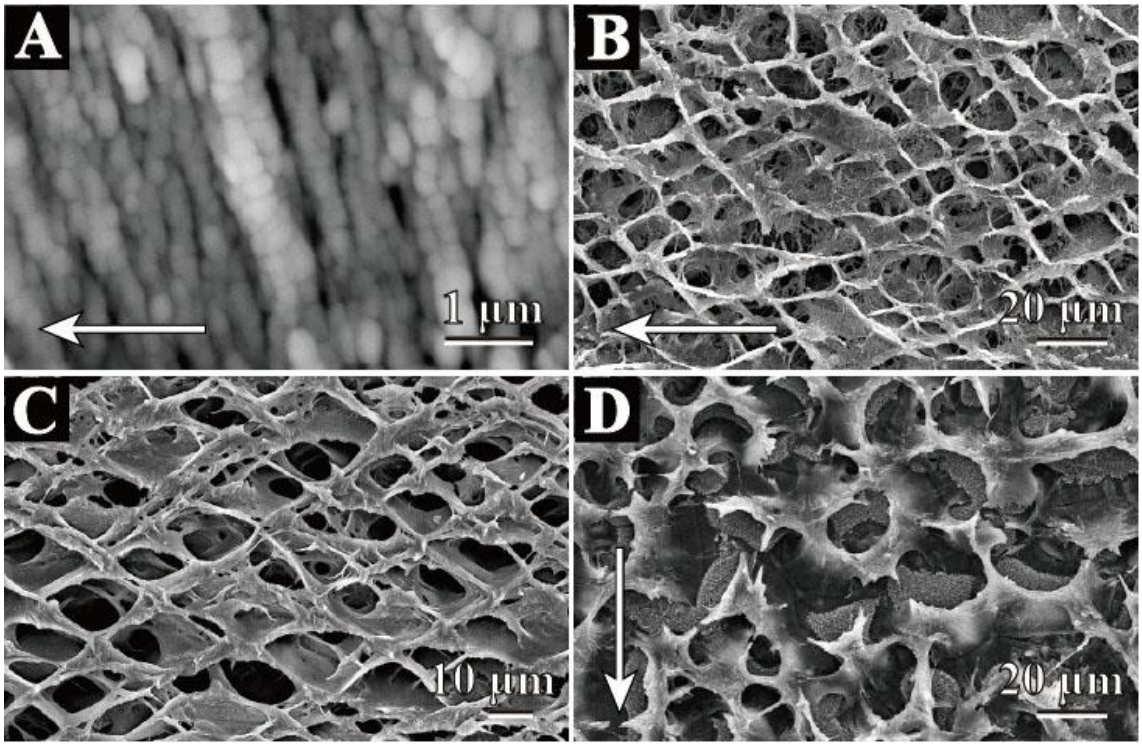

Figure3.29. Scanning electron micrographs of the outer layer of *A. johnsoni*. White arrows indicate growth direction. **A,** Radial section of B units of the reticulate structure; **B–D,** decalcified reticulate structure. Conchiolin sheets rolled up in B unit in a net-like shape. (B), radial section. (C), transverse section. (D), horizontal section. (A), . anterior part of shell. (B), posterior part. (C), anteroposterior part. (D), posterior part. (A), (B), (D), RM30912. (C), RM30913. Shell length = 62.9 (RM30913) and 91.7 mm (RM30912).

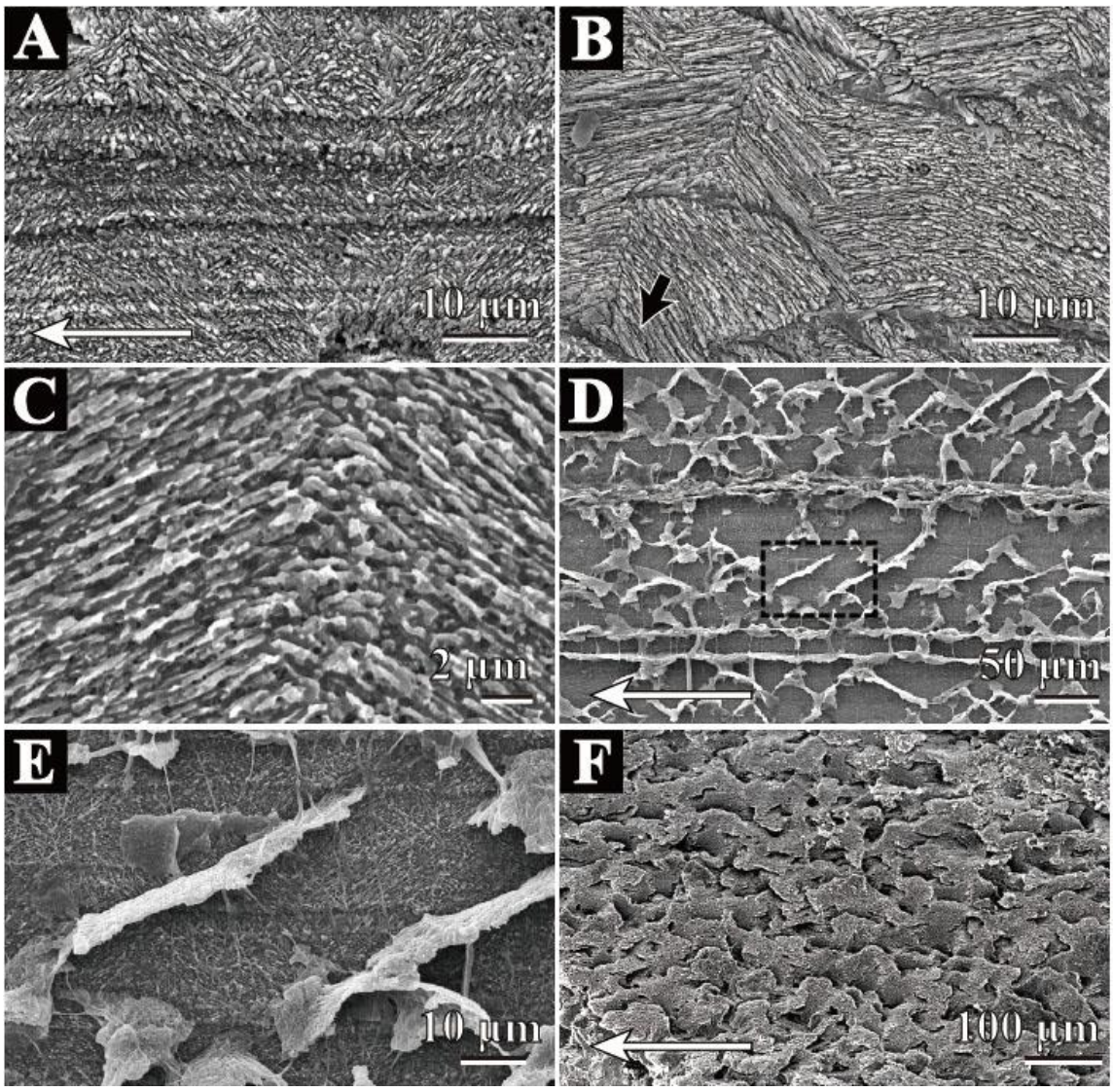

Figure 3.30. Scanning electron micrographs of cone complex crossed lamellar (cCCL) structure of the inner layer of *A. johnsoni*. White arrows indicate growth direction. **A, r**adial section of the cCCL structure; **B,** transverse section of the cCCL structure. Black arrow indicates the direction of the inner surface. **C,** transverse section of the cCCL structure at high magnification; **D,** radial section of the cCCL structure. Conchiolin sheets are inserted along growth lines or irregularly. **E,** closer view of the broken-lined square in D; **F,** inner surface of the cCCL structure. (A)-(E), anterodorsal part. (F), posterior part. (A)-(C), (F), RM30913. (D), (E), RM30912.

Superfamily Nuculanoidea

Family Nuculanidae

Nuculana soyoae Habe, 1958

Figures 3.31, 32

Shell layers.—Outer, myostracum and inner layers are present (Figure 3.31). The outer and inner layers are both homogeneous structures. A fine complex crossed lamellar structure is partly recognized in the outer layer. Granular crystals compose the homogeneous structures of both layers and decrease in diameter inwards. The myostracum is of obscure to irregular simple prismatic structure. The outer layer thickens ventrally. The myostracum and inner layer thickens dorsally. The shell is robust for this family and up to approximately 550 μm thick in the observed specimen.

Outer layer.—Homogeneous structure (Figures 3.32A–C, E) and fine complex crossed lamellar structure. The homogeneous structure is composed of granular crystals (Figures 3.32A, B). The diameter of granular crystals is around 1 μm and decreases in size inwards, up to around 0.5 μm. The first-order elements of the fine complex crossed lamellar structure are up to 4 μm long in the long axes. Several growth lines are comprised of irregular simple prismatic structures (Figures 3.32C). The shape and size never change along the concave-convex surface of the shell.

Myostracum.—Obscure to irregular simple prismatic structure (Figure 3.32D, E). Irregular simple prismatic structure is recognized at the dorsal part of the shell and consists of vertically aligned acicular crystals. The average width of these crystals is 0.5 μm

Inner layer.—Homogeneous structure (Figures 3.32D-F). Fine granular crystals (approximately 0.2 μm) compose this structure. Several growth lines are composed of relatively large granular crystals.

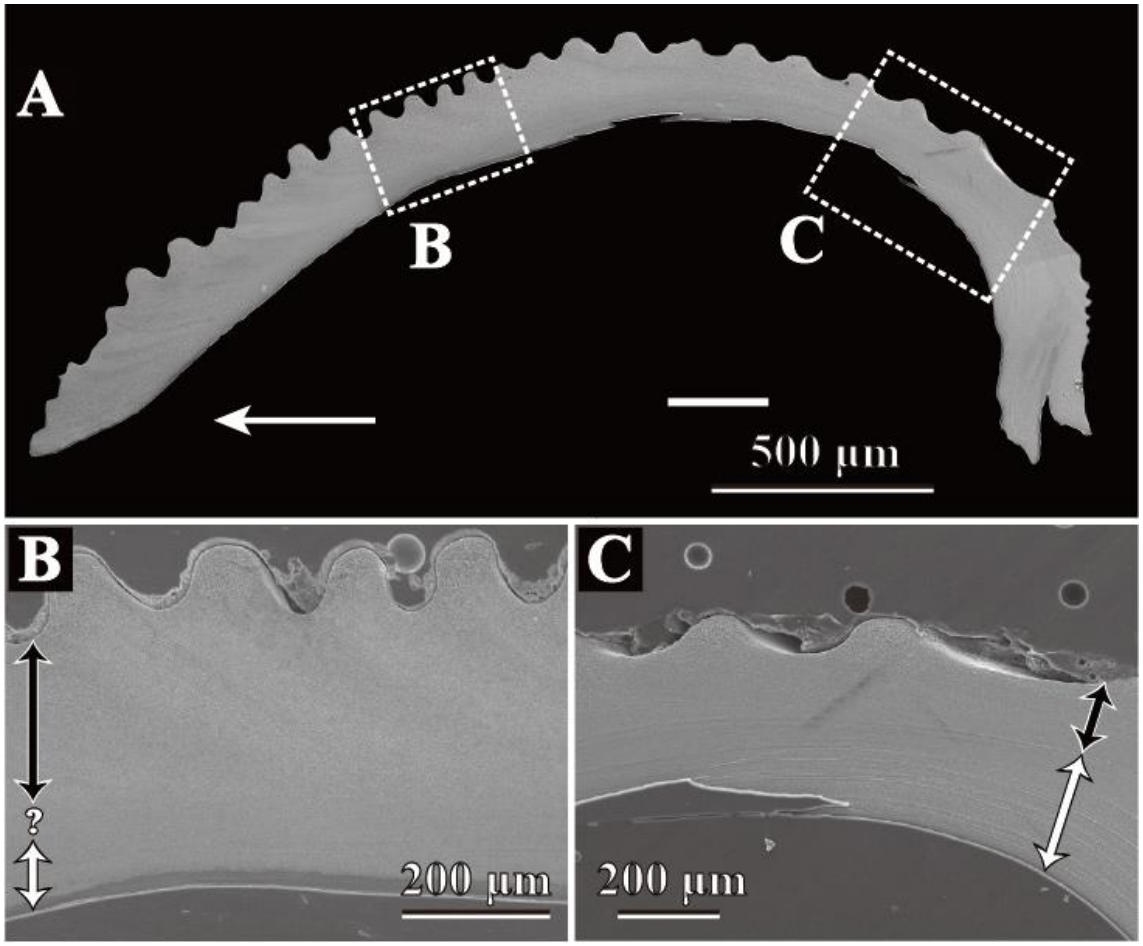

Figure 3.31. Scanning electron micrographs of *Nuculana soyoae* microstructure. White arrow indicate growth direction. **A** radial section of observed *Nuculana soyoae*. **B,** closer view of broken-lined square in A showing ventral part of the shell section. Black double-headed arrow, the outer layer; white double-headed arrow, inner layer; Question mark implies obscure margin of two layers. **C,** closer view of broken-lined square in A showing dorsal part of the shell section. Black double-headed arrow, the outer layer; white double-headed arrow, inner layer. . Shell lengh = 11 mm.

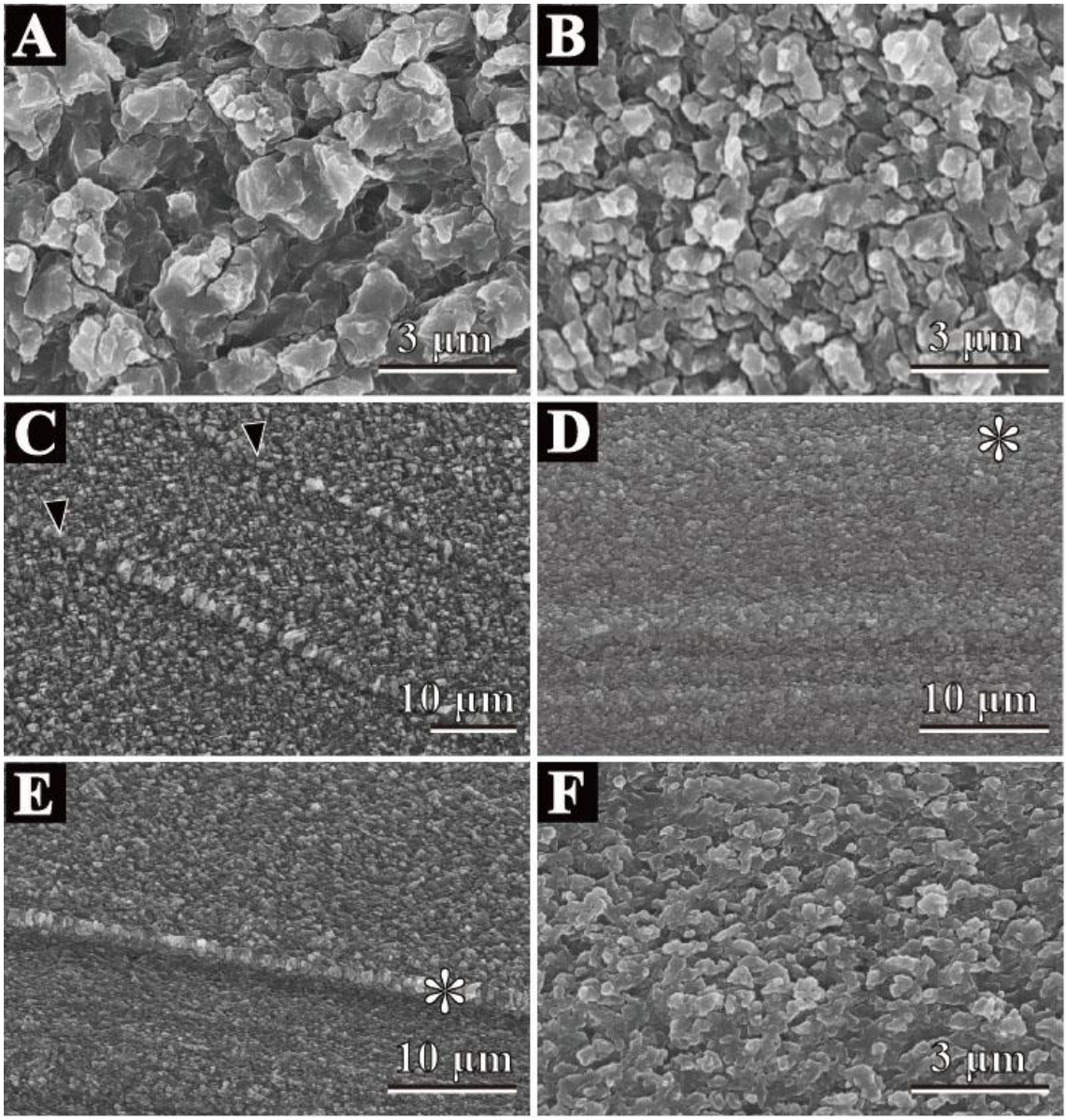

Figure 3.32. Scanning electron micrographs of *Nuculana soyoae* microstructure. White arrow indicate growth direction. **A** radial section of homogeneous structure of outer part of the outer layer. **B,** radial section of homogeneous structure of inner part of the outer layer. **C,** radial section of the outer layer. Black arrow-head indicates glowth lines. **D,** radial section of homogeneous structure of the inner layer. Asterisk mark indicates the myostracum layer. **E,** radial section of homogeneous structure of the inner layer at dorsal part. Asterisk mark indicates the myostracum layer. **D,** radial section of homogeneous structure of the inner layer. A-D, middle part of shell. E, F, dorsal part of shell. . Shell lengh = 11 mm.

Nuculana tanseimaruae Tsuchida & Okutani, 1985

Figure 3.33

Shell layers.—Outer, myostracum, and inner layers are present. The outer layer is composed of fibrous prismatic structures on the outermost part and homogeneous structures on the inner part, and partially of fine complex crossed lamellar structures. The myostracum is composed of an irregular simple prismatic structure. The inner layer is a homogeneous structure and the thickness of the inner layer is very thin. The outer layer thickens ventrally. The inner layer generally thickens ventrally, whereas the thickest part is distributed in the middle part of a radial section. The thickness of the shells are almost constant, being approximately 230 μm thick in the observed specimen.

Outer layer.—Fibrous prismatic structure, homogeneous structure, and partly fine complex crossed lamellar structure (Figure 3.33B-E). Fibrous prismatic structure is distributed only in the outermost part of the shell (Figure 3.33C). Its thickness is up to 50 μm. Acicular crystals comprising the fibrous prismatic structure are up to 8 μm long in the long axes, around 0.7 μm wide, and align vertically to the deposit surface. The homogeneous structure is composed of granular crystals whose diameter is around 0.5 μm (Figure 3.33D). Fine complex crossed lamellar structure is partially distributed at the ventral part of the shell where growth rings have accumulated. Acicular crystals are up to 4 μm long in the long axes.

Myostracum.—Irregular simple prismatic structure (Figure 3.33E). The of this family shows good thickness, up to 4 μm. The average width of these crystals is 0.4 μm.

Inner layer.—Homogeneous structure. Fine granular crystals of this structure are less than 0.3 μm wide. Growth lines in this layer consist of irregular simple

prismatic structures.

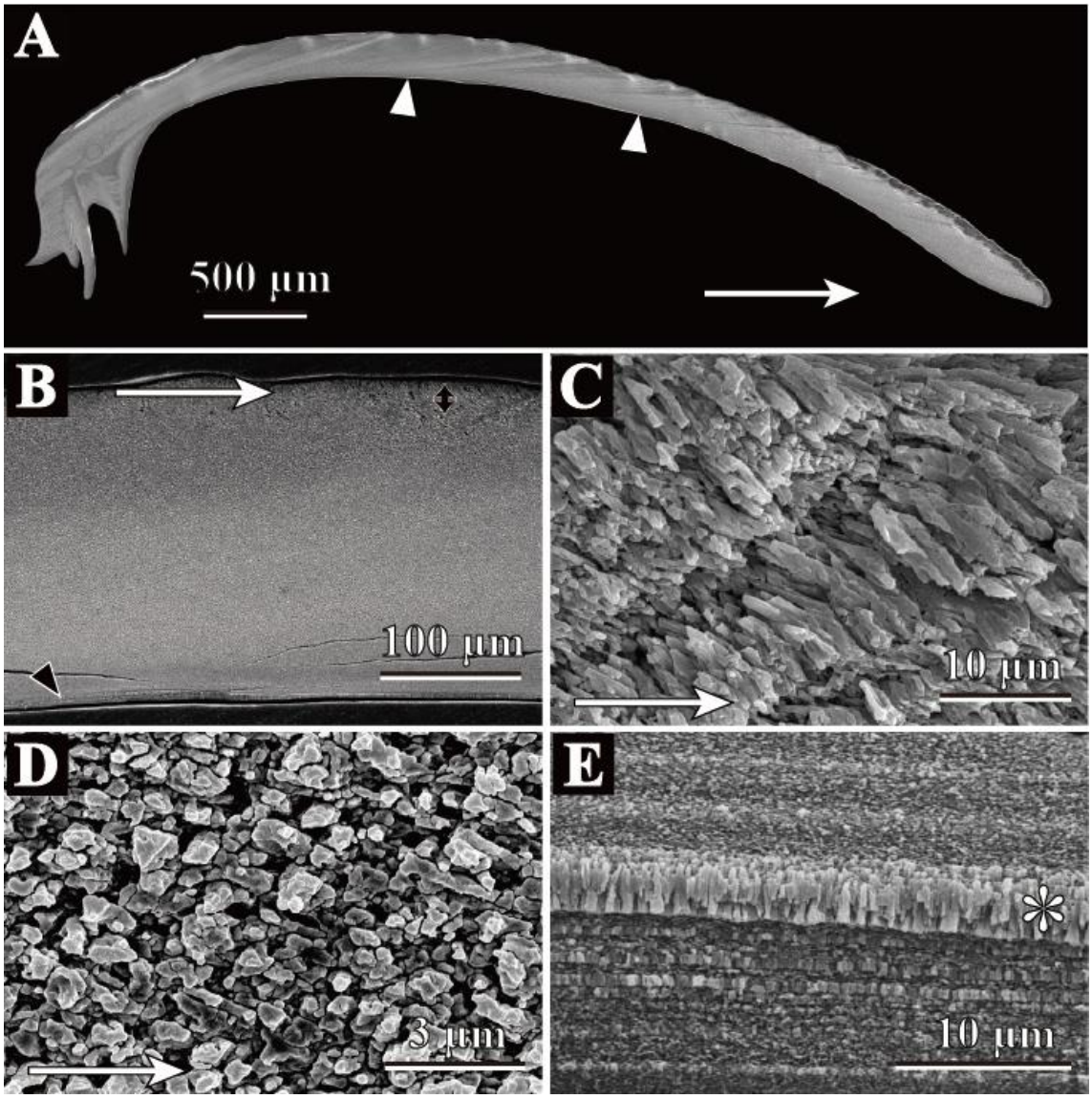

Figure 3.33. Scanning electron micrographs of *Nuculana tanseimaruae* microstructure. White arrow indicate growth direction. **A,** radial section of observed *Nuculana tanseimaruae*. White arrow heads indicate the beginning of the inner layer and end of it (i.e. the inner layer distributes between these two arrow heads). **B,** radial section of the outer and myostracum layers. Black double-headed arrow indicates fibrous prismatic structure and black arrow head indicates the myostracum layer. **C,** radial section of fibrous prismatic structure of the outer layer. **D,** radial section of homogeneous structure of the outer layer. **E,** radial section of the outer, myostracum and inner layers. Asterisk mark indicates the myostracum layer. B, D, middle part of shell. C, ventral part of shell, E, dorsal part of shell. . Shell length = 15 mm.

Nuculana leonina Okutani, 1962

Figure 3.34

Shell layers.—Outer and inner layers are present. The outer and inner layers are both composed of a homogeneous structure. The myostracum is obscure. The outer and inner layers thicken ventrally. The shell is up to approximately 280 μm thick in the observed specimen.

Outer layer.—Homogeneous structure (Figure 3.34B, C). The diameter of the granular crystals is around 0.4 μm and diminishes in size inwards, up to around 0.2 μm. Radial ribs on the shell surface do not change the crystal size and morphology.

Myostracum.— Obscure, but recognized as bright lines in the SEM observations with no change in crystal morphology (Figure 3.34C).

Inner layer.— Homogeneous structure (Figure 3.34C, D). The diameter of granular crystals is around 0.2 μm.

Figure 3.34 (next page)**.** Scanning electron micrographs of *Nuculana leonina* microstructure. White arrow indicate growth direction. **A,** radial section of dorsal part of the shell section. Black arrow, the outer layer; question mark, probable position of the myostracum; white arrow, the inner layer. **B,** radial section of homogeneous structure of the outer layer. **C,** radial section of the outer, myostracum and inner layers. Vertical black arrow indicates the outer layer. Asterisk mark shows the myostracum layer and white arrow is the inner layer. **D,** radial section of homogeneous structure of the inner layer. A-D, dorsal part of shell. A-D, Shell length = 20 mm.

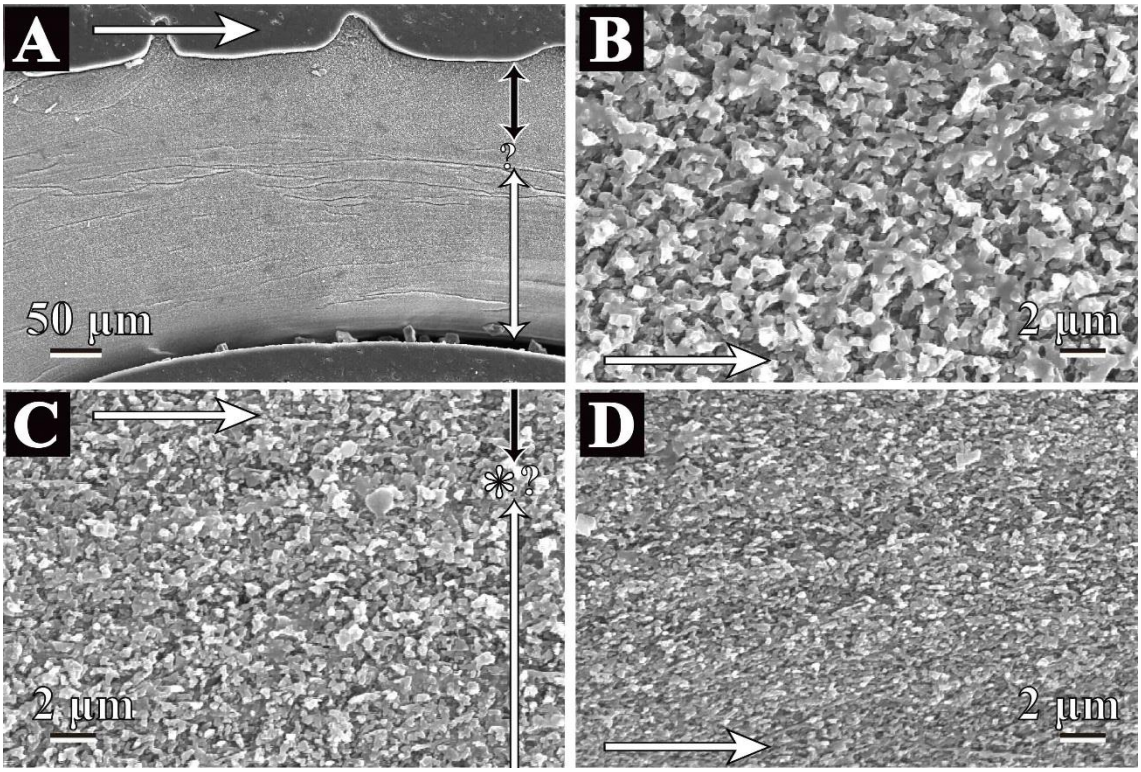

***Nuculana yokoyamai* Kuroda, 1934**

Figure 3.35

Shell layers.—Outer and inner layers are present (Figure 3.35A). The outer and inner layers are both of homogeneous structures. The myostracum is obscure. Both the inner and outer layers thicken ventrally. The shell is up to approximately 352 μm thick in the observed specimen.

Outer layer.—Homogeneous structure (Figures 3.35A-C). Granular crystals or partly acicular crystals compose this layer. The diameter of the granular crystals is around 0.5 μm and they slowly decrease in size inwards, up to around 0.3 μm. The

radial ribs on the shell surface do not alter the crystal size and morphology. Growth lines are recognized as bright lines in the observation using SEM, while the crystal morphology is not altered.

Inner layer.— Homogeneous structure (Figures 3.35C, D). The diameter of granular crystals is around 0.3 μm. Growth lines are recognized as bright lines in the observation using SEM, while the crystal morphology is constant.

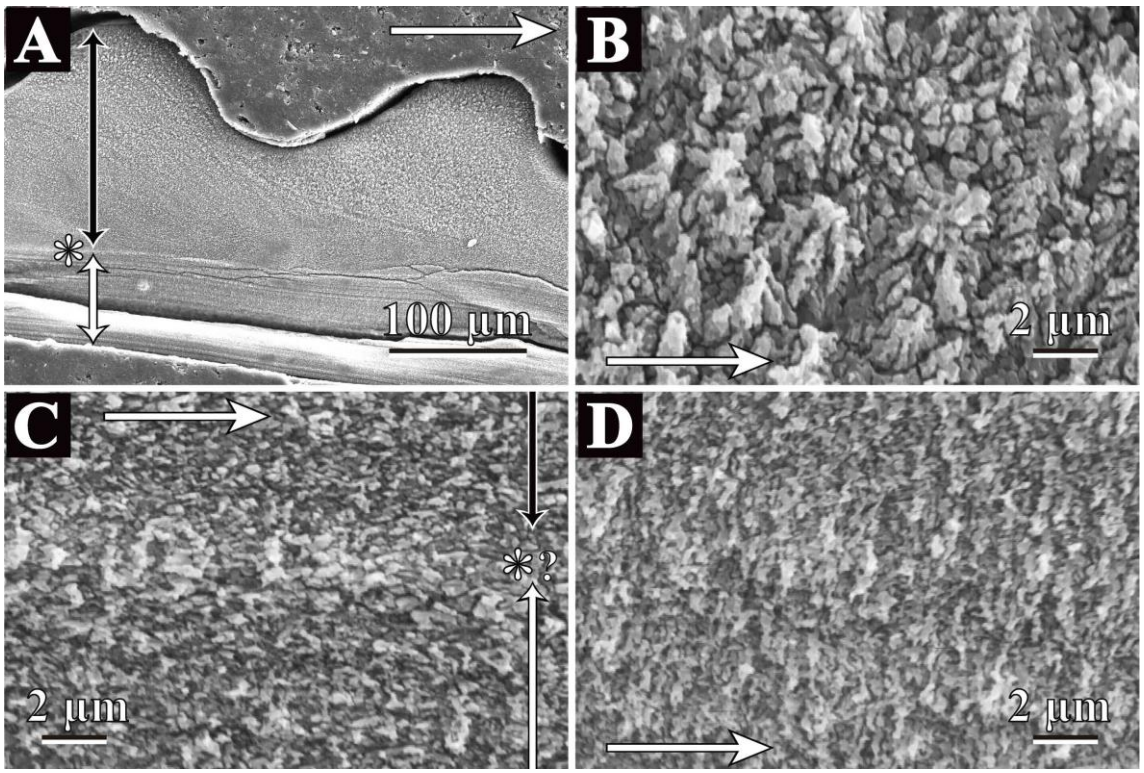

Figure 3.35. Scanning electron micrographs of *Nuculana yokoyamai* microstructure. White arrow indicate growth direction. **A,** radial section of middle part of the shell section. Black arrow, the outer layer; asterisk mark, myostracum; white arrow, the inner layer. **B,** radial section of homogeneous structure of the outer layer. **C,** radial section of homogeneous structure of the outer, myostracum and inner layers. Vertical black arrow indicates the outer layer. Asterisk mark shows the myostracum layer and white arrow is the inner layer. radial section of homogeneous structure of the outer layer. **D,** radial section of homogeneous structure of the inner layer. A-D, middle part of shell. A-D, Shell length = 9 mm.

Nuculana gordonis (Yokoyama, 1920)

Figure 3.36

Shell layers.—Outer, myostracum, and inner layers are present. The outer layer has two sublayers, fibrous prismatic structure in the outer sublayer and homogeneous structure and some fine complex crossed lamellar structures in the inner sublayer. The Myostracum is composed of obscure to irregular simple prismatic structures, and the inner layer of homogeneous structures. The outer and inner layers thicken ventrally. The shell is up to approximately 148 μm thick in the observed specimen.

Outer layer.—Fibrous prismatic (Figure 3.36C) and homogeneous structure (Figure 3.36D). Fibrous prismatic structure in the outer sublayer of the outer layer is distributed only in the outermost part of the shell. The thickness of the outer sublayer is up to 14 μm. Acicular crystals composing the outer sublayer are up to 4 μm long in the long axes, around 0.4 to 4 μm wide, and slant at angles of approximately 55° against the growth direction in a radial section. The inner sublayer of the outer layer consists of a homogeneous structure, whose granular crystals are 0.7 μm in diameter. Acicular crystals partly grow up to 6 μm long in the long axes and form fine complex crossed lamellar structures in the inner sublayer.

Myostracum.—Generally obscure, partly irregular simple prismatic structure. The average width of acicular crystals in the irregular simple prismatic structure is less than 0.5 μm.

Inner layer.— Homogeneous structure (Figure 3.36E). The diameter of the granular crystals is around 0.3 μm. Growth lines are recognized as bright lines in the observation using SEM, while no change in crystal morphology is recognized.

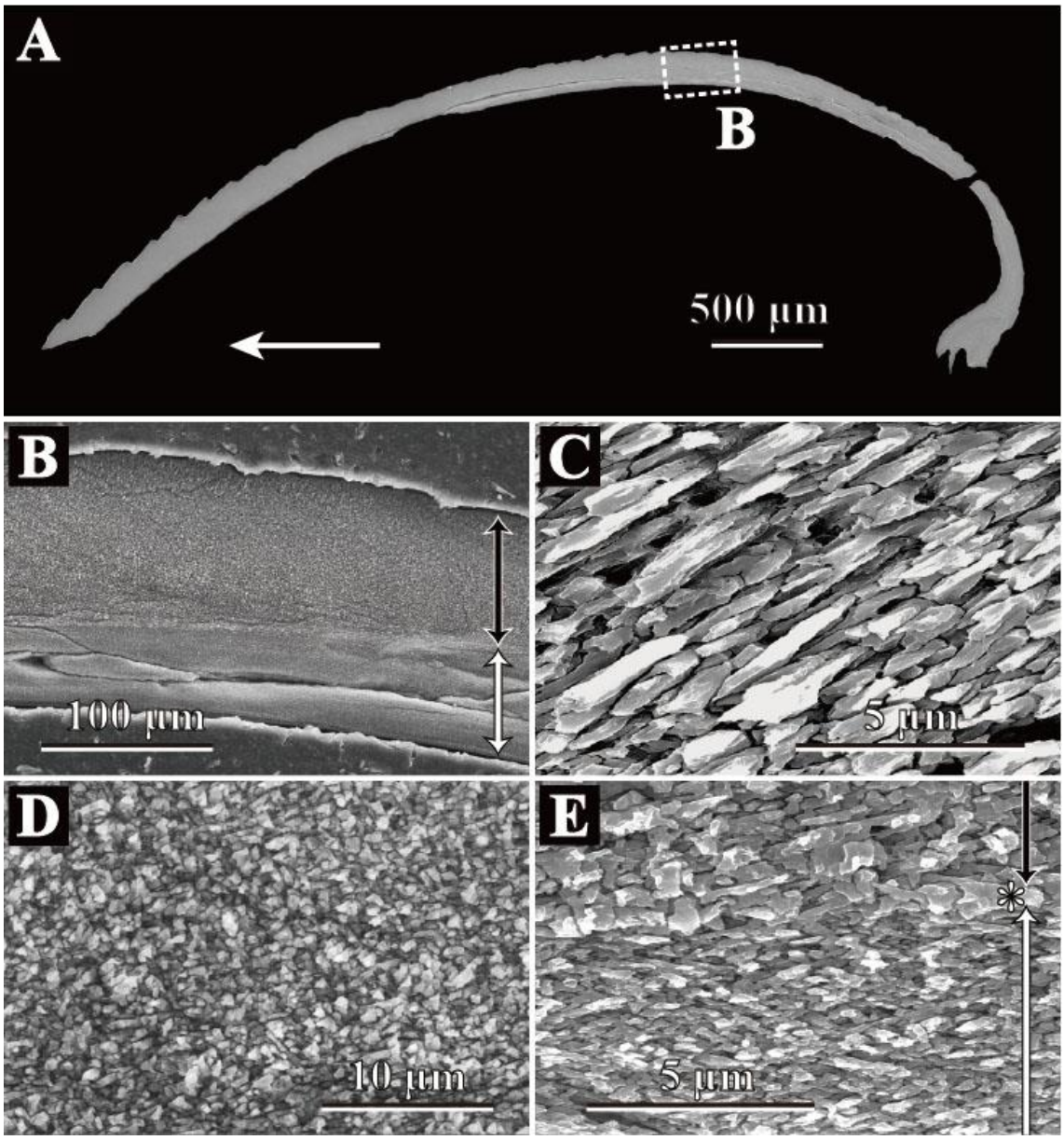

Figure 3.35. Scanning electron micrographs of *Nuculana gordonis* microstructure. Horizontal white arrow indicate growth direction. **A,** radial section of observed *Nuculana gordonis*. **B,** closer view of broken-lined square in A showing dorsal part of the shell section. Black double-headed arrow, the outer layer; white double-headed arrow, inner layer. **C,** radial section of fibrous prismatic structure of the outer sublayer of the outer layer. **D,** radial section of homogeneous structure of the inner sublayer of the outer layer. **E,** radial section of the outer, myostracum and inner layers. Vertical black double-headed arrow, the outer layer; Asterisk mark, the myostracum layer; white double-headed arrow, the inner layer. B-E, middle part of shell. . Shell length = 8 mm.

Family Bathyspinulidae

Bathyspinula calcarella (Dall, 1908)

Figure 3.37

Shell layers.—Outer and inner layers are present (Figure 3.37). The outer layer consists of a fibrous prismatic structure at the outermost part (outer sublayer) and a homogeneous structure (inner sublayer). Partly fine complex crossed lamellar structure is distributed in the inner sublayer of the outer layer. The myostracum is obscure. The inner layer is composed of a homogeneous structure. The outer layer thickens ventrally and the inner layer thicken dorsally. The shell is up to approximately 240 μm thick in the observed specimen.

Outer layer.—Fibrous prismatic structure (Figure 3.37B), homogeneous structure, and partly fine complex crossed lamellar structure (Figure 3.37C-E). The thickness of the outer sublayer is up to 30 μm. Acicular crystals that compose the outer sublayer are up to 4 μm long in the long axes, around 0.4 μm in width, and slant at angles of approximately 45° against the growth direction in a radial section. Crystals composing the outer layer decrease in size inwards and their morphology changes from acicular to granular crystals in the inner sublayer. Granular crystals are around 0.4 in diameter. A fine complex crossed lamellar structure is irregularly distributed in the inner sublayer.

Myostracum.—Obscure but recognized as bright lines in the observation using SEM, while crystal morphology is not altered (Figure 3.37A, E).

Inner layer.—Homogeneous structure (Figure 3.37E, F). Very fine granular crystals compose this layer and they are less than 0.3 μm in diameter.

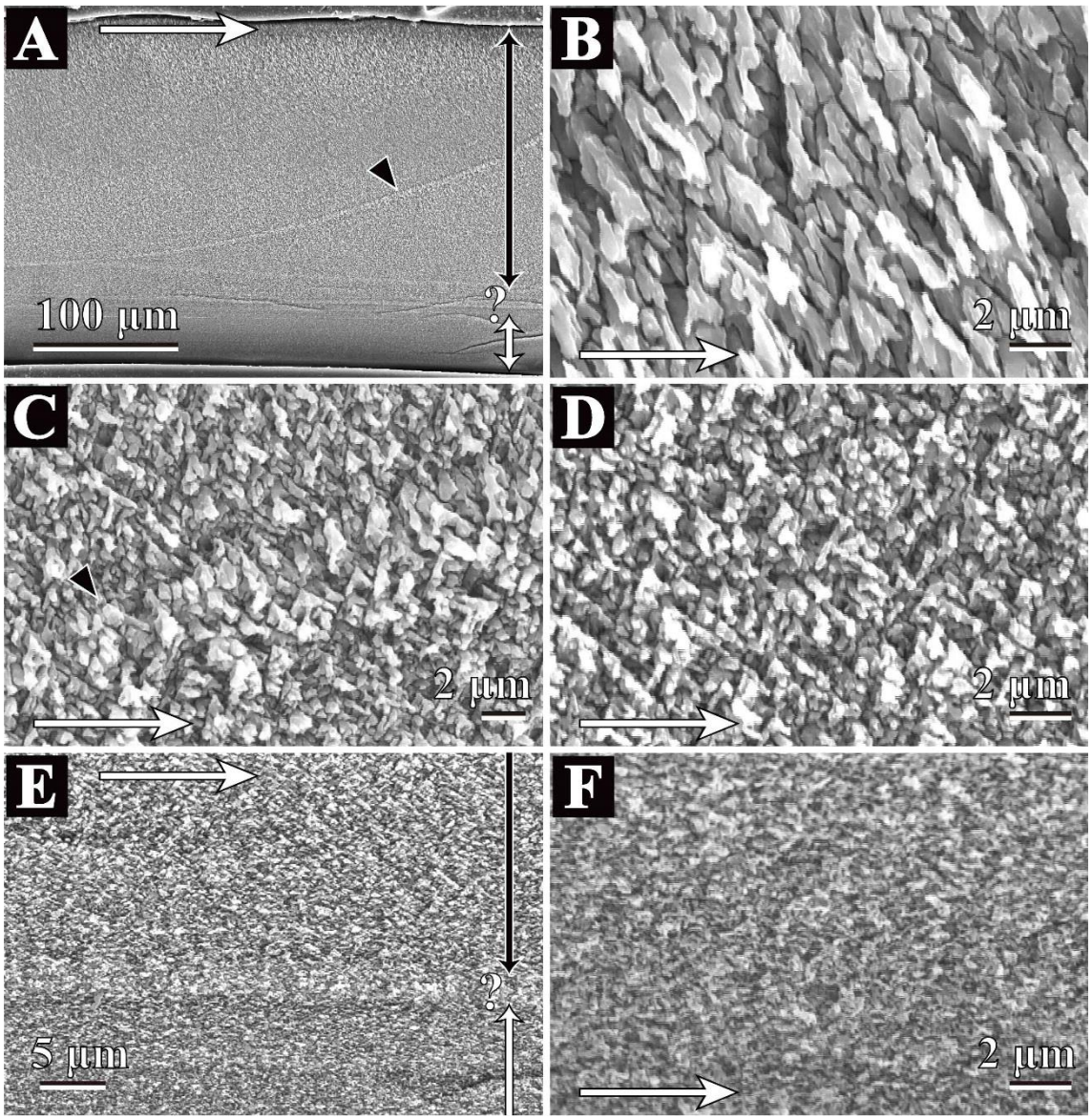

Figure 3.36. Scanning electron micrographs of *Bathyspinula calcarella* microstructure. Horizontal white arrow indicate growth direction. **A,** radial section of middle part of the shell section. Black arrow, the outer layer; question mark, probable position of myostracum; white arrow, the inner layer. Black arrow head indicates the myostracum layer. **B,** radial section of fibrous prismatic structure of the outer sublayer of the outer layer. **C,** radial section of fine complex crossed lamellar to homogeneous structure of the inner sublayer of the outer layer. Black arrow head indicates the myostracum layer. **D,** radial section of fine complex crossed lamellar to homogeneous structure of the inner sublayer of the outer layer. **E,** radial section of the outer, myostracum and inner layers. Vertical black double-headed arrow, the outer layer; Question mark, probable position of the myostracum layer; white double-headed arrow, the inner layer. **F,** radial section of homogeneous structure of the inner layer. A-F, middle part of shell. A-F, Shell length = 15 mm.

Family Malletiidae

Malletia takaii Okutani, 1968

Figure 3.38

Shell layers.—Outer, myostracum, and inner layers are present. The outer layer consists of a homogeneous structure, the myostracum consists of an irregular simple prismatic structure and the inner layer is composed of a fine complex crossed lamellar structure. The myostracum is composed of an irregular simple prismatic structure. Both the outer and inner layers thicken ventrally. The shell is up to approximately 125 μm thick in the observed specimen.

Outer layer.—Homogeneous structure (Figure 3.38A–C). Granular crystals consisting of homogeneous structure decrease in diameter inwards (from 1 to 0.7 μm). Second-order crystals are less than 200 nm in diameter (Figure 3.38C).

Myostracum.—Irregular simple prismatic structure consisting of vertically aligned acicular crystals (Figures 3.38B, F). The average width of these crystals is 0.6 μm

Inner layer.—Fine complex crossed lamellar structure (Figure 3.38B, D-F). Acicular crystals composing first-order lamellae of fine complex crossed lamellar structure are around 0.7 μm wide, up to 7 μm long in the long axes, and inclined at around 35° to the deposit surface.

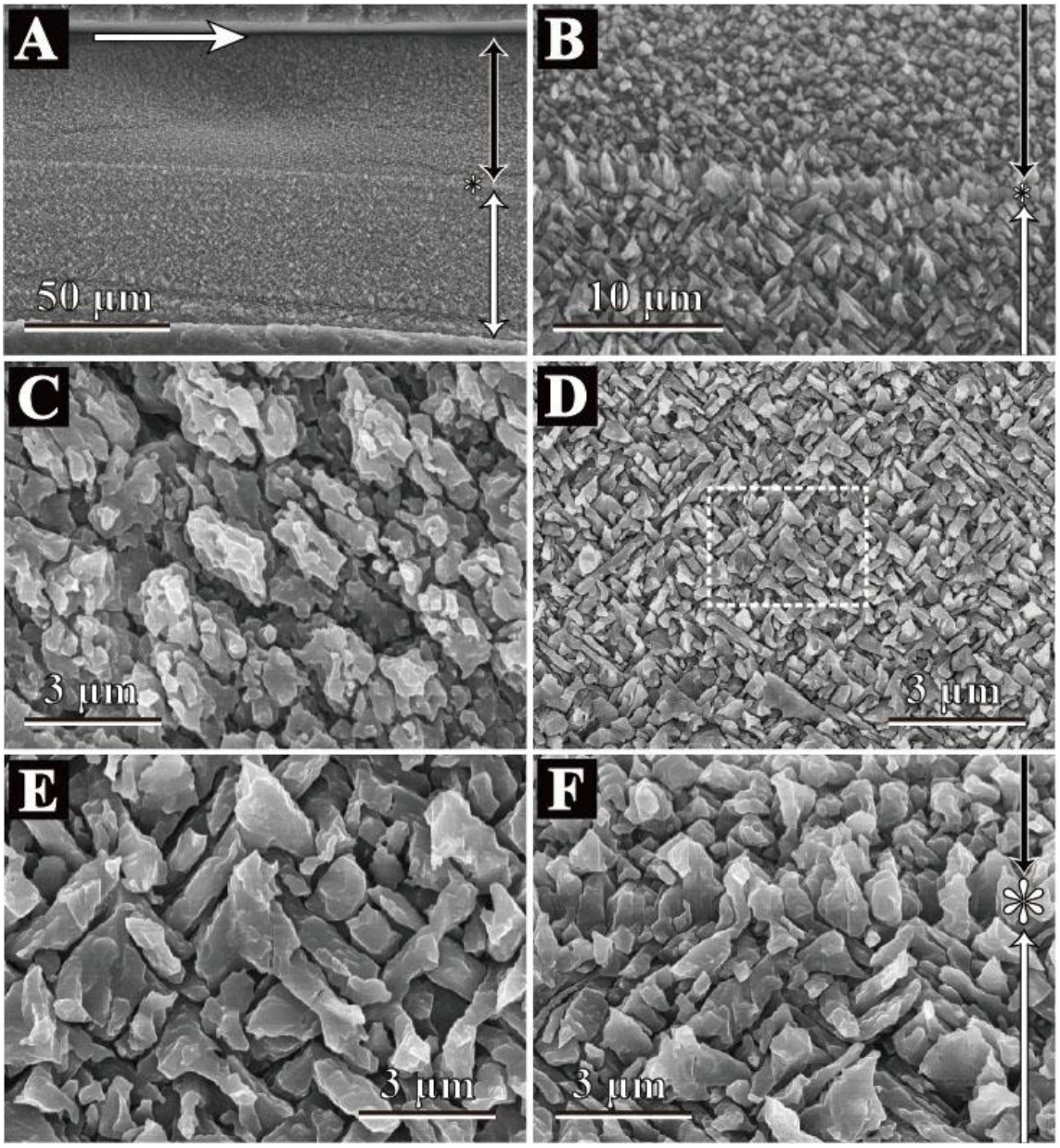

Figure 3.38. Scanning electron micrographs of *Malletia takaii* microstructure. Horizontal white arrow indicate growth direction. **A,** radial section of the outer, myostracum and inner layer. Vertical black double-headed arrow, the outer layer; Asterisk mark, the myostracum layer; white double-headed arrow, the inner layer. **B,** closer view of A. **C,** radial section of homogeneous structure of the outer layer. **D,** radial section of fine complex crossed lamellar structure of the inner layer. **E,** closer view of broken-lined square in D showing acicular crystals of the inner layer. **F,** closer view of radial section of the outer, myostracum and inner layer. Vertical black double-headed arrow, the outer layer; Asterisk mark, the myostracum layer; white double-headed arrow, the inner layer. . Shell length = 6 mm.

Malletia humilior Prashad, 1932

Figure 3.39

Shell layers.—Outer, myostracum, and inner layers are present (Figure 3.39). The outer layer consists of a homogeneous structure, the myostracum consists of an irregular simple prismatic structure, and the inner layer consists of a fine complex crossed lamellar structure. The myostracum consists of an irregular simple prismatic structure. The outer layer thickens ventrally. The inner layer generally thickens ventrally, while its thickest part is at the middle. The shell has almost constant thickness and is approximately 256 μm thick in the observed specimen.

Outer layer.—Homogeneous structure (Figure 3.39B-D). Granular crystals with homogeneous structure are 0.5 μm in diameter.

Myostracum.—Irregular simple prismatic structure consisting of vertically aligned acicular crystals (Figure 3.39D). The average width of these crystals is 1 μm

Inner layer.—Fine complex crossed lamellar structure (Figure 3.39E). Acicular crystals composing first-order lamellae of fine complex crossed lamellar structure are inclined at around 40° degree to deposit surface. Acicular crystals enlarge inwards. At the outermost part, crystals are around 0.8 μm wide and 5 μm long in the long axes. At the innermost part, crystals are around 1.8 μm in width and 18 μm in length.

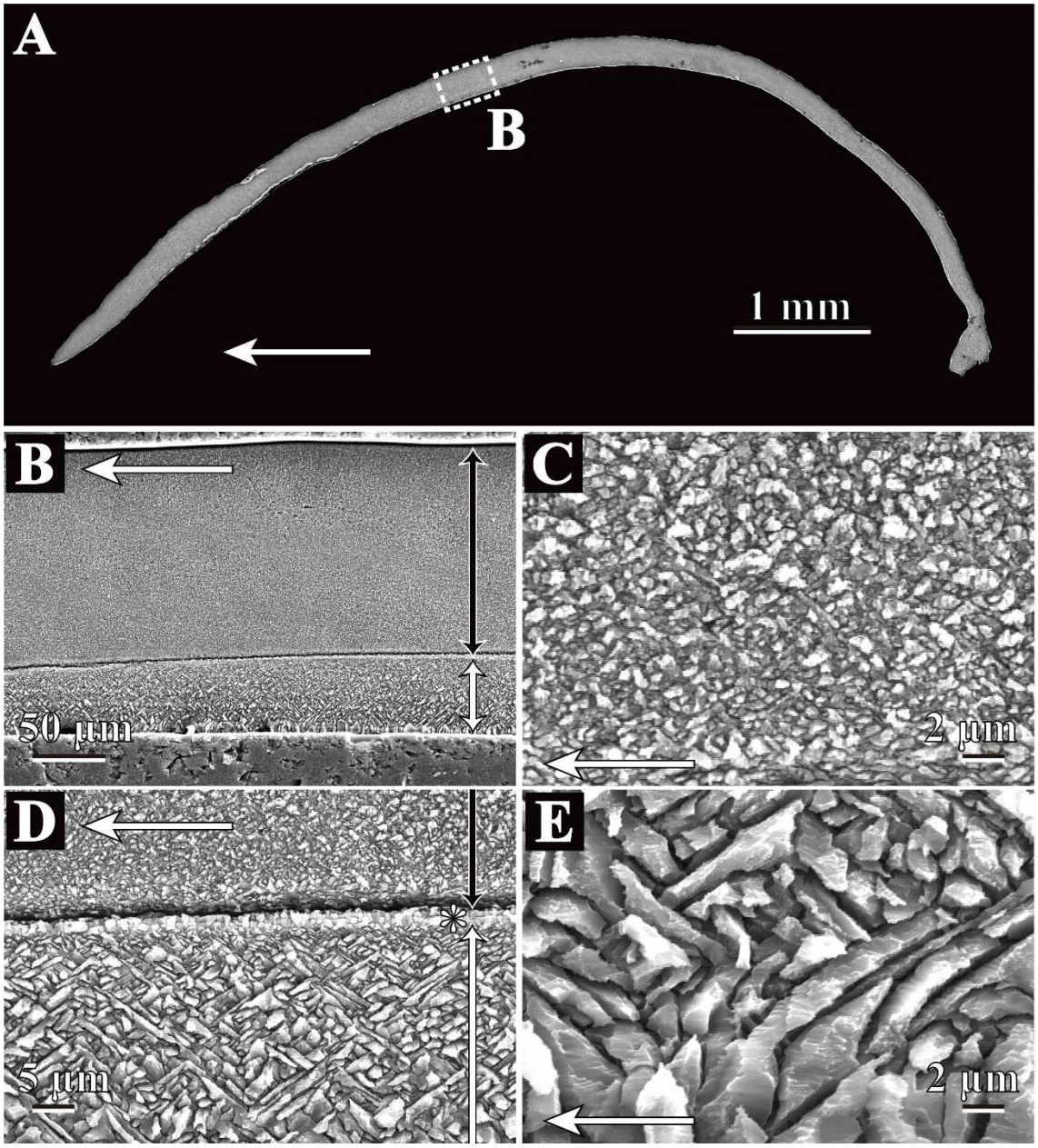

Figure 3.39. Scanning electron micrographs of *Malletia humilior* microstructure. Horizontal white arrow indicate growth direction. **A,** radial section of observed *Malletia humilior*. **B,** closer view of broken-lined square in A showing middle part of the shell section. Black double-headed arrow, the outer layer; white double-headed arrow, inner layer. **C,** radial section of homogeneous structure of the outer layer. **D,** radial section of the outer, myostracum and inner layers. Vertical black double-headed arrow, the outer layer; Asterisk mark, the myostracum layer; white double-headed arrow, the inner layer. **E,** radial section of fine complex crossed lamellar structure of the inner layer. B-E, middle part of shell. A-E, Shell length = 13 mm.

Family Neilonellidae

Neilonella soyoae Habe, 1958

Figures 3.40, 41

Shell layers.—Outer and inner layers are present. The myostracum is obscure. The outer layer is comprised of the outer sublayer with fibrous prismatic structure and inner sublayer with homogeneous structure. The inner layer is of a homogeneous structure. The outer and inner layers thicken ventrally (Figure 3.40B, C). The shell is up to approximately 380 μm thick in the observed specimen.

Outer layer.—Fibrous prismatic structure in the outer sublayer (Figure 3.41A) and homogeneous structure in the inner sublayer (Figure 3.41B, C). The thickness of the outer sublayer is up to 65 μm. Acicular crystals composing the outer sublayer are up to 6 μm long in the long axes, around 0.5 μm in width, and slant at an angle of approximately 50° against the growth direction in a radial section. The homogeneous structure is composed of granular crystals (Figure 3.41A, B). The average diameter of the granular crystals is around 0.5 μm and they diminish in size inwards, up to around 0.3 μm.

Myostracum.—Obscure, but recognized as bright lines in the SEM observations with no change in crystal morphology (Figure 3.41C).

Inner layer.—Homogeneous structure (Figure 3.41C, D). Very fine granular crystals that are less than 0.2 μm in diameter compose this layer.

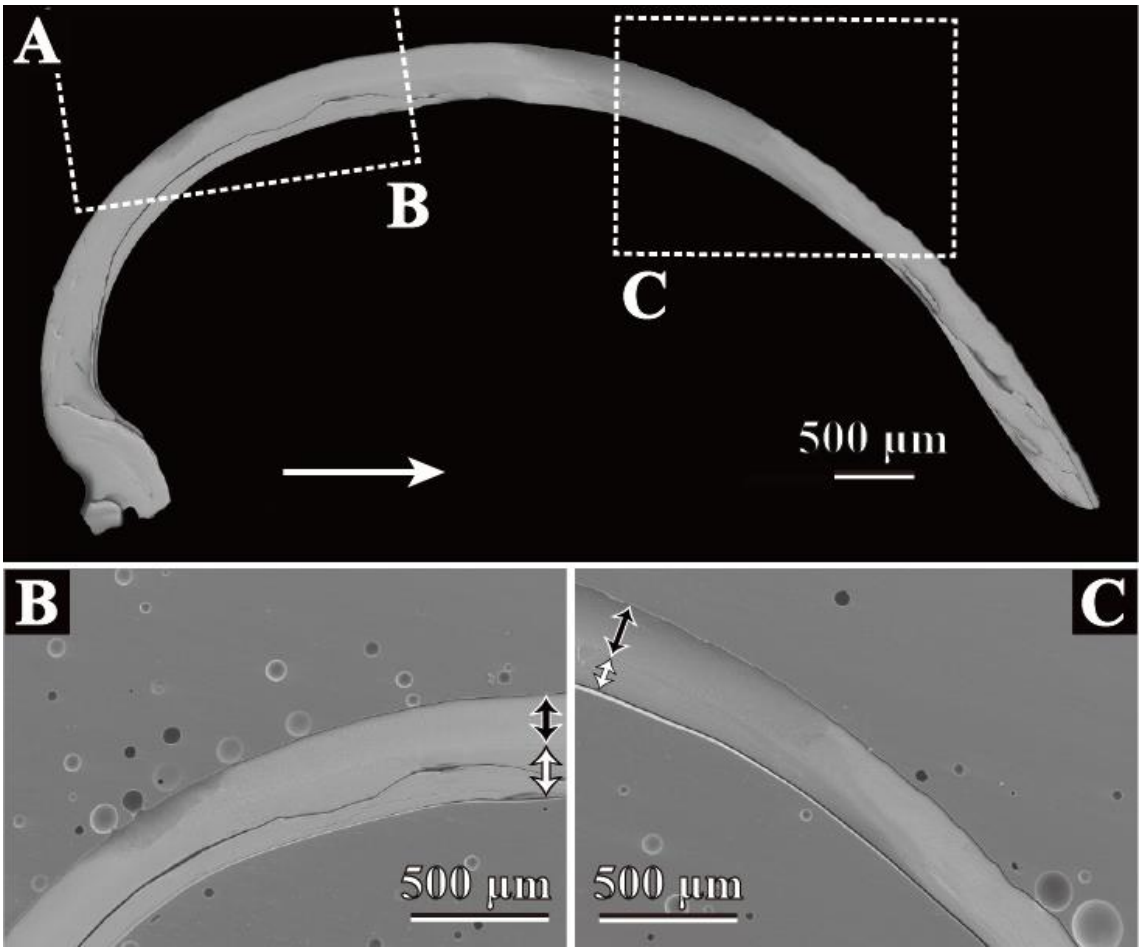

Figure 3.40. Scanning electron micrographs of *Neilonella soyoae* microstructure. Horizontal white arrow indicate growth direction. **A,** radial section of observed *Neilonella soyoae*. **B,** closer view of broken-lined square in A showing dorsal part of the shell section. Black double-headed arrow, the outer layer; white double-headed arrow, inner layer. **C,** closer view of broken-lined square in A showing ventral part of the shell section. Black double-headed arrow, the outer layer; white double-headed arrow, inner layer. . Shell length = 12 mm.

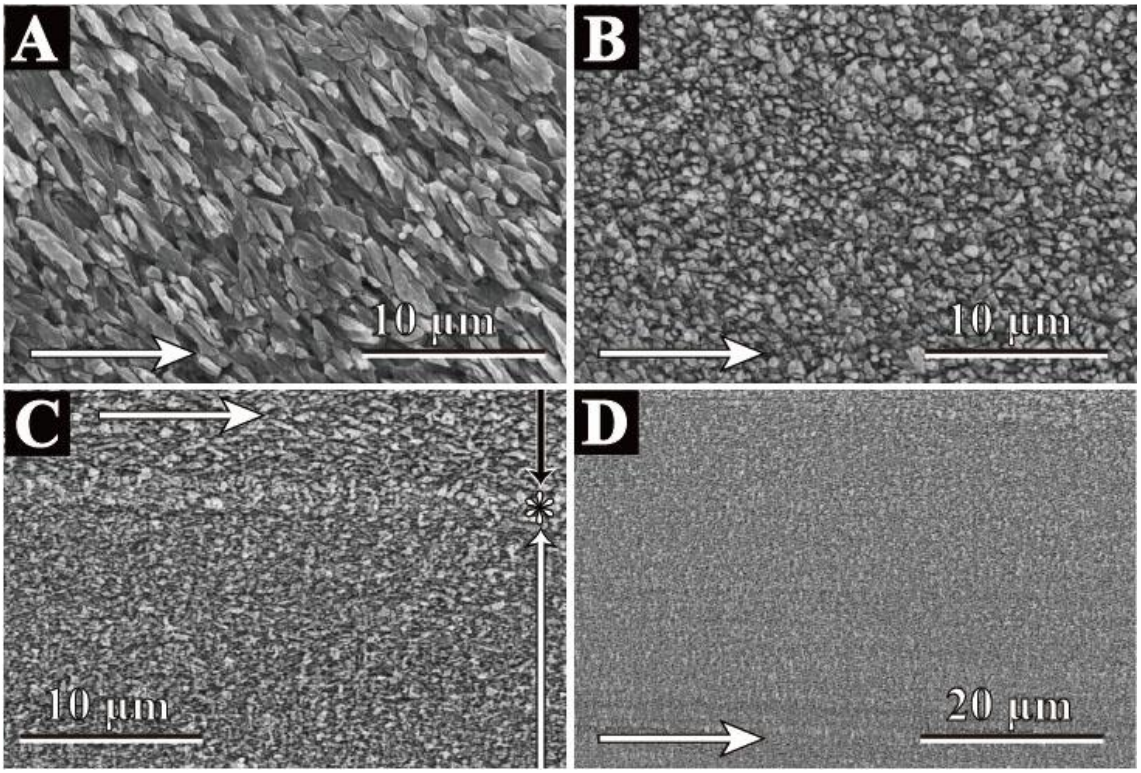

Figure 3.41. Scanning electron micrographs of *Neilonella soyoae* microstructure. Horizontal white arrow indicate growth direction. **A,** radial section of fibrous prismatic structure of the outer sublayer of outer layer. **B,** radial section of homogeneous structure of the inner sublayer of outer layer. **C,** radial section of the outer, myostracum and inner layers. Vertical black double-headed arrow, the outer layer; Asterisk mark, the myostracum layer; white double-headed arrow, the inner layer. **D,** radial section of homogeneous structure of the inner layer. A, B, ventral part of shell. C, D, middle part of shell. . Shell length = 12 mm.

***Neilonella dubia* Prashad, 1932**

Figures 3.42, 43

Shell layers.—Outer, myostracum, and inner layers are present (Figure 3.42). The outer layer is composed of a fibrous prismatic structure in the outer sublayer and homogeneous structure in the inner sublayer. The myostracum is of an irregular simple prismatic structure. The inner layer is homogeneous structure. The outer layer thickens

ventrally. The inner layer generally thickens ventrally but it distributed in the middle part of a radial section. The shell is up to approximately 203 μm thick in the observed specimen.

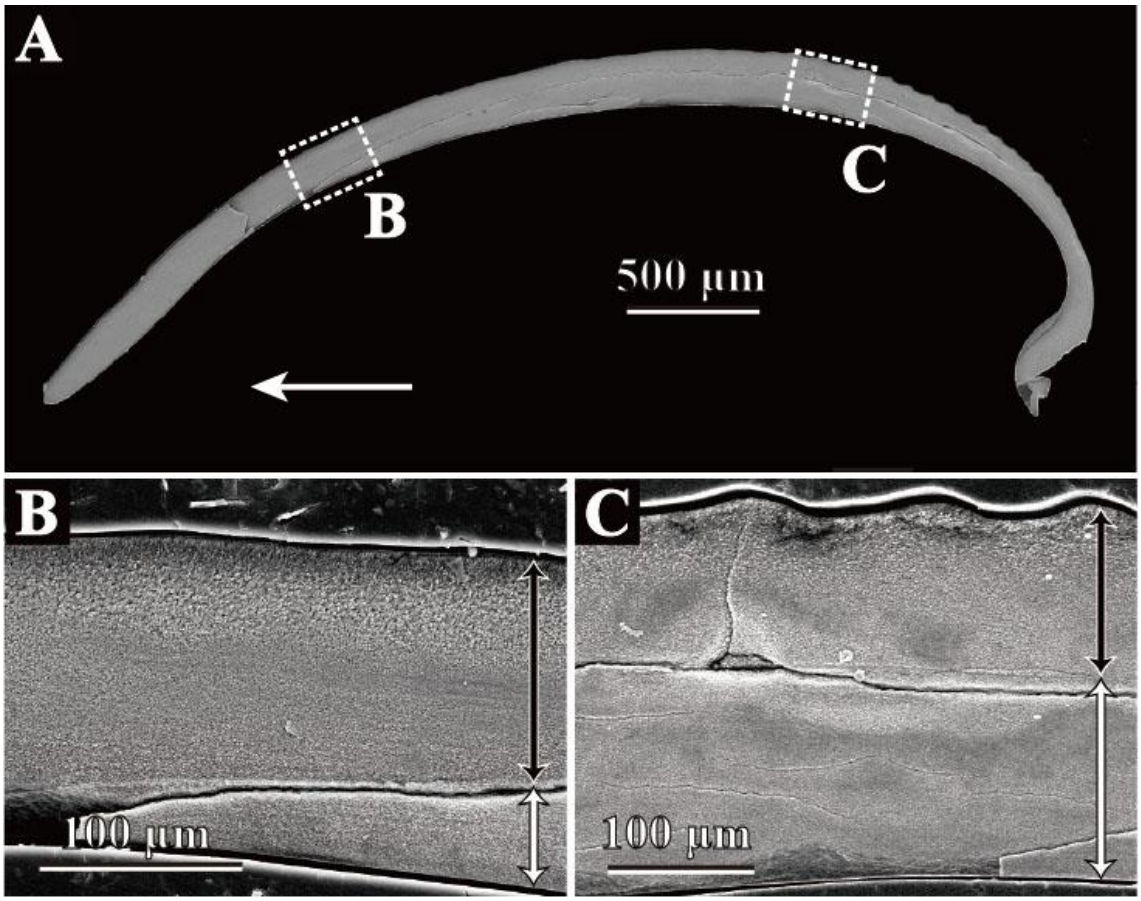

Figure 3.42. Scanning electron micrographs of *Neilonella dubia* microstructure. Horizontal white arrow indicate growth direction. **A,** radial section of observed *Neilonella dubua*. **B,** closer view of broken-lined square in A showing ventral part of the shell section. Black double-headed arrow, the outer layer; white double-headed arrow, inner layer. **C,** closer view of broken-lined square in A showing dorsal part of the shell section. Black double-headed arrow, the outer layer; white double-headed arrow, inner layer. . Shell length = 6 mm.

Outer layer.—Fibrous prismatic (outer sublayer; Figure 3.43A) and homogeneous structure (inner sublayer; Figures 3.43B, C). The thickness of the outer

sublayer is up to 16 μm. Acicular crystals composing the outer sublayer are up to 8 μm long in the long axes, around 0.6 μm in width, and slant at angles of approximately 35° against the growth direction in a radial section (Figure 3.43A). The homogeneous structure is composed of granular crystals (Figures 3.43B, C). The average diameter of the granular crystals is around 1 μm and they diminish in size inwards, up to around 0.5 μm.

Myostracum.— Irregular simple prismatic structure consisting of vertically aligned acicular crystals (Figure 3.43C). The average width of these crystals is 0.3 μm

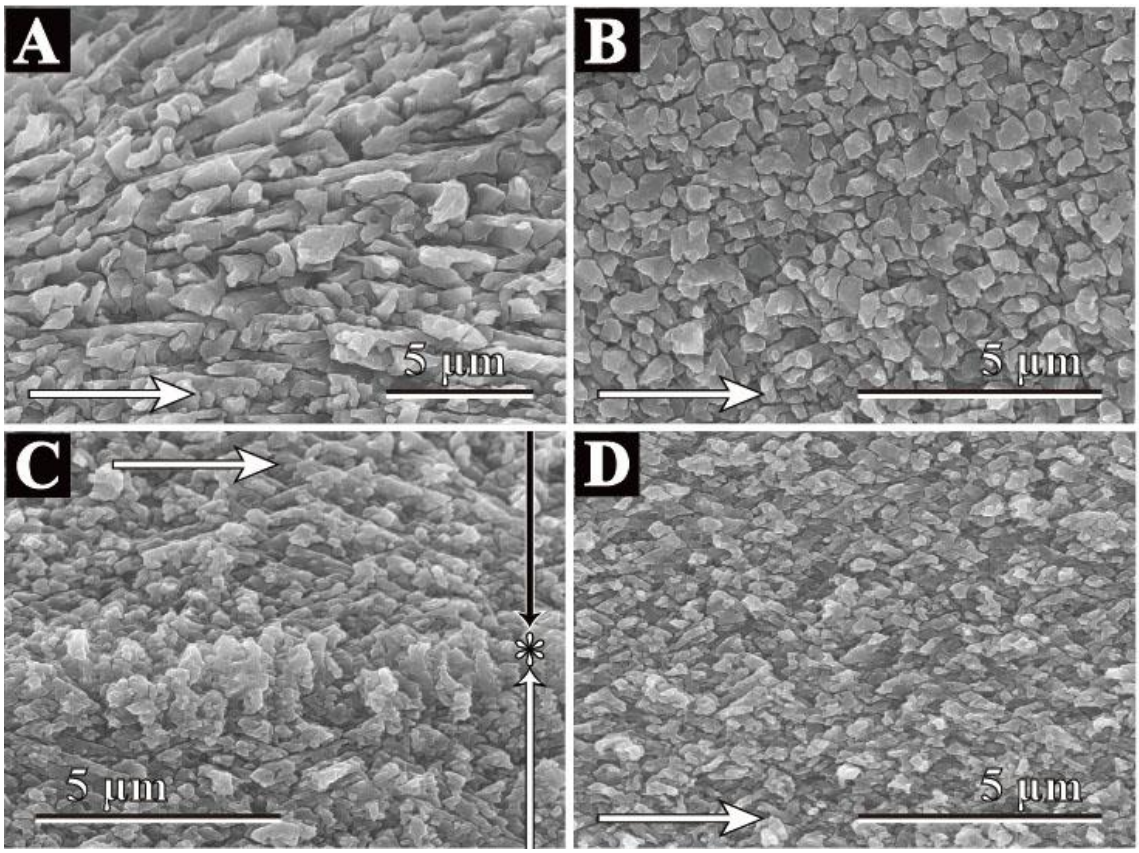

Figure 3.43. Scanning electron micrographs of *Neilonella dubia* microstructure. Horizontal white arrow indicate growth direction. **A,** radial section of fibrous prismatic structure of the outer sublayer of outer layer. **B,** radial section of homogeneous structure of the inner sublayer of outer layer. **C,** radial section of the outer, myostracum and inner layers. Vertical black double-headed arrow, the outer layer; Asterisk mark, the myostracum layer; white double-headed arrow, the inner layer. **D,** radial section of homogeneous structure of the inner layer. A-D, dorsal part of shell. . Shell length = 6 mm.

Inner layer.—Homogeneous structure (Figure 3.43C, D). Very fine granular crystals that are less than 0.2 μm in diameter form this layer.

Neilonella kirai Habe, 1953

Figure 3.44

Shell layers.—Outer, myostracum, and inner layers are present (Figure 3.44). The outer layer is composed of a fibrous prismatic structure in the outer sublayer and homogeneous structure in the inner sublayer. The boundary of the two sublayers is sharp for this family. The inner layer shows a homogeneous structure. The myostracum shows an irregular simple prismatic structure. The outer and inner layers thicken dorsally. The shell is up to approximately 400 μm thick in the observed specimen.

Outer layer.— Fibrous prismatic (Figure 3.44B) and homogeneous structure (Figure 3.44C, D). The thickness of the outer sublayer is up to 110 μm. Acicular crystals consisting of the outer sublayer are up to 5 μm long in the long axes and around 0.8 μm in width, and slant at an angle of approximately 50° against the growth direction in a radial section. The homogeneous structure is composed of granular crystals. The average diameter of the granular crystals is around 0.6 μm and they diminish in size inwards, up to around 0.4 μm.

Myostracum.— Irregular simple prismatic structure consisting of vertically aligned acicular crystals (Figure 3.44C, D). The average width of these crystals is 0.2 μm.

Inner layer.—Homogeneous structure (Figure 3.44C-E). Very fine granular crystals are less than 0.2 μm in diameter.

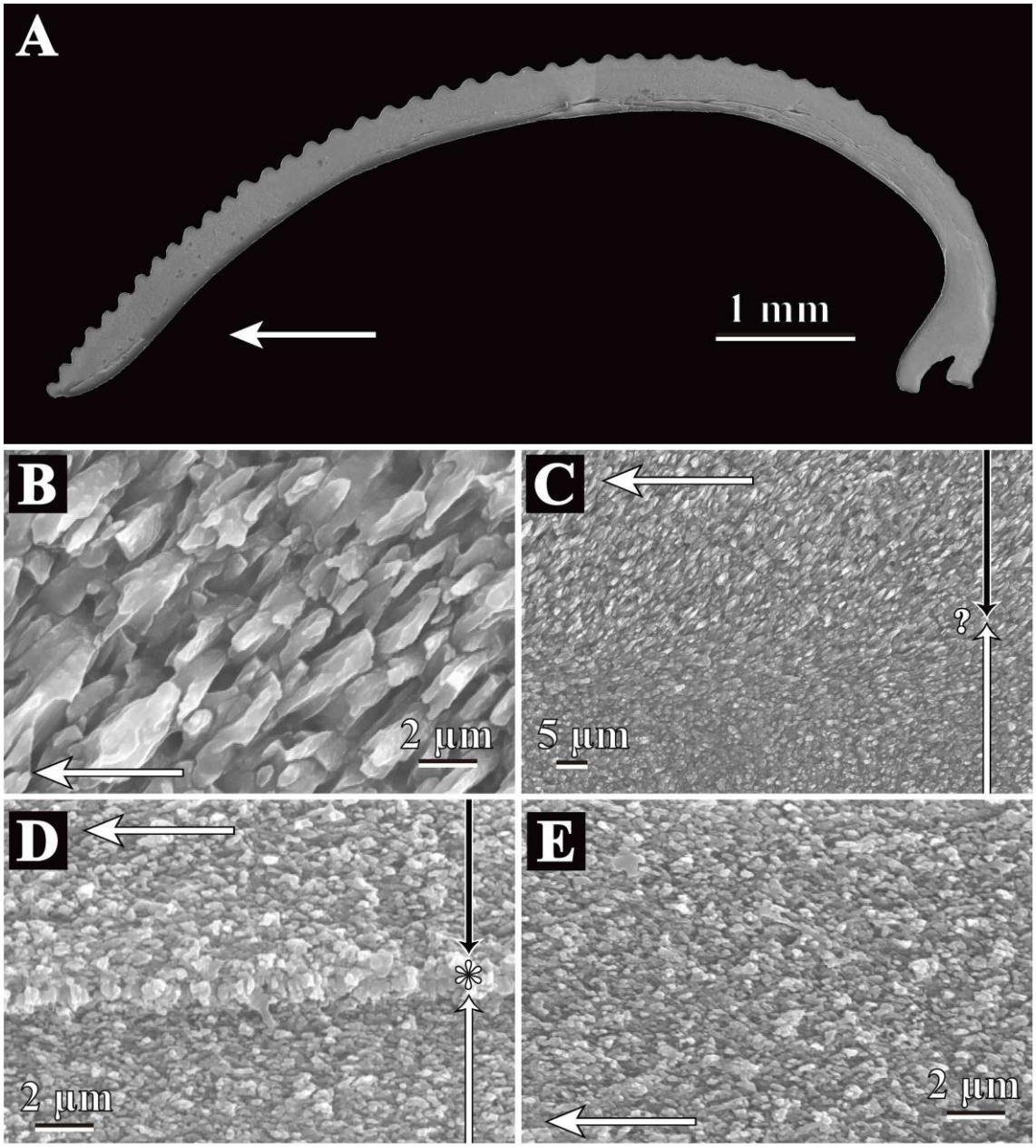

Figure 3.44. Scanning electron micrographs of *Neilonella kirai* microstructure. Horizontal white arrow indicate growth direction. **A,** radial section of observed *Neilonella kirai*. **B,** radial section of fibrous prismatic structure of the outer sublayer of outer layer. **C,** radial section of the outer, myostracum and inner layers. Vertical black double-headed arrow, the outer layer; Question mark, probable position of the myostracum layer; white double-headed arrow, the inner layer. **D,** radial section of the outer, myostracum and inner layers. Vertical black double-headed arrow, the outer layer; Asterisk mark, probable position of the myostracum layer; white double-headed arrow, the inner layer. **E,** radial section of homogeneous structure of the inner layer. B-E, middle part of shell. A-E, Shell length = 22 mm.

Family Tindariidae

Tindaria soyoae Habe, 1953

Figure 3.45

Shell layers.—Outer, myostracum, and inner layers are present (Figure 3.45). The outer and inner layers are both of a homogeneous structure. The myostracum is of an obscure to irregular simple prismatic structure. The outer and inner layers thicken ventrally. The shell is up to approximately 280 μm thick in the observed specimen.

Outer layer.—Homogeneous structure (Figure 3.45B, C). The diameter of the granular crystals is around 1.2 μm and they diminish in size inwards, up to around 0.5 μm. Radial ribs on the exterior surface do not alter the crystal size and morphology.

Myostracum.—Obscure to irregular simple prismatic structure (Figure 3.45A, C). Irregular prisms consist of vertically aligned acicular crystals. The average width of these crystals is 0.5 μm.

Inner layer.— Homogeneous structure (Figure 3.45C, D). The average diameter of the granular crystals is around 0.5 μm.

Figure 3.45 (next page)**.** Scanning electron micrographs of *Tindaria soyoae* microstructure. Horizontal white arrow indicate growth direction. **A,** radial section of the outer and inner layer. Vertical black double-headed arrow, the outer layer; white double-headed arrow, the inner layer. **B A,** radial section of the outer and inner layer. Vertical black double-headed arrow, the outer layer; Asterisk mark, the myostracum layer; white double-headed arrow, the inner layer. **B,** radial section of homogeneous structure of the outer layer. **C,** radial section of the outer, myostracum and inner layers. Vertical black double-headed arrow, the outer layer; Asterisk mark, probable position of the myostracum layer; white double-headed arrow, the inner layer. **D,** radial section of homogeneous structure of the inner layer. A-D, middle part of shell. A-D, Shell length = 13 mm.

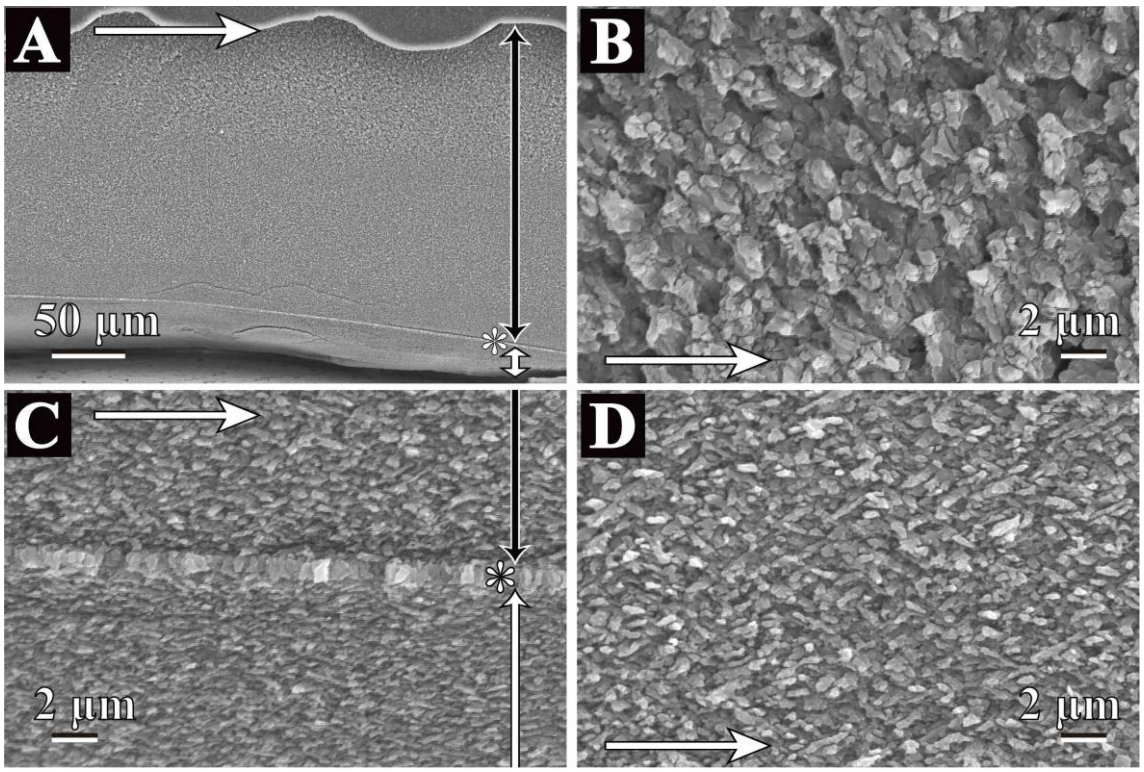

Family Yoldiidae

***Megayoldia lischkei* (Smith, 1885)**

Figure 3.46

Shell layers.—Outer, myostracum, and inner layers are present (Figure 3.46). The outer layer is composed of a homogeneous and partly spherulitic structure. The myostracum is of an irregular simple prismatic structure. The inner layer shows a fine complex crossed lamellar structure and has two sublayers, a fibrous prismatic structure in the outer sublayer and homogeneous structure in the inner sublayer. The inner layer is of a fine complex crossed lamellar structure. The outer layer thickens ventrally, and the

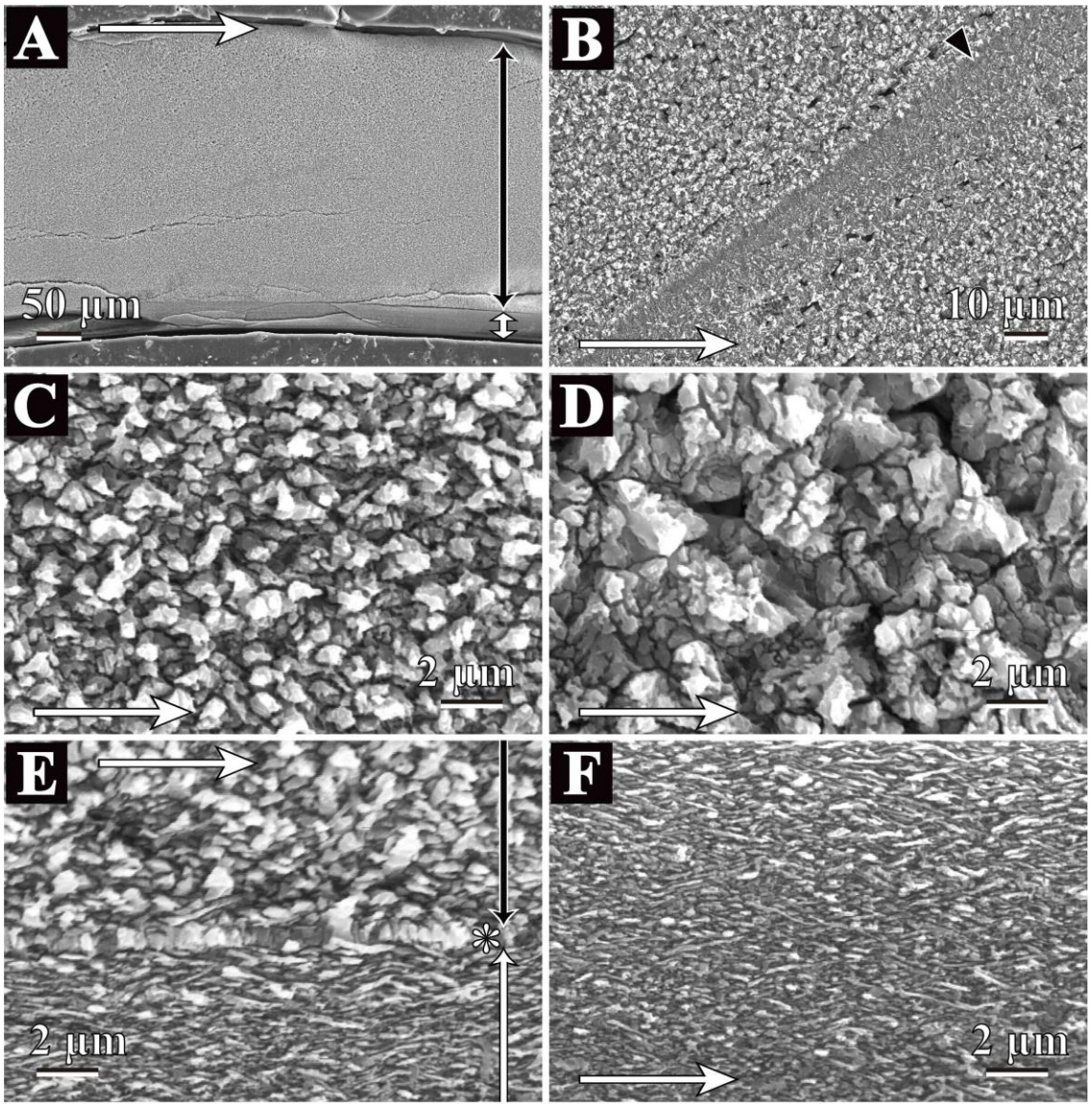

Figure 3.46. Scanning electron micrographs of *Megayoldia lischkei* microstructure. Horizontal white arrow indicate growth direction. **A,** radial section of the outer and inner layer. Vertical black double-headed arrow, the outer layer; white double-headed arrow, the inner layer. **B,** radial section of homogeneous and spherulitic structures of the outer layer. **C,** radial section of homogeneous structure of the outer layer. **D,** radial section of spherulitic structure of the outer layer. **E,** radial section of the outer, myostracum and inner layers. Vertical black double-headed arrow, the outer layer; Asterisk mark, probable position of the myostracum layer; white double-headed arrow, the inner layer. **F,** radial section of fine complex crossed lamellar structure of the inner layer. A, C, E, F, middle part of shell. B, dorsal part of shell. D, ventral part of shell. A-F, Shell length = 23 mm.

inner layer generally thickens ventrally in the middle part of a radial section. The shell is thickened in the ventral part and is approximately 360 μm thick in the observed specimen.

Outer layer.—Generally shows a homogeneous structure (Figures 3.46B, C, E) and partly a spherulitic structure (Figure 3.46B, D). Granular crystals composing the homogeneous structure are 1.5 μm in diameter at the outer part and diminish in size inwards, up to around 0.6 μm in diameter. Spherulitic structure is partly distributed along growth lines. Acicular crystals radiate equally in all directions from a central nucleation site and constitute the first-order spherulites, which are around 3 μm in diameter. Irregularly shaped acicular crystals in spherulites are around 1.5 in diameter.

Myostracum.—Irregular simple prismatic structure consisting of vertically aligned acicular crystals (Figure 3.46E). The average width of these crystals is 0.3 μm

Inner layer.—Fine complex crossed lamellar structure (Figure 3.46F). Acicular crystals composing the first-order lamellae of the fine complex crossed lamellar structure are around 0.1 μm wide and up to 2.5 μm long in the long axes and inclined at around 25° to the deposit surface.

***Megayoldia japonica* (Smith, 1885)**

Figure 3.47

Shell layers.—Outer, myostracum, and inner layers are present. The outer layer is composed of a fibrous prismatic structure in the outer sublayer and homogeneous structure in the inner sublayer. The myostracum is of an obscure to irregular simple prismatic structure. The inner layer is of a homogeneous or fine complex crossed

lamellar structure. The outer layer thickens ventrally. The myostracum and inner layer thicken ventrally. The shell is up to approximately 400 μm thick in the observed specimen.

Outer layer.—Fibrous prismatic and homogeneous structure (Figure 3.47A, B). The outer sublayer of the outer layer consists of a fibrous prismatic structure. The thickness of the outer sublayer is up to 16 μm. Acicular crystals in the outer sublayer are up to 16 μm long in the long axes, around 1.6 μm in width, and slant at an angle of approximately 65° against the growth direction in a radial section. The long axes of the acicular crystals shorten inwards and become granular crystals in the homogeneous structure of the inner sublayer of the outer layer. The average diameter of the granular crystals is around 0.6 μm.

Myostracum.—Obscure to irregular simple prismatic structure (Figure 3.47C). Vertically aligned acicular crystals in the irregular simple prismatic structure are around 0.8 μm in width and up to 4 μm long in the long axes. The thickness of the myostracum decreases ventrally and becomes obscure.

Inner layer.—Homogeneous or fine complex crossed lamellar structure (Figure 3.47C, D). The diameter of granular crystals in the homogeneous structure are around 0.3 μm. Acicular crystals composing the first-order lamellae of the fine complex crossed lamellar structure are around 0.3 μm wide, up to 2 μm long in the long axes, and inclined at around 25° degree to the deposit surface.

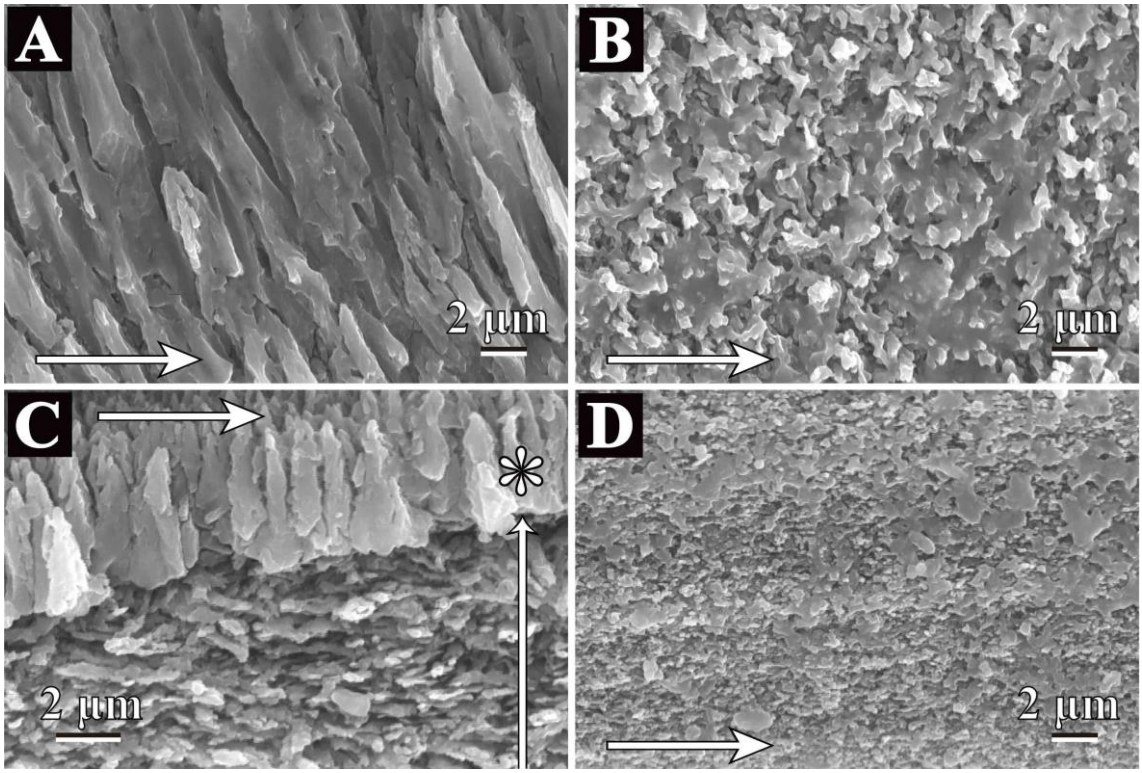

Figure 3.47. Scanning electron micrographs of *Megayoldia japonica* microstructure. Horizontal white arrow indicate growth direction. **A,** radial section of fibrous prismatic structure of the outer sublayer of the outer layer. **B,** radial section of homogeneous structure of the inner sublayer of the outer layer. **C,** radial section of the myostracum and inner layers. Asterisk mark, probable position of the myostracum layer; white double-headed arrow, the inner layer. **D,** radial section of homogeneous structure of the inner layer. A-D, middle part of shell. A-D, Shell length = 30 mm.

***Yoldia johanni* Dall, 1925**

Figures 3.48, 49

Shell layers.—Outer, myostracum, and inner layers are present. The outer layer is composed of a homogeneous structure and the inner layer of a fine complex crossed lamellar structure. The myostracum is of an irregular simple prismatic structure. The outer and inner layers thicken ventrally (Figure 3.48B, C). The shell is up to approximately 420 µm thick in the observed specimen.

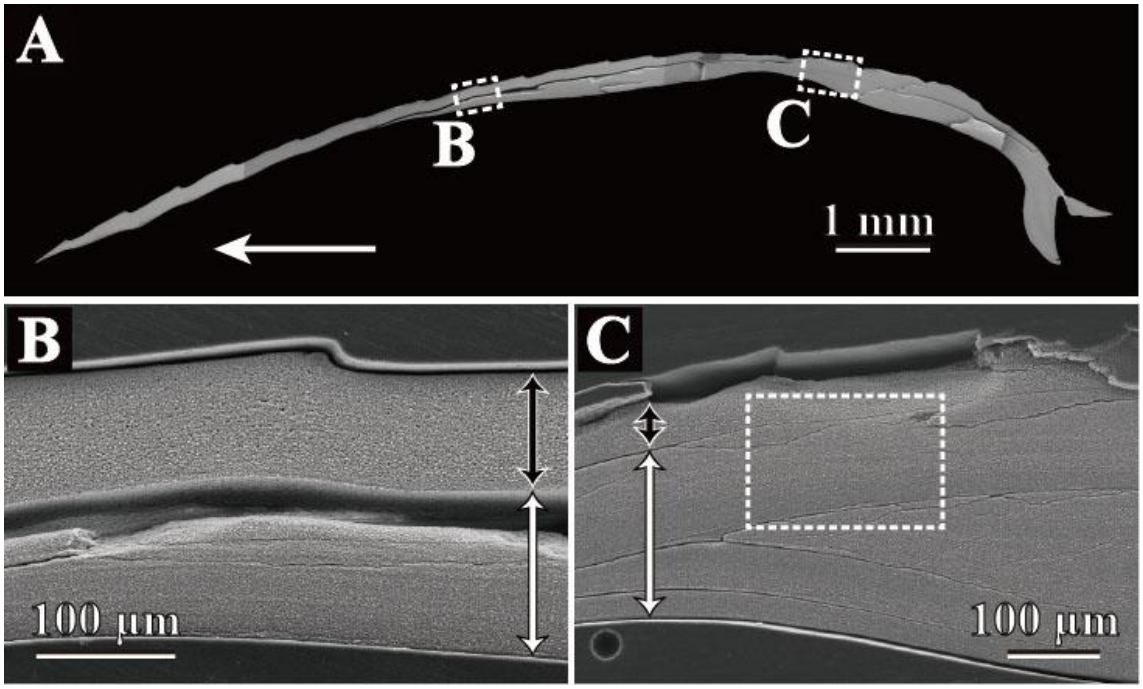

Figure 3.48. Scanning electron micrographs of *Yoldia johanni* microstructure. Horizontal white arrow indicate growth direction. **A,** radial section of observed *Yoldia johanni*. **B,** closer view of broken-lined square in A showing ventral part of the shell section. Black double-headed arrow, the outer layer; white double-headed arrow, inner layer. **C,** closer view of broken-lined square in A showing ventral part of the shell section. Black double-headed arrow, the outer layer; white double-headed arrow, inner layer. White broken-lined square is expanded in figure 32D. . Shell length = 25 mm.

Outer layer.—Homogeneous structure (Figure 3.49A, B). Granular crystals comprising the homogeneous structure are variable in size, but around 0.6 µm in diameter.

Myostracum.—Irregular simple prismatic structure consisting of vertically aligned acicular crystals (Figure 3.49B). The average width and length of these crystals are 0.5 µm and up to 4 µm long in the long axes, respectively.

Inner layer.—Fine complex crossed lamellar structure (Figure 3.49C). Acicular crystals composing the first-order lamellae of the fine complex crossed lamellar

structure are around 0.4 μm in width and up to 4 μm in length and inclined at around 30° to the deposit surface. Several growth lines composed of an irregular simple prismatic structure are present (Figure 3.49D).

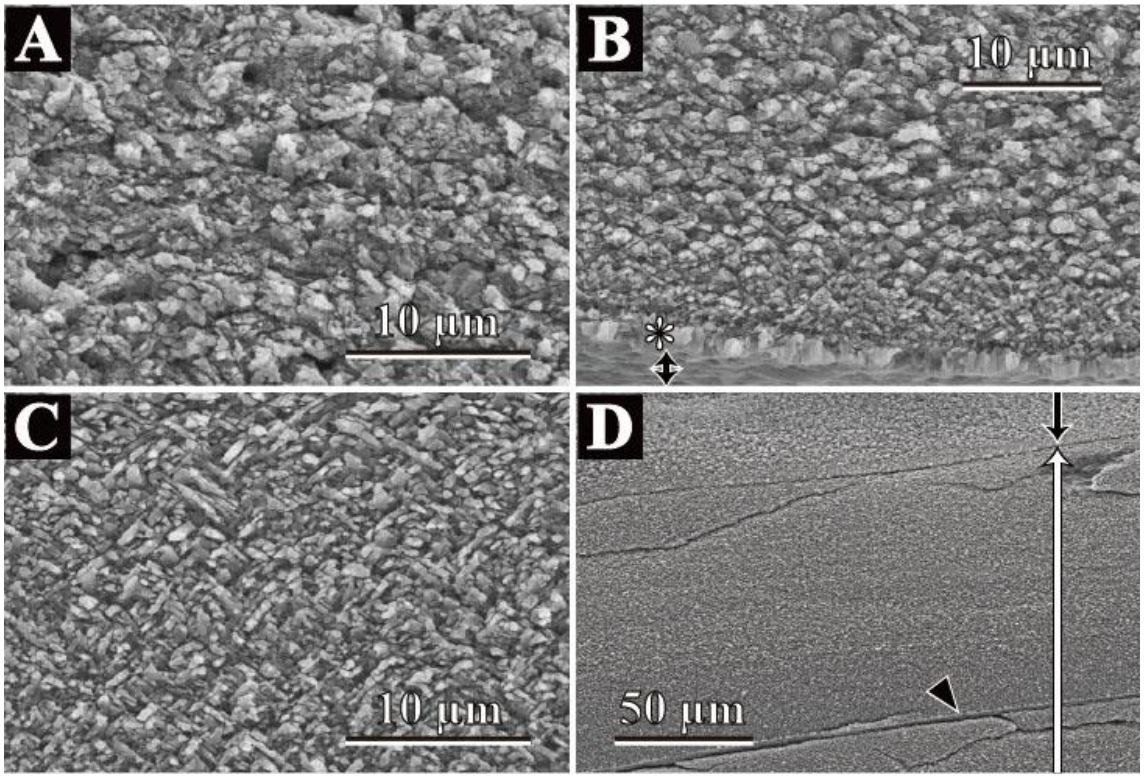

Figure 3.49. Scanning electron micrographs of *Yoldia johanni* microstructure. Growth direction is left side in all figures. **A,** radial section of homogeneous structure of the outer layer. **B,** radial section of the outer and myostracum layers. Asterisk mark, the myostracum layer; Black double-headed arrow, crack. **C,** radial section of fine complex crossed lamellar structure of the inner layer. **D,** radial section of the outer, myostracum and inner layers. Vertical black arrow, the outer layer; white double-headed arrow, the inner layer; Black arrow head, growth line. A-C, middle part of shell. D, dorsal part of shell. . Shell length = 25 mm.

Yoldia notabilis (Smith, 1885)

Figure 3.50

Shell layers.—Outer, myostracum, and inner layers are present (Figure 3.50). The outer layer is composed of a homogeneous structure. The inner layer is composed of a fine complex crossed lamellar structure. The myostracum is of an obvious to irregular simple prismatic structure. The outer and the inner layers thicken ventrally. In the outer layer, the growth lines are recognized as uniquely waved lines in a radial section along the oblique radial ribs and are well developed in a cyclic manner in the inner layer. The shell is up to approximately 360 μm thick in the observed specimen.

Outer layer.—Homogeneous structure (Figure 3.50B, C). Granular crystals in the homogeneous structure are variable in size but around 0.6 μm in diameter.

Myostracum.—Obscure to irregular simple prismatic structure (Figure 3.50C). Irregular simple prismatic structure consists of vertically aligned acicular crystals. The average width and length of these crystals are 0.6 μm and up to 0.7 μm, respectively.

Inner layer.—Fine complex crossed lamellar structure (Figure 3.50C-F). Acicular crystals composing the first-order lamellae of the fine complex crossed lamellar structure are around 0.3 μm wide, up to 10 μm long in the long axes, and inclined at around 35° to the deposit surface (i.e. inner surface of the shell). Growth lines are distributed periodically, and are composed of an irregular simple prismatic structure (Figure 3.50D, E). Acicular crystals are vertically aligned and around 1 μm in width and 4 μm long in the long axes.

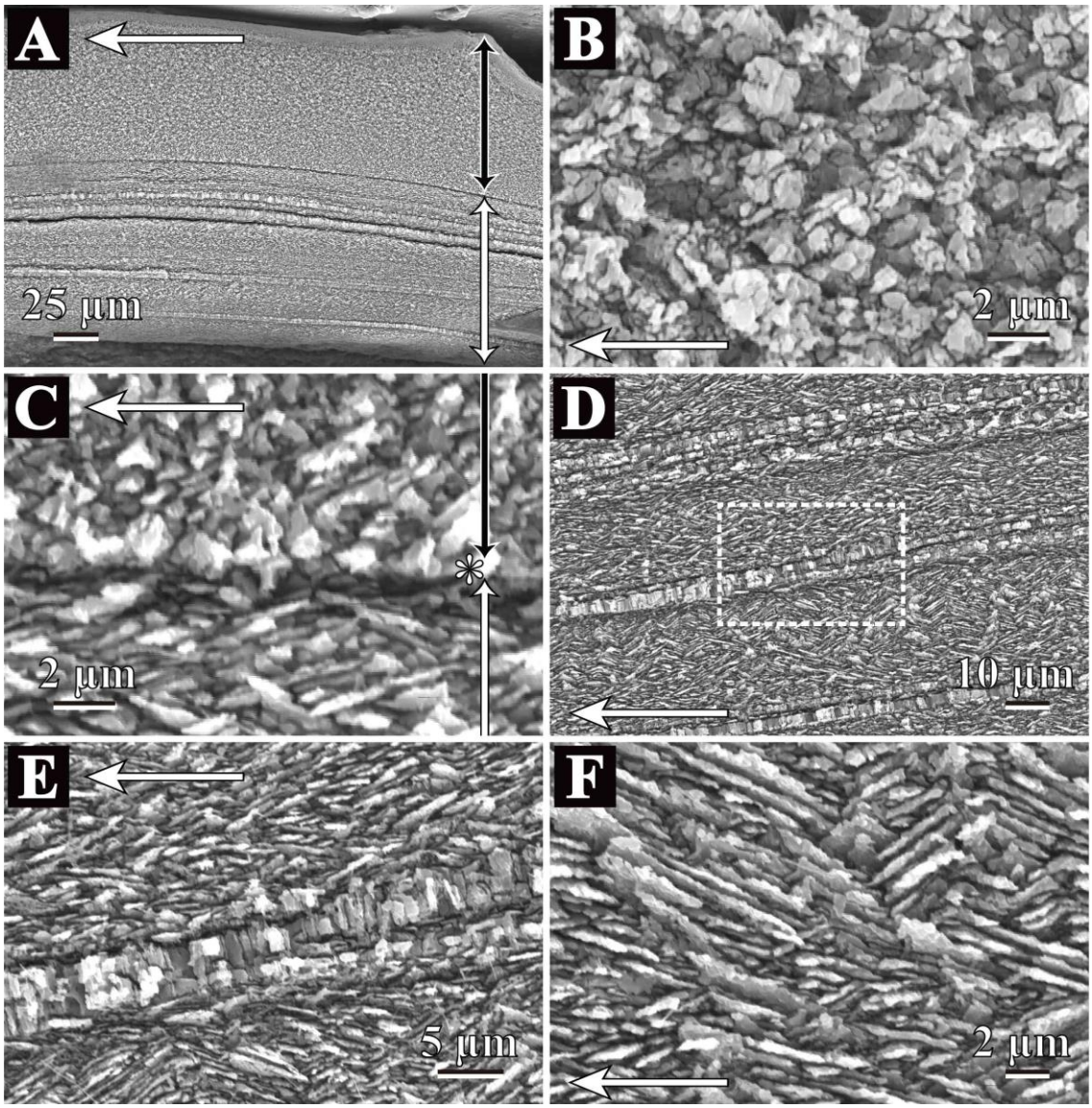

Figure 3.50. Scanning electron micrographs of *Yoldia notabilis* microstructure. Growth direction is left side in all figures. **A,** radial section of the outer and inner layer. Vertical black double-headed arrow, the outer layer; white double-headed arrow, the inner layer. **B,** radial section of homogeneous structure of the outer layer. **C,** radial section of the outer, myostracum and inner layers. Vertical black arrow, the outer layer; Asterisk mark, the myostracum layer; white double-headed arrow, the inner layer. **D,** radial section of fine complex crossed lamellar structure of the inner layer. Several growth lines was observed. **E,** closer view of broken-lined square in D. **F,** closer view of radial section of inner fine complex crossed lamellar structure. A-C, middle part of shell. D,E dorsal part of shell. A-F, Shell length = 33 mm.

3-5. Discussion

3-5-1. Summary of the shell microstructure observation of protobranchia

The shell microstructure of 35 species of protobranchs were newly described in this study based on the definition of the terminology by Carter & Clark (1985) and

Table 3.3. List of shell microstructures observed in each species. Abbreviations used in this table are listed in 3-3.

Classification	Species	Outer layer	Middle layer	Myostracum	Inner layer
Nuculoidea	*Acila mirabilis*	CP type-A	CN	ISP, Hom	SN
	Acia minutoides	CP type-A	CN	blocky	SN
	Acila insignis	CP type-A	CN	Hom	SN
	Brevinucula sp.	IFP type-A	SN	blocky/ ISP	SN
	Ennucula nipponica	CP type-B	CN	blocky/ ISP	SN
	Ennucula siberutensis	IFP type-B	SN	-	SN
	Ennucula tenuis	CP type-B	CN	ISP	SN
	Ennucula sp. 1	IFP type-B	CN	Hom	SN
	Ennucula sp. 2	CP type-A	CN	-	SN
	Nucula tokyoensis	DCP	SN	ISP	SN
	Nucula torresi	DCP	weakly CN	blocky	SN
Sareptidae	*Sarepta speciosa*	Hom (fCCL)	-	ISP	Hom
	Setigloma japonica	fCCL	-	ISP	fCCL
Manzanellidae	*Huxleyia sulcata*		Hom (fCCL)		
Solemyidae	*Acharax japonica*	RESP type C		-	Lam/ Hom
	Acharax johnsoni	Reticulate		-	cCCL
	Solemya pervernicosa	RESP typeA		-	ISP
	Solemya tagiri	RESP typeA		-	ISP
	Solemya pusilla	RESP type B		-	Hom
Nuculanidae	*Nuculana soyoae*	Hom (fCCL)		ISP	Hom
	Nuculana tanseimaruae	FP	Hom	ISP	Hom
	Nuculana leonina	Hom		-	Hom
	Nuculana yokoyamai	Hom		-	Hom
	Nuculana gordonis	FP	Hom (fCCL)	ISP	Hom
Bathyspinulidae	*Bathyspinula calcarella*	FP	Hom (fCCL)	-	Hom
Malletiidae	*Malletia takaii*	Hom		ISP	fCCL
	Malletia humilior	Hom		ISP	fCCL
Neilonellidae	*Neilonella soyoae*	FP	Hom	-	Hom
	Neilonella dubia	FP	Hom	ISP	Hom
	Neilonella kirai	FP	Hom	ISP	Hom
Tindariidae	*Tindaria soyoae*	Hom		ISP	Hom
Yoldiidae	*Megayoldia lischkei*	Hom (Spherulitic)		ISP	fCCL
	Megayoldia japonica	FP	Hom	ISP	Hom/ fCCL
	Yoldia seminuda	Hom		ISP	fCCL
	Yoldia notabilis	Hom		ISP	fCCL

Carter (1990). The results of shell microstructural observations in this study were summarized in Table 3.3. Newly found microstructures include the outer prismatic of Nuculidae and outer radially elongate simple prismatic structures of Solemyidae (Sato et al., 2013a; this study, Table 3.1, 2). Families or superfamilies confirmed by molecular phylogeny in chapter 2 can be diagnosed as follows according to shell microstructural composition.

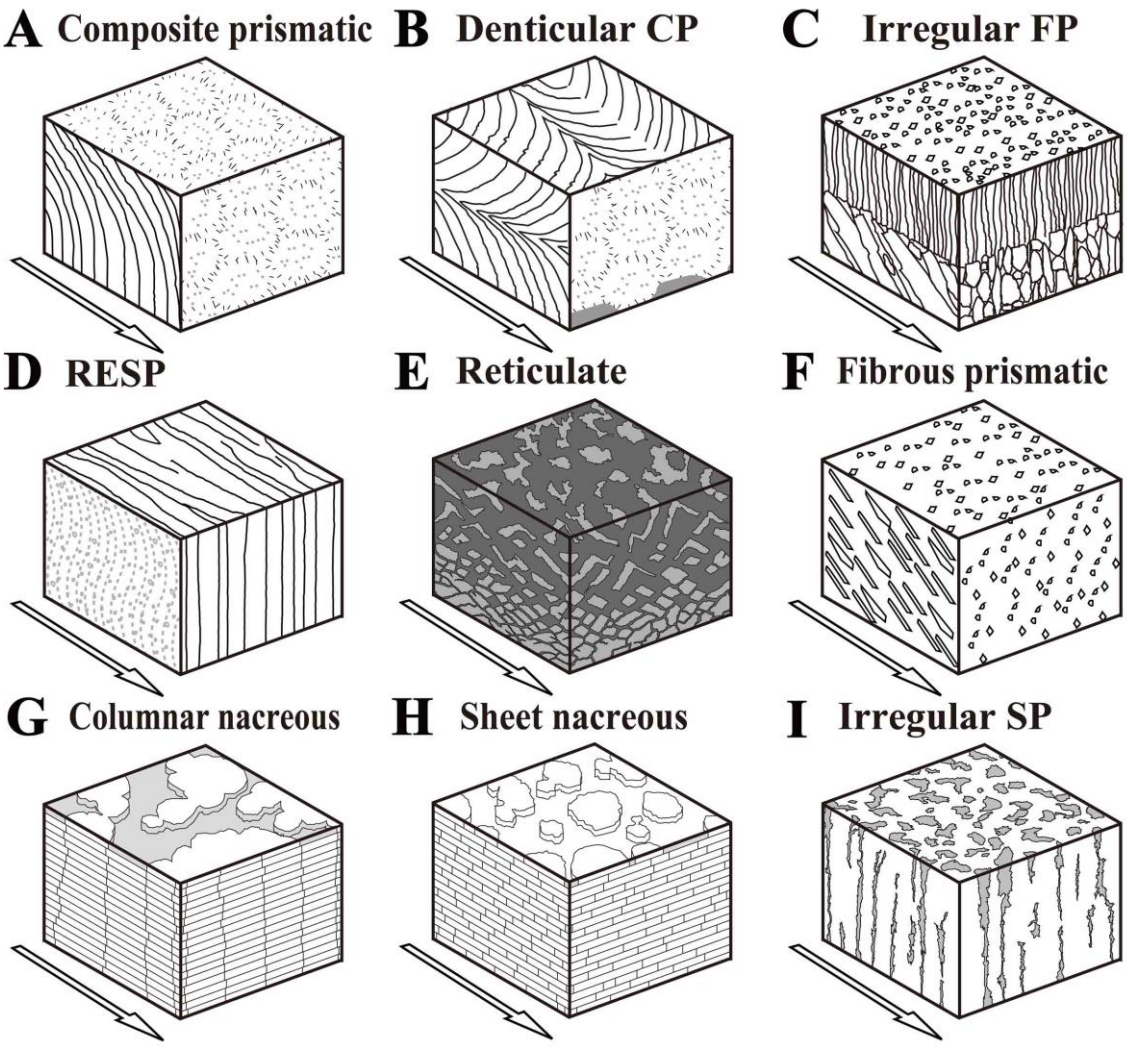

Figure 3.51. Schematic representation of the shell microstructures in protobranchs. White arrows indicate growth direction. Continued to next page.

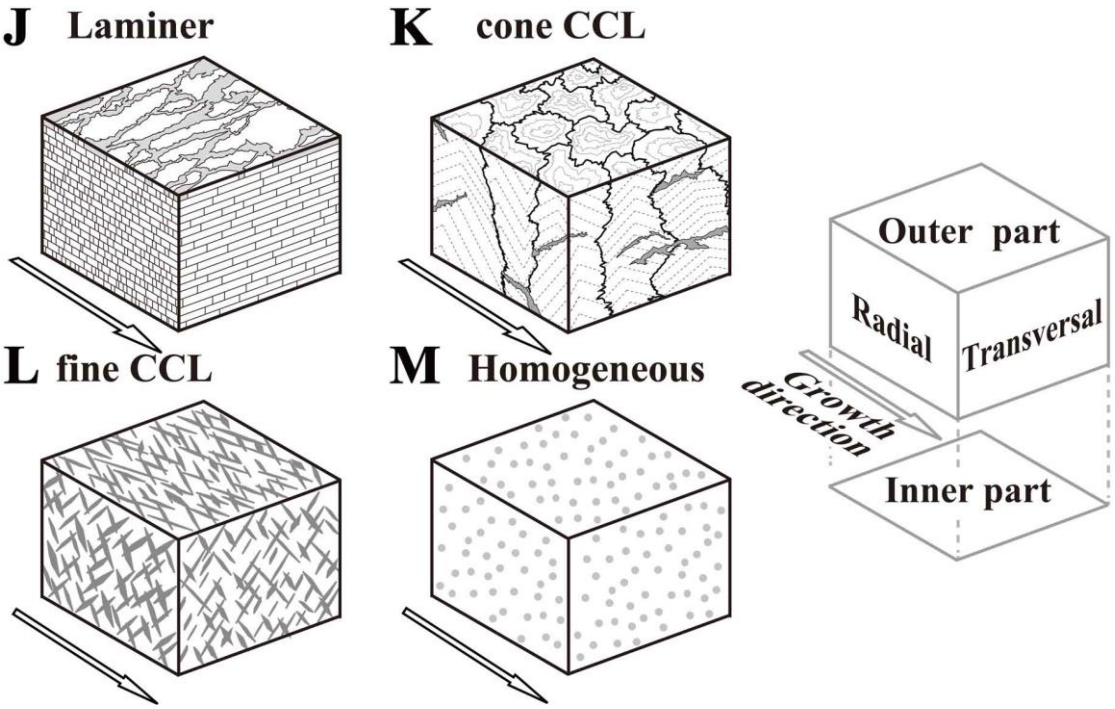

Figure 3.51. Continued.

3-5-2. Shell microstructural characteristics of Nuculidae

Previous studies characterized the shell microstructure of Nuculidae in having outer prismatic and middle/inner nacreous structures (e.g. Bøggild, 1930; Taylor et al., 1969; Carter, 1990a) except for *Condylonucula*. Carter (2001) reported that *Condylonucula maya* has fibrous to irregular prismatic structure in their outer layer, and middle and inner layers consist of nacreous structure in a juvenile stage. Later in ontogeny, the middle and inner layers are differentiated into homogeneous and irregular simple prismatic structures, respectively. This is rather unique to Nuculidae.

Prism-nacreous condition was confirmed in all observed species in Nuculidae.

Notable variations of outer prismatic structures were first detected within Nuculidae by this study. I divided prismatic structures into five types, viz. composite prismatic structure type-A, composite prismatic structure type-B, denticular prismatic structure, irregular fibrous prismatic structure type-A and irregular fibrous prismatic structure type-B; see Table 3.1. Composite prismatic structure type-A are observed only in three *Acila* species (*A. insignis, A. minutoides* and *A. mirabilis*) whose monophyly was supported by strong support value (bs = 91%). Two distinct prismatic microstructures were observed among *Ennucula* species. *Ennucula tenuis* and *E. nipponica* have composite prismatic structure type-B which differs from type-A in being composed of short acicular crystals. Their differences were also supported by crystallographic textures (see Figure5.1 and Chapter 4).The outer layers of *E. siberutensis* and *E*. sp. 1 were composed of irregular fibrous prismatic structure type-B. Two groups of *Ennucula* divided by shell microstructural character (CP type-B or IFP type-B) were separated into two clades with a weak support (bs = 31%). *Brevinucula* sp. has irregular fibrous prismatic structure type-A. *Nucula* (s.s.) and *Ennucula similis* which are paraphyletic to two *Brevinucula* species had denticular composite prismatic (DCP) structure. As described above, the outer layer of Nuculidae seems to provide crucial signals for their phylogenetic grouping in addition to the presence or absence of shell sculptures and crenulate inner ventral margin as in traditional classifications (e.g. Coan & Valentich-Scott, 2012). *Ennucula similis* is sister to *Nucula* s.s. species, and they have DCP structures. This consistency seems to confirm this hypothesis. Paraphyly of *Ennucula* was recognized in the molecular phylogenetic analysis in Chapter 2 and also by Sharma et al. (2013). If so, *Ennucula* sp. 2 could be genetically far from other *Ennucula* species, because its outer layer was composed of composite prismatic structure type-A which

was also observed in *Acila* species.

Sheet nacreous structures were observed in the inner layer. However occurrence of composite or sheet nacreous structure was irregularly found among species. No relationship was found between phylogeny, environment factors, body size and occurrence of columnar nacreous structure.

Nacreous structure appears in four of eight molluscan classes (Gastropoda, Bivalvia, Cephalopoda and Monoplacophora) (Checa et al., 2009; Frýda et al., 2010), although the arrangement patterns of nacreous tablets differ from each other. In Bivalvia, nacre tablets shows spiral growth and formed terraced arrangement (Wada, 1966; Cartwright et al., 2009), while nacre crystals stack in towers in Gastropoda (Weiner & Traub, 1980; Schäffer et al., 1997; Checa et al., 2009). The cephalopod nacre shows a mixed structure with towered and terraced growth (Mitchel & Phakey, 1995). In previous microstructural study generally defined nacre as sheet nacreous structure in bivalves and as columnar nacreous structure in gastropods and cephalopods (e.g. Taylor et al., 1969; Carter, 1990b). Vertically stacked nacre tablets were exceptionally observed in the middle layers of some species of Mytilidae (Subclass Pteriomorphia), Unioida, Trigonioida (both Subclass Palaeoheterodonta) and Nuculidae (subclass Protobranchia) (Taylor et al., 1969; Carter, 1990; Fryda et al., 2010; Génio et al., 2012; Carter et al., 2014). These two types of nacre have been defined as columnar nacreous structure by Carter (1990b). Taylor et al. (1969) have called them ‘lenticular nacreous’ structure but this appellative was rejected by authors after Carter (1990b). However, columnar nacreous structure of bivalves, gastropod and cephalopod seem to be distinguishable by the mode of crystal growth. Spiral growth of nacre tablets were observed in of *Acila mirabilis* (columnar nacre in figure 3.2F, sheet nacre in figure 3.3B), but that is not

recognized in gastropod and cephalopod columnar nacreous structure. Thus, two nacreous layers in the middle and inner layers of Nuculidae are regarded as the products created by the same mechanisms of crystal growth, and vertical nacre stacking seems not to be controlled by strict law as compared with that of gastropods and cephalopods. Columnar nacreous structure of protobranchs gradually shift to sheet nacreous structure towards the shell interior in the middle layer of nuculids. Such a trend has never been recognized in gastropods and cephalopods. Occurrence of columnar nacreous structure can be relate to the rate of shell growth. Generally columnar nacre associates with fast-growing surfaces and sheet nacreous structure associates with relatively slow-glowing surface (Wise, 1970; Checa et al., 2006).

3-5-3. Shell microstructural characteristics of Solemyoida

Three microstructures in solemyids, namely, RESP, reticulate structure, and ISP, have never been reported in other protobranchs, although RESP-like structure is also known in the cemented area of the oyster shell (Yamaguchi, 1994). No myostracum was observed in the solemyids in this study. The myostracum is frequently missing in other protobranchs, although bivalves and gastropod generally have a myostracum (Taylor *et al.*, 1969). The myostracum-lacking condition may be an apomorphic character of bivalves.

In terms of microstructural composition, Solemyidae is categorized into four groups: (1) Group 1 contains *S.* (*P.*) *pervernicosa* and *S.* (*S.*) *tagiri*. The outer layer of these species is composed of RESP type A, and the inner layer is composed of ISP. (2) Group 2 is represented by *S. pusilla*. The outer layer is composed of RESP type B, and

the inner layer is composed of homogeneous structure. (3) Group 3 is represented by *A. japonica*, whose outer layer is composed of RESP type C (4) Group 4 is represented by *A. johnsoni* and is distinguished from the other groups by the reticulate structure of the outer layer, reported here for the first time. These groupings have not been reported by earlier studies. Therefore, I have shown that shell microstructures are more diversified in this family than previously perceived.

These four groups determined on the basis of shell microstructure are not consistent with conventional solemyid systematics (Dall, 1908a, b; Vokes, 1955; Coan *et al*., 2000) in three respects. (1) Subgenus *Solemya*: Taylor *et al*. (1969) reported that the RESP of the outer layer of *S.* (*S.*) *togata*, the type species of *Solemya*, branches and bends ventrally when traced toward the inner shell surface. I did not observe this feature in the outer layer of *S.* (*S.*) *pusilla* or *S.* (*S.*) *tagiri*. (2) Subgenus *Zesolemya*: The shell microstructure of *Solemya* (*Zesolemya*) *parkinsoni* (Beedham & Owen, 1965; Taylor *et al*., 1969; Carter & Lutz, 1990) resembles the irregular simple prismatic structure of Group 1 [*S.* (*P.*) *pervernicosa* and *S.* (*S.*) *tagiri*] despite its different subgeneric assignment. (3) Genus *Acharax*: I observed notably different microstructures in both layers in the two species of genus *Acharax* that I examined (*A. japonica* and *A. johnsoni*). I assume that the character state distributions of the shell microstructures have a different pattern of character state distributions compared with macroscopic traits.

As mentioned in chapter 2, my molecular phylogenetic analysis in this study revealed that two subgenera (*Solemya* s.s. and *Petrasma*) are not monophyletic among three genera which used in ML analysis. This result implies traditional classification of solemyids mainly based on the characters in umbonal area is doubtful. In addition, *Solemya reidi*, which is regarded as a junior synonym of *S. pervernicosa* by Kamenev

(2009), and *S. pervernicosa* seem to be distinct two species. Shell microstructural diversification could provide important information about phylogenetic groupings in solemyids. Further observations and molecular data are required for this taxon to test this phylogenetic hypothesis more rigorously.

In contrast to Solemyoidea, *Huxleyia sulcata* which belong to Manzanelloidea, the sister group of Solemyidae had homogeneous structure in their shell. The component of shell microstructure of two superfamilies of Solemyoida differed completely despite their genetic affiliation which is confirmed by molecular analysis in Chapter 2.

3-5-4. Shell microstructural characteristics of Nuculanoidea

Molecular analysis in Chapter 2 suggested the systematic position of family Sareptidae should be revised from Nuculoidea to Nuculanoidea. Species of Nuculanoidea, including family Sareptidae, observed in this study share homogeneous structure expect for *Setigloma japonica*. Outer fibrous prismatic and inner fine complex crossed lamellar structures were observed in some species. Topology of this clade is doubtful due to insignificant support values (see Chapter 2). Thus, it is insecure to discuss the phylogenetic constraint of shell microstructural variations. However, provided shell microstructural and molecular data suggest occurrence of fibrous prismatic and fine CCL structures are not consistent with phylogeny. No relationship was found between the occurrence of these microstructure and the habitat (e.g. water depth).

3-6. Summary

Comparison with the molecular phylogenetic analysis in Chapter 2 corroborated that major clades of protobranchs have different microstructural composition at the superfamily level.

(1) Nuculoidea commonly had outer prismatic and middle/inner nacreous structures. I classified the outer prismatic layers into five types; this division is unique and has not been published in earlier studies. In particular, the irregular fibrous prismatic structure was first observed from the outer layer of Nuculoidea. The interspecific variation of outer prismatic layers seems to provide crucial signals for phylogenetic grouping. (2) The shell microstructural diversity of the inner layer was unique to Solemyoidea (Sato et al., 2013a): the radially elongate simple prismatic (RESP), and reticulate and irregular simple prismatic structures. (3) Nuculanoidea had non-nacreous structures including the homogeneous, fibrous prismatic and fine complex crossed lamellar structures. Sareptidae reclassified from Nuculoidea to Nuculanoidea also follows this trend.

Chapter 4

Crystallographic textures of protobranch bivalves

4-1. Introduction

Molluscan shells are one of the most studied biominerals. Current research on the molecular mechanism of molluscan biomineralization reveals that shell matrix proteins play an important role in this process. For instance, the shell protein *aspein*, which was identified by Tsukamoto et al. (2004) from the pearl oyster *Pinctada fucata*, controls the polymorphism of $CaCO_3$ (calcite/aragonite) during shell formation. Because magnesium (Mg) inhibits the growth of calcite (Berner, 1975), but not that of aragonite, the high levels of Mg observed recently in the global seawaters indicate that the precipitation of aragonite over calcite is currently favored (e.g. Ries, 2010; Hönisch et al., 2012). *Aspein* allows calcitic shell formation under this aragonite favored seawater chemistry (Takeuchi et al., 2008). Suzuki et al. (2009) reported that the proteins *Pif80* and *Pif97* specifically bind to the nacreous structure in *P. fucata*, and knockdown experiments during the study strongly suggest that *Pif80* and *Pif97* regulate nacre formation.

As mentioned before, biologically controlled calcium carbonates grow differently from authigenic carbonates in their mineral species, shape, and orientation of crystals. Shell microstructure is the product of such a complex molecular mechanism and several studies have recognized that crystallographic textures may differ even though the associated microstructures are similar and they show some systematic trends

(Chateigner et al., 2000; Frýda et al., 2010). Many studies of shell microstructure rely on SEM observations (as seen in Chapter 3), however, it is desirable to characterize shell microstructure by their crystallographic textures. Although studies on crystallographic textures have been conducted intensively for decades (nacreous structure of pteriid bivalve; Checa & Rodríguez-Navarro, 2005; Checa et al., 2006, monoplacophoran foliated aragonite structure; Checa et al., 2009, multi-layered shell microstructures of *Lottia kogamogai*; Suzuki et al., 2010, crossed lamellar structure: Rodriguez-Navarro et al., 2012; fibrous prismatic structure of mytilid bivalve; Checa et al., 2014), information on crystallographic textures is still unsatisfactory for a phylogenetic discussion. In this study, the crystallographic textures of shell microstructures in protobranch bivalves were analyzed and the relationships between crystallographic textures and morphological elements were investigated in order to discover further microstructural morphological characters; this was done using a single-crystal diffractometer equipped with an area detector.

4-2. Materials and Methods

4-2-1. Materials

A total of 182 specimens were investigated that comprised 14 samples of 13 different species (Table 2.1 in Chapter 2). All samples were cut into small chips (approximately 5 mm in length) using a hand cutter.

Samples used for texture analysis were planar and comprised a small portion of an already investigated shell to avoid the defocusing and uncontrolled absorption of the X-rays. The small chips were cut from an area near the center of the shells; this was

done to aid the analysis of the crystallographic textures of the outer and inner layers by exposing the outer and inner shell surfaces to the X-rays. Some small specimens had deeply concave inner surfaces, such as *Huxleyia sulcata*, and, therefore, the crystallographic textures of these surfaces could not be analyzed. Small chips from the ventral margins were used in the analysis of middle layer textural patterns in *Ennucula nipponica* and *Acila insignis*.

4-2-2. X-ray Diffraction

The three-dimensional orientation of the shell crystals was determined using an X-ray single diffractometer (D8 SMART APEX, Bruker). The working conditions for the experiments were as follows: Mo Ka radiation, 50 KV and 30 mA, collimator size, 0.5 mm in diameter. The shell samples were mounted on a goniometer head with the surface to be analyzed perpendicular to the ψ rotation axis. The ψ axis was rotated by 180°, with diffraction patterns being recorded every 5° of the rotation, giving a total of 36 frames for each analysis. The ω and 2θ axes were set as 10° and 20°. As a result, the orientation distribution for thousands of crystallites in an area of around 3 mm in diameter was determined.

Pole densities for strong aragonite reflections (110, 111, 012 and 002) were calculated and displayed as pole figures (Figure 4.1) using XRD2DScan software (http://www.ugr.es/~anava/xrd2dscan.htm). These pole figures display the intensity variation of a given hkl reflection (110, 111, 012, 002) as a function of the sample orientation (Figure 4.2). In this method, it is possible for multiple pole figures to be registered simultaneously (Rodriguez-Navarro, 2007).

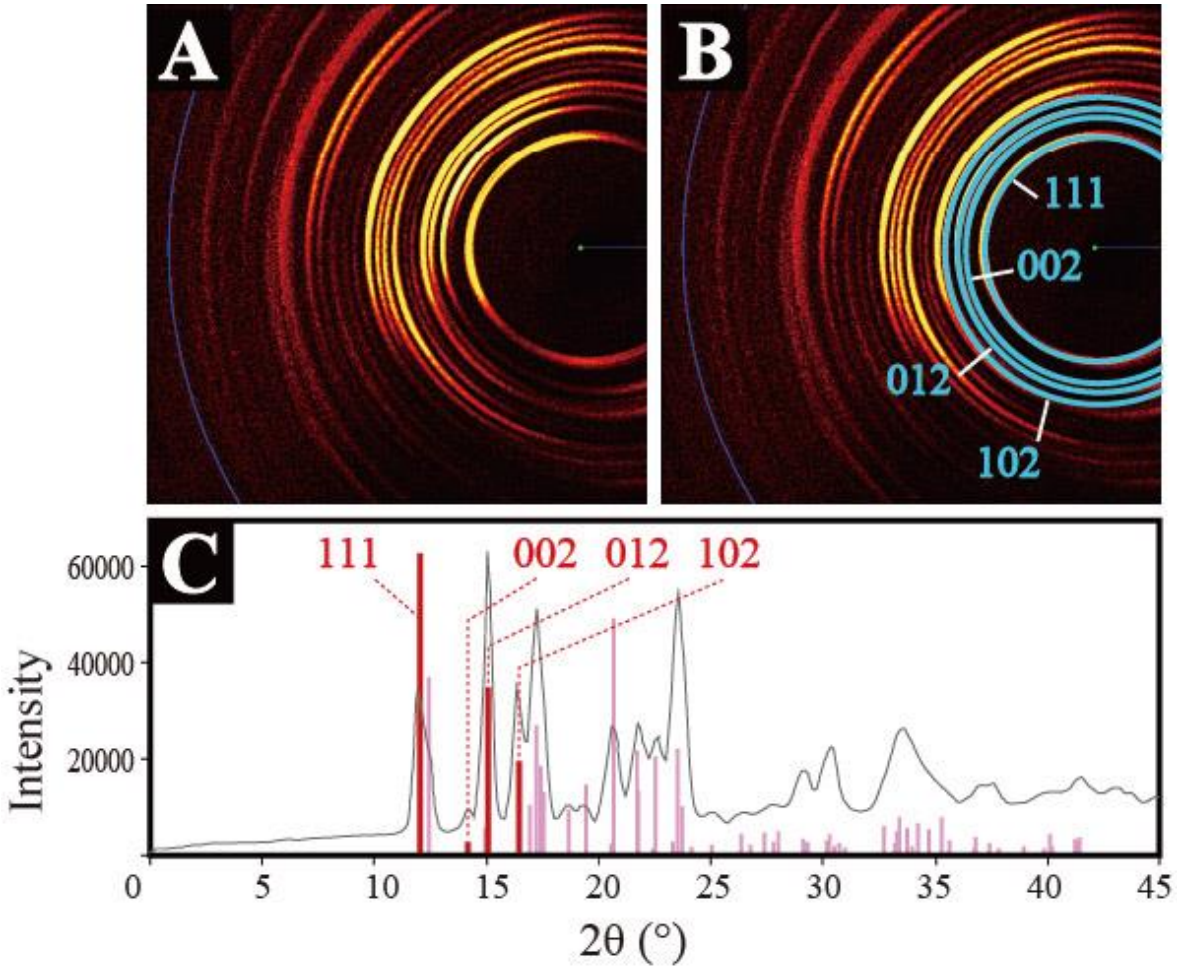

Figure 4.1. A, two dimensional diffraction pattern of $CaCO_3$ polycrystal in the outer layer of *Malletia takaii*, showing slightly spotty rings. **B,** same image as A with each ranges of crystal faces illustrated. **C,** calculated 2θ scans of $CaCO_3$ polycrystal in the outer layer of *Malletia takaii*. Red and pink colored bars indicate the mineral pattern of aragonite from the database.

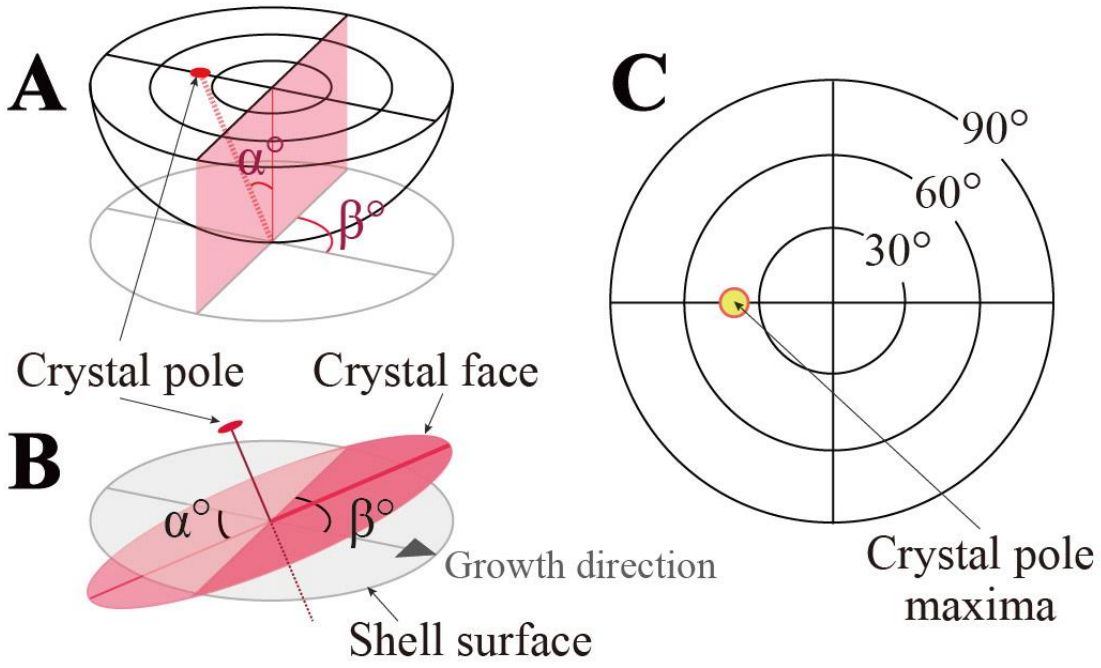

Figure 4.2. A, stereographic projection showing the position of projected crystal pole on the pole figure. The orientation of optimal crystal coincident with that in B. **B,** schematic image of optimal crystal face weakly inclined to shell surface. **C,** generated pole figure showing the pole densities of optimal crystal face in B.

4-3. Results

The outer layers of the family Nuculidae are characterized as having the prismatic structure. In the examined species, the composite prismatic structure was observed in *Ennucula nipponica* and *Acila insignis*, and the denticular composite structure was recognized in *Nucula tokyoensis* from SEM observations. The composite prismatic structure of the outer layer in *E. nipponica* showed a girdle pattern with a tendency to develop clusters in the pole of {111} and {002} reclined to the inner shell

surface (Figure 4.3). In contrast to the difference in the shell microstructure from SEM observation, the crystallographic textures of the outer layer of *A. insignis* and *N. tokyoensis* resemble each other in some aspects. The pole of {111} exhibits two linearly aligned patterns, which extend along the growth direction of the shell, and two or three peaks were found in the pole of {002}, clearly reclining to the outer shell surface (Figures 4.4, 4.5).

The middle and inner layers of the family Nuculidae are commonly composed of the nacreous structure (see Chapter 3). Also, differences in the stacking pattern of nacre tablets are obvious between the nacreous structure of the middle and inner layers in most nuculids. A columnar nacreous structure is dominant in the middle layers, and a sheet nacreous structure composes the inner layers of most nuculids. The crystallographic textures of the middle-layer nacreous structure of the two nuculid species *Ennucula nipponica* and *Acila insignis* were analyzed in this study (Figures 4.3, 4.4). Dyad symmetry patterns, which imply the single crystal like texture, were commonly found in the poles of {111} and {012} in the middle layers of the two species. On the other hand, the crystallographic textures of the sheet nacreous structure differed among three species of nuculids: *Acila insignis*, *Ennucula nipponica,* and *Nucula tokyoensis*. The poles of {111} and {012} of the sheet nacreous structure in *Acia insignis* showed a four-fold symmetry cluster pattern, which suggests single twinning of nacre tablets (Chateigner et al., 2000). In contrast, the six-maxima interpreted as a product of double twinning (Chateigner et al., 2000; Frýda et al., 2010) were found in the poles of {111} and {012} in *Ennucula nipponica* and *Nucula tokyoensis*. The {002} pole coinciding with the c-axes of aragonite of nacreous layers in all examined species were perpendicular to the inner shell surface.

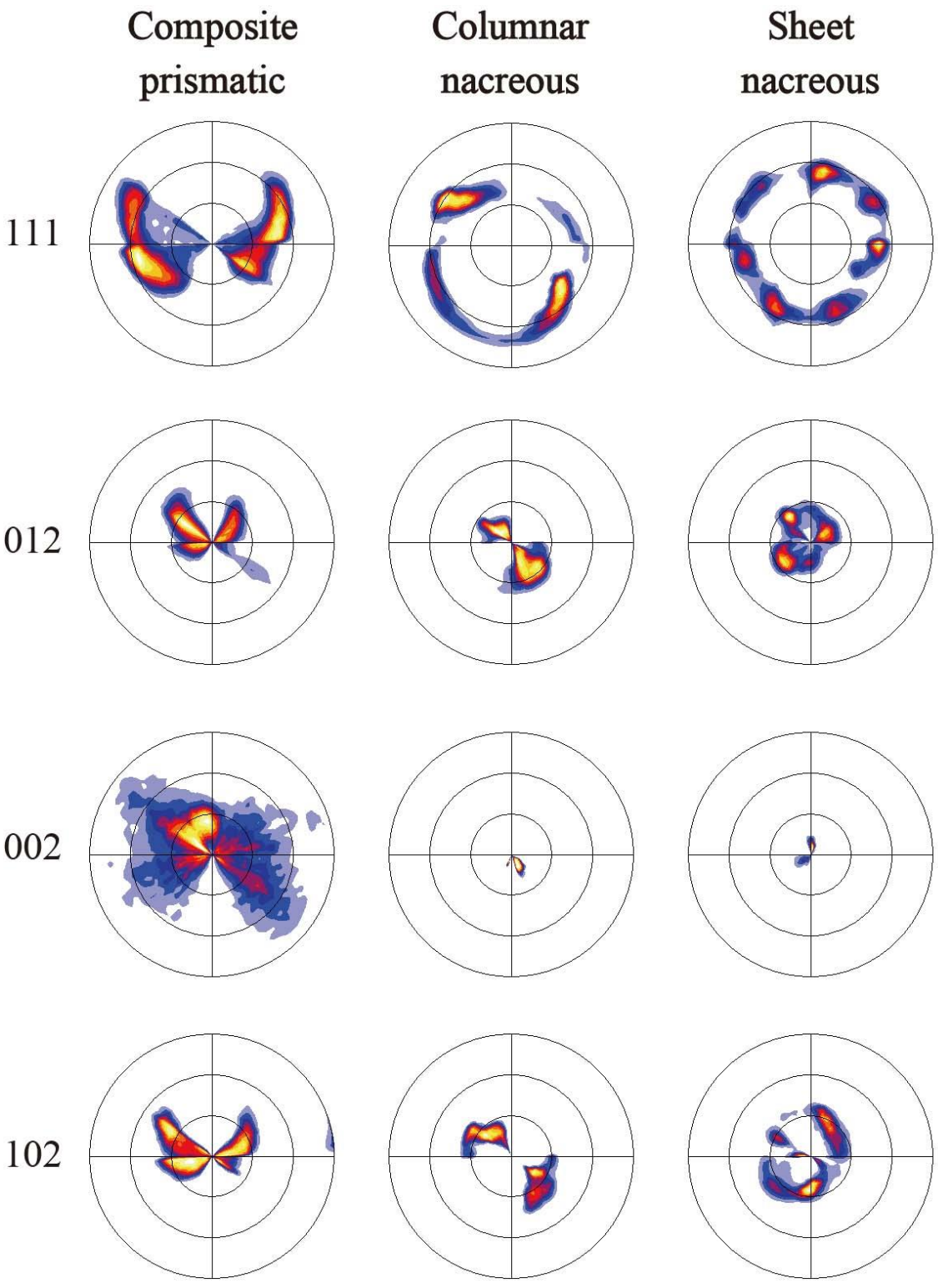

Figure 4.3. Results of X-ray diffraction texture analysis of composite prismatic structure type-B in the outer layer, columnar nacreous structure in the middle layer and inner sheet nacreous structure of *Ennucula nipponica*. The direction of growth is toward the right in all pole figures

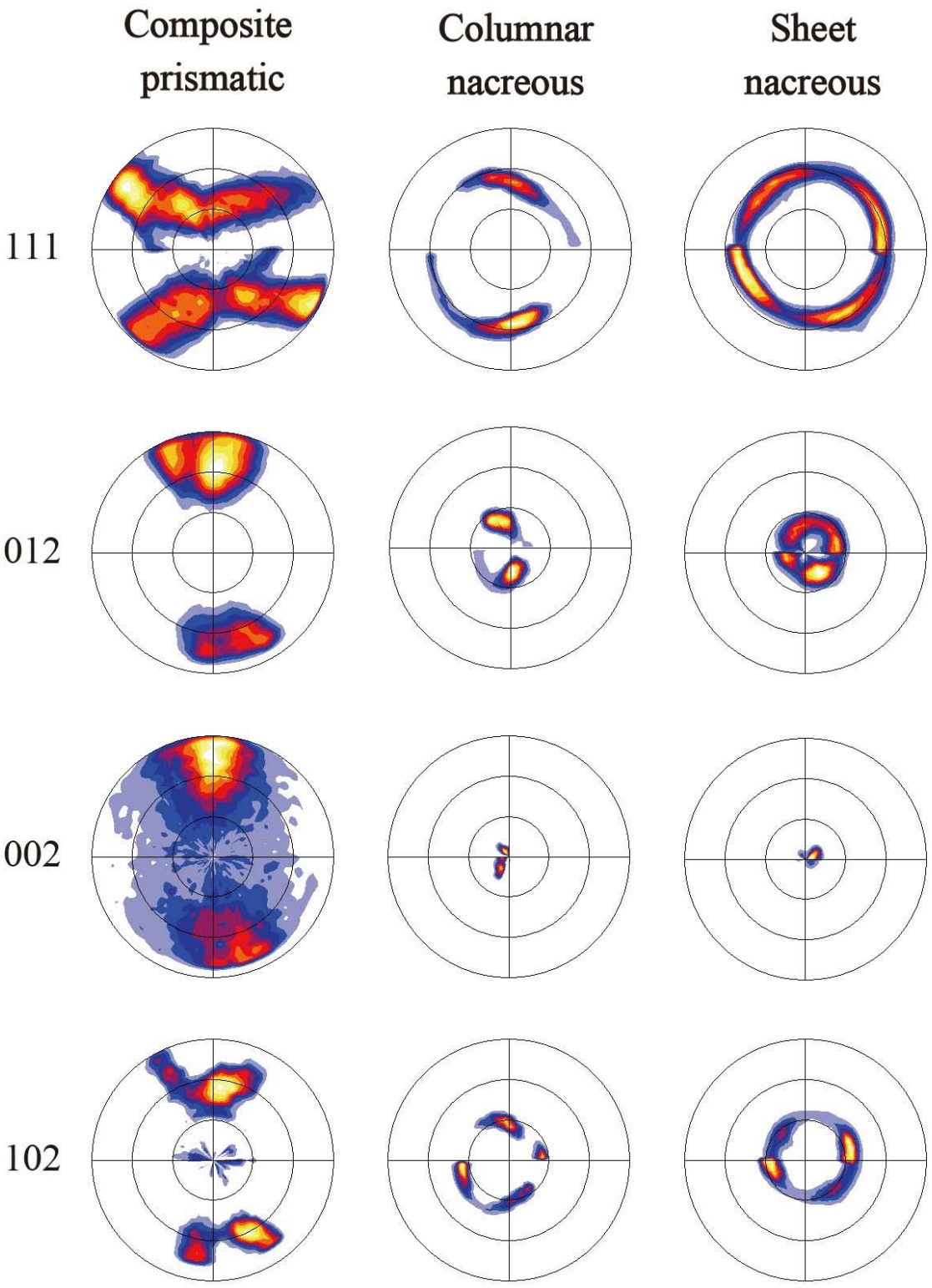

Figure 4.4. Results of X-ray diffraction texture analysis of composite prismatic structure type-A in the outer layer, columnar nacreous structure in the middle layer and inner sheet nacreous structure of *Acila insignis*. The direction of growth is toward the right in all pole figures.

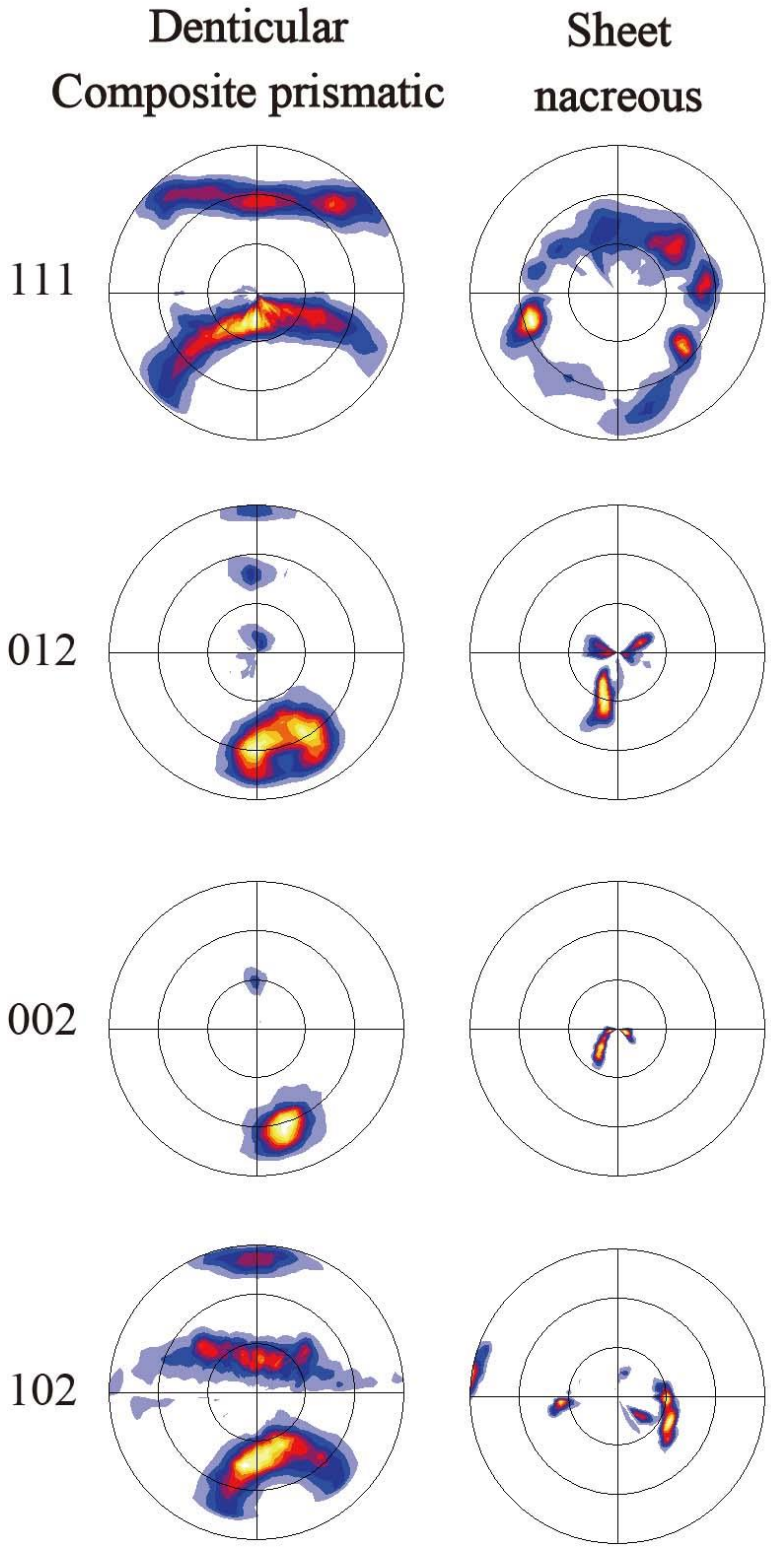

Figure 4.5. Results of X-ray diffraction texture analysis of denticular composite prismatic structure in the outer layer, columnar nacreous structure in the middle layer and inner sheet nacreous structure of *Nucula tokyoensis*. The direction of growth is toward the right in all pole figures.

The shell of *Huxleyia sulcata*, which belongs to the family Manzanellidae, is wholly composed of the homogeneous structure. The poles of {111}, {012} and {102} of the outer part of the homogeneous structure showed a moderately developed dyad symmetry pattern, and the {002} pole was perpendicular to the inner shell surface (Figure 4.6).

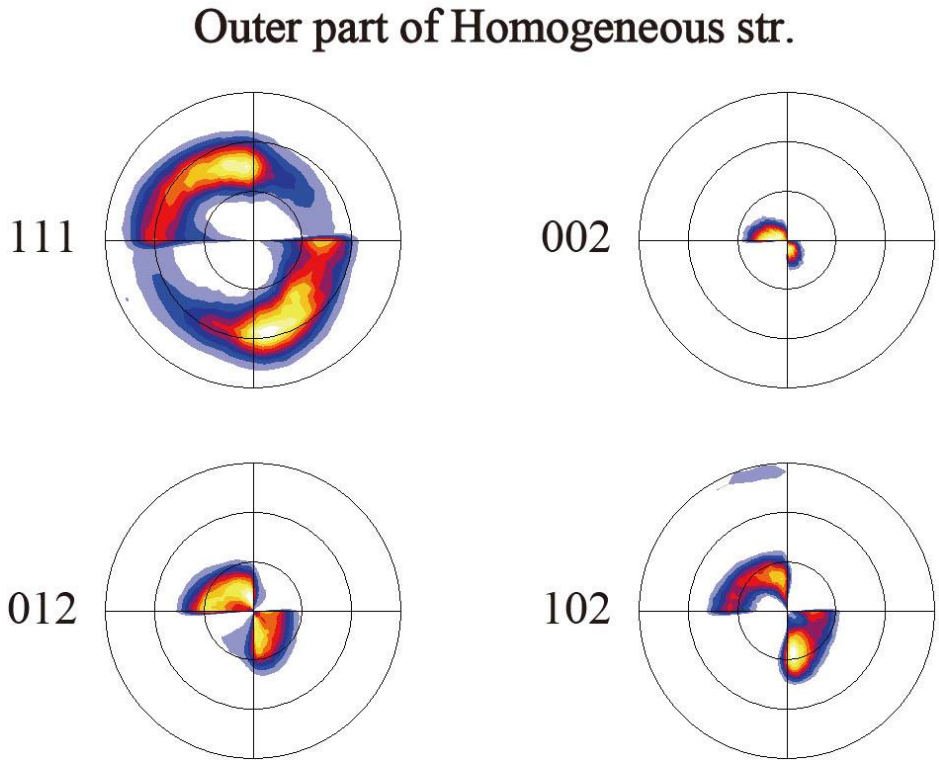

Figure 4.6. Results of X-ray diffraction texture analysis of homogeneous structure in outer most part of the shell of *Huxleyia sulcata*. The direction of growth is toward the right in all pole figures.

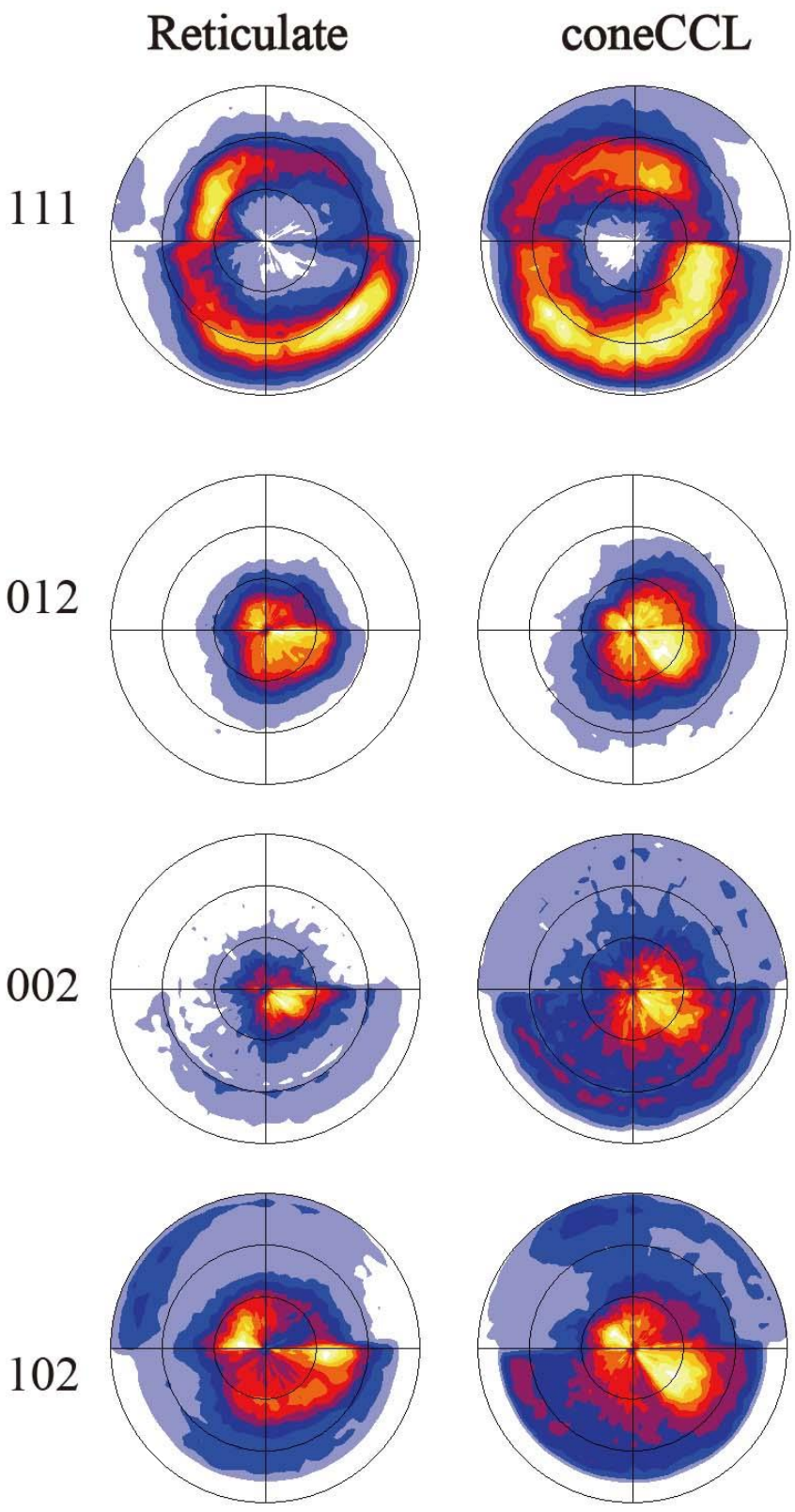

Figure 4.7. Results of X-ray diffraction texture analysis of raticulate structure in the outer layer and cone complex crossed lamellar structure in the inner layer of *Acharax johnsoni*. The direction of growth is toward the right in all pole figures.

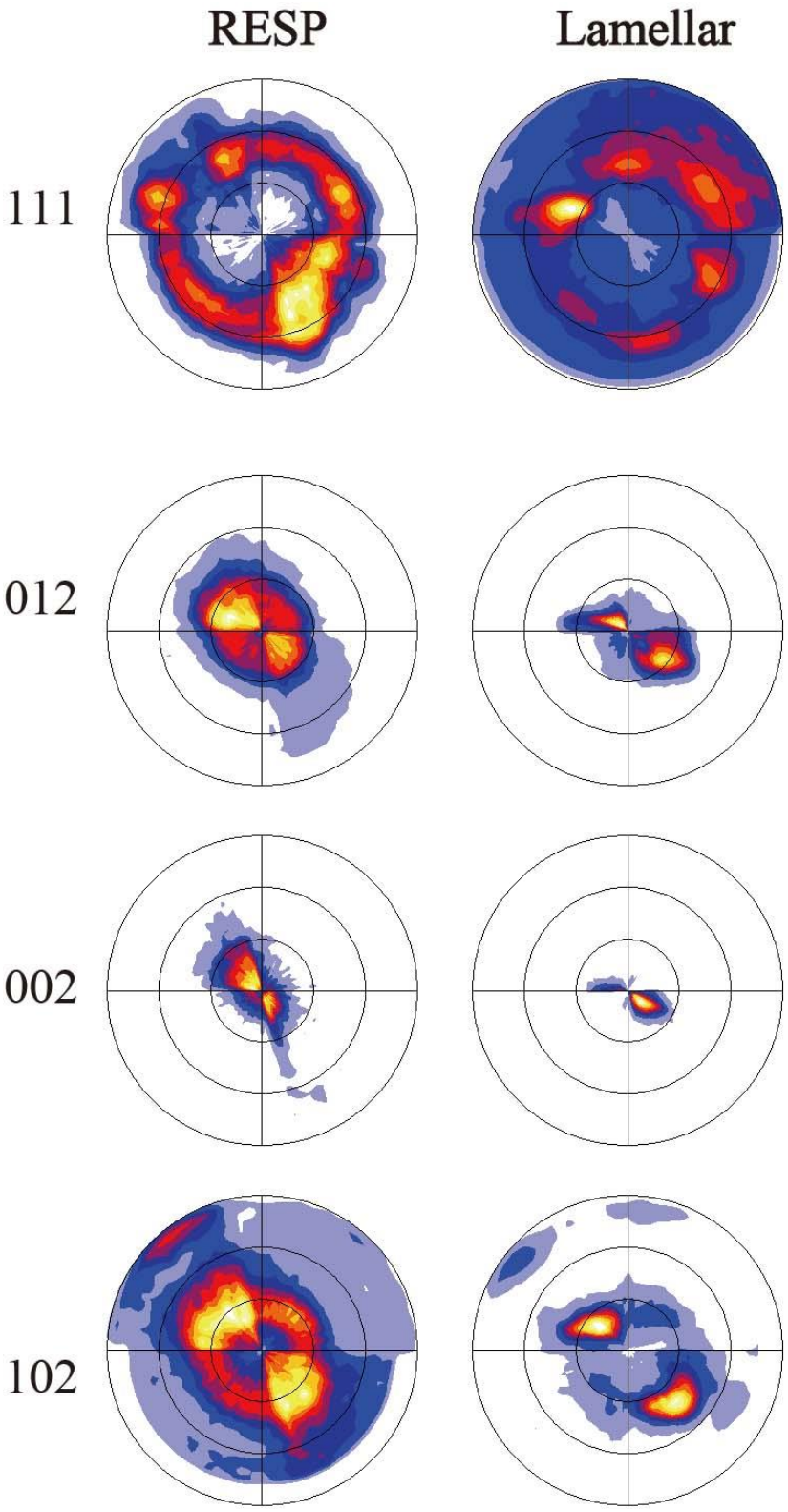

Figure 4.8. Results of X-ray diffraction texture analysis of radially elongate simple prismatic structure type-C in the outer layer and laminar structure in the inner layer of *Acharax japonica*. The direction of growth is toward the right in all pole figures**.**

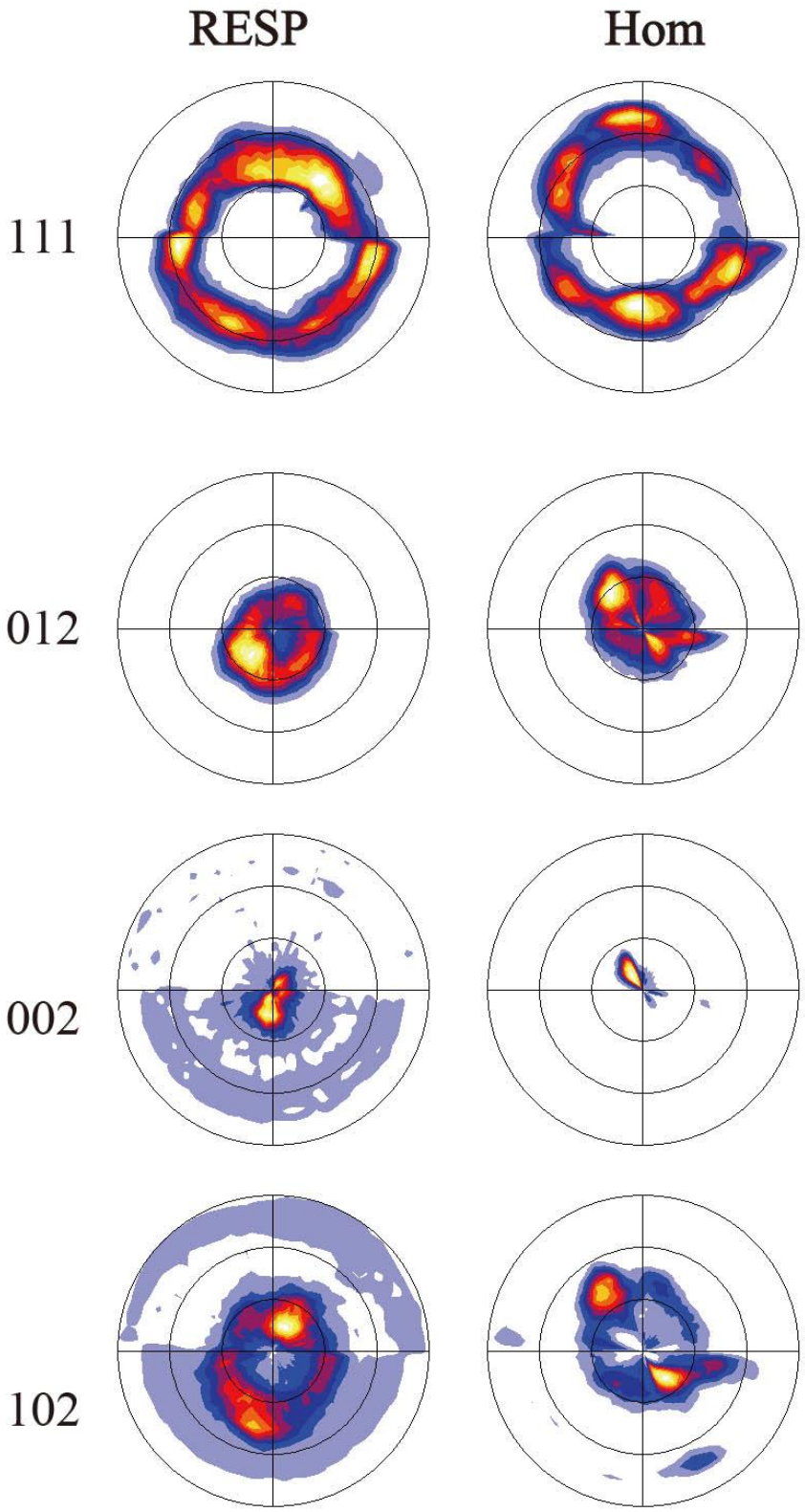

Figure 4.9. Results of X-ray diffraction texture analysis of radially elongate simple prismatic structure type-B in the outer layer and homogeneous structure in the inner layer of *Solemya pusilla*. The direction of growth is toward the right in all pole figures**.**

The family Solemyidae have variations in their shell microstructures (see Chapter 3), however, their crystallographic directions were monotonous. *Acharax johnsoni* (Figure 4.7) possesses the reticulate structure in the outer layer and cone Complex crossed lamellar structure (CCL) in the inner layer. Girdle-like patterns were commonly found in the poles of {111}, {012} and {102} in both layers. The pole of {002} of both layers converge moderately and were perpendicular to the inner shell surface. The crystallographic direction of the two layers in *Acharax japonica* (Figure 4.8) and *Solemya pusilla* (Figure 4.9) show the same tendency as that of *Acharax johnsoni*. The poles of {111}, {012} and {102} of the outer layers of these two species shows girdle-like patterns, and the {002} pole of both layers were perpendicular to the inner shell surface. Similar patterns were recognized in the crystallographic direction of their inner layers, but their crystal poles are more converged than that of the outer layer and showed a moderately clustered pattern.

In contrast to the above mentioned taxa, the shell microstructures of the superfamily Nuculanoidea are generally uncomplicated and the homogeneous structure was observed in all the studied species. Two species of the family Nuculanidae, *Nuculana tanseimaruae* (Figure 4.10) and *Nuculana gordonis* (Figure 4.11), have the fibrous prismatic structure in the outer layer and fine complex crossed lamellar structure in the inner layer. In these two examined species, the arrangements of the {111}, {012} and {102} axes showed a girdle pattern with a tendency to develop two clusters, and the pole of {002} is reclined to the inner shell surface in the fibrous prismatic structure. Crystallographic textures of the shell microstructures were different between the two species. Moderate dyad symmetry with nearly a girdle-like pattern was recognized in the arrangements of the {111}, {012}, and {102} poles in the homogeneous structure of

Nuculana tanseimaruae, while six-maxima for the {111}, {012} and {102} poles are present in *Nuculana gordonis*. Similar to the case of the family Nuculanidae, disagreement between shell structures and their crystallographic textures was frequently detected in the examined species of the superfamily Nuculanoidea. The homogeneous structure of the outer layer in *Malletia takaii* (Figure 4.12) showed a girdle-like pattern with a strong tendency to develop two clusters in the pole of {111}. Accumulation of the {111} pole into two clusters was slightly stronger in the homogeneous structure at the ventral part than that at the dorsal part. Weak dyad symmetry was found in the {111} and {102}poles of the fine complex crossed lamellar structure of the inner layer in *M. takaii*, although a girdle pattern with four-point maxima was recognized in the {012} pole. The shell of *Tindaria soyoae* (Figure 4.13) wholly consists of a homogeneous structure, with the pole of {111} showing a girdle-like pattern in the outer part of the homogeneous structure. On the other hand, two clusters in a dyad symmetry pattern were found in the {111} pole of the inner part of the homogeneous structure, while a four-maxima pattern was recognized in the {012} pole. The {002} pole of the inner part of homogeneous structure in *T. soyoae* is perpendicular to the inner shell surface, but that of the outer part is not. *Yoldia johanni* (Figure 4.14) and *Y. notabilis* (Figure 4.15) share the homogeneous structure in the outer layer and fine complex crossed lamellar structure in the inner layer. In the outer and inner layers of *Y. johanni* and dorsal part of the outer layer of *Y. notabilis*, girdle-like textural patterns of the {111}, {012} and {102} poles were found, and their {002} poles are similarly perpendicular to the inner shell surface. However, the arrangement of the {111}, {012} and {102} poles were nearly random in the ventral part of the outer layer in *Y. notabilis*, unlike the dorsal part of the same layer of the same structure. The pole of {111}, {012} and {102} axes of the fine complex crossed lamellar

structure of *Y. notabilis* showed a clustered arrangement; this was not seen in *Y. johanni*.

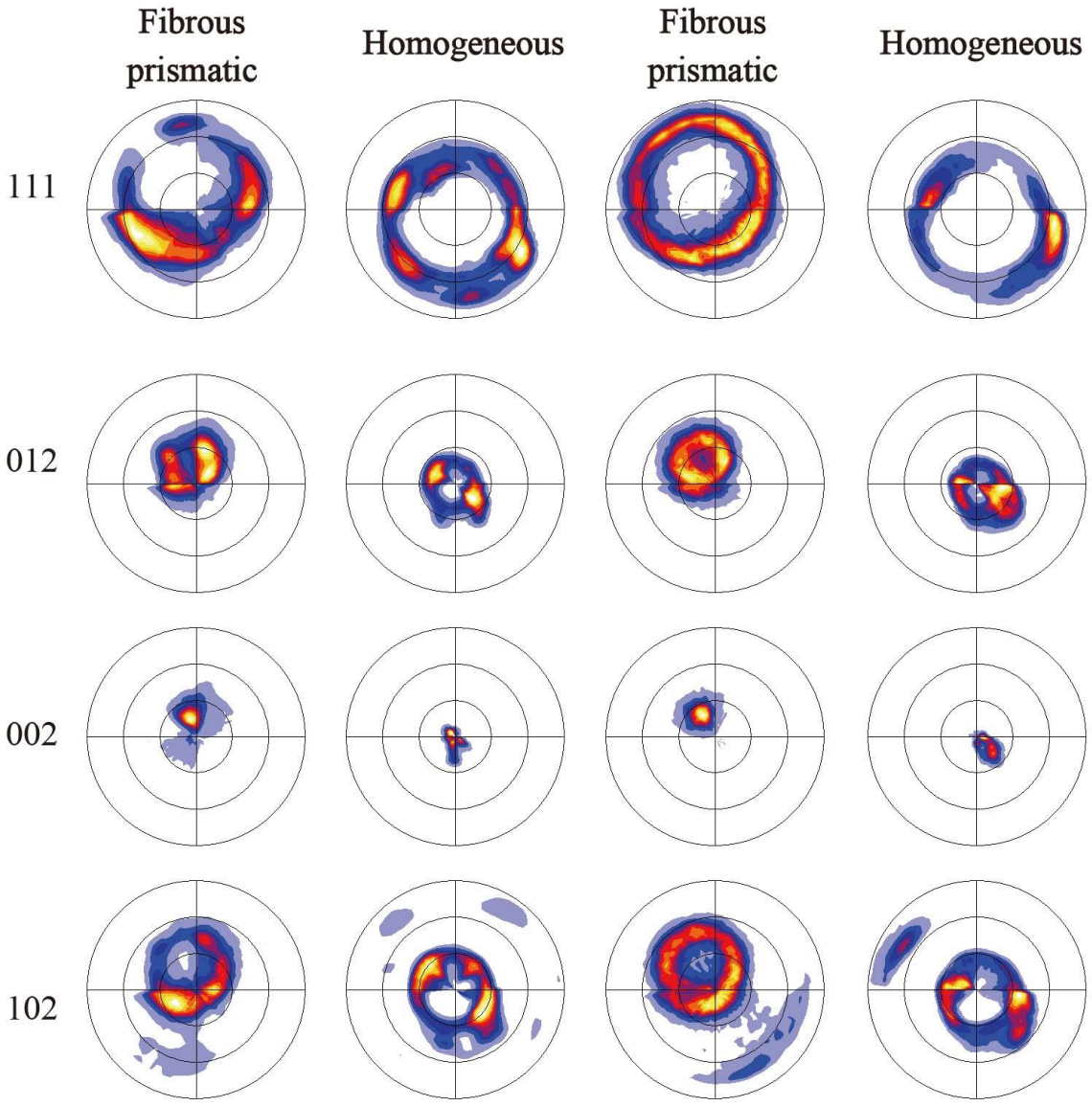

Figure 4.10. Results of X-ray diffraction texture analysis of outer fibrous prismatic and inner homogeneous structure of *Nuculana tanseimaruae*. The direction of growth is toward the right in all pole figures**.** The pole figures in left two columns are the data of the specimen collected from Okikasayama Bank and those in right from off Wakayama.

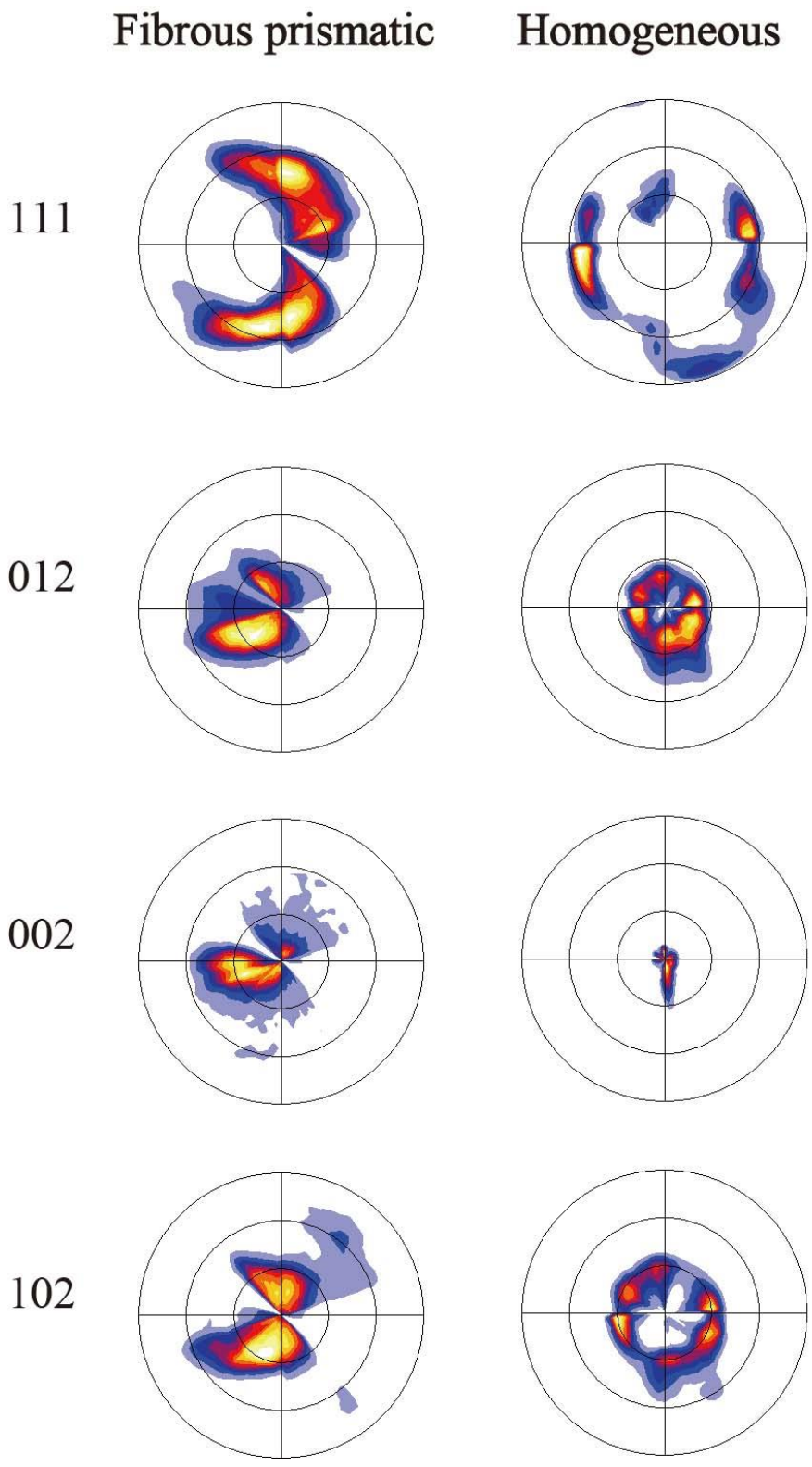

Figure 4.11. Results of X-ray diffraction texture analysis of outer fibrous prismatic and inner homogeneous structure of *Nuculana gordonis*. The direction of growth is toward the right in all pole figures**.**

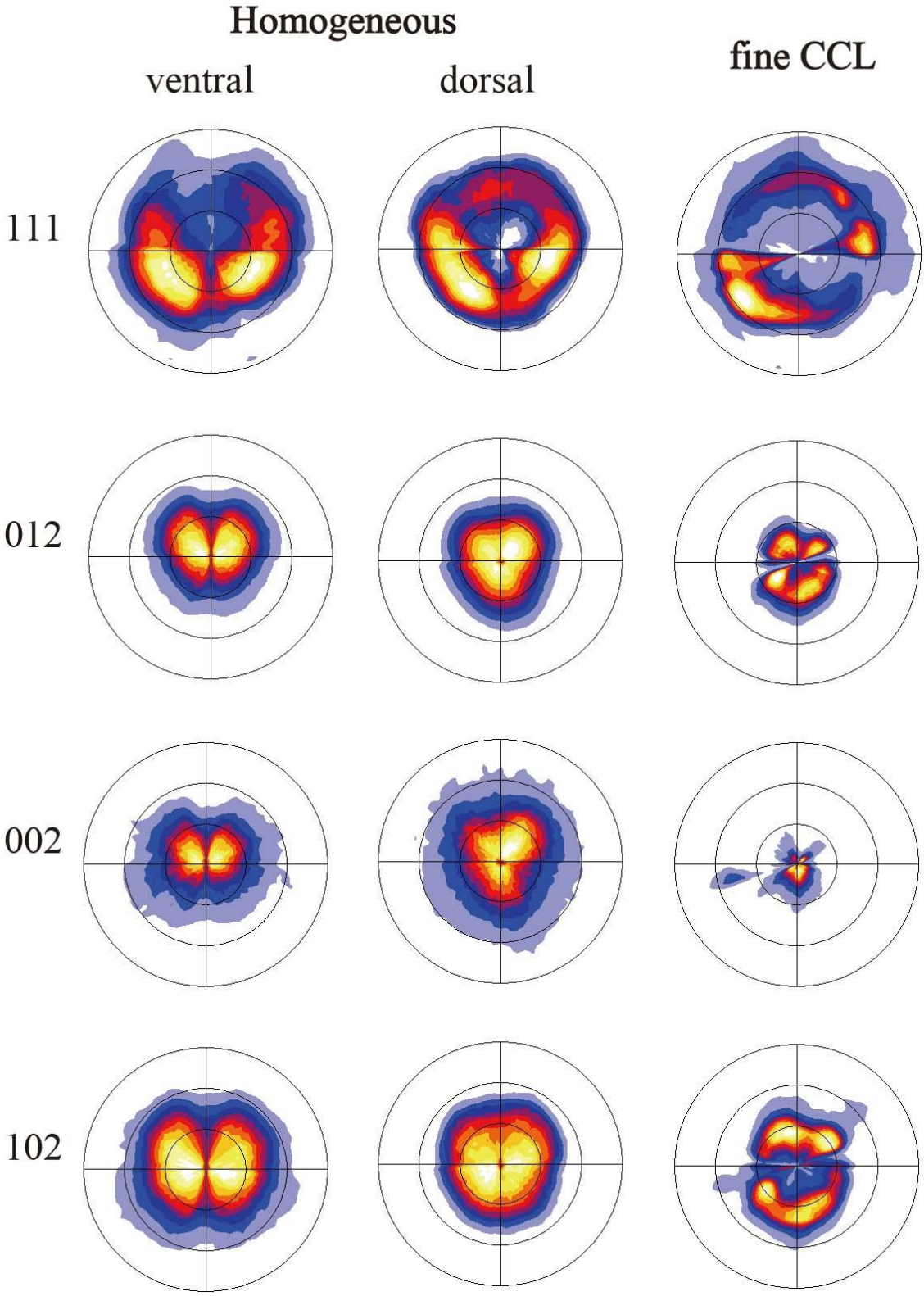

Figure 4.12. Results of X-ray diffraction texture analysis of outer homogeneous and inner fine complex crossed lamellar structure of *Malletia takaii*. Pole figures in left column were generated from ventral side of the outer layer and the right column from dorsal side. The direction of growth is toward the right in all pole figures**.**

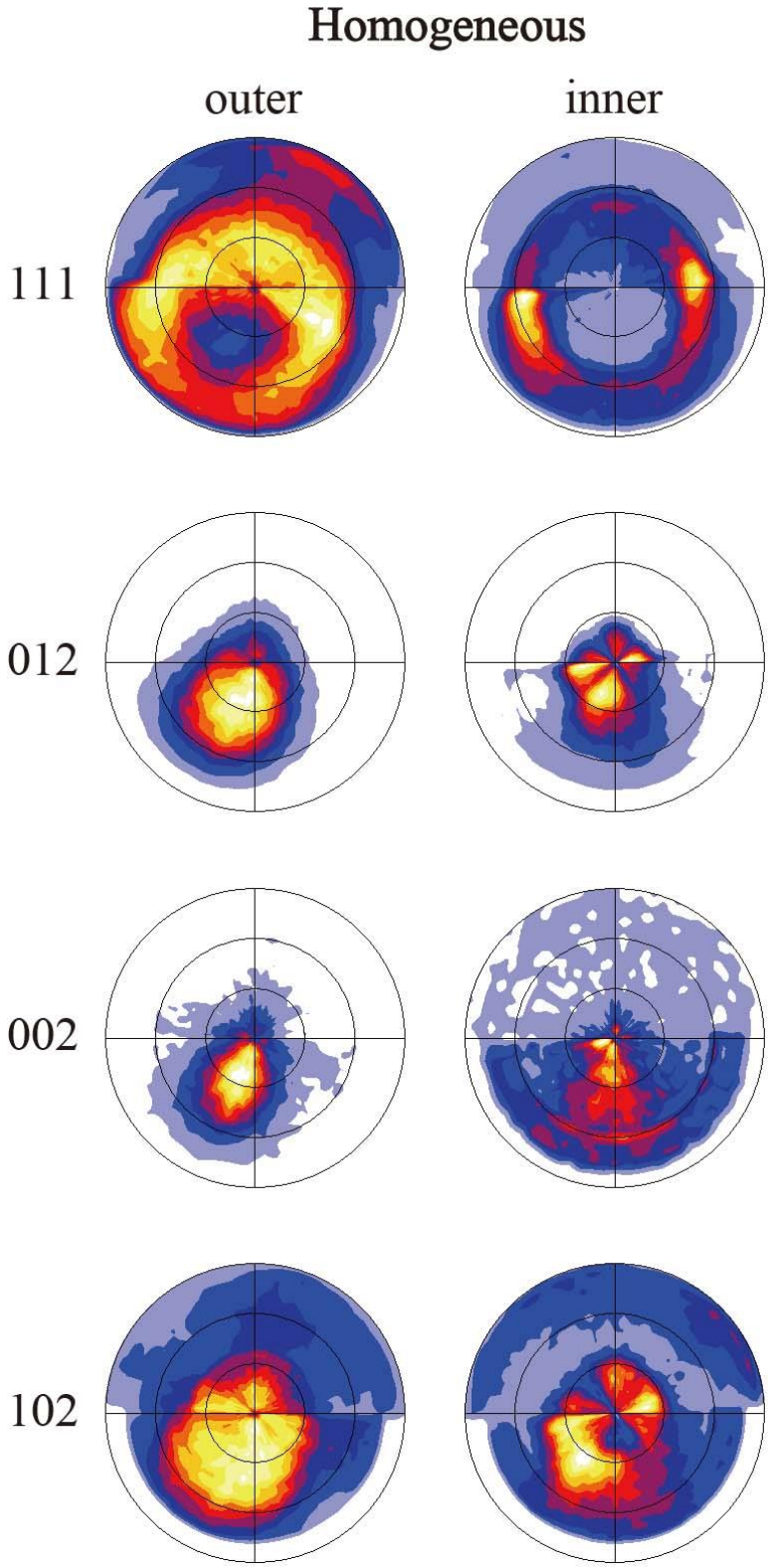

Figure 4.13. Results of X-ray diffraction texture analysis of outer side and inner side of homogeneous structures of *Tindaria soyoae*. The direction of growth is toward the right in all pole figures**.**

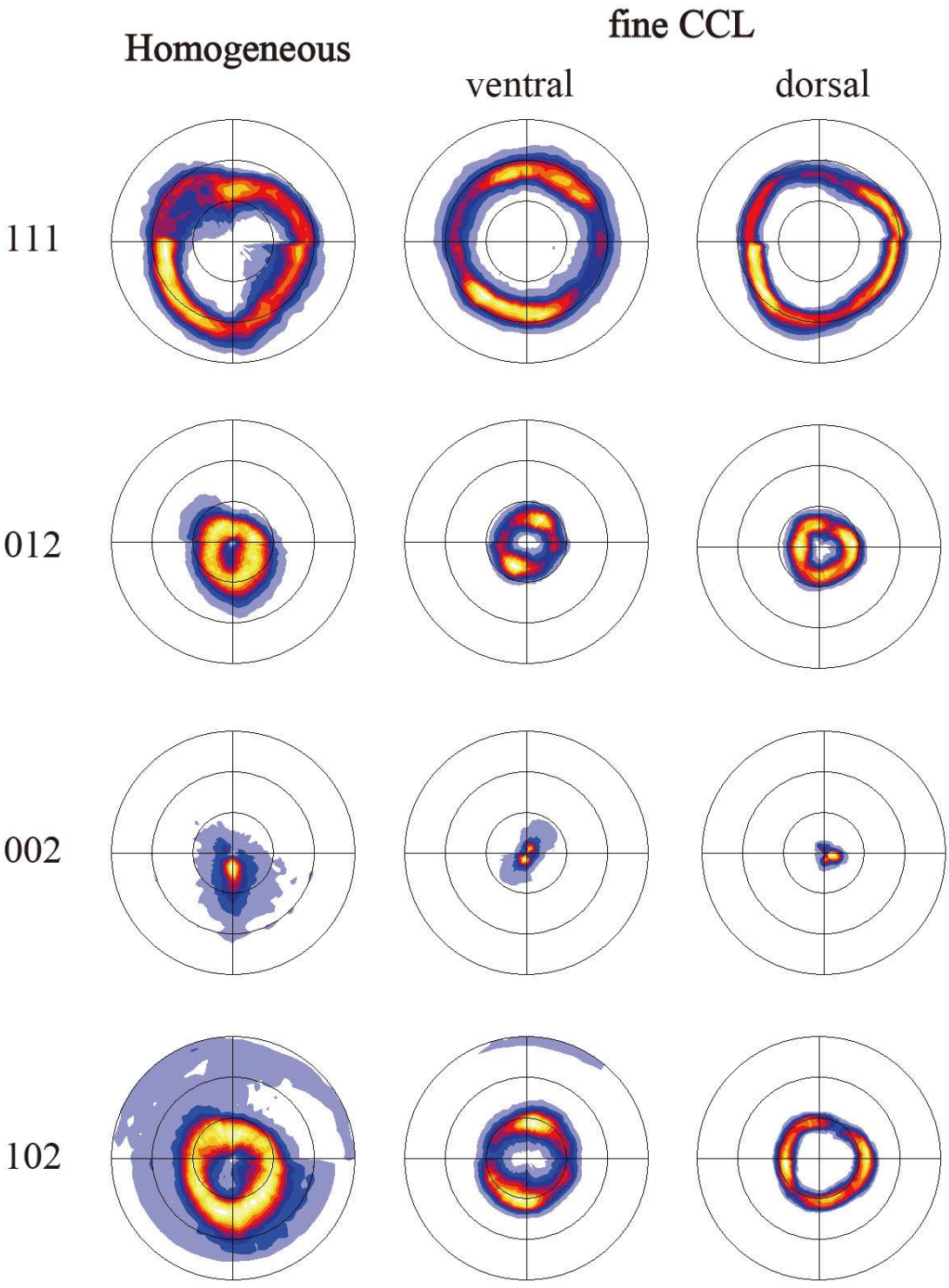

Figure 4.14. Results of X-ray diffraction texture analysis of outer homogeneous and inner fine complex crossed lamellar structure of *Yoldia johanni*. Pole figures of each microstructure in left column were generated from ventral side of the outer layer and the right column from dorsal side. The direction of growth is toward the right in all pole figures**.**

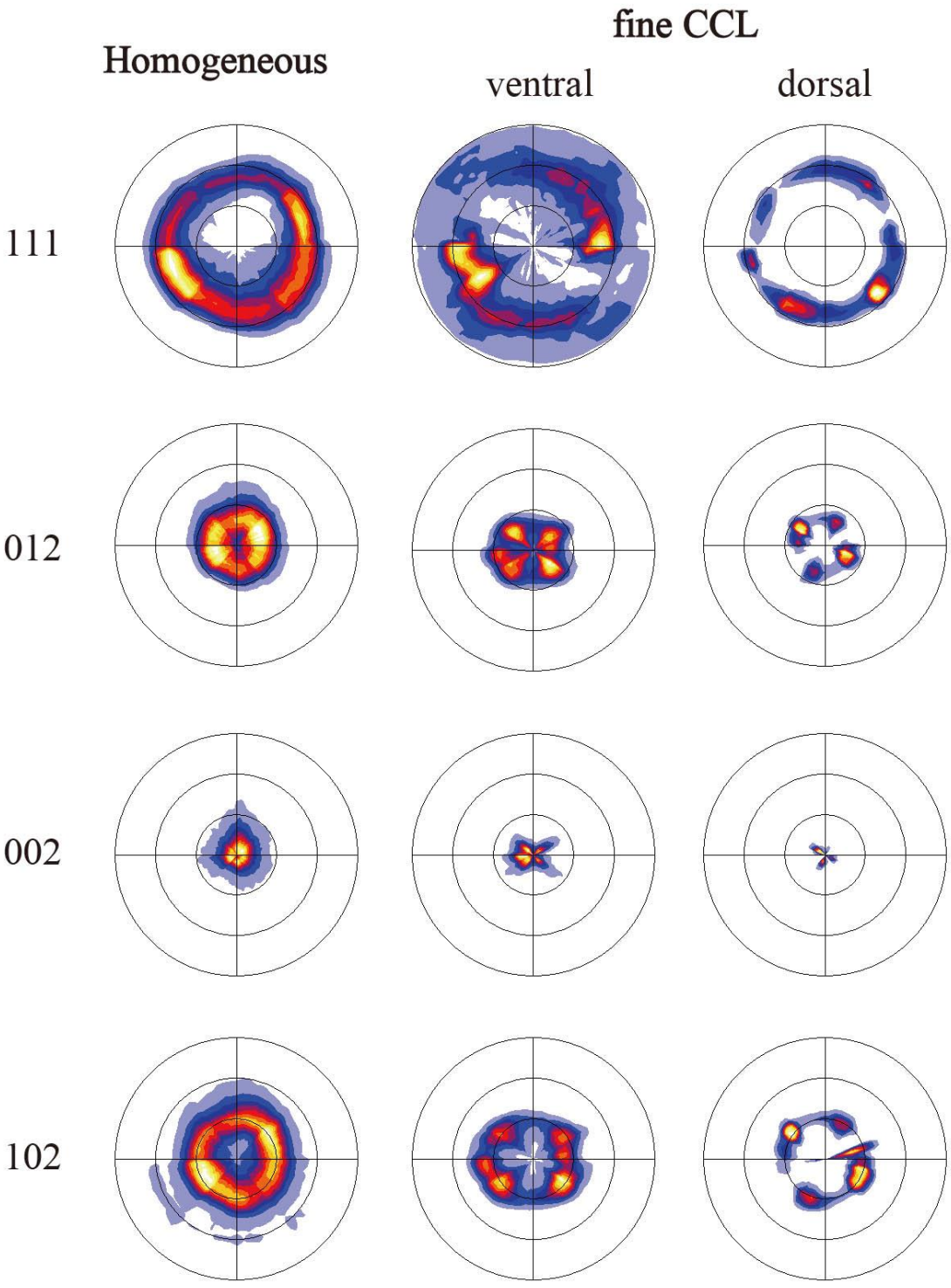

Figure 4.15 Results of X-ray diffraction texture analysis of outer homogeneous and inner fine complex crossed lamellar (CCL) structure of *Yoldia notabilis*. Pole figures of fine CCL in left column were generated from ventral side of the outer layer and the right column from dorsal side. The direction of growth is toward the right in all pole figures**.**

4-4. Discussion

4-4-1. Shell Microstructures and their Crystallographic Textural Patterns

In this study, the crystallographic texture of 12 microstructures in 14 species were analyzed and the observed crystallographic patterns were classified into six groups (Table 4.1 and Figure 4.16). A simple one-to-one relationship was not established between shell microstructures and crystallographic textures.

Table 4.1. The characterization of the types of crystallographic texture.

Defined crystallographic texture type	Direction 111, 012 and 102	Direction 002
Type-A	Two cluster to girdle-like patern	Inclined to the inner shell surface
Type-B	Two cluster in dyad symmetry	Perpendicular to the inner shell surface
Type-C	Six maxima pattern	Perpendicular to the inner shell surface
Type-D	Parallel two linearly pattern	Two or three peaks reclined to the inner shell surface
Type-E	Distinct or scarce four maxima	Perpendicular to the inner shell surface
Type-F	nearly girdle-like pattern with a tendenct ro develop two clusters	Perpendicular to the inner shell surface

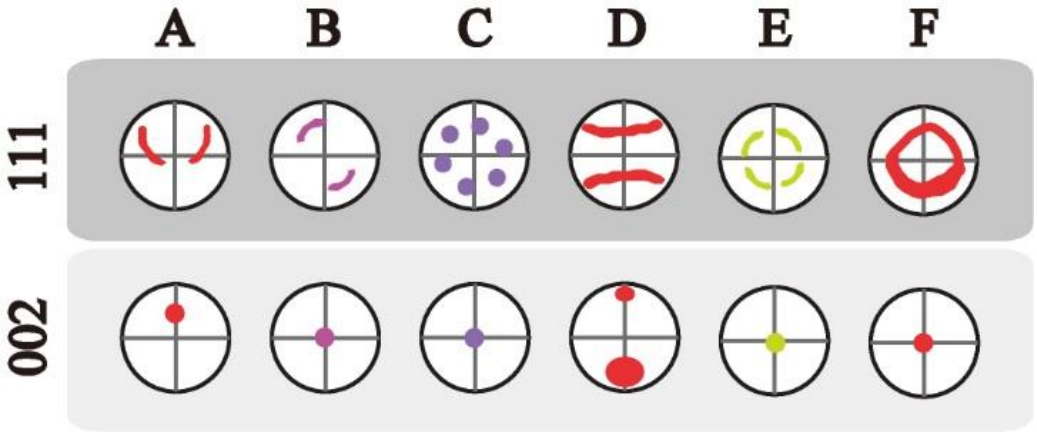

Figure 4.16 Six groups of the pattern diagrams of the crystallographic textures that found in this study.

A homogeneous structure, one of the most dominant microstructures in protobranchs, consists of granular or fine acicular crystals which seem to aggregate without any order. However, from this study, the crystals' c-axes were found to be concurrent and perpendicularly or slightly reclined to the inner shell surface in all species studied. Crystallographic textures of homogeneous structures showed the following five types: girdle-like pattern in the {111} pole, with the {002} pole inclined to the inner shell surface (type-A). Two-maxima in a dyad symmetry pattern with a tendency to develop girdle-like pattern in the {111} pole (type-B), six maxima pattern (type-C) and four cluster maxima (type-E) in the {111} pole and the girdle-like pattern in the {111} pole and the {002} pole perpendicular to the inner shell surface (type-F). On the other hand, those in the inner layers, whose granular crystals are smaller than those in the outer layer, were variable in crystallographic textures. Types B, C and E were found in the inner layers of different species. These three patterns are not consistent with their phylogenetic relationship.

While the crystallographic texture of the columnar nacreous structure showed a two-maxima pattern in dyad symmetry (type-B), the sheet nacreous structure showed a six-maxima pattern (type-C) and a four-maxima pattern (type-E). Six-maxima pattern (type-C) was found in *Acila castrensis* (Chateigner et al., 2000) and Frýda et al. (2010) recognized a girdle-like pattern in the nacreous structure of *Nucula nucleus*; these results also suggest the disagreement between the crystallographic textures and phylogenetic relationships.

Similar to the crystallographic texture of homogeneous and sheet nacreous structure, fine complex crossed lamellar and composite prismatic structures showed different textural patterns among species. The fine complex crossed lamellar structure is

often present in the inner layer of Nuculanoidea. In this study, fine CCL was observed in three species, *Yoldia johanni*, *Yoldia notabilis* and *Malletia takaii*, where the girdle-like pattern (type-F) and four-cluster maxima pattern (type-E) were recognized in the structure. Texture patterns were found to be different even in the closed species, such as *Yoldia johanni* and *Yoldia notabilis*. Composite prismatic structure was observed in the outer layers of *Ennucula nipponica* and *Acila insignis*, but their crystallographic texture showed different patterns: the former showed type-A pattern, and the latter type-D.

Fibrous prismatic structures showed a common type-A textural pattern in *Nuculana tanseimaruae*, *Megayoldia lischkei* and *Nuculana gordonis;* and radially elongate simple prismatic structure of the outer layer in *Solemya pusilla* and *Acharax japonica* showed type-F pattern.

The differences in crystallographic textures in the context of phylogenetic relationship have been generally discussed in the past. Chateigner et al. (2000) characterized the crystallographic texture of molluscan shell microstructures of 50 species using X-ray diffractometers. They found that the nacreous structure of bivalves and cephalopods have a six-maxima pattern for a-axis direction (type-C), and that those of gastropods and monoplacophora have a girdle pattern in the a-axis direction (type-F). Upon examining 12 species in the families Nuculoidea, Pterioida, Mytiloida, Unioida and Trigoniida, they concluded that all bivalves had the same textural pattern in their nacreous structure. On the other hand, Frýda et al. (2010) analyzed the crystallographic textures of the nacreous structure of four taxon of bivalvia (Nuculidae, Mytiloida, Pterioida and Unioida) by electron backscatter diffraction (EBSD). They considered that unordered nacre (girdle-like pattern; type-F) is found in ancestral groups of bivalves and that ordered nacre (type-B and-C) occurs in more derived taxa. In this study, a variety of ordered and

unordered nacreous structures were found, even within a family or genus. As well as this, the study also revealed that crystallographic textures are variable in composite prismatic, fine CCL and homogeneous structures among protobranch.

Kadar et al. (2008) reported that nacre tablet forms among the vent mytilid *Bathimodiolus azoricus* are variable and are dependent on the vent site parameters, such as the water depth, pH, and temperature. Although the crystallographic textures of the microstructures of that species were not analyzed, this result implies that environmental factors can result in intraspecific variations in the crystallographic textures of shell microstructures. Considering intraspecific variations, the crystallographic textures of two specimens of *Nuculana tanseimaruae* from different localities were analyzed during this current study. The first specimen, from Okikasayama Bank (32° 09.07’ - 32° 09.02’N, 128° 59.03’ - 129° 00.45 E, 508-514 m water depth), showed the girdle-like pattern with two clusters of the fibrous prismatic structure in the {111} pole in the outer layer, and two-maxima in dyad symmetry pattern with several weak clusters of the homogeneous structure in the inner layer, also in the {111} pole. However, the specimen from off of Wakayama (32° 34.6’ N, 135° 00.0’ E, 556.53 m water depth), showed the girdle-like pattern in the outer layer and two-maxima in dyad symmetry pattern in the inner layer the {111} pole. The crystallographic textures in these two specimens weakly differed in the concentration ratio of crystal orientations. Similar weak intraspecific variations were recognized in the nacreous structures of *Pinna nobilis* and *Mytilus edulis*; the six-maxima pattern was found in *Pinna nobilis* and the girdle-like pattern was found in *Mytilus edulis* (Frýda et al., 2000). The concentration ratios of crystal orientations were, however, different among the specimens from other localities. In this way, crystallographic textures of bivalves show insignificant intraspecific variations.

4-4-2. Crystallographic Textures and Phylogenetic Relationships

By comparing the crystallographic textures of each shell microstructure, several analogies were found between closed taxa (Figure 4.17). The composite prismatic structure of *Acila insignis* and the denticular composite prismatic structure of *Nucula tokyoensis* showed the same type-D textural pattern, but the composite prismatic structure of *Ennucula nipponica* exhibited the type-A textural pattern. These two microstructures resembled in crystal morphology and they consist, similarly, of well-developed acicular crystals, but not in the composite prismatic structure of *E. nipponica* (see Chapter 3). This resemblance is consistent with their phylogenetic relationships.

In the family Solemyidae, *Acharax johnsoni* is distinguished as having a unique shell microstructure (Sato et al., 2013a) and a deep-sea habitat (Okutani, 2000). Exclusive of *A. johnsoni*, the crystallographic textures of two solemyids, *Solemya pusilla* and *Acharax japonica*, were common despite the differences in shell microstructures. This trend suggests that these two species share identical mechanisms of shell formation, for instance the same shell matrix proteins. Regulating the crystal growth by shell matrix organic materials has been reported in (1) nacre formation in pearl oysters (Rousseau et al., 2009; Saruwatari et al., 2009), and (2) crystalline organization of the calcitic fibrous prismatic structure in *Mytilus galloprovincialis* (Checa et al., 2014). In addition, the homologs of shell matrix proteins were identified in closely related species (Isowa et al., 2012).

Nuculanoideans have a rich diversity of crystallographic textures even among different species that have the same morphological microstructures. As mentioned previously, it is important to check the presence or absence of intraspecific variations.

However, if we underestimate the variety of crystallographic textures due to insufficient data sampling, similar microstructures formed by different mechanisms (e.g. shell matrix proteins) may be misinterpreted as the same microstructure. Another possibility is that the degree of crystal growth relates to crystallographic textures. Acicular crystals in the fine complex crossed lamellar structures of *Yoldia notabilis* and *Malletia takaii* attain a length of more than 7 μm along their long axes, whose textures show the type-E pattern. By contrast, the type-F pattern in *Yoldia johanni* consists of acicular crystals of less than 4 μm along their long axes.

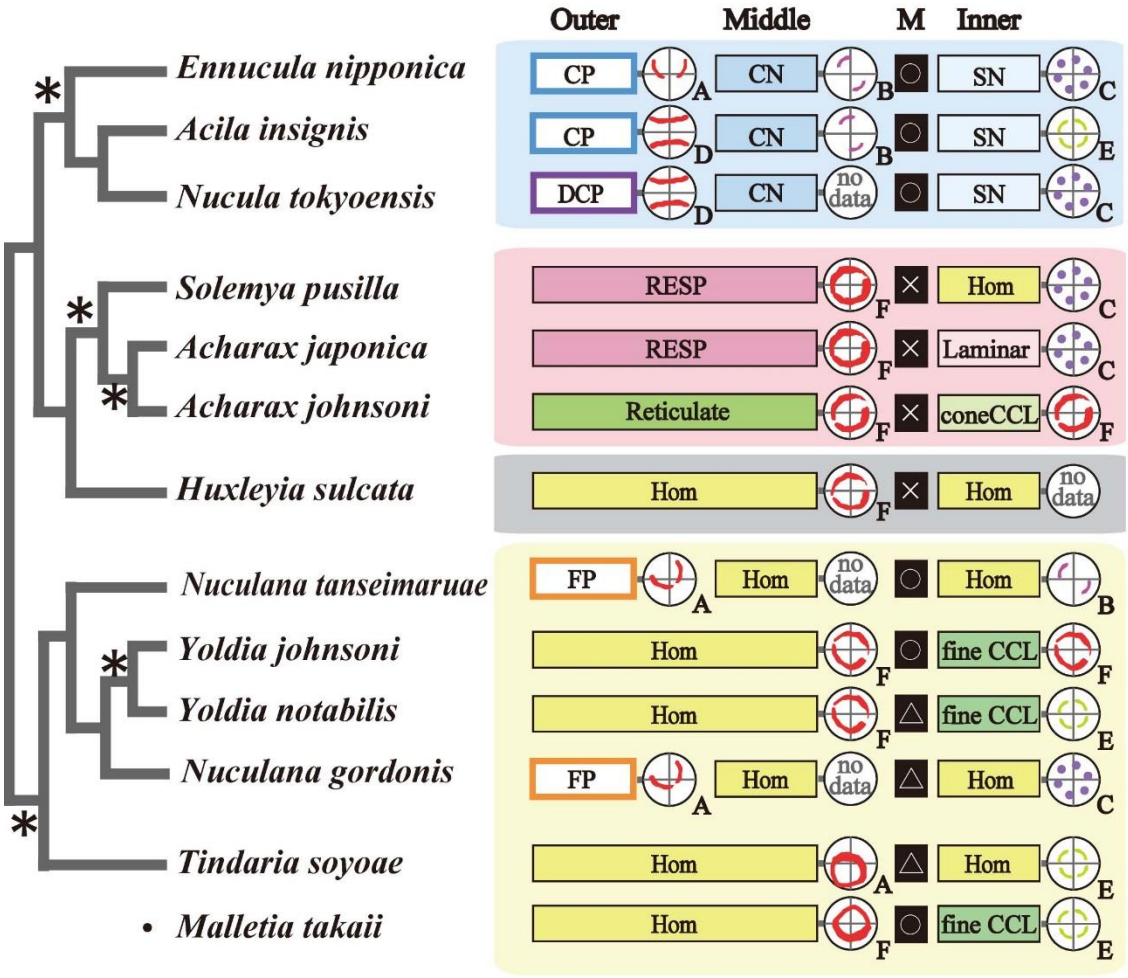

Figure 4.17. (previous page). Schematic illustration showing the genetic relationship based on the ML-based phylogenetic tree in Chapter 2 (right column), shell microstructure assemblages (data from Chapter 3) and crystallographic textures of the {111} pole with the note of crystallographic texture types. Abbreviations of shell microstructures names are listed in Chapter 3. Circle mark indicates the presence of myostracum. Triangle marks imply that myostracum is obscure. Cross marks mean abcence of myostracum. The clade with strong support (bs > 60%) is marked with the asterisk mark.

4-4-3. Shell Layers and Changes of Crystal Orientation

In this study, the crystallographic textures of the nacreous structures in the middle and inner layers of the two species *Acila insignis* and *Ennucula nipponica* clearly showed different patterns. The columnar nacreous structure in the middle layers of these two species showed dyad symmetry cluster pattern (type-B) in the {111} pole. On the other hand, the inner layer of three nuculid species, *Acila insignis*, *Ennucula nipponica* and *Nucula tokyoensis*, consist of sheet nacreous structure with nearly girdle-like patterns in the {111} pole. The six-maxima pattern, which implies double twinning (type-C), in the {111} was unmistakable in *Ennucula nipponica*, but more scarcely in *Nucula tokyoensis*. The four-maxima pattern, which implies single twinning (type-E), was recognized in the {111} pole of *Acila insignis*. This result implies that nacre tablets increase the level of twinning inwardly as the nacreous layer thickens, or that crystallographic textures drastically change around the boundary of the middle and inner layers, where the myostracum is inserted. The latter is more likely because of different nacre tablets stacking in two layers (Chapter 3). Frýda et al. (2010) recognized that both the girdle and cluster patterns exist among the four taxa of Bivalvia (Nuculidae, Mytiloida, Pterioida and Unioida), while Chateigner et al. (2000) concluded that all bivalves have

the same textural pattern in their nacreous structure; these results conflict with each other, although the studies analyzed the same species (*Pinna nobilis*, *Mytilus californianus* and *Mytilus edulis*). One probable reason for this conflict is that these studies did not consider the existence of two nacreous layers separated by the myostracum. Chateigner et al. (2000) appears to have analyzed the crystallographic texture of the nacreous structure near the shell surface for technical reasons, whereas Frýda et al. (2010) used shell fragments which were cut roughly in the middle of the nacreous shell layer.

A gradual change in crystallographic texture with layer thickening was recognized in the calcitic prismatic structures of the outer layers in pteriomorphs (*Malleus regulus*, *Propeamussium sibogai* and *Ostrea puelchana*; Delgado et al, 2008), and also probably in the nacreous structure of other pteriomorph (*Pinna nobilis* and *Pteria martensii*; see Figure 4 in Checa & Rodríguez-Navarro 2005). The latter study explained the increasingly preferred orientation of nacreous platelets by a competition model among the nacreous plates within growing lamellae. Checa et al. (2006) reported that the textural pattern was rapidly changed from a girdle-like pattern to single crystal-like texture during the growth within about 20 to 30 nacreous lamellae (about 10 to 15 μm thick) in the nacreous structure of *Pteria hirundo* and *Pinctada martensii*. This rapid change was not recognized in nacreous layers in other species of bivalves, including the family Nuculidae. At least the existence of two different nacreous structures (columnar and sheet nacreous) in the family Nuculidae implies the possibility of textural pattern change around two nacreous layers.

In the examined species of the families Solemyidae and Nuculanoidea, alteration from a girdle-like to a clustered pattern with shell growth was found, with the exception of *Acharax johnsoni* and *Yoldia johanni*. This progressive organization of crystal

orientation is probably due to the growth prevented by competition among crystals, as recognized in nacreous tablets of bivalves (Checa & Rodríguez-Navarro, 2005; Checa et al., 2006).

Chapter 5 General discussion

5-1. Overview of protobranch shell microstructure and their phylogenetic relationship

Here, the intraspecific differences in the detailed shell microstructure, including crystallographic textural variation, are provided for the species whose genetic relationship was reconstructed by molecular phylogenetic analysis. All results of Chapters 2–4 are summarized in Figure 5.1. Shell microstructural assemblages of the species whose molecular and shell microstructural data have been studied previously are illustrated together with the data of this study in Figure 5.1. In addition, all shell microstructural data of protobranchs from previous works and this study are summarized in Table 5.1. Table 5.1 contains the shell microstructural data of fossil taxa and the species whose genetic relationship was not reconstructed by molecular works.

As described in Chapter 2, molecular analysis reconstructed four major clades comprising of four superfamilies of protobranchs and a similarity of the shell microstructure assemblages of phylogenetically close taxa among four major clade was recognized in general. Shell microstructure in the nuculid clade is characterized by an outer prismatic and middle/inner nacreous structure. Species in the solemyid clade share a radially elongate prismatic structure (RESP) in their outer layer expect for one species—*Acharax johnsoni*. In the clade containing nuculanids and sareptids, the most common microstructure is granular to small acicular crystals composing homogeneous, fibrous prismatic, and fine CCL structures. Both molecular phylogenetic analyses and shell microstructure observations have been poorly made for manzanelids. However, according

to Carter (1990a) and this study, manzanelid species seem to have similar shell microstructures to that of nuculanids. An ML-based molecular phylogeny tree using nine genes formed the sister group of Solemyoida and Nuculanoidea (with anomalistic taxa family Sareptidae) was created in this study. The shell microstructures in that clade are not uniform but species in that sister group share granular crystals that constitute different

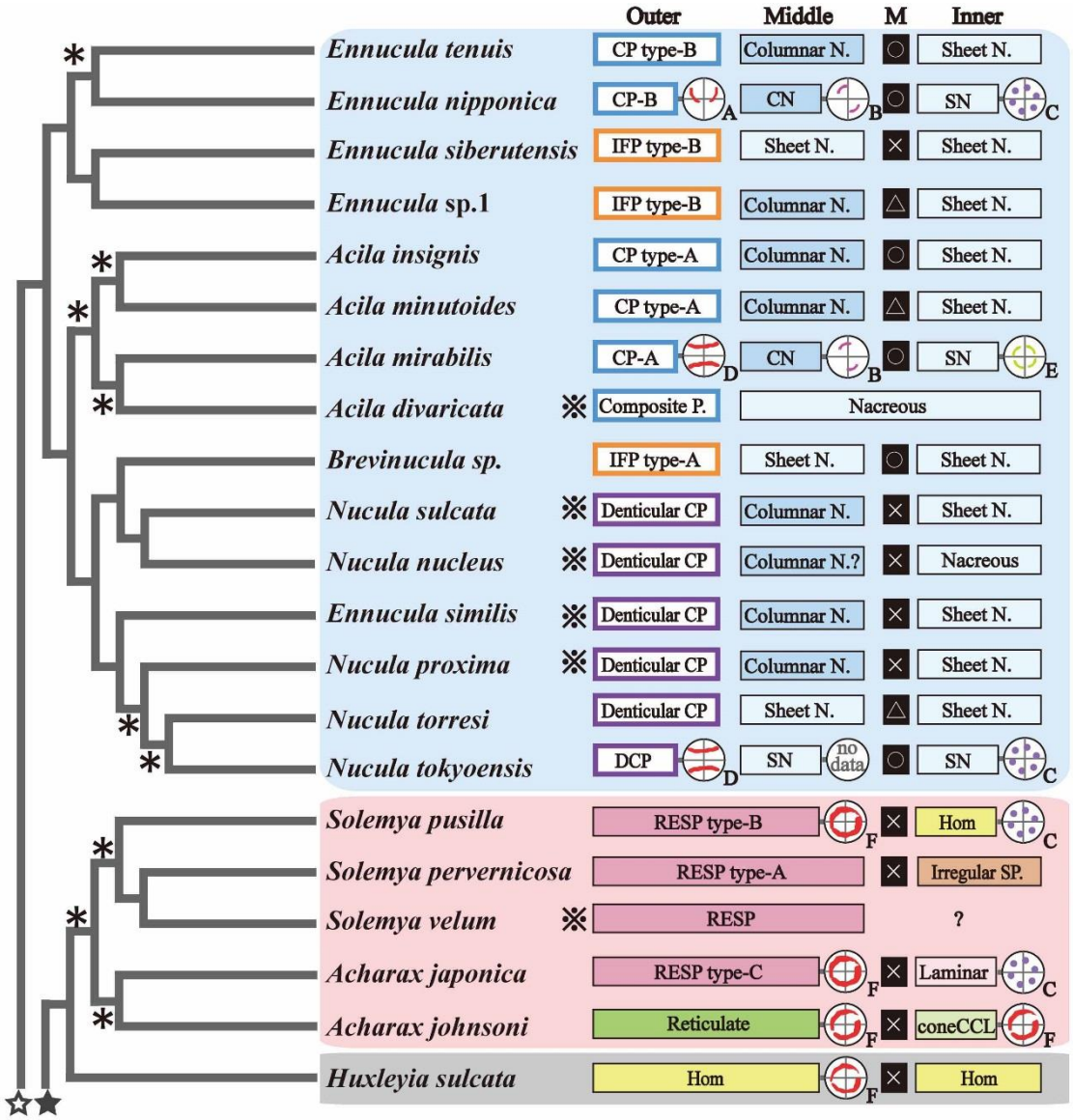

Figure 5.1. Continue to next page.

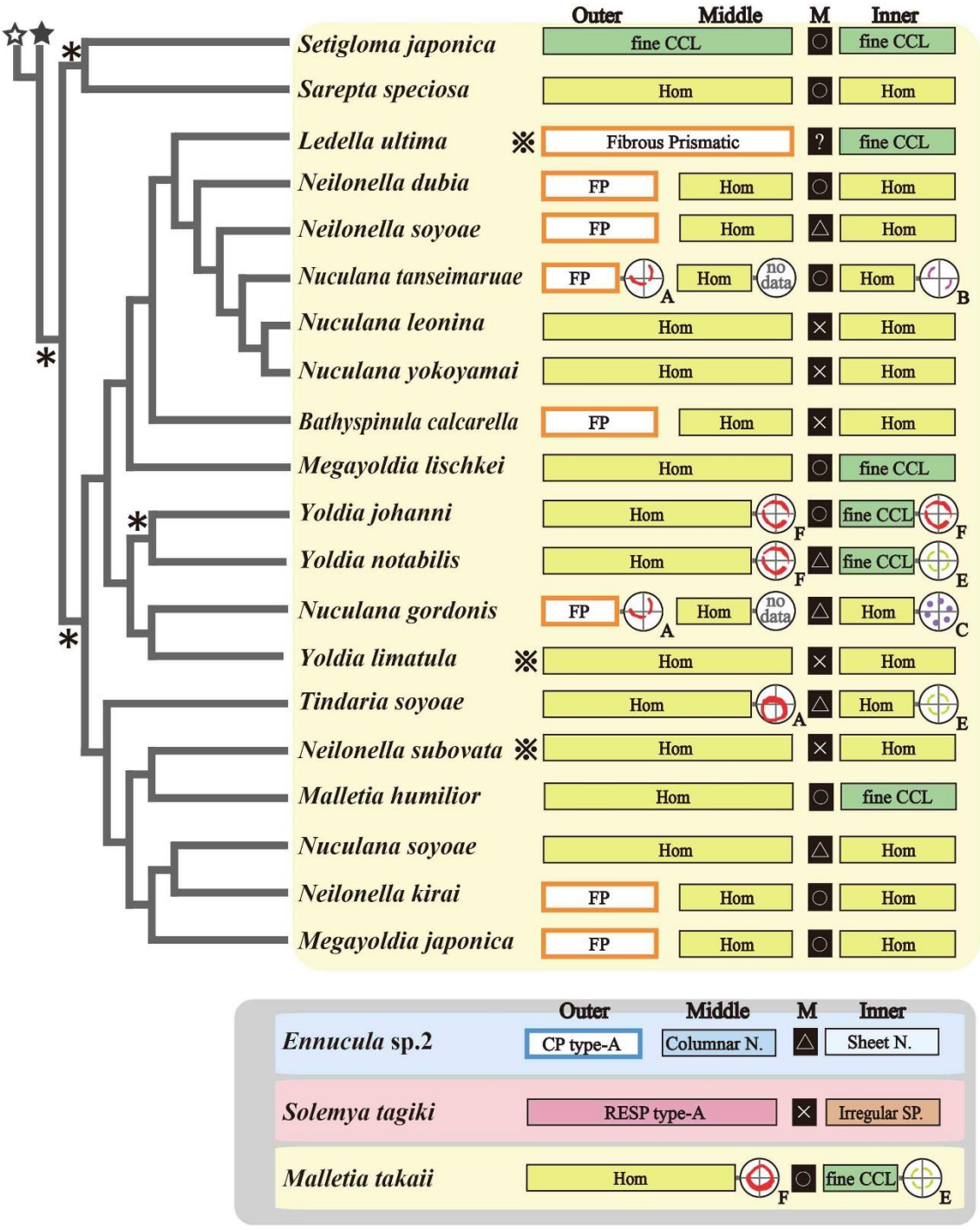

Figure 5.1. Schematic illustration of overall data of this study, showing the genetic relationship based on the ML-based phylogenetic tree in Chapter 2 (right column), shell microstructure assemblages (data from Chapter 3) and crystallographic textures of the {111} pole with the note of crystallographic texture types in Chapter 4. Abbreviations of shell microstructures names are listed in Chapter 3. Circle mark indicates the presence of myostracum. Triangle marks imply that myostracum is obscure. Cross marks mean abcence of myostracum. Black and white star marks connect the branchs crossing two pages. Species without molecular data were assembled in the bottom. The clade with strong support (bs > 60%) is marked with the asterisk mark. The shell microstructural data that have been described by previous studies was noted by (※).

Table 5.1. Comparison of layer distributions of shell microstructure in protobranchs. Discription highlighted in gray color is from this study. -, not observerd.

Species	Outer layer	Middle layer	Myostrucum	Inner layer	Age	Locality	Reference
Ctenodontidae							
Tancrediopsis gotlandica	ISP, FP?	N	-	N	Late Silurian	Sweden	Carter, 2001
Nuculoidea							
Deceptrix levata	nd	nd	nd	former N	Ordovician	Kentuchy, USA	Carter, 1990a
Paleoconcha sp.	nd	nd	nd	N ?	Late Ordovician	USA	Mutvei et al., 1985
Praenucula faba	finely P	N	-	N	Late Silurian	Sweden	Carter, 2001
Acila cobbolidiana	aragonitic CP	nd	nd	N	Pleistocene	England	Taylor et al., 1969
Acila divaricata	CP ?	nd	nd	N	nd	nd	Kobayashi, 1971a
Acila mirabilis	CP type A	CN	ISP to Hom	SN	Recent	Japan	This study
Acila (Truncacila) gottschei	nd	nd	nd	slight CN	Late Pliocene	Japan	Iwata, 1975a
Acila (Truncacila) insignis	CP type A	CN	Hom	SN	Recent	Japan	Iwata, 1975a; Suzuki, 1983; This study
Acila minutoides	CP type A	CN	ISP	SN	Recent	Japan	This study
Acila vigilia	CP ?	nd	nd	N	nd	nd	Kobayashi, 1971a
Brevinucula sp.	not DCP	nd	nd	N	nd	nd	Van de Poel, 1955
Brevinucula sp.	IFP type A	SN	ISP	SN	Recent	Japan	This study
Economolopsis gordoni	FP ?	N	nd	N	Late Mississippian	Arkansas, USA	Carter, 1990a
Nucula sp.	DCP	nd	nd	N	Recent	nd	Bøggild, 1930; Lucas, 1952; Van de Poel, 1955
Nucula (Gibbonucula) sp.	DCP	nd	nd	N	Eocene	Asia	Van de Poel, 1955
Nucula (Lamellinucula) sp.	DCP	nd	nd	N	nd	nd	Van de Poel, 1955
Nucula (Linucula) sp.	DCP	nd	nd	N	Miocene	New Zealand	Van de Poel, 1955
Nucula (Leionucula) bellotii	not DCP	nd	nd	nd	Recent	Arctic	Van de Poel, 1955
Nucula calcicora	nd	nd	nd	no N ?	Recent	Mexico	Moore, 1977
Nucula (Pectinucula) cancellata	finely crystalline	nd	nd	N	Late Cretaceous	South Dakota, USA	Speden, 1970
Nucula convexa	DCP	CN	P	SN	Recent	Monbasa, Kenya	Taylor et al., 1969
Nucula dixioni	DCP	nd	nd	N	Eocene	Selsey, England	Wrigley, 1946
Nucula greppini	(D) CP	nd	nd	N	Oligocene	probably Europe	Bøggild, 1930
Nucula laevigata	(D) CP	CN	nd	SN	Pleistocene	England	Taylor et al., 1969
Nucula (Nucula) mayaeri	DCP	nd	nd	N	Miocene	nd	Bøggild, 1930
Nucula nitida	(D) CP	nd	nd	N	Recent	nd	Bøggild, 1930
Nucula (Nucula) nucleus	DCP	CN ?	nd	N	Recent	Europe	Schmidt, 1924a,b; Bøggild, 1930; Suzuki, 1983; Taylor et al., 1969
Nucula (Leionucula) obliqua	no DCP	nd	nd	nd	nd	nd	Van de Poel, 1955
Ennucula tenuis	CP type B	CN	ISP	SN	Recent	Japan	This study
Ennucula nipponica	CP type B	CN	ISP	SN	Recent	Japan	This study
Ennucula siberutensis	IFP type B	SN	-	SN	Recent	Japan	This study
Ennucula sp1.	IFP type B	CN to SN	Hom	SN	Recent	Japan	This study
Ennucula sp2.	CP type A	CN to SN	-	SN	Recent	Japan	This study
Nucula (Pectinucula) pectinata	(D) CP	nd	nd	N	Cretaceous	England	Bøggild, 1930; Van de Poel, 1955
Nucula percrassa	finely crystalline	nd	nd	N	Late Cretaceous	South Dakota, USA	Speden, 1970
Nucula placentina	(D) CP	CN	thin P	SN	Pliocene	Italy	Taylor et al., 1969
Nucula planomarginata	finely crystalline	nd	nd	N	Late Cretaceous	South Dakota, USA	Speden,1970
Nucla (Nucula) proxima	DCP	CN	nd	SN	Recent	Massachusetts, USA	Wise,1970a; Carter, 1990a
Nucula tokyoensis	DCP	CN	ISP	SN	Recent	Japan	This study
Nucula torresi	DCP	SN	ISP	SN	Recent	Japan	This study

Table 5.1. Continued.

Species	Outer layer	Middle layer	Myostrucum	Inner layer	Age	Locality	Reference
Nucula (Leionucula) puelcha	no DCP	nd	nd	nd	Recent	South America	Van de Poel,1955
Nucula radiata	DCP	nd	nd	nd	nd	nd	Schmidt,1922
Nucula similis	DCP	CN	nd	SN	Eocene	France	Bøggild, 1930
Nucula (Nucula) sulcata	DCP	CN	nd	SN	Recent	Europe	Taylor et al., 1969
Nucula (Leionucula) superba	no DCP	nd	ISP	nd	Recent	nd	Van de Poel, 1955
Nucula trigona	fCL	nd	nd	no N	Eocene	Europe	Bøggild, 1930
Nuculoidea deceptroformis	FP	nd	nd	N	Middle Devonian	New York, USA	Carter and Tevesz,1978a; Bailey,1983
Nuculoidea pinguis	reclined P	nd	-	N	Late Silurian	Sweden	Carter, 2001
Nuculoidea opima	SP to FP	nd	nd	CN to SN	Middle Devonian	New York, USA	Carter and Tevesz,1978a
Nuculoma haesendonchi	not DCP	nd	nd	N	Jurassic	nd	Van de Poel, 1955
Nuculopsis croneisi	FP to ISPP	SN	ISP	SN	Late Carboniferous	Kentucky, USA	Carter, 1990a
Nuculopsis girtyi	FP, ISP, ISPP	SN	ISP	SN	Late Carboniferous	Texas, USA	Carter, 1990a
Nuculopsis pontotocensis	SP (calcitic?)	nd	nd	SN	Late Carboniferous	Oklahoma, USA	Bailey and Sandberg, 1985
Pronucula sp.	DCP	nd	nd	N	Late Oligocene to Recent	nd	Van de Poel, 1955
Condylonucula cynthiae	nd	nd	nd	Hom?	Recent	Caribbean nea Nicaragua	Moore,1977; Carter, 1990a
Condylonucula maya	FP to ISP	N (juvenile) to Hom, matted (adult)	nd	N (juvenile) to ISP (adult)	Recent	Mexico	Carter, 2001
Palaeonucula expansa	ISP	Hom	nd	Hom, fCCL, iCCL	Late Triassic	Italy	Schenck,1939; Carter, 1990a
Palaeonucula jugulata	ISP or FP	fCCL	nd	Hom	Late Triassic	Italy	Cater, 1990a
Palaeonucula strigilata	ISP to Hom	Hom	ISP	Hom	Late Triassic	Italy	Lucas, 1952; Cater, 1990a
Palaeonucula? cf. "Nucula" subrotundata	FP	nd	nd	Hom, fCCL, iCCL, CA	Late Carboniferous	Kentuchy, USA	Carter, 1990a
Palaeonucula sp. cf. *P. wewokana*	Hom	nd	nd	Hom	Late Carboniferous	Kentuchy, USA	Carter, 1990a
Pristigloma nitens	FP to ISP	CA	nd	fCCL, iCCL, Hom	Recent	Atlantic Ocean	Carter, 2001
Sarepta speciosa	Hom	-	ISP	Hom	Recent	Japan	This study
Setigloma japonica	fCCL	-	ISP	fCCL	Recent	Japan	This study
Solemyoidea							
Solemya (Solemya) pusilla	RESP type B	-	-	Hom	Recent	Japan	This study
Solemya (Solemya) tagiri	RESP type A	-	-	ISP	Recent	Japan	This study
Solemya (Solemya) togata	RESP	nd	nd	Lam. or Hom	Recent	Italy	Stempell, 1900; Taylor et al., 1969
Solemya sp.	RESP	nd	nd	Hom or indistinctly P	Recent	not described	Bøggild, 1930
Solemya (Austrosolemya) australis	RESP to ISP	nd	nd	Lam. or Hom	Recent	South Australia	Taylor et al., 1969
Solemya doderleini	RESP	nd	nd	nd	Oligocene	probably Europe	Bøggild, 1930
Solemya (Zesolemya) parkinsoni	RESP	ISP	-	fCCL or iCCL	Recent	New Zealand	Beedham and Owen, 1965
Solemya (Petrasma) velum	RESP	nd	nd	nd	Recent	Massachusetts, USA	Taylor et al., 1969; Kobayashi, 1971a
Solemya (Petrasma) pervernicosa	RESP type A	nd	nd	ISP	Recent	Japan	This study
Acharax (Nacrosolemya) trapezpoides	ISP to Hom	ICN	ISP	SN	Late Carboniferous	Kentucky, USA	Carter, 1990a
Acharax japonica	RESP type C	-	-	Lam. or Hom	Recent	Japan	This study
Acharax johnsoni	Reticulate	-	-	cCCL	Recent	Japan	This study

Table 5.1. Continued.

Species	Outer layer	Middle layer	Myostrucum	Inner layer	Age	Locality	Reference
Manzanelloidea							
Nucinella sohli	ISP, few FP	CA	FP, ISP	iCCL	Late Cretaceous	Georgia, USA	Carter, 1990a
Nucinella walvis	ISP, Hom	fCCL, Hom	ISP	fCCL or iCCL	Recent	USA	Carter, 1990a
Huxleyia sulcata	Hom	-	-	Hom	Recent	Japan	This study
Nuculanoidea							
Adrana sowerbyana	Hom?	Hom	nd	finely Laminated	Recent	Panama	Carter, 1990a
Ezonuculana mactraeformis	nd	nd	nd	not N	Cretaceous	Japan	Puri, 1969
Nuculana crassa	Hom	Hom	Trace	Hom	Recent	nd	Taylor et al., 1969
Nuculana emarginata	Hom	Hom	nd	Hom	Recent	nd	Taylor et al., 1969
Nuculana fragilis	Hom, fCCL, CA	nd	nd	nd	Recent	nd	Flajs, 1972
Nuculana (Nuculana) pernula	Hom	nd	present	Hom	Recent	Canada	Bøggild, 1930; Gilkinson et al., 1986
Nuculana tenuisulcata	nd	nd	nd	Porcelaneous	Recent	USA	Carter, 1990a
Nuculana tanseimaruae	FP	Hom	ISP	Hom	Recent	Japan	This study
Nuculana leonina	Hom	-	-	Hom	Recent	Japan	This study
Nuculana yokoyamai	Hom	-	-	Hom	Recent	Japan	This study
Nuculana gordonis	FP	Hom	ISP	Hom	Recent	Japan	This study
Nuculana soyoae	Hom	-	ISP	Hom	Recent	Japan	This study
Ledella messanensis	IFP, Hom, fCCL	nd	ISP	fLam., Hom	Recent, USA	nd	Carter, 1990a
Ledella ultima	FP	nd	nd	fCCL or Hom	Recent, USA	nd	Carter, 1990a
Bathyspinula scheltemai	Hom to IFP	Hom, few dCL	nd	Hom to fCCL	Recent, USA	nd	Carter, 1990a
Batyhspinula calcarella	FP	Hom	-	Hom	Recent	Japan	This study
Phestia (Polidevcia) arata	FP	SN to ICN	hardly trace	SN	Late Carboniferous	Kentucky, USA	Carter, 1990a
Phestia (Polidevcia) bellistriata	Hom and FP	SN	nd	SN	Late Carboniferous	Kentucky, USA	Carter, 1990a
Phestia corrugata	FP	N	nd	N	Late Mississippian	Oklahoma, USA	Carter, 1990a
Phestia sulcellata	IFP	SN	nd	SN	Late Triassic	Italy	Carter, 1990a
Dacryomya ovum	ISP	CN	nd	SN	Latest Early Jurassic	England	Carter, 1990a
'Nuculana (Nuculana)" grandensis	P	Lamellar	nd	N	Late Cretaceous	South Dakota, USA	Speden, 1970
'Nuculana (Jupiteria)" scitula	P	Lamellar	nd	N	Late Cretaceous	South Dakota, USA	Speden, 1970
Paleyoldia angustia	FP	N	nd	N	Late Mississippian	Arkansas, USA	Carter, 1990a
Paleyoldia glabra	ISP		nd	SN	Late Carboniferous	nd	Carter, 1990a
Ryderia graphica	nd	nd	nd	N	Early Jurassic	England	Taylor et al., 1969
Neilonella sericea striolata	IFP to Hom	Hom	nd	Hom (with few ISP)	Recent	USA	Carter, 1990a
Neilonella subovata	IFP (almost Hom)	Hom	hardly trace	Hom (with few FC)	Recent	USA	Carter, 1990a
Neilonella dubia	FP	Hom	ISP	Hom	Recent	Japan	This study
Neilonella soyoae	FP	Hom	-	Hom	Recent	Japan	This study
Neilonella kirai	FP	Hom	ISP	Hom	Recent	Japan	This study
Pseudotindaria erebrus	FP	Hom, dCL, CA	nd	fCCL, iCCL	Recent	USA	Carter, 1990a
Nuculites oblongatus	Hom, fCCL	-	nd	Hom, fCCL	Middle Devonian	New York, USA	Carter and Tevesz, 1978a
Palaeoneilo elliptica	Hom, FP	Hom, few dCL	nd	Hom or fCCL	Upper Triassic	Italy	Carter, 1990a
Palaeoneilo elliptica?	FP	Hom, fCCL	thin band	Hom or fCCL	Upper Triassic	Italy	Carter, 1990a

Table 5.1. Continued.

Species	Outer layer	Middle layer	Myostrucum	Inner layer	Age	Locality	Reference
Palaeoneilo filosa	ISP, SP(juvenile), Hom(adultl) as outer sublayer; FP as inner sublayer	dCL, fCCL, Hom	nd	fCCL or Hom	Middle Devonian	New York, USA	Carter, 1990a
Palaeoneilo oweni	ISP to Hom and IFP	dCL, CA, fCCL, Hom	ISP	Hom or fCCL, M	Late Carboniferous	Kentucky, USA	Carter, 1990a
Palaeoneilo sp.	nd	nd	nd	laminar	Ordovician	USA	Vendrasco et al., 2013
Ekstadia tricarinata	fine, reclined P	CA	ISP	fCCL	Late Silurian	USA	Carter, 2001
Prosoleptus lineata	Hom, IFP or ISP	Hom	nd	Hom	Late Triassic	Italy	Carter, 1990a
Malletia evansi	P	Lamellar	-	N	Late Cretaceous	South Dakota, USA	Speden, 1970
Malletia obtusa	IFP	CA	ISP	fCCL, iCCL, ISP	Recent	USA	Carter, 1990a
Malletia humilior	Hom	-	ISP	fCCL	Recent	Japan	This study
Malletia takaii	Hom	-	ISP	fCCL	Recent	Japan	This study
Yoldia (Calorhadia) compsa	Hom (locally dCL)	Hom, few ISP	nd	Hom, few ISP	Middle Eocene	Texas, USA	Carter, 1990a
Yoldia lacrima	P	Lamellar	nd	N	Late Cretaceious	South Dakota, USA	Speden, 1970
Yoldia (Yoldia) limatula	Hom	Hom	nd	Hom	Recent	Norway	Taylor et al., 1969
Yoldia (Yoldia) myalis	Hom	Hom	nd	Hom	Recent	St. Lawrence, USA	Taylor et al., 1969
Yoldia (Orthoyoldia) psammotaea	FP, ISP	Hom, few dCL	nd	Hom, few ISP, fCCL, iCCL	Middle Eocene	USA	Carter, 1990a
Yoldia rectangularis	P	Lamellar	nd	N	Late Cretaceous	South Dakota, USA	Speden, 1970
Yoldia (Megayoldia) thraciaeformis	Hom	Hom, dCL	nd	Laminated	Recent	off New Foundland, Canada	Gilkinson et al., 1986; Carter, 1990a
Yoldia seminuda	Hom	-	ISP	fCCL	Recent	Japan	This study
Yoldia notabilis	Hom	-	ISP	fCCL	Recent	Japan	This study
Portlandia (Portlandia) arctica	Hom or dCL	nd	nd	Hom or dCL	Recent	nd	Bøggild, 1930
Portlandia inflata	IFP	Hom	ISP	fCCL, iCCL, Hom, ISP	Recent	Atlantic Ocean	Carter, 1990a
Megayoldia lischkei	Hom, Sph	-	ISP	fCCL	Recent	Japan	This study
Megayoldia japonica	FP	Hom	ISP	Hom, fCCL	Recent	Japan	This study
Silicula sp.	nd	nd	nd	N	Recent	nd	Nevesskaya et al., 1971
Phaseolus sp.	nd	nd	nd	N	Recent	nd	Nevesskaya et al., 1971
Tindaria (Deminucula) sp.	not CP	nd	nd	nd	Recent	nd	Van de Poel, 1955
Tindaria callistiformis	Hom, FP	Hom	nd	Hom	Recent	nd	Carter, 1990a
Tindaria soyoae	Hom	-	ISP	Hom	Recent	Japan	This study
Isoarca	nd	nd	nd	N	Middle Jurassic - Late Cretaceous	nd	Cox et al., 1969

microstructures among species. Homogeneous structures in the Manzanelloidea and Nuculanoidea are composed of granular crystals, and RESP and reticulate structures containing granular crystals are observed in Solemyidae. Thus, crystallographic textures are more diversified than crystal morphologies.

5-2. Paleontological view of shell microstructure and their evolutionary hypothesis

5-2-1. Archetype molluscs and their shell microstructures

Shell microstructures of ancestral molluscs have been studied for decades (Runnegar, 1985; Runnegar & Pojeta, 1992; Kouchinsky, 1999; Kouchinsky, 2000; Feng & Sun, 2003; Vendrasco et al., 2009; Vendrasco et al., 2010; Vendrasco et al., 2011; Vendrasco et al., 2013). While Cambrian molluscan shells have been generally replaced with phosphates, traces of shell microstructures are sometimes preserved, especially in the internal moulds of specimens. Thus far, eight kinds of shell microstructures have been observed in Cambrian molluscs (Table 5.2).

The probable ancestor of bivalves is compressed monoplacophoran-like molluscs, and several species, such as *Watsonella*, *Anabarella* (both Stenothecidae), and *Pseudimyona* (Pseudomyonidae), were considered as taxa close to bivalves (Carter et al., 2000; Zong-Jie & Sanchez, 2012). Two species of Stenothecidae from early Cambrian have complex three shell layers consisting of fibrous, foliated (or semi-foliated), aragonite, and prismatic textures (Kouchinsky, 1999), and *Pseudimyona* from the middle Cambrian has a foliated calcite microstructure (Runneger & Pojeta, 1992). On the other hand, three bivalve genera were found from the lower to middle Cambrian (*Pojetaia* and *Fordilla* as Fordillidae, *Tuarangia* as Tuarangiidae; Runnegar & Pojeta, 1992), although

several scholars doubt whether *Tuarangia* is a true bivalve (Runnegar & Pojeta, 1992; Pojeta, 2001). They were classified into Euprotobranchia. Shells of Fordillidae were constructed of foliated aragonite (Vendrasco et al., 2011) whose structure was composed of elongate blade-like laths. Foliated aragonite is also possessed by recent monoplacophoras (Checa et al., 2009). Checa et al. (2009) first recognized that the inner layer of Monoplacophora consists of foliated aragonite, not nacre. The two species of monoplacophorans they examined (*Rokopella euglypta* and *Micropilina arntzi*) have foliated aragonite and *Veleropilina zografi* has a nacreous structure. Co-occurrence of foliated aragonite in the Cambrian and recent monoplacophorans and fordillid bivalves implies that microstructure is a plesiomorphy for these taxon (Carter, 2001; Vendrasco et al., 2011; Vendrasco et al., 2013). Compared with Fordillidae, *Tuarangia* has unique morphological characteristics (Runnegar & Pojeta, 1992) and foliated calcite (Runnegar, 1985; Vendrasco et al., 2010). The other candidates for archetype bivalves, *Arhouriella* and *Camya*, have many uncertainties regarding their identity as true bivalves (Carter et al., 2000; Elicki & Gursu, 2009) and their shell microstructures are unknown.

The Cambrian Euprotobranchia lineage became scarce during the late Cambrian (Dark ages; Fang, 2006a). No unequivocal bivalve fossils were found from the upper Cambrian and they completely disappeared before the Ordovician (Hinz-Schallreuter, 2000; Cope, 2002). Fang (2006a) explained the reason for their disappearance as substrate change due to increase of the bioturbation frequency. Euprotobranchia bivalves were not anatomically well adapted to such environments. The latest common ancestor of Eubivalvia Nevesskaja, 2009, which is a modern-type bivalve consisting of Protobranchia, Pteriomorphia, and Heteroconchia (i.e. crown-group bivalves) appeared at least as early as the early Ordovician (Zon-Jie & Sanchez, 2012). While the relationship between

Table 5.2. Shell microstructure data for Cambrian molluscs (modified the Table in Vendrasco et al., 2013). Possilbe ancesters of Bivalvia were highlighted in gray colors. F: Fibrous; P: Prismatic; X: Crossed-Lamellar; LF: Lamello-fobrillar; CN: Calcitic semi-nacre; FC: Foliated calcite; FA: Foliated aragonite; L: Laminar of undetermined type. Possibly foliated aragonite.

Cambrian	Species name	family	outer layer	inner layer
Upper	Yochelcionella	Yochelcionellidae	P	L
	Tuarangia	Tuarangiidae	FC	
	Ribeiria	Ribeiriidae	CN	
	Protowenella	Helcionellidae	P	LF
	Pelagiella	Pelagiellidae	P	LF
	Mellopegma	Stenothecidae	P	CN
	Figurina	Helcionellidae	P	L
	Eurekapegma	Stenothecidae	CN	
	Eotebenna	Yochelcionellidae	FC	
	Costipelagiella	Pelagiellidae	F	LF
Middle	Aequiconus	Stenothecidae	L	
	Anabarella	Stenothecidae	P	
	Anabarella	Stenothecidae	P	
	Anhuiconus	Helcionellidae	P	
	Bemella	Helcionellidae	P	
	Calyptroconus	Helcionellidae	FC	
	Figurina	Helcionellidae	P	
	Fordilla	Foldillidae	FA	
	Ilsanella	Scenellidae	P	
	Leptostega	Helcionellidae	P	
	Mackinnonia	Trenellidae	P	
	Mackinnonia	Trenellidae	P	L
	Mellopegma	Stenothecidae	P	CN
	Obtusoconus	Helcionellidae	P	
	Parailsanella	Trenellidae	P	
	Pararaconus	Helcionellidae	P	
	Pelagiella	Pelagiellidae	P	
	Pelagiella	Pelagiellidae	LF	L
	Pojetaia	Foldillidae	FA	
	Yochelcionella	Yochelcionellidae	P	
	Yuwenia	Onychochilidae	F	P
	Watsonella	Stenothecidae	F	FA?
	Securiconus	Helcionellidae	F	P
Lower	Ocruranus	Halkieriidae	LF	
	Mellopegma	Stenothecidae	P	CN
	Ilsanella	Scenellidae	F	LF
	Ceratoconus	Ceratoconidae	F	P
	Bemella	Helcionellidae	P	
	Archaeospira	Coreospiridae	F	
	Anabarella	Stenothecidae	F	P
	Aldanella	Aldanellidae	F	P

Euprotobranchia and Eubivalvia is unclear, several anatomical similarities were recognized between Foldiliidae and Paleotaxodonta (Runnegar & Bentley, 1983; Pojeta & Runnegar, 1985; Carter, 1990a).

5-2-2. General trends in the evolution of the shell microstructures of Protobranchia

Pathways of evolution within the protobranch bivalves are uncertain. However, their earliest representative was most likely a nuculoid (Waller, 1998). Ctenodontidae with nuculoid-like shell are considered as the ancestral taxa to Solemiyoidea, Manzenelloidea (Pojeta, 1988), and possibly Praenuculidae (Carter, 2001). Praenuculidae is also a likely ancestor for early Nuculidae since it has similar shell and ligament microstructures (Carter, 2001). An ancestor of Nuculanoidea is unclear, but they were separated from nuculoid-like species on the basis of water flow into the mantle (Allen, 1985; Zardus, 2002). The molecular phylogenetic analysis in this study suggests that Nuculanoidea are closer to Solemyoidea.

Stratigraphical ranges of protobranchs with descriptions of shell microstructures are shown in Table 5.3. The oldest fossil specimen whose shell microstructure has been observed are both from the middle Ordovician for Nuculoidea (Carter, 1990a) and from upper Ordovician for Nuculanoidea (Vendrasco et al., 2013). Carter (1990a) observed the shell microstructure of *Deceptrix levata* (Praenuculidae) and found relict horizontal lamination which may indicate a primitive nacreous structure. *Paleoneilo* sp. (Nuculanoidea) has a laminar shell microstructure that is also similar to the primitive nacreous structure. Such a nacreous structure is found in gastropods and cephalopods from the same formation at the same locality as *Paleoneilo* sp. (Vendrasco et al., 2013).

Therefore, there were no molluscan species having nacreous structures before the Ordovician when all the major molluscan classes had diverged (Vendrasco et al., 2010; Vendrasco et al., 2013). Thus, co-occurrence of the nacreous structure in four molluscan classes (Gastropoda, Bivalvia, Cephalopoda, and Monoplacophora) was due to convergence and the ancestral character of nacre was probably foliated aragonite. Pathways from foliated aragonite to laminar to nacreous structures is recognized in the early evolution of protobranchs, like the other major molluscan classes. Foliated aragonite is found in Fordillidae, which is a probable ancestor of modern-type bivalves; laminar microstructure was found in Ordovician Nuculoidea and Nuculanoidea. In addition, Carter (2001) observed the shell microstructures of Silurian protobranchs and reported a nacreous structure in *Praenucula* (Praenuculidae), *Nuculoidea* (Nuculidae), and *Tancrediopsis* (Ctenodontidae). In addition, Carter (1990a) recognized a nacreous structure in Carboniferous Solemyidae, *Acharax (Nacrosolenya) trapezoides,* which has morphological similarity in their ligament to *Tancrediopsis gotlandica* and several nuculanoidean species, *Malletia, Nuculana, Jupiteria, Dacryomya, Paleyoldia, Silicula, Phsetia, Ryderia,* and *Yoldia,* which are probable descendants of *Paleoneilo,* which had nacreous structures.

Observations of the shell microstructures of recent protobranch bivalves in this study reveals sister groups consisting of Solemyoidea, Manzanelloidea, and Nuculanoidea, which do not have a nacreous structure while the Nuculoidea have nacreous structure. However, this trend is not common in fossil taxa. The evolutionary pathway in the shell microstructure seems to be characterized by the acquiring of a nacreous structure in protobranchs.

Table 5.3. Geological occurrence of protobanch genera and their shell microstructure. Blue bar: Occurence of the species with nacreous structure; Yellow bar ; non-nacreous species; Red: species with RESP structure; Green: species with Reticulate structure. Detail assamblage of the shell microstructure was described in Table 5.1.

Superfamily	Family	Genus	Paleozoic						Mesozoic			Cenozoic			Recent
			Cam.	Ord.	Sil.	Dev.	Car.	Per.	Tri.	Jur.	Cre.	Pal.	Neo.	Qua.	
Solemyoidea	Ctenodontidae	*Ctenodonta*													
		Clinopistha													
		Ditichia													
		Praectenodonta													
		Tancrediopsis													
		Tellinopsis													
	Solemydae	*Solemya*													
		Janeia													
		Psiloconcha													
		Acharax													
	Manzanellidae	*Manzanella*													
		Huxleyia													
		Nucinella													
Nuculoidea	Praenuculidae	*Praenucula*													
		Cardiolaria													
		Deceptrix													
		Ledopsis													
		Palaeoconcha													
		Similodonta													
	Nuculidae	*Nucula*													
		Ennucula													
		Linucla													
		Acila													
		Brevinucula													
		Nuculoidea													
		Nuculoma													
		Nuculopsis													
		Palaeonucula													
		Condylonucula													
		Pronucula													
		Ptychostolis													
		Trigonucula													
	Sareptidae	*Pristigloma*													
		Sarepta													
Nuculanoidea	'Malletidae"	*Malletia*													
		Arisaigia													
		Bicrenula													
		Cadomia													
		Ctenodontella													
		Dysodonta													
		Ekstadia													

Table 5.3. Continued.

Superfamily	Family	Genus	Paleozoic Cam.	Ord.	Sil.	Dev.	Car.	Per.	Mesozoic Tri.	Jur.	Cre.	Cenozoic Pal.	Neo.	Qua.	Recent
		Koenenia													
		Metapalaeoneilo													
		Myoplusia													
		Neilo													
		Neilonella													
		Nuculites													
		Palaeoneilo													
		Phaenodesmia													
		Prosoleptus													
	'Malletidae"	*Pseudarca*													
		Pseudoglomus													
		Quadratonucula													
		Saturnia													
		Sluha													
		Tindaria													
		Tropinuculites													
		Nuculana													
		Jupiteria													
		Ledella													
		Politoleda													
		Poroleda													
		Propeleda													
		Saccella													
		Adrana													
Nuculanoidea		*Costatoleda*													
		Dacryomya													
		Ezonuculana													
		Hilgardia													
		Ledina													
	'Nuculanidae"	*Lithorhadia*													
		Mesosaccela													
		Paleyoldia													
		Silicula													
		Phestia													
		Portlandia													
		Adranella													
		Hataiyoldia													
		Yoldiella													
		Ryderia													
		Veteranella													
		Yoldia													
		Katadesmia													
		Megayoldia													
		Orthoyoldia													
	Isoarchidae														

5-2-3. Shell microstructural evolution in Nuculoidea

The shell microstructure of Nuculoidea is more conservative than other protobranch bivalves in that they have a nacreous structure in common. However, their outer prismatic layer is rich in variety. They seem to provide important information about phylogenetic groupings. The earliest mollusc was considered to have an outer prismatic and inner lamello-fibrillar texture (Feng & Sun, 2003), but the oldest bivalve Foldillidae has a foliated aragonite mono-layer. The outer layer has not been described for nuculids from the Ordovician (Mutvei et al., 1985; Carter, 2001). However, it is uncertain whether these species are truly mono-layered or bi-layered species, because absence of the outer layer in those species could be the result of poor preservation or unsatisfactory observation. The first occurrence of the outer layer in nuculids is known be from at least the Sirulian; *Praenucula faba* (Praenuculidae) had thin and nearly vertical to slightly reclined, finely prisms, and *Nuculoidea pinguis* (Nuculidae) had relatively thin and vertical to slightly reclined prisms (Carter, 2001). Because similar microstructure are found among the two nuculoid families, these thin, nearly vertical prismatic layers are considered as the ancestral state of the outer layer of nuculids. Carboniferous *Nuculopsis* species had the outer layer consisting of several sublayers, which included an irregular spherulitic prismatic structure (ISPP) (Carter, 1990a). ISPP was found only in this genus. *Nuculoidea optima* from the Middle Devonian had an outer prismatic layer consisting of two sublayers, a vertical simple (?) prismatic outer sublayer and a reclined fibrous prismatic inner sublayer (Carter & Tevesz, 1978a; Carter, 1990a). Compared to the shell microstructures of recent Nuculidae, the reclined prisms in the Sirulian Praenuculidae and Nuculidae (Carter, 2001) seem to resemble the composite prismatic structure type-A

found in recent *Acila* and *Ennucula*. The outer layer of *Nuculoidea optima* consists of two prismatic sublayers that appear to resemble the irregular fibrous prismatic structure type-A and B which are found in some *Ennucula* species and *Brevinucula* sp. If so, the composite prismatic structure type-B and denticular composite prismatic structure are the secondary structure in nuculids. The first occurrence of nuculid species with DCP is reported from the Cretaceous (Bøggild, 1930; Van de Poel, 1955).

The above-mentioned nuculid species commonly had columnar or sheet nacreous structures; however, the *Palaeonucula* species from the Carboniferous and Triassic (Schenck, 1939; Lucas, 1952; Carter, 1990a) and adult *Condylonucula* species (Moore, 1977; Carter1990a; Carter, 2001) had non nacreous shells. *Condylonucula* are very small and appear to be confined to small areas in the western Caribbean (Moore, 1977). *Condylonucula maya* had a nacreous structure in the middle and inner layers at a juvenile stage and lost its nacre later in ontogeny (Carter, 2001). Carter (2001) allocated them to the new subfamily Palaeonuculinae according to their shell microstructural character. The validity of this classification is unknown, because molecular phylogenetic data for *Condylonucula* is lacking currently. Molecular analysis in this study reveals a systematic position of Sareptidae transferred from Nuculoidea to Nuculanoidea. A similar change can occur in Palaeonuculinae. If they are true Nuculoidea, it is reasonable to consider that loss of nacre occurred at least after the Carboniferous among Palaeonuculinae, like the other protobranch superfamilies.

5-2-4. Shell microstructural evolution in Solemyoidea

Recent solemyids contain two genera, *Solemya* and *Acharax*. These are clearly distinguished by the ligament position (e.g. Taylor et al., 2008). The former has an internal ligament, and the latter possess an external ligament. My observations of the shell microstructures of solemyids reveals that *Solemya* and one species of *Acharax* (i.e. *Acharax japonica*) have similar microstructural composition, while *Acharax johnsoni* has an exceptionally unique microstructure.

Among solemyids, their ancestral states can be inferred from the several available fossil records from the Paleozoic because even Paleozoic solemyids are similar to recent solemyids in many features (Bailey, 2011). (1) The Ordovician solemyid genus *Psiloconcha* and the Carboniferous and Permian solemyid genus *Janeia* are similar in having an external ligament (Pojeta, 1988). Therefore, an internal ligament must have evolved from an external ligament. (2) In terms of shell microstructure, the outer shell layer of *Acharax* (*Nacrosolemya*) *trapezoides* from the Upper Carboniferous has a RESP-like vertical irregular prismatic structure (Carter, 1990a). This fossil record probably represents the origin of the RESP microstructure found in recent solemyids. In addition, the reticulate structure in the outer shell layer of *A. johnsoni* is an apomorphic characteristic in the family. Huber (2010) suggests that *Acharax japonica* differs from other *Acharax* species in morphology and habitat and proposes a new subgenus *Pseudacharax* within *Solemya* for *Acharax japonica* and *Acharax occidentalis*. This definition may be reasonable to distinguish *Acharax* based on the RESP structure and reticulate structure. (3) The middle shell layer of *Acharax* (*Nacrosolemya*) *trapezoides* is characterized by a columnar nacreous structure, and the inner shell layer by a sheet

nacreous structure (Carter, 1990a). In addition, both Solemyidae and Manzanelloidea evolved from Ctenodontidae (Pojeta, 1988) as mentioned above, and the occurrence of nacre is known in Ctenodontidae (Carter, 2001). Therefore, the absence of a nacreous structure in recent species may be a secondary condition in Solemyidae and probably in Manzanelloidae.

Habitat depth may be related to phylogeny in solemyids. *Acharax johnsoni* is distributed from a depth of 100 to 5379 m (Okutani, 2000; Okutani & Fujikura, 2002), whereas the depth range of the genus *Solemya* is from 0 to 600 m (Kuznetsov & Schileyko, 1984; Métivier & von Cosel, 1993; Coan et al., 2000) and that of *A. japonica* is from 0 to 20 m (Okutani, 2000; Yamanaka et al., 2008). Seep-associated *Acharax* appear in the Early Cretaceous (Kiel & Little, 2006). From my shell microstructural data, published molecular trees, and the fossil record, we assume that cold-seep-dwelling *Acharax* diverged from an *Acharax*-like ancestor, and that shallow-water-dwelling *Acharax* moved into deep-sea chemosynthetic communities during an early stage of their evolution. Kiel et al. (2008) reported a new shell microstructure in *Acharax cretacea* from a Cretaceous cold seep that is similar to the reticulate structure in that it is composed of two types of units. The reticulate structure in the outer shell layer of *A. johnsoni* has reticulate conchiolin sheets, and the c-CCL of the inner layer is crossed by oblique conchiolin sheets, unlike the c-CCL of other bivalves (Carter, 1990b). In *A. johnsoni*, the organic content of both shell layers is high, which probably protects the shells against corrosion in the deep sea (Pytkowicz, 1970).

5-2-5. Shell microstructural evolution in Nuculanoidea

Recent Nuculanoidea show non-nacreous microstructures as shown in this study. In contrast, previous studies found a nacreous structure in many fossil taxa of Nuculanoidea (e.g. Cox et al., 1969; Taylor et al., 1969; Speden, 1970; Carter, 1990a). As mentioned above, *Palaeoneilo*, the oldest species of Nuculanoidea, has a shell microstructure with a laminar microstructure, which could be a primitive nacreous structure. On the other hand, Silurian "Malletidae", *Ekstadia tricarinata* have outer fine, reclined prismatic structure. The middle and inner layer are the crossed acicular and fine complex crossed lamellar structure (Carter, 2001). Devonian and Carboniferous *Palaeoneilo* species, which is also classified into "Malletidae", have non-nacreous shell layers—outer prismatic, middle homogenous to fine complex crossed lamellar structure, and inner homogeneous, fine complex crossed lamellar, and matted structures (Carter, 1990a). The possibility that misidentification have occurred in nacre having *Paleoneilo* cannot be denied, because Vendrasco et al. (2013) didn't show the photograph of the specimen used for SEM observation. But if it is true, this difference seems to imply evolutionary transitions between nacreous and non-nacreous structures such as fine CCL and homogeneous structures. Like *Palaeoneilo*, shell microstructural transition from nacreous to non-nacreous structures was observed simultaneously in Nuculanoidea: the Cretaceous *Nuculana* and *Yoldia* had nacreous structures (Speden, 1970), while the recent species have non-nacreous shells. Thus, nacreous structure is probably a plesiomorphy of Nuculanoidea rather than a synapomorphy, but this character is lost almost completely in the recent taxa. Nevesskaya et al. (1971) reported a nacreous structure in the recent Nuculanoidea, *Silicula* sp. and *Phaseolus* sp.. Although this result is doubtful due to

insufficient description, some taxa of Nuculanoidea may have maintained a nacreous layer until recently.

Reconstructing the precise phylogeny of Nuculanoidea is rather difficult. Paleontologists traditionally divided Nuculanoidea into two families; Malletidae and Nuculanidae (Cox et al., 1969). These two families are distinguished by the presence or absence of a resilifer. However, this classification is doubtful, because molecular studies do not support this definition (Sharma et al., 2013 and this study). Microstructural evolution from nacreous to non-nacreous structures in the same taxon and/or the appearance of non-nacreous taxa occurred around the Silurian to Devonian in 'Malletidae' and after the Cretaceous in 'Nuculanidae'.

The hypothesis that a nacreous structure is a plesiomorphy of Nuculanoidea also means that the similar shell microstructural character in the recent Nuculanoidea (e.g. the homogeneous, fine complex crossed lamellar structures) shows convergence. Variation of crystallographic texture was found even within the same microstructure (see chapter 4). This may imply that their microstructure is a product of convergent evolution. Further study on shell microstructure and classification is required, especially in this taxon

5-2-6. possible driving force of nacre deprivation in Protobranchia

Molecular and shell microstructural data from previous studies and this study indicate that shell microstructure in protobranch bivalves has remained uniform through geological time (Figure 5.2). Shell microstructures of ancestral bivalves from Cambrian Fordillidae were constructed of foliated aragonite, which is considered a primitive nacreous structure (Vendrasco et al., 2011) (Event 1 in Figure 5.2). The oldest fossil

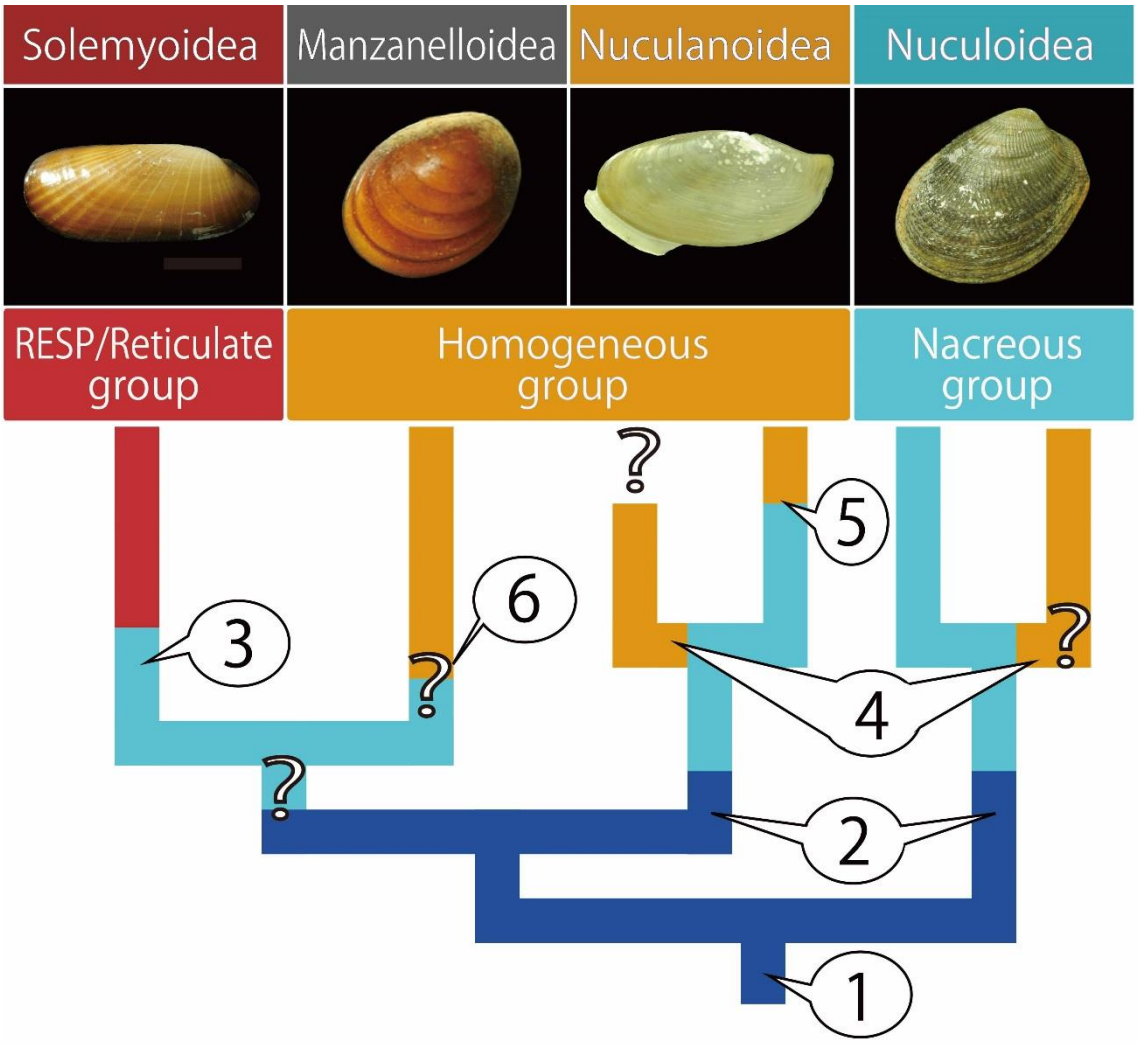

Figure 5.2. Schematic illustration of shell microstructural evolution of protobranchs. Characteristics of the shell microstructural components of each protobranch superfamily were classified into three major groups: (1) RESP/Reticulate group, (2) Homogeneous group, and (3) Nacreous group. The brief cladogram of four protobranch superfamilies is shown at the bottom. Each branch is colored differently, distinguishing each shell microstructural group: red: RESP/Reticulate group; yellow: homogeneous group; light blue: Nacreous group; blue: "primitive" nacreous. Numbers in the balloons exhibit some events that are described in the text.

Specimens of Nuculoidea and Nuculanoidea, whose shell microstructures have been observed, were from the Ordovician (Carter, 1990a; Vendrasco et al., 2013). They possessed the primitive nacreous structure (Event 2 in Figure 5.2). Solemyoidea also had nacreous structure in the Carboniferous (Carter, 1990a) (Event 3 in Figure 5.2). Molecular and shell microstructural data indicate that Solemyoidea, Nuculanoidea and Palaeonuculinae lost their nacre during their evolution. According to descriptions of protobranch shell microstructures in previous studies and my observations (Table 5.3), changes from nacre to non-nacre may have occurred between the Silurian to Carboniferous: Silurian to Devonian in "Malletidae-like" nuculanids, Carboniferous in Palaeonuculinae nuculids (Event 4 in Figure 5.2), probably after the Carboniferous in solemyids, and after the Cretaceous for non-nacreous taxa of nuculanids (Event 5 in Figure 5.2). Fossil Manzanelloidea having the nacreous structure have not been observed. However, a non-nacreous condition in Recent Manzanelloidea is also considered as a secondary condition because the probable ancestor of Manzanelloidea, Ctenodontidae, and the sister group of Solemyoidea in the Carboniferous commonly had the nacreous structure (Pojeta, 1988; Carter, 1990a) (Event 6 in Figure 5.2).

Molluscs have experienced remarkable shell microstructural evolution during the Phanerozoic. Mineralogical evolution of molluscan shells leading to a change from nacreous to non-nacreous microstructures has been well studied to date. Molluscan shells are mainly composed of calcium carbonate of two common polymorphs of the biominerals, aragonite and calcite (see Table 1.1 in Chapter 1). The precipitation rate of calcite is higher than that of aragonite in lower temperatures in inorganic systems (Burton & Walter, 1987). In addition, high pCO_2 and low oceanic Mg/Ca inhibit the biological deposition of aragonite (Wilkinson, 1979; Wilkinson et al., 1985). Ancient sea water

altered the amount of pCO_2 and Mg/Ca cyclically due to marine transgression-regression cycles (Carter et al., 1998). This cycle controls the saturation state of calcium carbonate, resulting in a "calcite sea" and "aragonite sea." (e.g., Porter, 2007; Hönisch et al., 2012). The mineralogy of molluscan shells is weakly controlled by seawater chemistry compared to other calcareous organisms (e.g., corals and sponges; Ries, 2010). However, a mineralogical switch from aragonite to calcite occurred during the Cambrian. Species with calcitic shells increased during the Middle Cambrian, when seawater changed from aragonite to calcite seas. However, aragonite shell mineralogy was common in early Cambrian molluscs (Vendrasco et al., 2013). On the other hand, Carter et al. (1998) recognized bivalve species with a calcitic layer occurring concurrently during the Permian to Triassic, times with aragonite seas, not calcite seas. In this period, predators such as shell chemical boring algae, which could have been the driving force of microstructural evolution, did not increase. Carter et al. (1998) emphasized that thermal potentiation was the most important factor controlling the timing of shell mineralogical evolution. During the Permian to Triassic, it was colder than average. However, there is no apparent relationship between the shell microstructural evolution from nacre to non-nacre and the change of global sea water chemistry or temperature.

Shell microstructural changes in various mollusc lineages seem to reflect complex biotic/abiotic factors and therefore promoted their adaptive radiation. Shell microstructural differences influence the following factors (Vendrasco et al., 2013): (1) the energy cost of shell formation (Palmer, 1983, 1992), which is related to shell formation rate and energy demand of the animal; (2) shell strength as resistance to predatory attacks. The mechanical properties of bivalve shell structures are variable, and the nacreous structure is known as the strongest shell microstructure (Taylor & Layman,

1972; Palmer, 1983; Currey, 1988); and (3) the dissolution ratio in seawater chemistry. Harper (2000) concluded that the shell microstructural difference affects the dissolution rate together with the carbonate mineralogy.

The nacreous structure is present in basal bivalve lineages (Nuculidae and basal Autolamellibranchia) but not in derived taxa (Frýda et al., 2010). Nacreous structure simultaneously occurred not only in protobranch bivalves but also in different molluscan classes (gastropods and cephalopods) during the Ordovician. The assumed driving force of this evolution is strong selective pressure due to increasing intensity of predation (Great Ordovician Biodiversification Event) (Vendrasco et al., 2013). On the other hand, Cartwright & Chaca (2007) summarized the paleontological presence of nacre (see their Figure 8) and the gradual increasing of species with non-nacre layers as follows; the nacreous structure is a high-cost material due to its high proportion of the organic matrix. Energy costs of calcification (1–2 J/mg) are assumed to be considerably less than the total costs of proteins (29 J/mg) (Palmer, 1992). Although nacre is the strongest microstructure, it gradually lost its market share. As discussed above, Nuculanoidea diversification accompanied shell microstructural change from nacreous to non-nacreous microstructures, such as homogeneous, fine CCL structure, around the K/T boundary. Shell strength and organic content of non-nacreous microstructures, such as homogeneous structures, have been measured in previous studies. The mechanical strength of homogeneous structures is significantly lower than that of nacreous structures. The bending strength of the homogeneous structure of *Arctica islandica* (Hetrodontia) is 60 MPa, while that of the nacreous structure is 117 MPa in *Anodonta cygnea* (Paleoheterodonta) and 238 MPa in *Modiolus modiolus* (Pteriomorphia) (Currey, 1976; Taylor & Layman, 1972). Thus, acquisition of a non-nacreous shell cannot be explained

as the result of strengthening of shell hardness in resistance to predatory attacks. Raup (1979) reported that the organic content of the homogeneous structure of *Arctica islandica* (Heteroconchia) is 0.4 wt %; in contrast, that of the nacreous structure of several species ranges from 0.69 to 2.3 wt % (Taylor & Layman, 1972; Harper, 2000). Because of its low organic content, the homogeneous structure is less costly to produce and, therefore, might be advantageous.

Different habitats of each protobranch taxon seem to have been established in the early in their evolution. In general, Recent Nuculanoidea are characterized by the inhalant siphon and posterior elongated shell that allow the deep burrowing habitat (Allen, 1985). The posterior elongated shell and internal septum, which imply the presence of a siphon are recognized in the Ordovician Nuculanoidea (Cox et al., 1969). Thus, based on their shell morphology, Nuculanoidea's habitats presumably underwent little change between nacre-bearing and nacre-lacking members. For example, *Paleoneilo* had the posterior elongated shell, despite having the primitive nacreous structure in the Ordovician. Other nacre-bearing fossil nuculanoidean taxa such as *Dacryomya*, *Phestia* and *Phaseolus* all have similar morphology to Recent Nuculanoidea. Thus, shell microstructural evolution was not apparently synchronized with the life habitat change in Nuculanoidea (Event 4 and 5 in Figure 5.2). This applies to Nuculoidea, because their shell morphology is the most conservative (Allen, 1985), implying that their life habitat did not change during or after their shell microstructural evolution (Event 4 in Figure 5.2). Solemyoida are characterized by their chemosynthetic nutrition (e.g., Oliver & Taylor, 2012). It is not clear whether the origin of the chemosymbiosis can be traced back to the common ancestor of Solemyoidea and Manzenelloidea. If so, the acquisition of chemosymbiotic bacteria did not trigger shell microstructural evolution from the nacreous

to non nacreous structure. This scenario can be hypothesized because Solemyoidea maintained their nacreous structure after the divergence of two superfamilies of Solemyoida.

With respect to the microstructural change after the Cretaceous (Event 5 in Figure 5.2), the dominant taxa of deposit-feeding bivalves transitioned from protobranchs to tellinids (Heterodontia) during the early Cretaceous to Miocene (Nicol, 1972). The fossil occurrence of protobranchs suggests that they became less abundant in warm shelf waters (Nicol, 1972) due to the appearance of tellinids in the Early Cretaceous, which prefer warm water environments. Thus, it is likely that protobranchs moved to high-latitude regions (Nicol, 1972) or deep water as a result of competition against tellinids. Probably in association with this transition, Nuculanoidea increased their diversity drastically during the late Mesozoic to early Paleogene (Nevesskaya, 2008). Among protobranchs, Nuculanoidea most resemble tellinids with their siphons in the life habitat (Rhoads, 1974). As a low-cost material for molluscan shells, the homogeneous structure was an advantage for this diversification event in Nuculanoidea. This may be also the driving force of other events when nacre decreased.

5-3. Conclusion

Shell microstructures of 38 protobranch species were newly described and crystallographic textures of 13 species were examined in this study. Molecular phylogenetic analysis supports the monophyly of four superfamilies of Protobranchia with a major change in the position of the family Sareptidae. However, multiple polyphyletic conditions were revealed among genera and families. Compared with the

provided topology of the ML tree, the shell microstructural composition is consistent with the phylogeny among superfamilies in protobranchs.

Shell microstructural groupings and molecular phylogenetic analysis of the recent protobranchs in this study provide reliable clues for higher-level identification of fossil taxa. However, descriptions of the shell microstructures in previous studies and results of this research suggest that all protobranch superfamilies had nacreous structure in their ancestral taxa and underwent radical changes from nacreous to non-nacreous structures. Thus, current shell microstructural components may be convergent among different superfamilies. Different patterns of crystallographic textures among the same shell microstructure suggest different origins, most notably in the homogeneous structure. Changes from nacre to non-nacreous structures seem to have occurred during the Silurian to Carboniferous in “Malletidae-like” nuculanids and Nuculoidea, and again later than the Cretaceous in Nuculanoidea. Global sea water chemistry, temperature, and life habitat change were probably not the driving forces of shell microstructural evolution. The possible driving force is inexplicable for the former event. The latter event occurred in synchronicity with the diversification event of Nuculanoidea, suggesting that the shell microstructure has evolutionary significance in the adaptive radiation of protobranchs, contributing to conserving energy costs of shell formation.

Acknowledgements

My deepest appreciation goes to Takenori Sasaki. His persistent teaching has guided me through a tough time since the day I came to here, The University of Tokyo. I have enormous respect for him. I thank Kazuyoshi Endo, Toshihiro Kogure, Takanobu Tsuihiji, Yasunori Kano (The University of Tokyo) for valuable comments and suggestions. I also thank the members of paleontological seminar, especially the members who belong Sasaki laboratory, Yusuke Takeda, Shinnosuke Teruya and Takashi Muranaka. They gave me valuable comments and devoted their time to supporting my writing. Hiromi Watanabe (Japan Agency for Marine-Earth Science and Technology: JAMSTEC) and Davin H. E. Setiamarga (The University of Tokyo) taught me the technical method of the molecular phylogenetic analysis. Antonio Checa (The University of Granada) taught me the technical method on SEM. I am grateful to them for supporting my research.

I thank Katsunori Fujikura (JAMSTEC), Yoshihiro Fujiwara (JAMSTEC), Koji Seike (The University of Tokyo), Robert G. Jenkins (Kanazawa University) and Takuma Haga (National Museum of Nature and Science) for donating specimens for me. I also thank Koji Inoue (The University of Tokyo) and Toshiro Saruwatari (The University of Tokyo), who gave me the opportunity for participating in a research voyage.

Kazuyoshi Tanabe (The University of Tokyo) and Yuta Shiino (Niigata University) provided many valuable advices on my research during my doctoral program. Rei Nakashima (AIST), Ryuichi Majima (Yokohama National University) and Kozue Nishida (AIST) have supported my work since I was an undergraduate student. I

have a renewed appreciation for them, and all the person who supported and encouraged me many times.

References

Allen, J. A., 1978: Evolution of the deep sea protobranch bivalves. *Philosophical Transactions of the Royal Society of London. Series B, Biological Sciences*, vol. 284, pp. 387–401.

Allen, J. A., 1983: The ecology of deep-sea molluscs. *In*, Russell-Hunter, W. D., *ed*., *Evolution, The Mollusca, Volume 6*, pp. 29–75. Academic Press, Orlando.

Allen, J. A., 1985: The Recent Bivalvia: their form and evolution. *In*, Trueman, E. R. and Clarke, M. R., *eds*., *Evolution, The Mollusca, Volume 10*, pp. 337–399. Academic Press, New York.

Allen, J. A. and Hannah, F. J., 1986: A reclassification of the Recent genera of the subclass Protobranchia (Mollusca: Bivalvia). *Journal of Conchology*, vol. 32, pp. 225–249.

Allen, J. A. and Sanders, H. L., 1969: *Nucinella serrei* Lamy (Bivalvia: Protobranchia) a monomyarian solemyid and possible living actinodont. *Malacologia*, vol. 7, pp. 381–426.

Allen, J. A. and Sanders, H. L., 1982: Studies on the deep sea Protobranchia; the subfamily Spinulinae (family Nuculanidae). *Bulletin of the Museum of Comparative Zoology at Harvard College*, vol. 150, pp. 1–30.

Allen, J. A. and Sanders, H. L., 1996: Studies on the deep-sea Protobranchia (Bivalvia): the family Neilonellidae and the family Nuculanidae. *Bulletin of The Natural History Museum (Zoology)*, vol. 62, pp. 101–132.

Amano, K., Jenkins, R. G. and Hikida, Y., 2007: A new gigantic nucinella (Bivalvia: Solemyoida) from the Cretaceous cold-seep deposit in Hokkaido, Northern Japan.

The Veliger, vol. 49, pp. 84–90.

Atkins, D., 1937: On the ciliary mechanisms and interrelationships of Lamellibranchs: Part III: Types of lamellibranch gills and their food currents. *The Quarterly Journal of Microscopical Science*, vol. 79, pp. 375–421.

Bailey, J. B., 2011: Paleobiology, paleoecology, and systematics of Solemyidae (Mollusca: Bivalvia: Protobranchia) from the Mazon Creek lagerstätte, Pennsylvanian of Illinois. *Bulletins of American Paleontology*, vol. 382, pp. 1–74.

Bandel, K., 1990a: Cephalopod shell structure and general mechanisms of shell formation. *In*, Carter, J. G., *ed*., *Skeletal Biomineralization: Patterns, Processes and Evolutionary Trends, vol. 1*, pp. 97–115. Van Nostrand Reinhold, New York.

Bandel, K., 1990b: Shell structure of the Gastropoda excluding Archaeogastropoda. *In*, Carter, J. G., *ed*., *Skeletal Biomineralization: Patterns, Processes and Evolutionary Trends, vol. 1*, pp. 117–134. Van Nostrand Reinhold, New York.

Beedham, G. E. and Owen, G., 1965: The mantle and shell of *Solemya parkinsoni* (Protobranchia: Bivalvia). *Proceedings of the Zoological Society of London*, vol. 145, pp. 405–430.

Berner, R. A., 1975: The role of magnesium in the crystal growth of calcite and aragonite from sea water. *Geochimica et Cosmochimica Acta*, vol. 39, pp. 489–504.

Bernard, F. R., Cai, Y. Y., and Morton, B., 1993: *Catalogue of the Living Marine Bialve Molluscs of China*. 146 pp. Hong Kong University Press, Hong Kong.

Bieler, R. and Mikkelsen, P. M., 2006: Bivalvia – a look at the branches. *Zoological Journal of the Linnean Society*, vol. 148, pp. 223–235.

Bieler, R., Mikkelsen, P. M., Collins, T. M., Glover, E. A., González, V. L., Graf, D. L.,

Harper, E. M., Healy, J., Kawauchi, G. Y., Sharma, P. P., Staubach, S., Strong, E. E., Taylor, J. D., Temkin, I., Zardus, J. D., Clark, S., Guzmán, A., McIntyre, E., Sharp, P. and Giribet, G., 2014: Investigating the bivalve tree of life – an exemplar-based approach combining molecular and novel morphological characters. *Invertebrate Systematics*, vol. 28, pp. 32–115.

Bøggild, O. B., 1930: The shell structure of the mollusks. *Det Kongelige Danske Videnskabernes Selskabs Skrifter. Naturvidenskabelig og Mathematisk Afdeling, Raekke 9*, vol. 2, pp. 231–326.

Bouchet, P., Rocroi, J., Bieler, R., Carter, J. G. and Coan, E. V., 2010: Nomenclator of bivalve families with a classification of bivalve families. *Malacologia*, vol. 52, pp. 1–184.

Boyle, E. E., 2011: Evolutionary patterns in Deep-Sea Mollusks. Ph. D thesis, University of Massachusetts Boston.

Burton, E. A., and Walter, L. M., 1987: Relative precipitation rates of aragonite and Mg calcite from seawater: temperature or carbonate ion control? *Geology*, vol. 15, pp. 111-114.

Campbell, D. C., Hoekstra, K. J. and Carter, J. G., 1998: 18S ribosomal DNA and evolutionary relationships within the Bivalvia. *In*, Johnston, P. A. and Haggart, J. W., *eds.*, *Bivalves: An Eon of Evolution—Palaeobiological Studies Honoring Norman D. Newell*. pp. 75–85. University of Calgary Press, Calgary.

Carter, J. G., *ed.*, 1990a: *Skeletal Biomineralization: Patterns, Processes and Evolutionary Trends, vol. 1*, 832 pp. Van Nostrand Reinhold, New York.

Carter, J. G., *ed.*, 1990b: *Skeletal Biomineralization: Patterns, Processes and Evolutionary Trends, vol. 2, Atlas and Index*, 302 pp. Van Nostrand Reinhold,

New York.

Carter, J. G., 2001: Shell and ligament microstructure of selected Silurian and Recent palaeotaxodonts (Mollusca: Bivalvia). *American Malacological Bulletin*, vol. 16, pp. 217–238.

Carter, J. G., Altaba, C. R., Anderson, L. C., Araujo, R., Biakov, A. S., Bogan, A. E., Campbell, D. C., Campbell, M., Jin-hua, C., Cope, J. C. W., Delvene, G., Dijkstra, H. H., Zong-jie, F., Gardner, R. N., Gavrilova, V. A., Goncharova, I. A., Harries, P. J., Hartman, J. H., Hautmann, M., Hoeh, W. R., Hylleberg, J., Bao-yu, J., Johnston, P., Kirkendale, L., Kleemann, K., Koppka, J., Kříž, J., Machado, D., Malchus, N., Márquez-Aliaga, A., Masse, J., McRoberts, C. A., Middelfart, P. U., Mitchell, S., Nevesskaja, L. A., Özer, S., Pojeta, J., Polubotko, I. V., Pons, J. M., Popov, S., Sánchez, T., Sartori, A. F., Scott, R. W., Sey, I. I., Signorelli, J. H., Silantiev, V. V., Skelton, P. W., Steuber, T., Waterhouse, J. B., Wingard, G. L. and Yancey, T., 2011: A synoptical classification of the Bivalvia (Mollusca). *Paleontological Contributions*, vol. 4, pp. 1–47.

Carter, J. G., Campbell, D. C. and Campbell, M. R., 2000: Cladistic perspective on early bivalve evolution. *In*, Haper, E. M., Taylor, J. D. and Crame, J. A., *eds.*, *The Evolutionary Biology of the Bivalvia.* pp. 47–79.

Carter, J. G. and Clark II, G. R., 1985: Classification and phylogenetic significance of molluscan shell microstructure. *In*, Broadhead, T. W., *ed*., *Mollusks: Notes for a Short Course, organized by Bottjer, D. J., Hickman, C. S. and Ward, P. D., Studies in Geology*. vol. 13, pp. 50–71. Department of Geological Sciences, University of Tennessee, Knoxville.

Carter, J. G. and Lutz, R. A., 1990: Part 2 Bivalvia (Mollusca). *In*, Carter, J. G., *ed*.,

Skeletal Biomineralization: Patterns, Processes and Evolutionary Trends, vol. 2, pp. 5–28, pls. 1–121. Van Nostrand Reinhold, New York.

Cartwright, J. H. E. and Checa, A. G., 2007: The dynamics of nacre self-assembly. *Journal of The Royal Sociery Interface*, vol. 4, pp. 491–504.

Cartwright, J. H. E., Checa, A. G., Escribano, B. and Sainz-Diaz, C. I., 2009: Spiral and target patterns in bivalve nacre manifest a natural excitable medium from layer growth of a biological liquid crystal. *PNAS*, vol. 106, pp. 10499–10504.

Castresana, J., 2000: Selection of conserved blocks from multiple alignments for their use in phylogenetic analysis. *Molecular Biology and Evolution*, vol. 17, pp. 540–552.

Chase, M. R., Etter, R. J., Rex, M. A. and Quattro, J. M., 1998: Bathymetric patterns of genetic variation in a deep-sea protobranch bivalve, *Deminucula Atacellana*. *Marine Biology*, vol. 131, pp. 301–308.

Chateigner, D., Hedegaard, C. and Wenk, H. R., 2000: Mollusc shell microstructures and crystallographic textures. *Journal of Structural Geology*, vol. 22, pp. 1723–1735.

Checa, A. G., Okamoto, T. and Ramírez, J., 2006: Organization pattern of nacre in Pteriidae (Bivalvia: Mollusca) explained by crystal competition. *Proceedings of the Royal Society B*, vol. 273, pp. 1329–1337.

Checa, A. G., Pina, C. M., Osuna-Mascaro, A. B. and Harper, E. M., 2014: Crystalline organization of the fibrous prismatic calcitic layer of the Mediterranean mussel *Mytilus galloprovincialis*. *European Journal of Mineralogy*, vol. 26, pp. 495–505.

Checa, A. G., Ramírez-Rico, J., González-Segura, A. and Sánchez-Navas, A., 2009: Nacre and false nacre (foliated aragonite) in extant monoplacophorans

(=Tryblidiida: Mollusca). *Naturwissenschaften*, vol. 96, pp. 111–122.

Checa, A. G. and Rodríguez-Navarro, A. B., 2005: Self-organisation of nacre in the shells of Pterioida (Bivalvia: Mollusca). *Biomaterials*, vol. 26, pp. 1071–1079.

Coan, E. V. and Valentich-Scott, P., 2012: *Bivalve Seashells of Tropical West America. Marine bivalve mollusks from Baja California to Northern Perú*. 1258 pp. Santa Barbara Museum of Natural History, Santa Barbara.

Coan, E.V., Valentich-Scott, P. and Bernard, F. R., 2000: *Bivalve Seashells of Western North America.* 766 pp. Santa Barbara Museum of Natural History, Santa Barbara.

Cope, J. C., 1996: Early Ordovician (Arenig) bivalves from the Llangynog Inlier, South Wales. *Palaeontology*, vol. 39, pp. 979–1026.

Cope, J. C. W., 1997: The early phylogeny of the class Bivalvia. *Palaeontology*, vol. 40, pp. 713–746.

Cope, J. C. W., 2000: A new look at early bivalve phylogeny. *Geological Society, London, Special Publications*, vol. 177, pp. 81–95.

Cox, L. R., 1969: Superfamily Solemyacea. *In*, Moore, R. C. *ed., Treatise on Invertebrate Paleontology, Part N, Mollusca 6* (*Bivalvia*)*, Vol. 1,* pp. 241–243. Geological Society of America, New York and University of Kansas, Lawrence.

Currey, J. D., 1976: Further studies on the mechanical properties of mollusc shell material. *Journal of Zoology*, vol. 180, pp. 445–453.

Currey, J. D., 1988: Shell form and strength. *In*, Trueman, E. R. and Clarke, M. R., *eds.*, *The mollusca: form and function*, pp. 183–210. Academic Press, London.

Dall, W. H., 1908a: A revision of the Solenomyacidae. *Nautilus*, vol. 22, pp. 1–2.

Dall, W. H., 1908b: Reports on the dredging operations off the west coast of Central

America to the Galapagos, to the west coast of Mexico, and in the Gulf of California, in charge of Alexander Agassiz, carried on by the U.S. Fish Commission Steamer “Albatross,” during 1891, Lieut. Commander Z. L. Tanner, U. S. N., Commanding. XXXVII. Reports on the scientific results of the expedition to the Eastern Tropical Pacific, in charge of Alexander Agassiz, carried on by the U.S. Fish Commission Steamer “Albatross,” from October, 1904, to March, 1905, Liuet. Commander L. M. Garrett, U. S. N., Commanding. XIV. The Mollusca and Brachiopoda. *Bulletin of the Museum of Comparative Zoology at Harvard College*, vol. 43, pp. 205–487.

Distel, D. L., 1998: Evolution of chemoautotrophic endosymbioses in bivalves—bivalve-bacteria chemosymbioses are phylogenetically diverse but morphologically similar. *Bioscience*, vol. 48, pp. 277–286.

Don, R. H., Cox, P. T., Wainwright, B. J., Baker, K. and Mattick, J. S., 1991: 'Touchdown' PCR to circumvent spurious priming during gene amplification. *Nucleic acids research*, vol. 19, p. 4008.

Elicki, O. and Gürsu, S., 2009: First record of *Pojetaia runnegari* Jell, 1980 and *Fordilla* Barrande, 1881 from the Middle East (Taurus Mountains, Turkey) and critical review of Cambrian bivalves. *Paläontologische Zeitschrift*, vol. 83, pp. 267–291.

Esteban-Delgado, F. J., Harper, E. M., Checa, A. G. and Rodríguez-Navarro, A. B., 2008: Origin and expansion of foliated microstructure in pteriomorph bivalves. *The Biological Bulletin*, vol. 214, pp. 153–165.

Etter, R. J., Rex, M. A., Chase, M. C. and Quattro, J. M., 1999: A genetic dimension to deep-sea biodiversity. *Deep Sea Research Part I: Oceanographic Research*

Papers, vol. 46, pp. 1095–1099.

Etter, R., Rex, M. A., Chase, M. R. and Quattro, J. M., 2005: Population differentiation decreases with depth in deep―sea bivalves. *Evolution*, vol. 59, pp. 1479–1491.

Fang, Z., 2006: An introduction to Ordovician bivalves of southern China, with a discussion of the early evolution of the Bivalvia. *Geological Journal*, vol. 41, pp. 303–328.

Feng, W. and Sun, W., 2003: Phosphate replicated and replaced microstructure of molluscan shells from the earliest Cambrian of China. *Acta Palaeontologica Polonica*, vol. 48, pp. 21–30.

Filatova, Z. A. and Schileyko, A. A., 1984: Size, structure and distribution of the deep-sea Bivalvia of the family Ledellidae (Protobranchia). Journal of USSR Academy of Science, Oceanology Institute, vol. 119, pp. 106–139. (*in Russian with English abstract*)

Fisher, C. R., 1990: Chemoautotrophic and methanotrophic symbioses in marine invertebrates. *Reviews in Aquatic Sciences*, vol. 2, pp. 399–436.

Frýda, J., Klicnarová, K., Frýdová, B. and Mergl, M., 2010: Variability in the crystallographic texture of bivalve nacre. *Bulletin of Geosciences,* vol. 85, pp. 645–662.

Frýda, J., Šepitka, J., Frýdová, B., Hrabánková, I., Lukeš, J. and Klicnarová, M., 2013: Crystallographic texture determines mechanical properties of molluscan nacre. *Computer Methods in Biomechanics and Biomedical Engineering*, vol. 16, pp. 292–293.

Fuchigami, T. and Sasaki, T., 2005: The shell structure of the Recent Patellogastropoda (Mollusca: Gastropoda). *Paleontological Research,* vol. 9, pp. 143–168.

Fujikura, K., Okutani, T. and Maruyama, T., 2008: *Deep-sea Life-biological Observations Using Research Submersibles*, 512 pp. Tokai University Press, Kanagawa. (in Japanese).

Fujiwara, Y., 2003: Symbiotic adaptation for deeper habitats in chemosynthetic environments. *Journal of Geography*, vol. 112, pp. 302–308.

Génio L., Kiel, S., Cunha, M. R., Grahame, J. anb Little, C. T. S., 2012: Shell microstructures of mussels (Bivalvia: Mytilidae: Bathymodiolinae) from deep-sea chemosynthetic sites: Do they have a phylogenetic significance? *Deep-Sea Research Part I*, vol. 64, pp. 86–103.

Giribet, G., 2008: Bivalvia. *In*, Ponder, W. F. and Lindberg, D. R., *eds.*, *Phylogeny and Evolution of the Mollusca*. pp. 105–142. University of California Press, Berkeley.

Giribet, G. and Distel, D.L., 2003: Bivalve phylogeny and molecular data. *In*, Lydeard, C. and Lindberg, D.R., *eds.*, *Molecular Systematics and Phylogeography of Mollusks*. pp. 45–90. Smithsonian Books, Washington.

Giribet, G., Okusu, A., Lindgren, A. R., Huff, S. W., Schrödl, N. and Nishiguchi, M. K., 2006: Evidence for a clade composed of molluscs with serially repeated structures: monoplacophorans are related to chitons. *Proceedings of the National Academy of Sciences of the United States of America*, vol. 103, pp. 7723–7728.

Giribet, G. and Wheeler, W., 2002: On bivalve phylogeny: a high-level analysis of the Bivalvia (Mollusca) based on combined morphology and DNA sequence data. *Invertebrate Biology*, vol. 121, pp. 271–324.

Glazier, A. E. and Etter, R. J., 2014: Cryptic speciation along a bathymetric gradient. *Biological Journal of the Linnean Society*, vol. 113, pp. 897–913.

Gofas, S. and Salas, C., 1996: Small Nuculidae (Bivalvia) with functional primary hinge

in the adults. *Journal of Conchology*, vol. 35, pp. 427–435.

Griffin, M. and Nielsen, S. N., 2008: A revision of the type specimens of Tertiary molluscs from Chile and Argentina described by d'Orbigny (1842), Sowerby (1846) and Hupé (1854). *Journal of Systematic Palaeontology*, vol. 6, pp. 251–316.

Habe, T., 1958: Report on the Mollusca chiefly collected by the S. S. Soyo-Maru of the Imperial Fisheries Experimental Station on the continental shelf bordering Japan during the years 1922-1930. Part 3. Lamellibranchia (1). *Publications of the Seto Marine Biological Laboratory*, vol. 6, pp. 241–280.

Harper, E. M., 2000: Are calcitic layers an effective adaptation against shell dissolution in the Bivalvia? *Journal of Zoology*, vol. 251, pp. 179–186.

Harries, P. J. and Little, C. T. S., 1999: The early Toarcian (Early Jurassic) and the Cenomanian-Turonian (Late Cretaceous) mass extinctions: similarities and contrasts. *Palaeogeography, Palaeoclimatology, Palaeoecology*, vol. 154, pp. 39-66.

Hashimoto, J., Miura, T., Fujikura, K. and Ossaka, J., 1993: Discovery of vestimentiferan tube-worms in the euphotic zone. *Zoological Science*, vol. 10, pp. 1063-1067.

Hashimoto, J., Ohta, S., Fujikura, K. and Miura, T., 1995: Microdistribution pattern and biogeography of the hydrothermal vent communities of the Minami-Ensei Knoll in the Mid-Okinawa Trough, Western Pacific. *Deep Sea Research Part I: Oceanographic Research Papers*, vol. 42, pp. 577–598.

Hickman, C. S., 1974: Characteristics of bathyal mollusk faunas in the Pacific Coast Tertiary. *Annual Report of the Western Society of Malacologists*, vol. 1, pp. 41–

50.

Hinz-Schallreuter, I., 2000: Middle Cambrian Bivalvia from Bornholm and a review of Cambrian bivalved Mollusca. *Revista Española de Micropaleontología*, vol. 32(2), pp. 225-242.

Hönisch, B., Ridgwell, A., Schmidt, D. N., Thomas, E., Gibbs, S. J., Sluijs, A., Zeebe, R., Kump, L., Martindale, R. C., Greene, S. E., Kiessling, W., Ries, J., Zachos, J. C., Royer, D. L., Barker, S., Marchitto Jr.,T. A., Moyer, R., Pelejero, C., Ziveri, P., Foster, G. L. and Williams B., 2012: The geological record of ocean acidification. *Science*, vol. 335, pp. 1058–1063.

Huber, M., 2010: *Compendium of Bivalves*. 901 pp. Conchbooks, Hackenheim.

Imhoff, J. F., Sahling, H., Süling, J. and Kath, T., 2003: Bacterial endosymbionts in marine bivalves from cold-seep habitats. *Marine Ecology Progress Series*, vol. 249, pp. 39–51.

Isowa, Y., Sarashina, I., Setiamarga, D. H. E. and Endo, K., 2012: A comparative study of the shell matrix protein aspein in pterioid bivalves. *Journal of molecular evolution*, vol. 75, pp. 11–18.

Kadar, E., Checa, A. G., Oliveira, A. N. D. P. and Machado, J. P., 2008: Shell nacre ultrastructure and depressurisation dissolution in the deep-sea hydrothermal vent mussel *Bathymodiolus azoricus*. *Journal of comparative physiology. B, Biochemical, systemic, and environmental physiology*, vol. 178, pp. 123–130.

Kamenev, G. M., 2009: North Pacific species of the genus *Solemya* Lamarck, 1818 (Bivalvia: Solemyidae), with notes on *Acharax johnsoni* (Dall, 1981). *Malacologia*, vol. 51, pp. 233–261.

Katoh, K. and Standley, D. M., 2013: MAFFT Multiple Sequence Alignment Software

Version 7: Improvements in performance and usability. *Molecular biology and evolution*, vol. 30, pp. 772–780.

Keen, A. M., 1969: Isoarcidae. *In*, Moore, R. C., *ed.*, *Treatise on Invertebrate Paleontology, Part N, Mollusca 6 (Bivalvia)*, vol. 1, p. 241. Geological Society of America, New York and University of Kansas, Lawrence.

Kiel, S., Amano, K. and Jenkins, R.G., 2008: Bivalves from Cretaceous cold−seep deposits on Hokkaido, Japan. *Acta Palaeontologica Polonica*, vol. 53, pp. 525–537.

Kiel, S. and Little, C. T. S., 2006: Cold-seep mollusks are older than the general marine mollusk fauna. *Science*, vol. 313, pp. 1429–1431.

Kilburn, R. N., 1999: The family Nuculidae (Bivalvia: Protobranchia) in South Africa and Mozambique. *Annals of the Natal Museum*, vol. 40, pp. 245–268.

Kobayashi, I., 1971: Internal shell microstructure of Recent bivalvian molluscs. *Science Reports of Niigata University, Series. E, Geology and Mineralogy*, vol. 2, pp. 27–50.

Kouchinsky, A.V., 1999: Shell microstructures of the Early Cambrian *Anabarella* and *Watsonella* as new evidence on the origin of the Rostroconchia. *Lethaia*, vol. 32, pp. 173–180.

Kuznetsov, A. P. and Schileyko, A. A., 1984: On gutless Protobranchia (Bivalvia). *Nauchnye Doklady Vysshei Shkoly, Biologicheskie Nauki*, vol. 2, pp. 39–49. (in Russian)

Liljedahl, L., 1984: *Janeia silurica*, a link between nuculoids and solemyoids (Bivalvia). *Palaeontology*, vol. 27, pp. 693–698.

Liljedahl, L., 1991: Contrasting feeding strategies in bivalves from the Silurian of

Gotland. *Palaeontology*, vol. 34, pp. 219–235.

Lucas, G., 1952: Étude microscopique et pétrographique de la coquille des Lamellibranches. *In*, Piveteau, J., *ed.*, *Traité de Paléontologie, vol. 2*, p. 246–260. Masson, Paris.

Maddison, W. P. and Maddison, D. R., 2011: Mesquite: a modular system for evolutionary analysis. Version 2.75. http://mesquiteproject.org.

Matsumoto, R., Okuda, Y., Aoyama, C., Hiruta, A., Ishida, Y., Sunamura, M., Numanami, H., Tomaru, H., Snyder, G. T., Komatsubara, J., Takeuchi, R. and Hiromatsu, M., 2005: Methane plumes over a marine gas hydrate system in the eastern margin of Japan Sea: a possible mechanism for the transportation of subsurface methane to shallow waters. *Proceedings of the 5th International Conference on Gas Hydrates, Trondheim*, pp. 749–754.

Métivier, B. and von Cosel, R., 1993: *Acharax alinae* n. sp., a giant solemyid (Mollusca: Bivalvia) from the Lau Basin. *Comptes rendus de l'Académie des sciences. Série 3, Sciences de la vie*, vol. 316, pp. 229–237.

Moore, D. R., 1977: Small species of Nuculidae (Bivalvia) from the tropical Western Atlantic. *Nautilus*, vol. 91, pp. 119–128.

Morris, N. J. and Fortey, R. A., 1976: The significance of *Tironucula* gen. nov. to the study of bivalve evolution, *Journal of Paleontology*, vol. 50, pp. 701-709.

Mortimer, J. E., 1962: A comparative study of post-larval feeding mechanisms in the Bivalvia. Ph. D thesis, University of Glasgow.

Morton, B., 1996: The evolutionary history of the Bivalvia. *In*, Taylor, J. D., *ed.*, *Origin and Evolutionary Radiation of the Mollusca*. pp. 337–359. Oxford University Press, Oxford.

Mutvei, H., Dauphin, Y. and Cuif, J. P., 1985: Observations sur l'organisation de la couche externe du test des *Haliotis* (Gastropoda): un cas exceptionnel de variabilité minéralogique et microstructurale. *Bulletin du Muséum Nationale d'Histoire Naturelle*, vol. 7, pp. 73–91.

Neulinger, S. C., Sahling, H., Süling, J. and Imhoff, J. F., 2006: Presence of two phylogenetically distinct groups in the deep-sea mussel *Acharax* (Mollusca: Bivalvia: Solemyidae). *Marine Ecology Progress Series*, vol. 312, pp. 161–168.

Nevesskaya, L. A., 2008: Dynamics of Taxonomic Diversity of Bivalves in the Phanerozoic. *Paleontological Journal*, vol. 42, pp. 335–342.

Nevesskaja, L. A., 2009: Principles of Systematics and the System of Bivalves. Paleontological Journal, vol. 43(1), pp. 1-11.

Nevesskaya, L. A., Scarlato, O. A., Starobogatov, Ya, I. and Eberzin, A. G., 1971: New ideas on bivalves systematics. *Paleontological Journal*, vol. 2, pp. 141–155.

Newell, N. D., 1965: Classification of the Bivalvia. *American Museum Novitates*, vol. 2206, pp. 1–25.

Nicol, D., 1972: Geologic history of deposit-feeding pelecypods. *The Nautilus*, vol. 86, pp. 11–15.

Nishida, K., Ishimura, T., Suzuki, A. and Sasaki, T., 2012: Seasonal changes in the shell microstructure of the bloody clam, *Scapharca broughtonii* (Mollusca: Bivalvia: Arcidae). *Palaeogeography, Palaeoclimatology, Palaeoecology*, vol. 363, pp. 99-108.

Ockelmann, K. and Waren, A., 1998: Taxonomy of and biological notes on the bivalve genus Microgloma, with comments on protobranch nomenclature. *Ophelia*, vol. 48, pp. 1–24.

Ohta, S. and Kim, D., 2001: Submersible observations of the hydrothermal vent communities on the Iheya Ridge, Mid Okinawa Trough, Japan. *Journal of Oceanography*, vol. 57, pp. 663–677.

Okutani, T., 2000: *Marine Molluscs in Japan.* 1221 pp. Tokai University Press, Tokyo.

Okutani, T. and Egawa, K., 1985: The first underwater observation on living habit and thanatocenoses of *Calyptogena soyoae* in bathyal depth of Sagami Bay. *Venus*, vol. 44, pp. 285–289.

Okutani, T. and Fujikura, K., 2002: Abyssal gastropods and bivalves collected by Shinkai 6500 on slope of the Japan Trench. *Venus*, vol. 60, pp. 211–224.

Oliver, G., Rodrigues, C. F. and Cunha, M. R., 2011: Chemosymbiotic bivalves from the mud volcanoes of the Gulf of Cadiz, NE Atlantic, with descriptions of new species of Solemyidae, Lucinidae and Vesicomidae. *Zookeys*, vol. 113, pp. 1–38.

Oliver, P. G. and Taylor, J. D., 2012: Bacterial symbiosis in the Nucinellidae (Bivalvia: Solemyida) with descriptions of two new species. *Journal of Molluscan Studies*, vol. 78, pp. 81–91.

Palmer, A. R., 1983: Relative cost of producing skeletal organic matrix versus calcification: evidence from marine gastropods. *Marine Biology*, vol. 75, pp. 287–292.

Palmer, A. R., 1992: Calcification in marine molluscs: How costly is it? *PNAS*, vol. 89, pp. 1379–1382.

Plazzi, F., Ceregato, A., Taviani, M. and Passamonti, M., 2011: A molecular phylogeny of bivalve mollusks: ancient radiations and divergences as revealed by mitochondrial genes. *PLOS one*, vol. 6, e27147.

Plazzi, F. and Passamonti, M., 2010: Towards a molecular phylogeny of mollusks:

bivalves' early evolution as revealed by mitochondrial genes. *Molecular phylogenetics and evolution*, vol. 57, pp. 641–657.

Pojeta, Jr., J., 1988: The origin and Paleozoic diversification of solemyid pelecypods. *New Mexico Bureau of Mines & Mineral Resources Memoir*, vol. 44, pp. 201–271.

Pojeta, Jr., J. and Runnegar, B., 1985: The early evolution of diasome molluscs. *In*, Trueman, E. R. and Clarke, M. R., *eds*., *Evolution, The Mollusca, Volume 10*, pp. 295–336. Academic Press, New York.

Pojeta, Jr., J., 2001 Cambrian Pelecypoda (Mollusca). *American Malacological Bulletin*, vol. 15(2), pp. 157-166.

Porter, S. M., 2007: Seawater chemistry and early carbonate biomineralization. *Science*, vol. 316, p. 1302.

Purchon, R. D. 1987: Classification and evolution of the Bivalvia: an analytical study. *Philosophical Transactions of the Royal Society B: Biological Sciences*, vol. 316, pp. 277–302.

Pytkowicz, R. M., 1970: On the carbonate compensation depth in the Pacific Ocean. *Geochimica et Cosmochimica Acta*, vol. 34, pp. 836–839.

Reid, R. G. B., 1980: Aspects of the biology of a gutless species of *Solemya* (Bivalvia: Protobranchia). *Canadian Journal of Zoology*, vol. 58(3), pp. 386-393.

Rhoads, D. C., 1974: Organism-sediment relations on the muddy seafloor. *Oceanography and Marine Biology - An Annual Review*, vol. 12, pp. 263–300.

Ridewood, W. G., 1903. On the structure of the gills of the Lamellibranchia. *Philosophical Transactions of the Royal Society of London B*, vol. 195, pp. 147-284.

Ries, J. B. 2010: Review: geological and experimental evidence for secular variation in seawater Mg/Ca (calcite-aragonite seas) and its effects on marine biological calcification. *Biogeosciences*, vol. 7, pp. 2795–2849.

Rodrigues, C. F., Duperron, S. and Gaudron, S. M., 2011: First documented record of a living solemyid bivalve in a Pockmark of the Nile Deep-Sea Fan (eastern Mediterranean Sea). *Marine Biodiversity Records*, vol. 4, pp. 1–4.

Rodriguez-Navarro, A. B., 2007: Registering pole figures using an X-ray single-crystal diffractometer equipped with an area detector. *Journal of Applied Crystallography*, vol. 40, pp. 631–634.

Rodriguez-Navarro, A. B., Checa, A., Willinger, M., Bolmaro, R. and Bonarski, J., 2012: Crystallographic relationships in the crossed lamellar microstructure of the shell of the gastropod *Conus Marmoreus*. *Acta biomaterialia*, vol. 8, pp. 830–835.

Rousseau, M., Meibom, A., Gèze, M., Bouratt, X., Angellier, M. and Lopez, E., 2009: Dynamics of sheet nacre formation in bivalves. *Journal of structural biology*, vol. 165, pp. 190–195.

Runnegar, B., 1985: Shell microstructures of Cambrian molluscs replicated by phosphate. *Alcheringa*, vol. 9, pp. 245–257.

Runnegar, B. and Bentley, C., 1983: Anatomy, ecology and affinities of the Australian Early Cambrian bivalve *Pojetaia runnegari* Jell. *Journal of Paleontology*, vol. 57, pp. 73–92.

Runnegar, B. and Pojeta, J., 1992: The earliest bivalves and their Ordovician descendants. *American Malacological Bulletin*, vol. 9, pp. 117–122.

Salvini-Plawen, L. V. and Steiner, G., 1996: Synapomorphies and plesiomorphies in higher classification of Mollusca. *In*, Taylor, J. D., *ed.*, *Origin and Evolutionary*

Radiation of the Mollusca. pp. 29–51. Oxford University Press, Oxford.

Sanders, H. L. and Allen, J. A., 1973: Studies on deep sea Protobranchia (Bivalvia): prologue and the Pristiglomidae. *Bulletin of The Museum of Comparative Zoology*, vol. 145, pp. 237–261.

Sanders, H. L. and Allen, J. A., 1977: Studies on deep sea Protobranchia (Bivalvia): the family Tindariidae and the genus *Pseudotindaria*. *Bulletin of The Museum of Comparative Zoology*, vol. 148, pp. 23–59.

Saruwatari, K., Matsui, T., Mukai, H., Nagasawa, H. and Kogure, T., 2009: Nucleation and growth of aragonite crystals at the growth front of nacres in pearl oyster, *Pinctada Fucata*. *Biomaterials*, vol. 30, pp. 3028–3034.

Sato, K., Nakashima, R., Majima, R., Watanabe, H. and Sasaki, T., 2013a: Shell microstructures of five Recent solemyids from Japan (Mollusca: Bivalvia). *Paleontological Research* vol. 17, pp. 69–90.

Sato, K., Watanabe, H. and Sasaki, T., 2013b: A new species of *Solemya* (Bivalvia: Protobranchia: Solemyidae) from a hydrothermal vent in the Iheya Ridge in the mid-Okinawa Trough, Japan. *NAUTILUS*, vol. 127, pp. 93–100.

Schenck, H. G., 1936: Nuclid bivalves of the genus *Acila*.*Geological Society of America Special Papers*, vol. 4, 149 pp.

Schenck, H. G., 1939: Revised nomenclature for some nuculid pelecypods. *Journal of Paleontology*, vol. 13, pp. 24–41.

Schneider, J. A. and Carter, J. G., 2001: Evolution and phylogenetic significance of cardioidean shell microstructure (Mollusca, Bivalvia). *Journal of Paleontology*, vol. 75, pp. 607–643.

Sharma, P. P., González, V. L., Kawauchi, G. Y., Andrade, S. C. S., Guzmán, A., Collins,

T. M., Glover, E. A., Harper, E. M., Healy, J. M., Mikkelsen, P. M., Taylor, J. D., Bieler, R. and Giribet, G., 2012: Phylogenetic analysis of four nuclear protein-encoding genes largely corroborates the traditional classification of Bivalvia (Mollusca). *Molecular phylogenetics and evolution*, vol. 65, pp. 64–74.

Sharma, P. P., Zardus, J. D., Boyle, E. E., González, V. L., Jennings, R. M., McIntyre, E., Wheeler, W. C., Etter, R. J. and Giribet, G., 2013: Into the Deep: a phylogenetic approach to the bivalve subclass Protobranchia. *Molecular phylogenetics and evolution*, vol. 69, pp. 188–204.

Shimamoto, M., 1986: Shell microstructure of the Veneridae (Bivalvia) and its phylogenetic implications. *Science Reports of the Tohoku University, Second Series (Geology)*, vol. 56, pp. 1–39.

Silvestro, D. and Michalak, I., 2011: raxmlGUI: a graphical front-end for RAxML. *Organisms Diversity & Evolution*, vol. 12, pp. 335–337.

Smith, E. A., 1892. Descriptions of new species of *Nucula*, and a list of the species belonging to the subgenus *Acila*. Journal of Conchology, vol. 7, pp. 110-112.

Smith, S. A., Wilson, N. G., Goetz, F. E., Feehary, C., Andrade, S. C. S., Rouse, G. W., Giribet, G. and Dunn, C. W., 2011: Resolving the evolutionary relationships of molluscs with phylogenomic tools. *Nature*, vol. 480, pp. 364–367.

Speden, I. G., 1970: The type Fox Hills Formation, Cretaceous (Maestrichtian), South Dakota. Systematics of the Bivalvia. Bulletin of the Peabody Museum, Yale University, vol. 33, pp. 1–222.

Stanley, S. M., 1970: Relation of shell form to life habits of the Bivalvia (Mollusca). *GSA Memoirs*, vol. 125, pp.1–282.

Steiner, G. and Hammer, S., 2000: Molecular phylogeny of the Bivalvia inferred from

18S rDNA sequences with particular reference to the Pteriomorphia. *Geological Society, London, Special Publications*, vol. 177, pp. 11–29.

Stewart, F. J. and Cavanaugh, C. M., 2006: Bacterial endosymbioses in *Solemya* (Mollusca: Bivalvia)—Model systems for studies of symbiont – host adaptation. *Antonie van Leeuwenhoek*, vol. 90, pp. 343–360.

Suzuki, M., Kameda, J., Sasaki, T., Saruwatari, K., Nagasawa, H. and Kogure, T., 2010: Characterization of the multilayered shell of a limpet, *Lottia Kogamogai* (Mollusca: Patellogastropoda), using SEM-EBSD and FIB-TEM techniques. *Journal of structural biology*, vol. 171, pp. 223–230.

Suzuki, M., Saruwatari, K., Kogure, T., Yamamoto, Y., Nishimura, T., Kato, T. and Nagasawa, H., 2009: An acidic matrix protein, Pif, is a key macromolecule for nacre formation. *Science*, vol. 325, pp. 1388–1390.

Takeuchi, T., Sarashina, I., Iijima, M. and Endo, K., 2008: In vitro regulation of CaCO3 crystal polymorphism by the highly acidic molluscan shell protein Aspein. *FEBS letters*¸ vol. 582, pp. 591–596.

Tamura, K., Stecher, G., Peterson, D., Filipski, A. and Kumar, S., 2013: MEGA6: Molecular Evolutionary Genetics Analysis Version 6.0. *Molecular biology and evolution*, vol. 30, pp. 2725–2729.

Taylor, J. D. and Glover, E. A., 2010: Chemosymbiotic bivalves. *In*, Kiel, S., *ed.*, *The vent and seep biota: Aspects from Microbes to Ecosystems*. pp. 107–135.

Taylor, J. D., Glover, E. A. and Williams, S. T., 2008: Ancient chemosynthetic bivalves: systematics of Solemyidae from eastern and southern Australia (Mollusca: Bivalvia). *Memoirs of the Queensland Museum-Nature*, vol. 54, pp. 75–104. Springer, Dordrecht.

Taylor, J. D., Kennedy, W. J. and Hall, A., 1969: The shell structure and mineralogy of the Bivalvia. Introduction. Nuculacea-Trigonacea. *Bulletin of the British Museum (Natural History), Zoology*, vol. 22, pp. 1–125.

Taylor, J. D. and Layman, M., 1972: The mechanical properties of bivalve (Mollusca) shell structures. *Palaeontology*, vol. 15, pp. 73–87.

Taylor, J. D. and Reid, D. G., 1990: Shell microstructure and mineralogy of the Littorinidae; ecological and evolutionary significance. *Hydrobiologia*, vol. 193, pp. 199–215.

Tsukamoto, D., Sarashina, I. and Endo, K., 2004: Structure and expression of an unusually acidic matrix protein of pearl oyster shells. *Biochemical and biophysical research communications*, vol. 320, pp. 1175–1180.

Ueshima, R., 2002: Simple Methods for DNA Preservation in Molluscan Specimens. *Venus*, vol. 61, pp. 91-94. (*in Japanese with English abstract*).

Uozumi, S. and Suzuki, S., 1981: The evolution of shell structures in the Bivalvia. *In*, Habe, T. and Omori, M., *eds*., *Study of Molluscan Paleobiology, Professor Masae Omori Memorial Volume*, pp. 63–77. Niigata University, Niigata. (*in Japanese with English abstract*).

Van de Poel, L., 1955. Structure du test et classification des Nucules. Institut Royal des Sciences Naturelles de Belgiques Bulletin, vol. 31(3), pp. 1-11.

Vendrasco, M. J., Checa, A. G., Heimbrock, W. P. and Baumann, S. D. J., 2013: Nacre in molluscs from the Ordovician of the Midwestern United States. *Geosciences*, vol. 3, pp. 1–29.

Vendrasco, M. J., Checa, A. G. and Kouchinsky, A. V., 2011: Shell microstructure of the early bivalve *Pojetaia* and the independent origin of nacre within the Mollusca.

Palaeontology, vol. 54, pp. 825–850.

Vendrasco, M. J., Porter, S. M., Kouchinsky, A., Li, G. and Fernandez, C. Z., 2010: New data on molluscs and their shell microstructures from the Middle Cambrian Gowers Formation, Australia. *Paleontology*, vol. 53, pp. 97–135.

Vokes, H. E., 1955: Notes on Tertiary and Recent Solemyacidae. *Journal of Paleontology*, vol. 29, pp. 534–545.

Wada, K., 1966: Spiral growth of nacre. *Nature*, vol. 211, p. 1427.

Waller, T. R., 1990: The evolution of ligament systems in the Bivalvia. *In*, Morton, B., *ed.*, *The Bivalvia: Proceedings of a Memorial Symposium in honour of Sir Charles Maurice Yonge (1899-1986) at the 9th International Malacological Congress, 1986, Edinburgh, Scotland, UK*. pp. 49–71. Hong Kong University Press, Hong Kong,

Waller, T. R., 1998: Origin of the molluscan class Bivalvia and a phylogeny of major groups. I. *In*, Johnston, P. A. and Haggart, J. W., *eds.*, *Bivalves: An Eon of Evolution—Palaeobiological Studies Honoring Norman D. Newell*. pp. 1–45. University of Calgary Press, Calgary.

West, K. and Cohen, A., 1996: Shell microstructure of gastropods from Lake Tanganyika. *Evolution*, vol. 50, pp. 672–681.

Weiner, S., Traub, W., 1980: X-ray diffraction study of the insoluble organic matrix of mollusk shells. *FEBS letters*, vol. 111, pp. 311-316.

Wignall, P. B., Newton, R. J. and Little, C. T., 2005: The timing of paleoenvironmental change and cause-and-effect relationships during the Early Jurassic mass extinction in Europe. *American Journal of Science*, vol. 305, pp. 1014–1032.

Wilkinson, B. H., 1979: Biomineralization, paleooceanography and the evolution of

calcareous marine organisms. *Geology*, col. 7, pp. 524-527.

Wilkinson, B. H., Owen, R. M. and Carroll, A. R., 1985: Submarine hydrothermal weathering, global eustacy, and carbonate polymorphism in Phanerozoic marine oolites. Journal of Sedimentary Petrology, vol. 55, pp. 171-183.

Wilson, N. G., Rouse, G. W. and Giribet, G., 2010: Assessing the molluscan hypothesis Serialia (Monoplacophora+Polyplacophora) using novel molecular data. *Molecular phylogenetics and evolution*, vol. 54, pp. 187–193.

Wise, S. W., Jr., 1970: Microarchitecture and mode of formation of nacre (mother of pearl) in pelecypods, gastropods and cephalopods. *Eclogae Geologicae Helvetiae*, vol. 63, pp. 775–797.

Xu, F. S., 1984: Preliminary study on the Protobranchia (Mollusca) from the shallow waters of China. II. Nuculidae. *Studia Marina Sinica*, vol. 22, pp. 179-188.

Xu, F. S., 1999: *Fauna Sinica Phylum Mollusca Class Bivalvia Subclass Protobranchia and Anomalodesmata*. 244 pp. Science Press, Beijing.

Xu, F. S. and Zhang, J. L., 2008: *An Illustrated Bivalvia Mollusca Fauna of China sea*. 336 pp. Science Press, Beijing.

Yamaguchi, K., 1994: Shell structure and behavior related to cementation in oysters. *Marine Biology*, vol. 118, pp. 89–100.

Yamanaka, T., Mizota, C., Matsuyama-Serizawa, K., Kakegawa, T., Miyazaki, J., Mampuku, M., Tsutsumi, H. and Fujiwara, Y., 2008: Stable isotopic characterization of carbon, nitrogen and sulfur uptake of *Acharax japonica* from central Japan. *Plankton and Benthos Research*, vol. 3, pp. 36–41.

Yamanaka, T., Mizota, C., Miura, T. and Hashimoto, J., 1999: A currently forming petroleum associated with hydrothermal mineralization in a submarine caldera,

Kagoshima Bay, Japan. *Geochemical Journal*, vol. 33, pp. 355–367.

Yonge, C. M., 1939: The protobranchiate Mollusca; a functional interpretation of their structure and evolution. *Philosophical Transactions of the Royal Society of London B*, vol. 230, pp. 79-147.

Yokoyama, M., 1925: Molluscan remains from the uppermost part of the Jo-Ban Coal-Field. *Journal of the College of Science, Imperial University of Tokyo*. vol. 45, pp. 1–34.

Zardus, J. D., 2002: Protobranch bivalves. *Advances in marine biology*, vol. 42, pp. 1–65.

Zardus, J. D., Etter, R. J., Chase, M. R., Rex. M. A. and Boyle, E. E., 2006: Bathymetric and geographic population structure in the Pan-Atlantic deep-sea bivalve *Deminucula Atacellana* (Schenck, 1939). *Molecular ecology*, vol. 15, pp. 639–651.

Zhang, J., Shi, H., Xu, F. and Sha, Z., 2014: Are *Acila Divaricata* and *Acila Mirabilis* one species or two distinct species? Evidence from COI mitochondrial DNA. *Journal of Ocean University of China*, vol. 13, pp. 283–289.

Zong-jie, F. and Sánchez, T. M., 2012: Part N, Revised, Volume 1, Chapter 16: Origin and Early Evolution of the Bivalvia. *Treatise Online*, vol. 43, pp. 1–21.

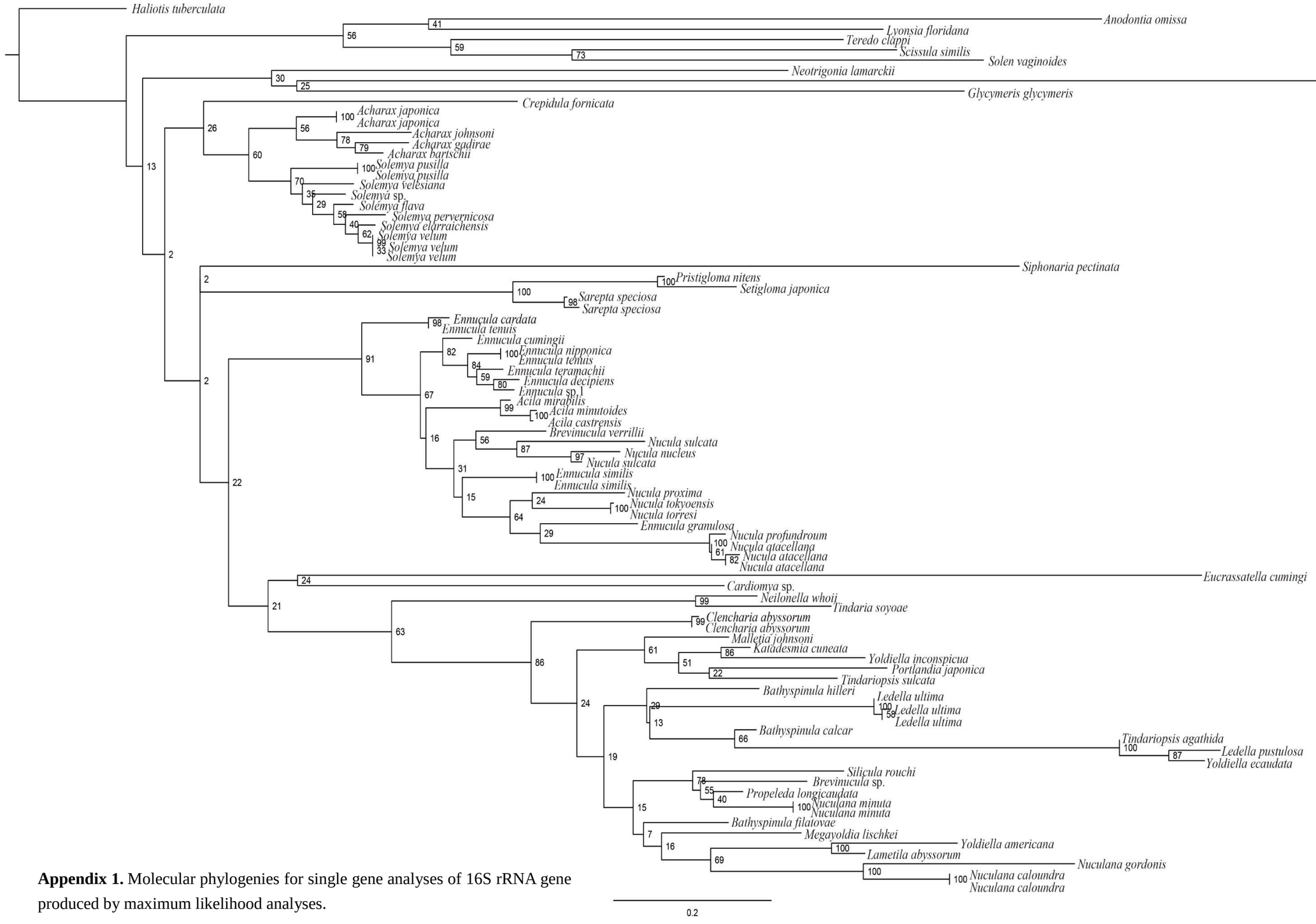

Appendix 1. Molecular phylogenies for single gene analyses of 16S rRNA gene produced by maximum likelihood analyses.

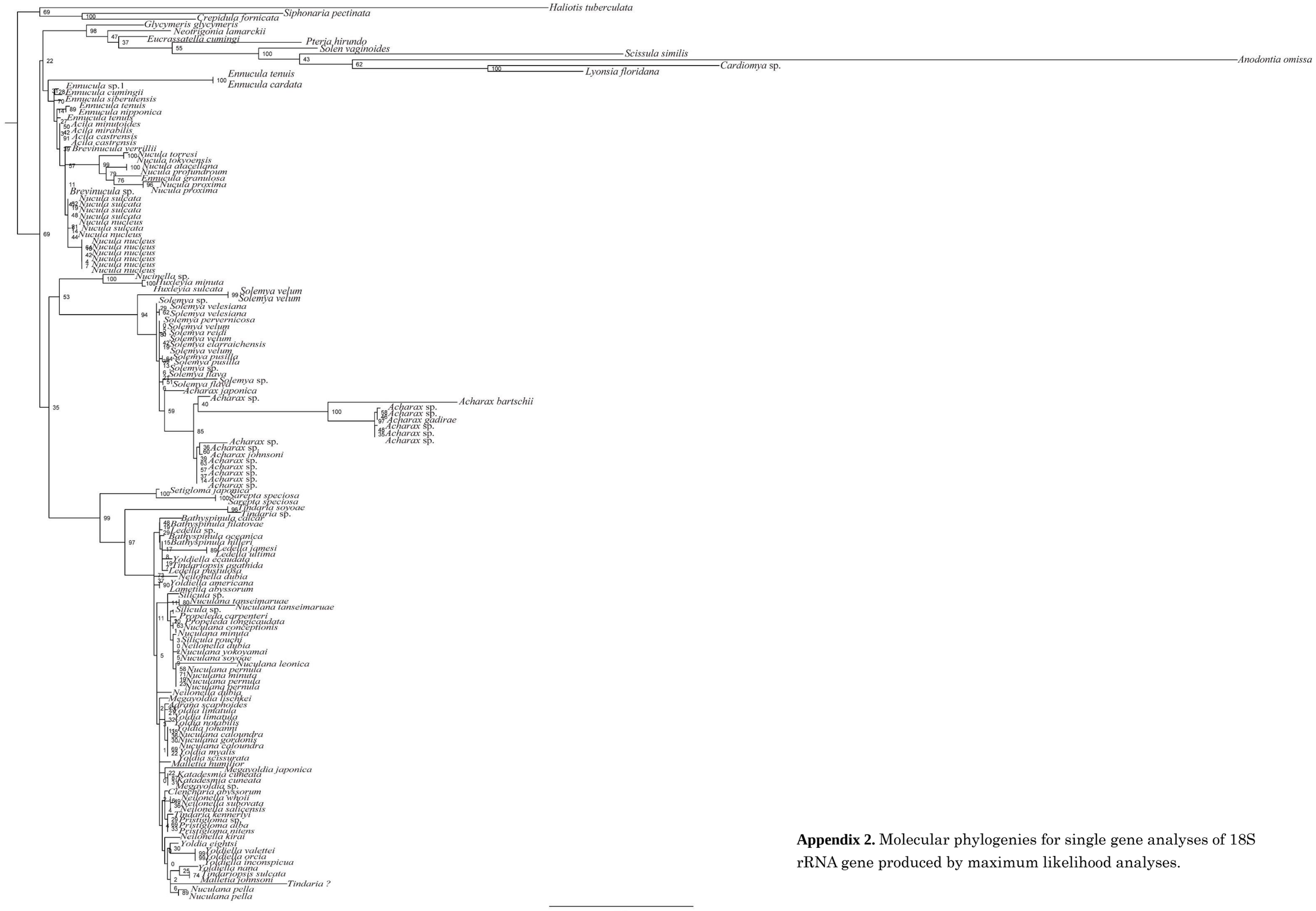

Appendix 2. Molecular phylogenies for single gene analyses of 18S rRNA gene produced by maximum likelihood analyses.

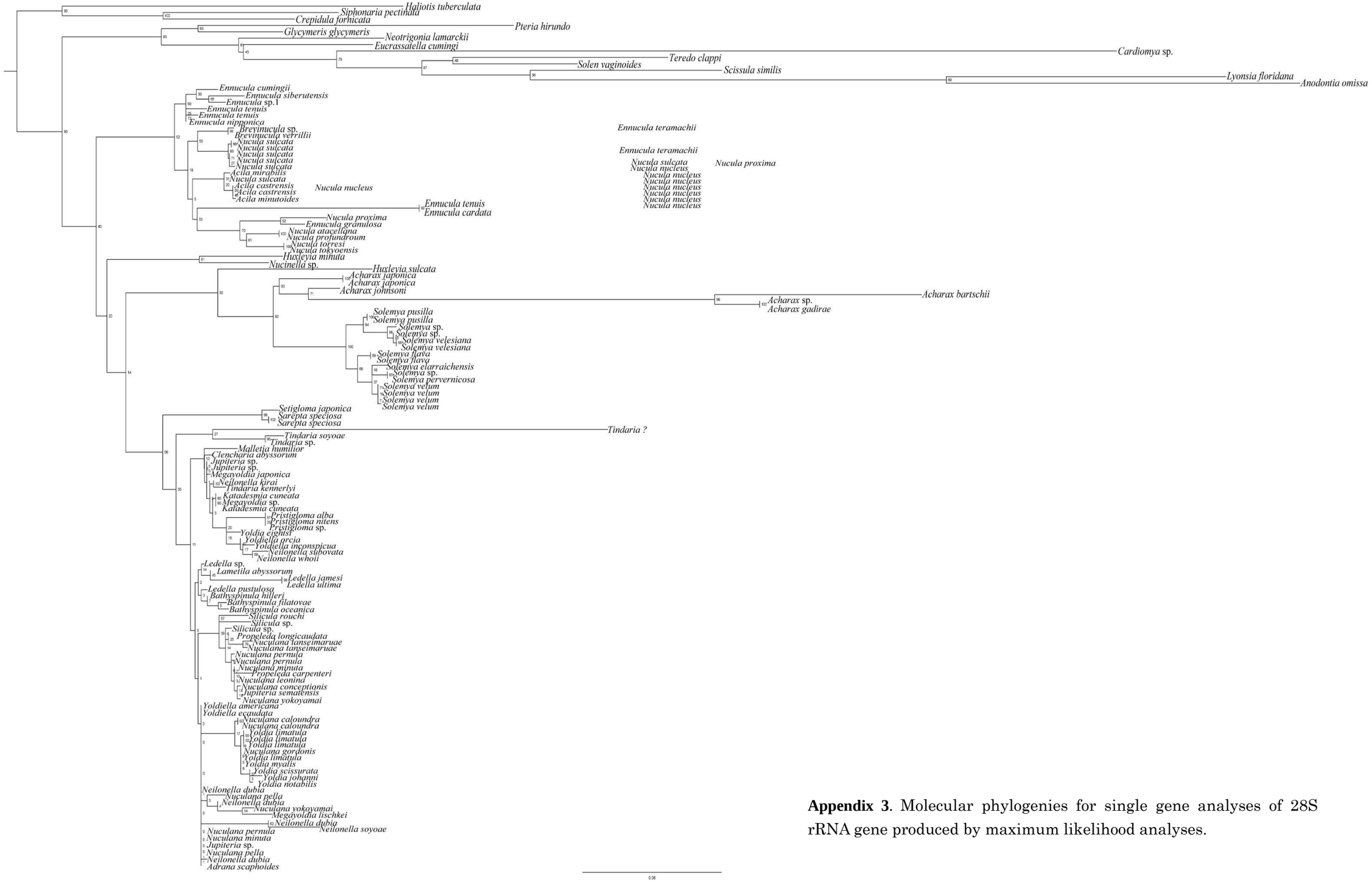

Appendix 3. Molecular phylogenies for single gene analyses of 28S rRNA gene produced by maximum likelihood analyses.

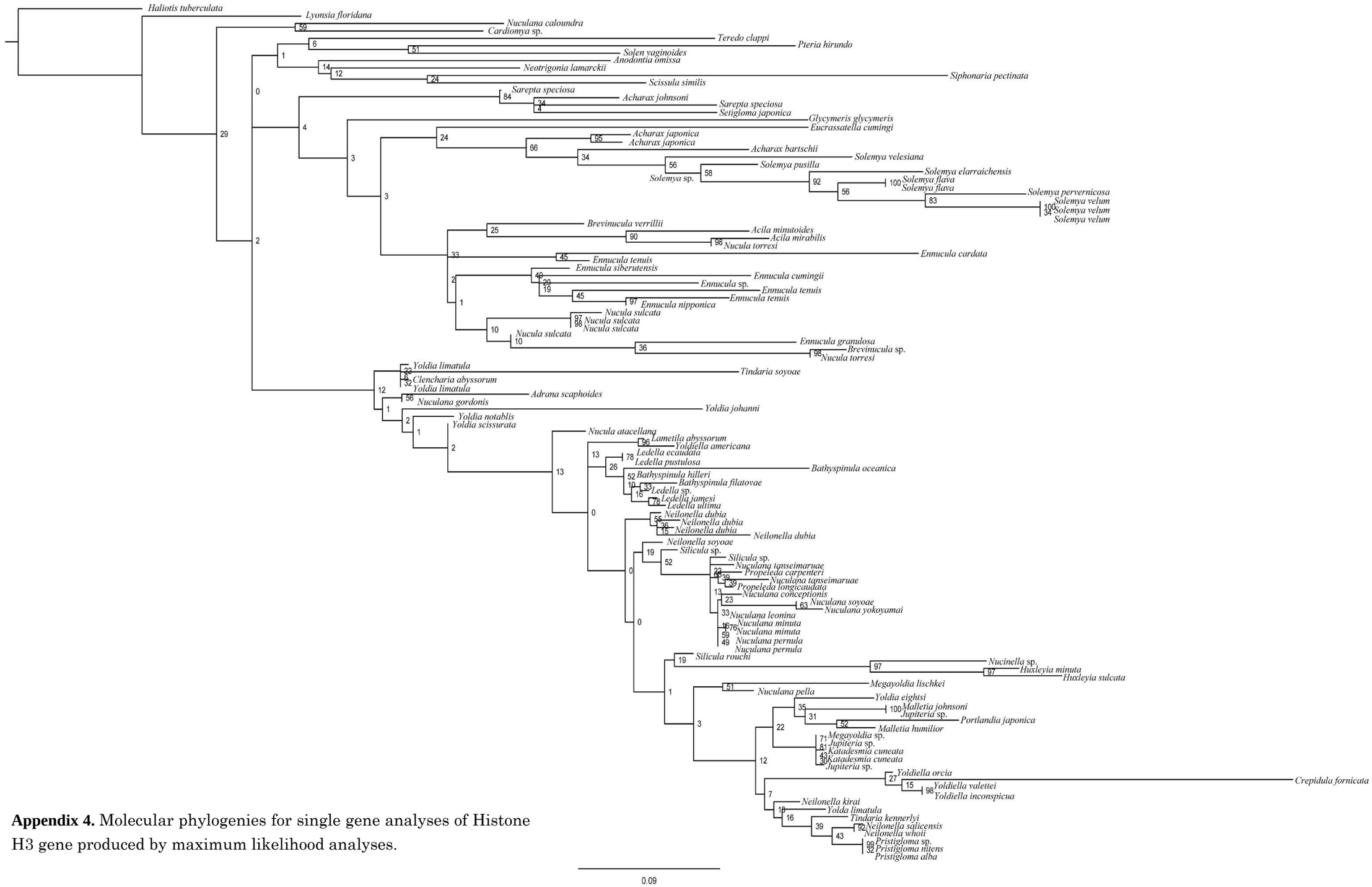

Appendix 4. Molecular phylogenies for single gene analyses of Histone H3 gene produced by maximum likelihood analyses.

Appendix 5. Molecular phylogenies for single gene analyses of COI gene produced by maximum likelihood analyses.